Università degli studi di Padova

Dipartimento di Astronomia

Dottorato di ricerca in Astronomia

Ciclo XX

Variable stars and planetary transit search in super metal-rich open clusters

Coordinatore: Ch.mo Prof. Giampaolo Piotto

Supervisori: Ch.mo Prof. Giampaolo Piotto,
Dott. Silvano Desidera

Dottorando: Fabrizio De Marchi

DATA CONSEGNA TESI

31-01-2008

Abstract

This PhD thesis presents the analysis of a large sample of photometric data relative to the super metal–rich open clusters NGC 6791 and NGC 6253.

The primary target of the observations in both clusters was the search for extrasolar planets; but my work was focused on the analysis of the database in order to search for and to study the variable stars contents of NGC 6791 and NGC 6253 and their surrounding areas.

The database of NGC 6791 consists in several thousands of light curves. obtained in July 2002 from 3 telescopes: the Canada–France-Hawaii telescope (3.6m), the San Pedro Mártir telescope (2.2m) and the Loiano telescope (1.5m); the light curves (about 30,000 units) are all in the V band. and the field covers an area of 42×28 arcmin^2 (the cluster diameter is nearby 20').

Among the entire sample of light curves, we have discovered 260 new variables and re-determined periods and amplitudes of 70 already known variable stars. By means of a photometric evaluation of the membership and preliminary membership based on the proper motions, we give a full description of the variable content of the cluster and surrounding field in the range $16 \lesssim V < 23.5$. Accurate determinations for the periods were obtained for the variables with $P \lesssim 4.0$ d, while for the variables with longer periods (168 stars) the limited time–baseline hampered precise determinations. An interesting result obtained is the discovery of an U Geminorum cataclysmic variable belonging to NGC 6791; it is worthwhile to note that the number of known U Gem systems in all open clusters is actually no more than four objects (three of them belong to NGC 6791). A complete description of this

study is reported in Chapter 3, while the data relative to the variables and their light curves are reported in Appendix A.

Moreover, I considered also the incidence of the variability and the statistical properties of peculiar stellar populations as Blue and Yellow Stragglers stars, where, with the term "Yellow Stragglers" I mean the stars located (into a Color-Magnitude diagram) between the Blue Stragglers region and the Red Giant Branch.

I found no variable stars among the Blue Stragglers of NGC 6791, and for the Yellow Stragglers I infer that most of them are non-eclipsing binary systems composed by a couple of Main Sequence stars or a Main Sequence star and a slightly evolved star. The type of the variability detected among the Yellow Stragglers is fully compatible with chromospheric activity enhanced by magnetic winds and/or tidal forces between the two components. The lack of variables among the Blue Stragglers is mostly due to the fact that at brighter magnitudes our light curves were saturated. This topic is treated in Chapter 4.

The other cluster, NGC 6253, was observed at La Silla with the 2.2m telescopes, the database consists in about 327,000 light curves (mainly field stars) in R band, and the area covered is 32×32 arcmin^2 (the cluster diameter is no more than 8-10'). Observations and data reduction procedure (for both clusters) are described in Chapter 2. The high number of light curves collected in this survey is due to the severe field contamination towards the Galactic Center on which the cluster is projected.

From the variability study in NGC 6253, even if still in progress, I individuate 597 variable stars. However, a preliminary study using proper motions, even if the information about membership are incomplete at faint magnitudes, allows us to retain that no more than 20–30 of them are real members of the cluster. The details on this study are described in Chapter 5, while the light curves and their classification are reported in Appendix B.

Finally, I contributed to the planetary transits search in both clusters by making several accurate simulations in order to give a realistic estimate

of the number of expected *detectable* transiting planets, taking into account also the Transit Detection Efficiency of the algorithm involved in the search of transit-like events into the light curves. These simulations represent a necessary implementation of our transit search in open clusters, moreover, they also strongly influenced the conclusions of our work. The details of the procedure are described in Chapter 6, while, the numerical results are reported in Appendix C.

Contents

Chapter 1

Introduction

In this section the wide range of astrophysical information that can be achieved by studying variable stars[1] is listed and discussed (Sect. 1.1), while a description of the characteristics and behaviours of different types of variable stars is reported in Sect. 1.2. In Sect. 1.4 I will describe the selection criteria that allowed us to choice as our targets NGC 6791 and NGC 6253. At the very end of the Chapter, there will be briefly summarized the results obtained by some variability surveys in stellar environment similar to our clusters.

1.1 Variable stars: why study them?

The study of variable stars is important for many reasons: it can provide fundamental information about the internal structure and the evolution of stars. Moreover, the measurement of the distance scale of the Universe is strictly connected to the period-luminosity relations typical of certain pulsating variables.

Eclipsing binaries are important because from their spectroscopic and/or

[1] I want to highlight that in this class of objects I will include also phenomena as the extrasolar transits or the microlensing, following the scheme of Eyer & Mowlavi, 2007 [28] and represented in Figure 1.1.

photometric observations we can obtain information on masses and radii, while in contact or semi-detached systems many kind of interactions (tidal, magnetic, thermal, etc.) between the components can be studied. In particular, it is quite probable that one of the way of formation of Blue Stragglers stars strictly depends on evolution and interaction of these objects with the surrounding stellar environment; therefore, also statistical data about the incidence of these systems are needful in order to resolve the question.

Recently, the study of certain kinds of pulsating variables provides a powerful tool to find the internal structure of stars (one of the parts of the Universe more difficult to observe). The pulsation frequencies give the information about the density profile of the region where the waves originate and travel (different oscillation modes penetrate to different depths inside the star); on the other hand, the spectra give the information about the chemical constituents.

Another important reason to study variable stars is the distances determination. There are classes of pulsating variable stars such as Cepheids, W Virginis, δ Scuti, RR Lyrae etc. that exhibit definite relationships between their periods and their intrinsic luminosities. Such period-luminosity relationships represent a vital method in calculating distances within and beyond the Milky Way and, historically, the study of these objects has strongly influenced our understanding of the scale of the Universe.

Supernova explosions are interesting mostly because an explosion represents the only way to see *directly* the internal deep structure of a star, but supernovae can be used also as "standard-chandles" to calculate distances, such as the pulsating variables. Moreover, the expansion of a remnant gives information about the interstellar medium.

Finally, the study of cataclysmics variables, pulsars and other objects on which high-energy processes are in act, provides information about the physical behaviour of the matter subject to extreme conditions such high temperatures, ionization, strong magnetic fields, degenerate states, etc.

To summarize, the study of variable stars is a powerful system, and in

some cases the only, to achieve information on diverse astrophysical processes and to extend our knowledge about the geometry of the large scale Universe.

1.2 Different types of variable stars

Manifestations of variability in astrophysical sources are very diverse. Regarding the timescales, the variations go from the the order of milliseconds for Gamma Ray Burst to centuries for secular evolution. Amplitudes range from parts per million for solar-like oscillations to many orders of magnitudes for hypernovae; and finally, we can have extremely regular pulsations of, for example, Cepheids to unique events such as cataclysmic phenomena or supernovae explosions.

In this thesis, several kinds of variable stars will be analyzed and discussed. We now briefly describe the main characteristics of some classes of variability. Our list is limited to those classes to which belong the variables that we found (see Chapters 3, 5, and 4).

Many phenomena can be at the origin of the variations of the brightness of certain stars. Variables are generally sampled in two distinct classes: *extrinsic* and *intrinsic* variables.

Extrinsic variables are those in which the light output varies either due to processes external to the star itself as geometrical effects (i.e.: the position of the object relative to the observer) or due to the rotation of the star. The two main classes of extrinsic stars are the eclipsing binaries and the rotating variables.

Intrinsic variables, on the other hand, result from changes within the star itself. They are extremely important and useful objects to astronomers as they can provide important information about the internal structure of the stars (see Sect. 1.1) and needful data for the models of stellar evolution. Moreover, some types of intrinsic variables, such as Cepheids and supernovae are used in distance determination. Four subsamples are generally identified: pulsating, cataclysmic, eruptive, and secular variables, however, we limit our

description to the first two categories.

Pulsating variables are stars showing periodic expansion and contraction (radially or non-radially) of their surface layers. A radially pulsating star remains spherical in shape, while in the case of non-radial pulsations the star's shape periodically deviates from a sphere. In the process they change their size, effective temperature and spectral properties.

The pulsating variables that will described in this thesis belong to the following subtypes:

- δ **Scuti** Pulsating variables of spectral types A0-F5 III-V (see Figure 1.2) displaying light amplitudes from 0.003 to 0.9 mag in V (usually several hundredths of a magnitude) and periods from 0.01 to 0.2 d. The shapes of the light curves, periods, and amplitudes usually vary greatly. Radial as well as non-radial pulsations are observed. The maximum of the surface layer expansion does not lag behind the maximum light for more than 0.1 periods. DSCT stars are representatives of the galactic disk and are phenomenologically close to the SX Phoenicis variables (see below).

- **High-amplitude δ Scuti stars** (hereafter HADS) form an interesting subgroup of short-period pulsators located inside the classical instability strip near the main-sequence. Their light variation is characterized by relatively large amplitudes (a conventional limit is $A_V \geq 0.30$) The variability of these stars is likely due to radial pulsation in fundamental or low-order radial overtone pulsation (Rodriguez et al. 1996 [89]; Petersen & Christensen-Dalsgaard, 1996 [79]), It also appears that they exhibit a period-luminosity relation which has been studied by several authors (e.g. McNamara, 1997 [65], 2000 [66] and [67]; Petersen & Hog 1998 [81]).

- **SX-Phoenicis** are the metal-poor counterpart of δ Scuti variables. They are pulsating subdwarfs of the spherical component, or old disk

galactic population, with spectral types in the range A2-F5 (see Figure 1.2). They may show several simultaneous periods of oscillation, generally in the range 0.04-0.08 d, with variable-amplitude light changes that may reach 0.7 mag in V.

- **RR Lyrae** are radially-pulsating giant A-F stars having amplitudes from 0.2 to 2 mag in V. Cases of variable light curve shapes as well as variable periods are known. Periodic variations of the period are called the "Blazhko effect".

  RRab are RR Lyrae stars that show asymmetric light curves (steep ascending branches); their periods range from 0.3 to 1.2 d, and amplitudes from 0.5 to 2 mag in V. Instead, RRc are stars that have nearly symmetric, sometimes sinusoidal, light curves, periods from 0.2 to 0.5 d, and amplitudes not greater than 0.8 mag in V.

Cataclysmic Variables are variable stars showing outbursts caused by thermonuclear burst processes in their surface layers (novae) or deep in their interiors (supernovae). Many cataclysmic variables are close binary systems and their components having strong mutual influence on the evolution of each star. It is often observed that the hot dwarf component of the system is surrounded by an accretion disk formed by matter lost by the other, cooler, and more extended component. In particular, the U Geminorum type variables, also called *dwarf novae*, are close binary systems consisting of a dwarf or subgiant K-M star that fills the volume of its internal Roche lobe and a white dwarf surrounded by an accretion disk (Warner, 1995 [108]). Orbital periods are in the range of 0.05-0.5 d. Usually only small, in some cases rapid, light fluctuations are observed, but from time to time the brightness of a system increases rapidly by several magnitudes and, after an interval of from several days to a month or more, returns to the original state. Intervals between two consecutive outbursts for a given star may vary greatly, but every star is characterized by a certain mean value of these intervals, i.e., a mean cycle that corresponds to the mean light amplitude. The longer the

cycle, the greater the amplitude. These systems are also frequently sources of X-ray emission.

Among the other group, the *extrinsic* variables, we have the eclipsing binaries and the rotational variables; however, as said above, to this group belong also the brightness variation due to transiting planets and the effects of the so called microlensing. This latter topic lies outside the purpose of this thesis, while the transits phenomena will be discussed in details in Chapter 6.

Eclipsing binaries are binary systems with orbital planes so close to the observer's line of sight ($i \sim 90\circ$) that the components periodically eclipse each other. Consequently, the observer finds changes of the apparent combined brightness of the system with the period coincident with that of the components' orbital motion. basing on the degree of interaction between the two members, we have:

- **EA-Type** : they are eclipsing binaries with spherical or slightly ellipsoidal components. It is possible to specify, for their light curves, the moments of the beginning and end of the eclipses. Between eclipses the light remains almost constant or varies insignificantly because of reflection effects, slight ellipticity of components, or physical variations. Secondary minima may be absent. An extremely wide range of periods is observed, from 0.2 to $\geq$ 10000 d. Light amplitudes are also quite different and may reach several magnitudes. The prototype is Algol (β Persei).

- **EB-Type**: these are eclipsing systems have ellipsoidal components and light curves for which it is impossible to specify the exact times of onset and end of eclipses because of a continuous change of a system's apparent combined brightness between eclipses; secondary minimum is observed in all cases, its depth usually being considerably smaller than that of the primary minimum; periods are mainly longer than 1 d, . while Light amplitudes are usually $<$ 2 mag in V. The prototype is β Lyrae.

- **EW-Type**: they consist of ellipsoidal components almost in contact and having light curves for which it is impossible to specify the exact times of onset and end of eclipses. The depths of the primary and secondary minima are almost equal or differ insignificantly. Light amplitudes are usually < 0.8 mag in V. The periods are generally shorter than 1 d (typically 0.3-0.4 d, but some EW have period of near 2 d), The prototype is W Ursae Majoris. For this important class of object exist a period-color-luminosity relation by Rucinski et al. (2003) [92] (see pag. 52) that will be useful several times during our analysis.

Rotational variables are stars with nonuniform surface brightness and/or ellipsoidal shapes due to the presence of a companion. In particular:the BY Draconis type variables (G, K or M Main Sequence stars) show quasi-periodic light variations (periods: from less than 1 d to 120 d) and amplitudes generally smaller than 0.5 mag in V. The light variation is caused by axial rotation of the star with a variable degree of non-uniformity of the surface brightness (spots) and chromospheric activity.

A peculiar type of binary system (several variables of our databases belong to it) is represented by the RS Canum Venaticorum class (RS-CVn). They are close binary systems on which the primary is generally the cooler component (a subgiant branch or a red giant branch star) and the secondary is a MS star. The variability of these object, when non eclipsing, is due to chromospheric spots combined with the stellar rotation. The result is a light curve that exhibits quasi sine waves outside eclipses, with amplitudes and positions changing slowly with time. The presence of this wave (often called a distortion wave) is explained by differential rotation of the star, its surface being covered with groups of spots; the period of the rotation of a spot group is usually close to the period of orbital motion. The variability of the wave's amplitude (which may be up to 0.2 mag in V) is explained by the existence of a long-period stellar activity cycle during which the number and total area of spots on the star's surface vary.

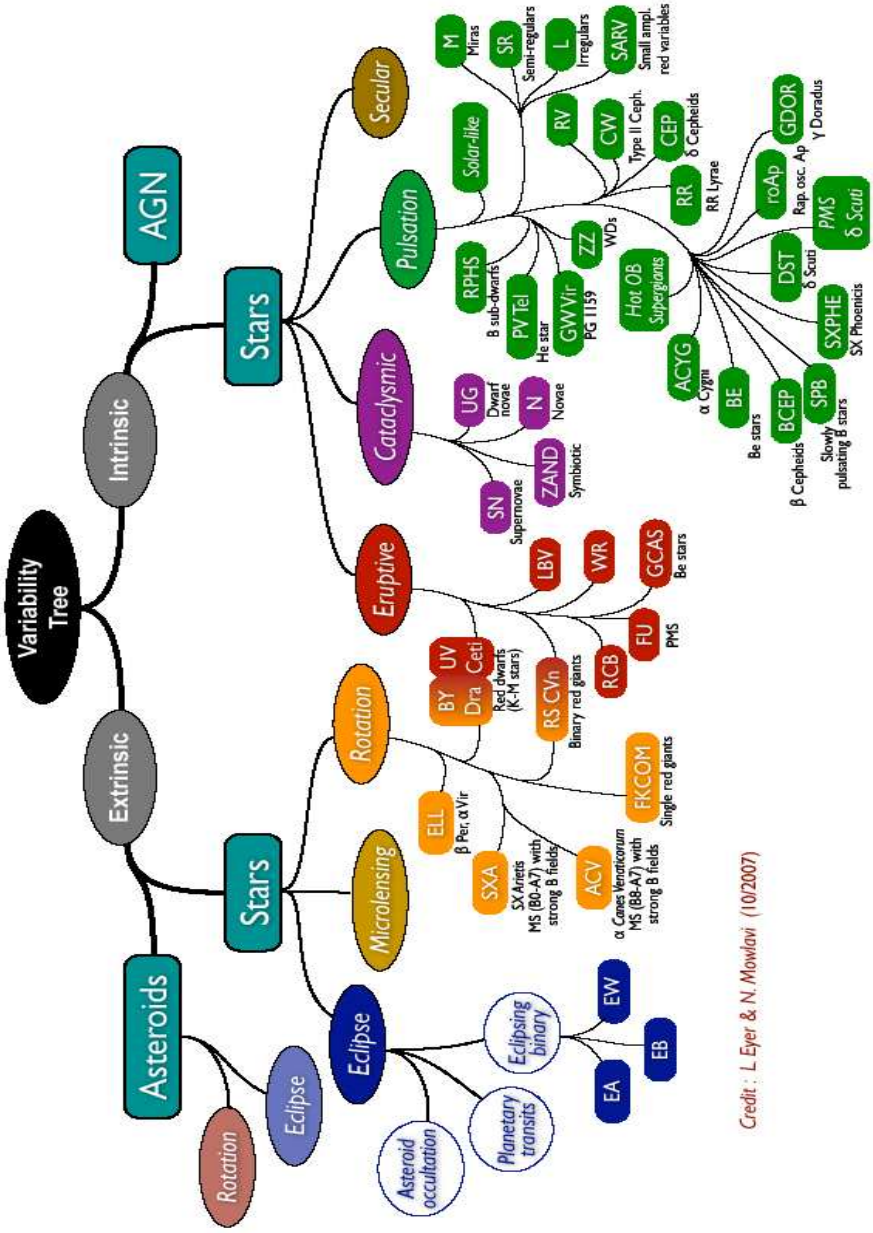

Figure 1.1: Variability tree. A tentative organization of variable objects (image taken from Eyer & Mowlavi, 2007 [28]).

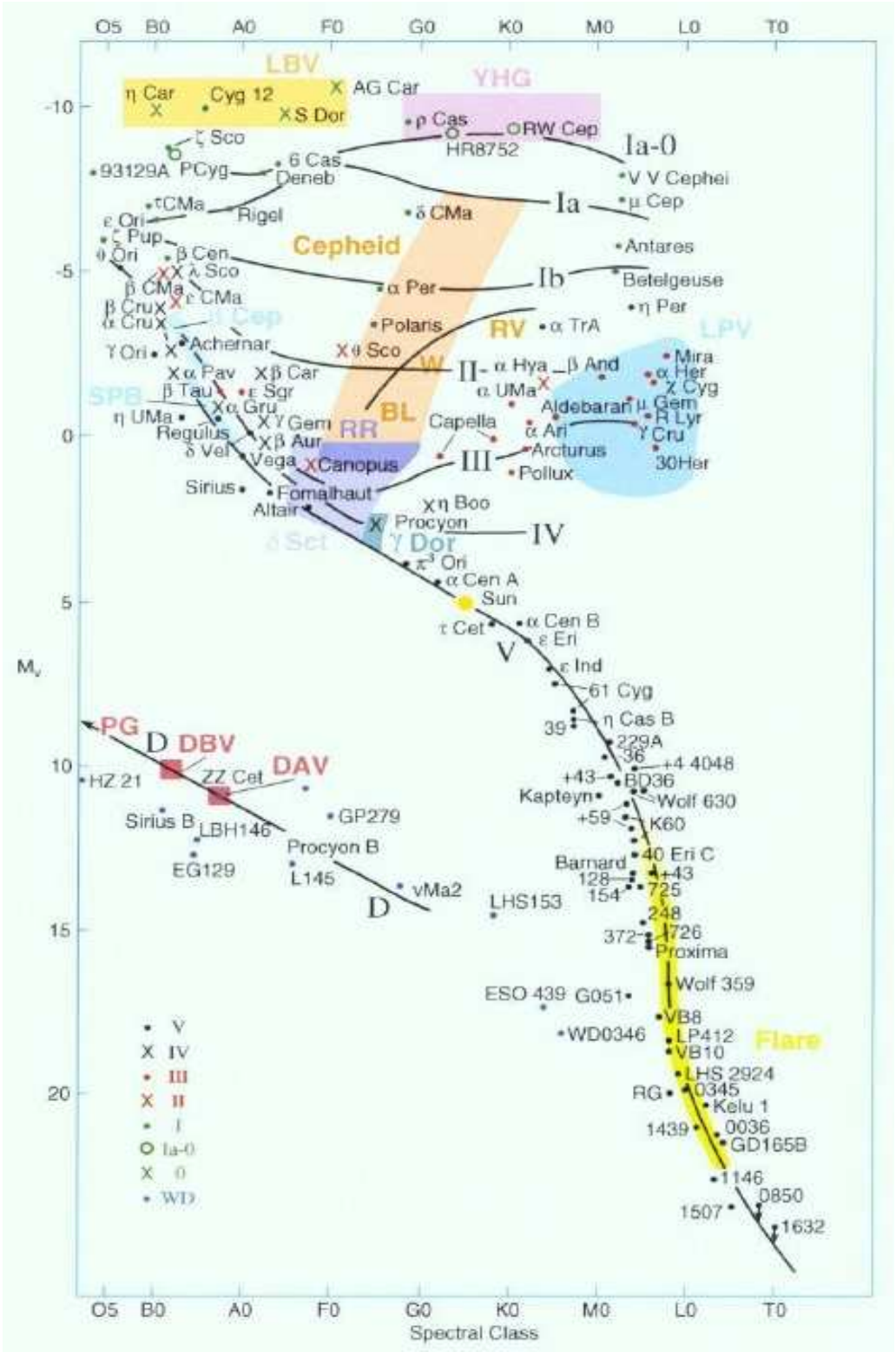

Figure 1.2: Theoretical HR diagram with superimposed the areas occupied by variable stars (Figure taken from `www.astro.uiuc.edu`) .

1.3 Synergy between searches for transiting planets and variable stars

During the last years, several searches for transiting planets were made. The requirements of a planet search survey are:

1. Many stars (several thousands), to have a significant chance of success.

2. High photometric precision (transits amplitudes are $\sim$0.01 mag for a solar type star (see Chapter 6).

3. Continue observations over days/weeks depending on the observing strategy of the survey.

These characteristics are ideal also for the search of short-period variables; indeed, several studies on variable stars are based on the observational material of transit searches.

1.4 Advantages of open clusters

Galactic clusters are substantially coeval sets of stars with homogeneous properties. For this reason, they are ideal laboratories for the study of many different astrophysical topics. In fact, all stars of a cluster are expected to have the same age, chemical composition, reddening and distance from the Sun, consequently, much more informations can be obtained for a cluster member than from an isolated field star.

Regarding the observations, the morphology of a stellar cluster allows us to obtain simultaneous photometry of hundreds of stars in a single CCD frame; therefore, it is possible to perform complete monitoring of several astrophysical phenomena as, for example, stellar variability or, in the last years, planetary transit searches.

It seems that a planetary survey on an open cluster rather than a globular cluster has many probabilities of success: a search for planets in the globular

cluster 47 Tucanae using HST and ground-based wide-field facilities gave null results. This indicate that planetary systems are at least one order of magnitude less common in 47 Tuc than in Solar vicinity (Gilliland et al. 2000 [37]; Weldrake et al. 2005) [110]. The lack of planets in 47 Tuc may be due either to the low metallicity of the cluster (see below), or to environmental effects caused by the high stellar density (or both).

One planet has been identified in the globular cluster M 4 (Sigurdsson et al. 2003 [98]), but this is a rather peculiar case, as the planet is in a circumbinary orbit around a system including a pulsar and it may have formed in a different way from the planets orbiting solar type stars (Beer et al. 2004 [7]).

Open clusters are not as dense as globular clusters. The dynamical and photoevaporation effects at work should then be less extreme than in globular clusters. Furthermore, their metallicity (typically Solar) should, in principle, be accompanied by a higher planet frequency.

Moreover, open clusters have a wide spread in age, and that give us the possibilty of studying different types of stars at different epochs of dynamical evolution. For example, young clusters are useful in the developement of models of star formation, while from the older ones we can obtain informations about the stellar and dynamical evolution.

The specific interests for planet searches are: dynamical effects, better determination of stellar parameters and look for differences between stars with/without planets (e.g. chemical composition).

Targeting cluster stars in order to look for transits involves other specific issues:

- The total number of monitored stars in clusters is in general lower than in rich Galactic fields where tens of thousand of stars can be monitored simultaneously. The richest open clusters can have up to 10,000 stars (Friel, 1995 [32]), and this reduces the number of expected transits. Moreover, only a relatively small fraction of these stars (i.e.: 10-20%) are monitored with the required high photometric precision.

- Contamination of field stars represents another important challange in

the search for transits in clusters. Because of open clusters are typically located in the Galactic disk, it follows that without any additional information on radial velocities and on proper motions isolating cluster stars on the basis of the only photometry could result in an highly contaminated sample. Handle the problem of contamination is important because any statistical statement about the results is based on surveyed cluster members.

1.5 Our project: searching for planets in super metal-rich open clusters

In a typical open cluster of solar metallicity with about 1000 members, less than one star is expected to show a planetary transit if the same frequencies as for nearby field stars are valid. Considering the unavoidable losses due to the observing window and photometric errors, it turns out that the probability of success of such efforts is fairly low unless several clusters are monitored. The fact that, up to now, only three planets were discovered in clusters have been found should not come as a surprise. However, it was found that the probability that a star hosts a planet is proportional to the metallicity (Fischer & Valenti, 2005 [30]; see Figure 1.3 and Sect. 6.3.1). Therefore, the metallicity is our first selection criterium.

The second criterium is the age:younger stars have in general an higher level of activity; which could add noise to the light curves and increase the number of false candidates. Moreover, the same type of stellar activity corresponds to high rotational velocities (i.e. up to 50 $\mathrm{m\,s^{-1}}$ Paulson et al. 2004 [78]), and consequently to a less precision in a radial velocity follow-up (which is necessary to confirm a transit candidate). Transits surveys are also heavily limited by the stellar sizes: the depth of a planetary eclipse is proportional to R^{-2} where R is the host star radius. Conversely, older stars (age >1.5 Gyr, Pace & Pasquini 2004 [77]) have significantly less surface activity, and, in addition, old clusters are generally richer than younger ones

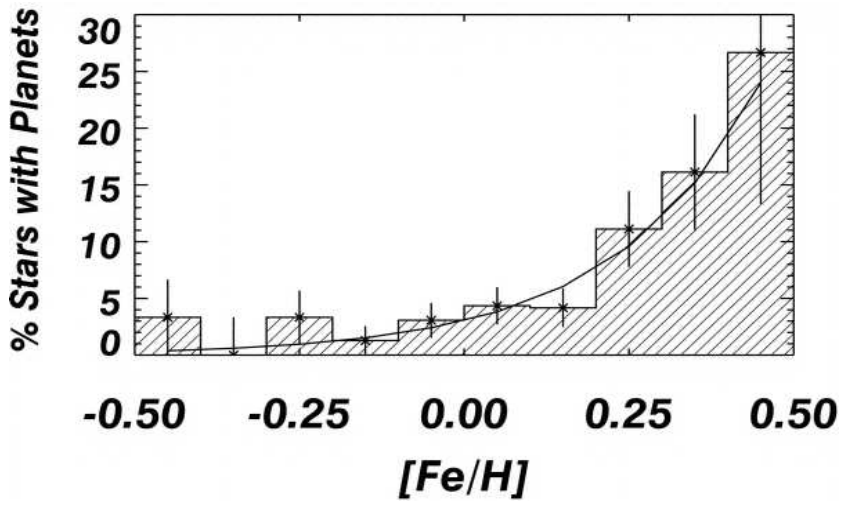

Figure 1.3: Probability that a star has a planet as a function of its metallicity, the continuous curve represents the Equation. 6.9 (Figure taken from FV05.

(Friel, 1995 [32]). Old clusters have also few pulsating variable stars (this means a smallest number of false positives transit candidates).

Finally, the last criterium is the richness: monitoring a rich cluster obviously increases the probability to observe transits and at the same time, the results of the survey will have a greater statistic significance. However, an estimate of the richness of an open cluster is not so easy because of the field contamination that is significant especially at the low Galactic latitudes, that are typical for Open Clusters.

The two open clusters that fulfill these criteria are NGC 6791 and NGC 6253. They were both observed by us with the main goal of search for transiting planets. The cluster properties are described in Sect. 2

Chapter 2

Our targets: NGC 6791 and NGC 6253

2.1 The open cluster NGC 6791

NGC 6791 (α_{2000}=19^h 20^m 53^{sec}, δ_{2000}= 37° 46' 18.0" (l=69.96 deg, b=-10.90 deg) appears to be the best choice for surveys devoted to planet search on the basis of the characteristics listed above, because it is thought to be one of the oldest and high–metallicity open clusters (OCs) of our Galaxy. Its age is estimated about 8–9 Gyr (Carraro et al. 2006 [16], King et al. 2005 [53]; Chaboyer, Green, & Liebert 1999 [19], Stetson et al. 2003 [102], Kaluzny & Rucinski 1995 [49]), while its metallicity is estimated to be [Fe/H]$\sim$ 0.4 dex (Carraro et al. (2006), [16], Gratton et al. (2006) [39]). Determinations of the metallicity of NGC 6791 are shown in Table 2.1.

Another characteristic of this OC is its richness: its mass is estimated to be about 4070 $M_\odot$ (Kaluzny & Udalski, 1993 [47]).

The cluster is located at about 4.1 kpc from the Sun, at a relatively high galactic latitude (i.e.: b=10.9 deg), that implies a relatively small reddening ($E(B-V)$=0.09-0.12 mag); while the high distance is the cause of a big field contamination. The extension of the cluster was estimated to be "at least 9.3 arcmin" by Kaluzny & Udalski (1992) [51], and no greater than 10 arcmin

Reference	[Fe/H]
Friel & James, (1993) [31]	0.18±0.18
Kaluzny & Rucinski, (1995) [49]	∼0.5
Chaboyer et al. (1999) [19]	0.4
Worthey & Jowett, (2003) [112]	0.32
Carraro et al. (2006) [16]	0.39
Gratton et al. (2006) [39]	0.47

Table 2.1: Determinations of the metallicity of NGC 6791.

in our work (De Marchi et al. 2007 [25], hereafter D07).

Characteristics as metallicity, age and richness, made NGC 6791 the target for transiting exoplanets surveys during the last 5 years: Mochejska et al. (2002 and 2005) [69] [72], with a survey of 18 nights found no good transiting candidates, and Bruntt (2003) [13] (8 nights, taken at the NOT), proposed some single–transit candidates, unconfirmed by our subsequent survey (Montalto et al., 2007 [75]).

2.1.1 Observations

Our observative campaign covers 10 consecutive nights (from July 4, 2002 to July 13, 2002) and it was characterized by the continuous monitoring of the target on each clear night.

Three telescopes were used:

1. The Canada–France–Hawaii Telescope (CFHT) in Hawaii equipped with the CFHT12k detector, composed of 12 CCDs of 4128 × 2048 pixels and covering a field of 42 × 28 arcmin^2. However, owing to the large number of bad columns, data from chip 6 could not be used, so we could get data over a 0.29 deg^2 field;

2. The San Pedro Mártir (SPM) 2.1–m telescope equipped with the Thomson 2k detector and covering a field of about 6 × 6 arcmin^2;

	Loiano		SPM		CFHT	
Night	t_{start} (HJD–2452400)	t_{end}	t_{start} (HJD–2452400)	t_{end}	t_{start} (HJD–2452400)	t_{end}
1^{st}					59.82	59.96
2^{nd}					60.83	61.02
3^{rd}	62.48	62.63	61.68	61.95	61.94	62.07
4^{th}	63.41	63.63	62.68	62.96	62.76	63.07
5^{th}	64.38	64.64	63.68	63.96	63.88	64.10
6^{th}	65.39	65.62	64.69	64.98	64.77	65.11
7^{th}			65.70	65.82		
8^{th}			66.69	66.97		
9^{th}			67.67	67.98	67.77	68.10
10^{th}			68.69	68.87	68.76	69.11
α_{min}	$19^h\ 20^m\ 25.8$		$19^h\ 20^m\ 36.3^s$		$19^h\ 19^m\ 23.7^s$	
α_{max}	$19^h\ 21^m\ 30.4$		$19^h\ 21^m\ 10.4^s$		$19^h\ 22^m\ 58.0^s$	
δ_{min}	37° 41' 22.6"		37° 43' 15.4"		37° 36' 6.7"	
δ_{max}	37° 53' 42.7"		37° 50' 3.1"		38° 4' 21.2"	

Table 2.2: NGC 6791. The observation log for each night and the limits of the field of view at the 3 different observatories.

3. The Loiano 1.5–m telescope equipped with BFOSC + the EEV 1300×1348B detector and covering a field of 11.5 × 11.5 arcmin^2.

With the CFHT data the number of light curves collected is 28464. For the SPM and Loiano surveys, the light curves are 2152 and 6055, respectively. All light curves are in V band. The coordinates of the edges of our fields are also listed in Tab. 2.1.1. Table 2.1.1 gives details about the length of the observing nights while Figure 2.1 shows the field of the CFHT survey and the edges of the Loiano and SPM surveys. The field of the SPM observations is entirely included within chip 9 and the field of the Loiano observations partially covers chips 2, 3, 4, 8, 9 and 10 of CFHT (see Fig. 2.1). stars brighter than 1 mag above the turn–off are saturated. The calibration of the CFHT, Loiano and SPM data have been performed by using the Kaluzny & Rucinski photometry ([49]). More details on the data reduction procedure can be found in Montalto et al. (2007) [75].

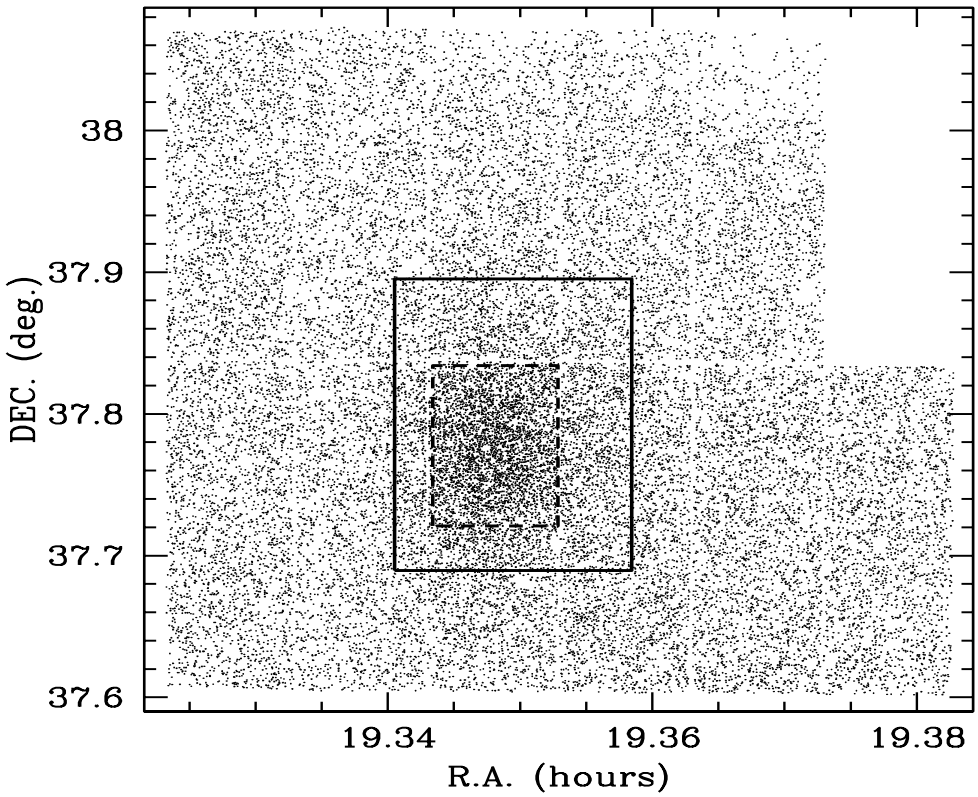

Figure 2.1: Field of view (42×28 arcmin^2) of the CFHT image. The chips are numbered in increasing order from left to right from chip 1 (top left) to chip 12 (bottom right); stars of chip 6 are not plotted since we found it impossible to derive accurate photometry. Dashed and solid lines are the edges of the SPM and Loiano fields, respectively.

2.2 Photometric data reduction

The data-sets described in Sect. 2.1.1 and 2.3.1 were reduced with three different techniques: aperture photometry, PSF fitting photometry and image subtraction. An accurate description of these techniques is given in the next sections. The goal was to compare their performances to see if one of them performed better than the others. For what concerned aperture and PSF fitting photometry the DAOPHOT (Stetson, 1987 [101]) package was used. In particular the aperture photometry routine was slightly different from that one commonly used in DAOPHOT and was provided by P. B. Stetson. It performed the photometry after subtracting all the neighbors stars of each target star. Image subtraction was performed by means of the ISIS2.2 package (Alard & Lupton, 1998 [1]) except for what concerned the final photometry on the subtracted images which was performed with the DAOPHOT aperture routine.

Subsequent comparisons among the results obtained using the three different techniques, demonstrated that, applying the image subtraction technique, we were able to improve the photometric precision with respect to that obtained by means of the aperture photometry and the PSF fitting techniques.

For the image subtraction reduction, the photometric precision overcame the 0.001 mag level for the brightest stars in the CFHT data-set,and for the other sites it was around 0.002 mag (for the NOT) or better (for SPM and Loiano). This clearly allowed the search for planets in all these different data-sets.

Given the results of the previous comparisons, we decided to adopt the photometric data set obtained with the image subtraction technique. Figure 2.2, shows the photometric precision that we obtained for the four different sites. The photometric precision is very close to the theoretical noise for all the datasets.

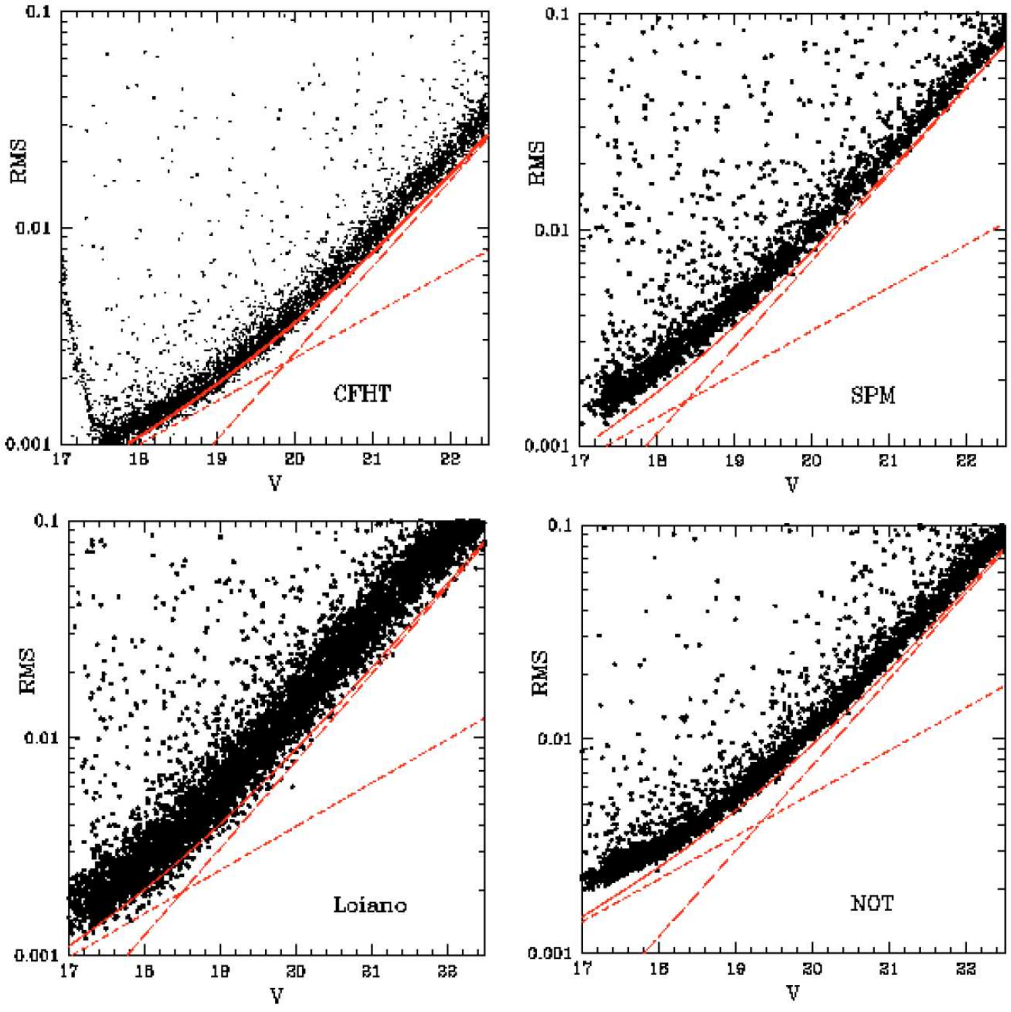

Figure 2.2: The expected rms noise for the observations taken at the different sites as a function of the visual apparent magnitude, is compared with therms of the observed light curves obtained with the image subtraction technique (figure taken from Montalto et al. 2007 [75]).

2.3 The open cluster NGC 6253

The second target of our study is another metal–rich old open cluster located towards the Galactic center, NGC 6253, (α_{2000}=16^h 59^m 05^s, δ_{2000}= -52° 42' 30.2" (l=335.46 deg, b=-6.25 deg). Its importance consists also in the fact that, together with NGC 6791, it is one of the most metal rich open

clusters of the Galaxy.

NGC 6253 was the target of five previous photometric studies to date: Bragaglia et al. (1997) [11]; Piatti et al. (1998) [83]; Sagar, Munari, & de Boer (2001) [94]; Twarog, Anthony-Twarog, & De Lee (2003) [106], Anthony-Twarog, Twarog, & Mayer (2006) [4]. Other three spectroscopic studies have been devoted to NGC 6253: Carretta et al. (2000) [17], Carretta, Gratton & Bragaglia (2007) [18] and Sestito et al. (2007) [97]. The fundamental parameters obtained by these studies are: $E(B-V)$=0.2-0.26 mag, $(m-M)_V$=12.3 mag, age ranging from 2.5 to 5 Gyr, and [Fe/H]=0.2–0.7 dex. The resulting distance of NGC 6253 from the Sun is about 1.5-2 Kpc

2.3.1 Observations

Observations were made at two telescopes:

1. The ESO2.2m telescope of La Silla where 10 consecutive observing nights were dedicated on NGC 6253 from June 14, 2004 to June 23, 2004. The WFI detector was used, which consisted of a mosaic of 8 CCDs 2k× 4k. The pixel scale was 0.238 arcsec/pixel. The cluster was imaged on chip 2 and in total ∼45.3 hours of observation on the cluster were collected, mainly in the R filter. Images in the B, V and I filters were also acquired, along with a standard field to allow the calibration of the data. In total 918 images of the cluster were obtained, with a mean exposure time of 178 seconds.

2. In Siding Spring 10 observing nights were allocated at the AAT3.9m telescope from 13 to 22 of June 2004. However, observations were performed during 3 out of the 10 allocated nights, because of bad weather conditions, and the frequent shifts between the field and the cluster inevitably deteriorate the precision of the telescope pointing (only 7% of the images have been shifted with respect to the mean of the telescope shifts inside 1 seeing radius).

   For these reasons, in this work, only the La Silla database was used.

	La Silla	
Night	t_{start}	t_{end}
	(HJD–2453100)	
1^{st}	70.57	70.91
2^{nd}	71.49	71.91
3^{rd}	72.46	72.90
4^{th}	73.69	73.87
5^{th}	74.49	74.89
6^{th}	75.48	75.90
7^{th}	76.46	76.67
8^{th}	77.84	77.87
9^{th}	78.44	78.76
10^{th}	79.46	79.90
α_{min}	16^h 56^m 42.3	
α_{max}	17^h 00^m 23.9	
δ_{min}	-53° 05' 54.1"	
δ_{max}	-52° 33' 04.2"	

Table 2.3: NGC 6253. The observation log for each night and the limits of the field of view at the La Silla observatory.

In the case of NGC 6253, mean $BVRIJHK$ photometry is available for each star of our database, but for our purposes, we considered only the $B-V$ and $V-I$ colors.

NGC 6253 is a relatively small cluster, but it is projected towards the Galactic Bulge, therefore our database contains a large number of field stars. A proper motion analysis, performed by Montalto et al. 2008 (in preparation), provided membership probabilities for about 28,000 stars contained into the chip 2 on which the cluster was imaged. The stars with membership probabilities greater than 50% are only 977.

2.3.2 Data reduction

The reduction process that allow us to obtain the R-band light curves database is identical to that used for NGC 6791 data (Sect. 2.2), In Figure 2.4 we reported the RMS as a function of the R-band magnitudes.

To obtain the $BVRIJHK$ photometry of the cluster, we reduced the La Silla and Siding Springs separately, but we followed the same procedure

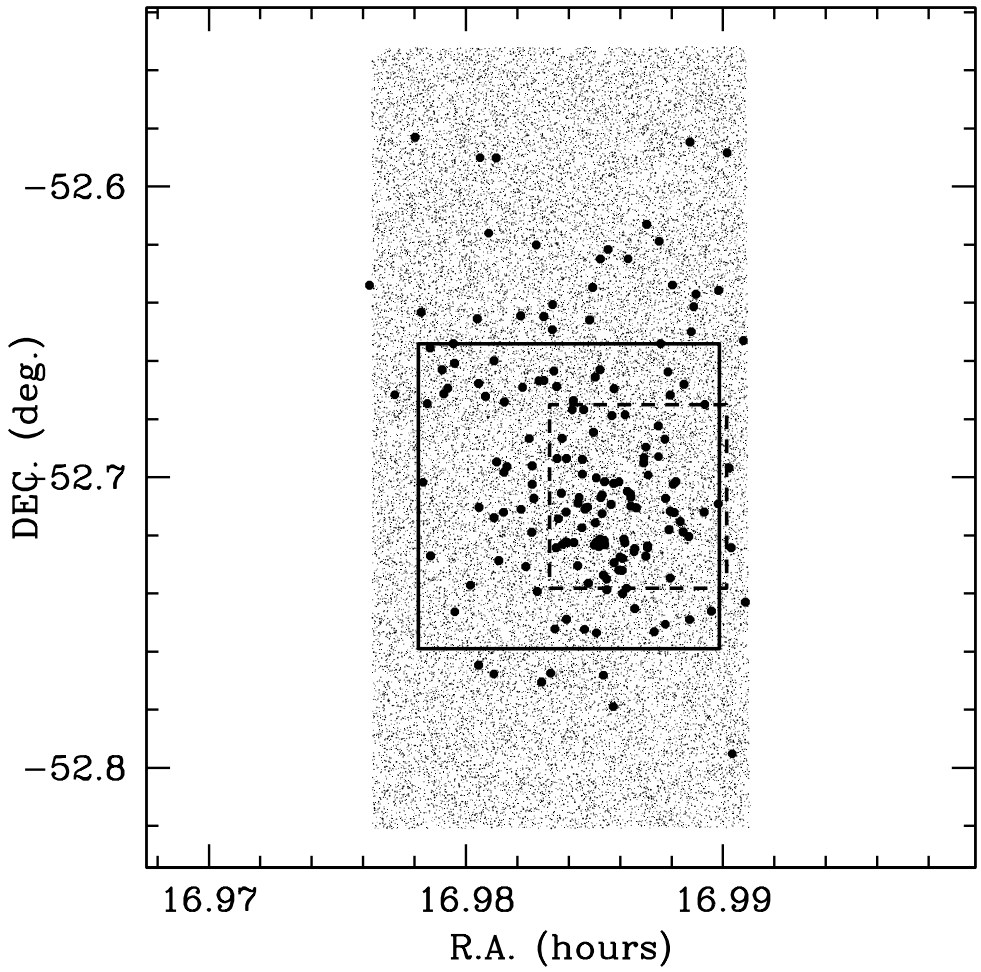

Figure 2.3: Image of the chip 2 (8×16 arcmin^2). Solid and dotted lines represent the edges of the surveys of Bragaglia et al. (1997) [11] and Piatti et al. (1998) [83], respectively. Black points are stars with membership probabilities greater than 90%. The chip contains 25823 light curves.

for both of them. Firstly we calculated a PSF for each image in each dataset with DAOPHOT. We chose a second order spatially variable PSF for La Silla images, while for Siding Spring ones, after some tests, we decided to apply a constant PSF. The PSF was calculated through an iterative process which progressively eliminate those stars which shown the highest residuals. We verified that after 3-4 iterations the PSF didn't change significantly and so we chosen to apply 4 iteration for each image.

After that we applied ALLSTAR in order to refine stellar positions and magnitudes and then DAOMATCH and DAOMASTER to calculate the coordinate transformations among the frames. To do this we chose as reference the best seeing image in each dataset. Stacking the 50 best seeing images with MONTAGE2 allowed us to calculate a reference master frame from which we derived a master list of stars. La Silla master-list had 36537 stars while Siding Spring master-list had 11715 stars. We applied ALLFRAME to the 918 images of La Silla and to the 974 images of Siding Spring.

At the end we averaged the magnitudes in the same filters considering all the stars present at least in half of the images. Fig.2.5 shows the standard deviation of the mean (internal error) for our photometry in each filter. For R and J bands the internal error was much smaller than for the other filters, (being <0.001 mag for the brightest stars), because of the greater number of images acquired in that filters. In those two filters we calculated also the zero magnitude points between each image and our adopted master frame, and correct for that to build up the light curves of the stars. This allowed us to search for extrasolar planetary transits and star variability.

2.3.3 Proper motions and cluster membership of NGC 6253

NGC 6253 is projected towards a very rich stellar field at low galactic latitude, making the identification of cluster members from photometry alone highly uncertain. The measurement of proper motion is a powerful tool to determine cluster membership and we applied this technique to NGC 6253 thanks to

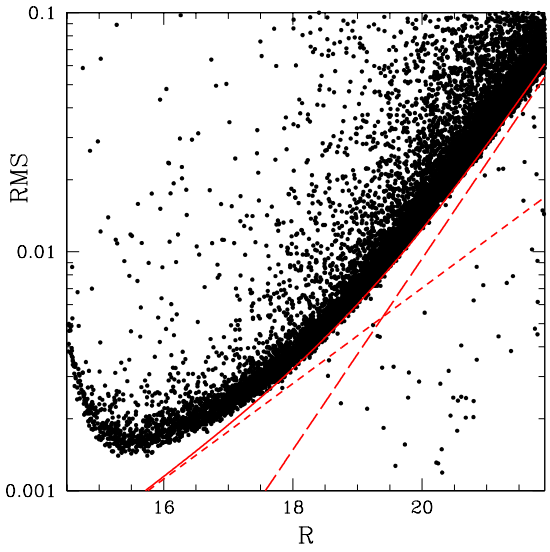

Figure 2.4: The expected rms noise for the observations taken at the La Silla telescope as a function of the R band magnitude. The rms is compared with therms of the observed light curves obtained with the image subtraction technique (figure taken from Montalto et al. 2008, in preparation).

the availability, in the ESO archive, of 8 B,V images acquired with the $ESO@WFI$ on March 30, 2000 as part of the $PRE-FLAMES$ survey, as shown in Tab. 2.3.3. Thus we had a 4 year temporal baseline taking into account that our $ESO@WFI$ data were collected in 2004.

Proper motions were calculated with the software described in Anderson et al. (2006) [3] This software characterizes specifically the WFI geometric distortions, and applies a local transformation approach for proper-motion

Date	Filter	Exp.Time(sec)	N.images
30/3/2000	B	30	2
30/3/2000	B	240	2
30/3/2000	V	30	2
30/3/2000	V	240	2

Table 2.4: Journal of observations taken from the $ESOWFI$ archive.

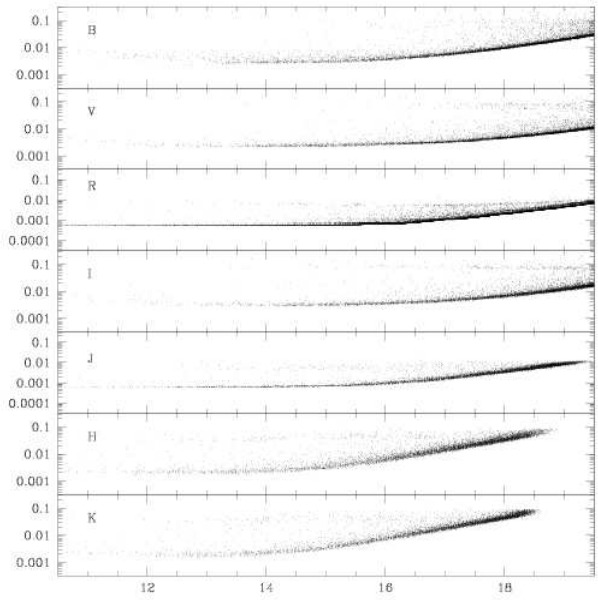

Figure 2.5: Internal errors in the different photometric bands (figure taken from Montalto et al. 2008, in preparation).

measurements. This method allows to obtain accuracies in proper motions of the order of 7 mas in both coordinates for well exposed stars, as demonstrated by the authors.

For an open cluster like NGC 6253, the expected cluster star proper motion dispersion is negligible with respect to measurement errors. Actually, the proper motion dispersion is given by:

$$\sigma_\mu = \frac{V}{K\,d} \tag{2.1}$$

where V is the velocity dispersion of cluster stars ($\sim$1 Km/sec), K is a constant, and it is equal to 4.74 AU/yr, and d is the distance of the cluster in Kpc, being for NGC 6253 $\sim$ 1.5 Kpc. With these numbers, we obtained σ_μ=0.14 ,mas yr^{-1}, which is much lower than the measurement accuracy. This means that, even if cluster stars move with respect to field stars, they maintain the same relative positions each other. Thus, once the frames have been distortion corrected, (by definition a distortion free image is an image

that can be transformed to any other distortion free image applying only linear transformations) the 50 cluster stars, (well isolated, with good photometry, non saturated), nearest to one target star, are used as reference to calculate the linear transformations of coordinates between the two frames in that region, thus correcting for residual local distortion patterns. In general, this is performed by means of an iterative process in which cluster stars, at the beginning, are selected only photometrically around a main sequence fiducial line, and then by means also of proper motions as long as these become more accurate.

More frames taken in different epochs allow to obtain independent estimates of the stars' proper motions, and to reduce the measurement uncertainties statistically combining these independent quantities. The individual errors of proper motions for single stars have been obtained as described in Sect. 7.3 of Anderson et al. (2006) [3].

The stars located on the region of the chip where it was possible to adequately correct for distortion effects were selected (see Figure 2.6, right panel). Starting from the 3309 stars for which we were able to calculate proper motions, this selection leaved 1435 stars.

The vector-point diagram, (Fig. 2.6, left panel), of our proper motions shows clearly two populations: a tight clump at μ_x=μ_y=0.0 mas yr^{-1} mainly representing the cluster stars and an overlapping broad distribution of field stars.

For membership probability calculations, we have chosen the local sample method, which is equally reliable in rich open clusters such as NGC 188 (Platais et al. 2003 [85]) as well as in sparse clusters like IC 2391 (Platais et al. 2007 [86]). In this method, a local sample of stars is selected to represent the properties of a target star as close as possible. It assures a smooth transition of calculated membership probabilities as a function of magnitude and also accounts for the changes in the magnitude dependent cluster-to-field star ratio. Another component of our approach is to parametrize the magnitude dependence of proper motion dispersions for cluster and field stars.

That can be done using photometrically selected samples of cluster and field stars. Finally, the center of proper-motion distribution for cluster stars was adopted at μ_x^c=μ_y^c=0.0 mas yr^{-1} but for field stars it was estimated from the photometrically selected field stars and also parametrized as a function of magnitude.

Calculation of the two remaining parameters (heights of Gaussian peaks) needed to fully characterize the cluster and field distributions in the VPD is straightforward (Platais et al. 2003 [85]). The distribution of membership probabilities (Figure 2.6, bottom panel) reflects the degree of reliability of our proper motions. Thus, the separation between the cluster and field is convincing for $V < 17.5$ mag, conversely, in the range $V >$20 mag it is clear a steadily growing contamination by field stars, and the accuracy of proper motions becomes inadequate for reliable calculations of membership probability.

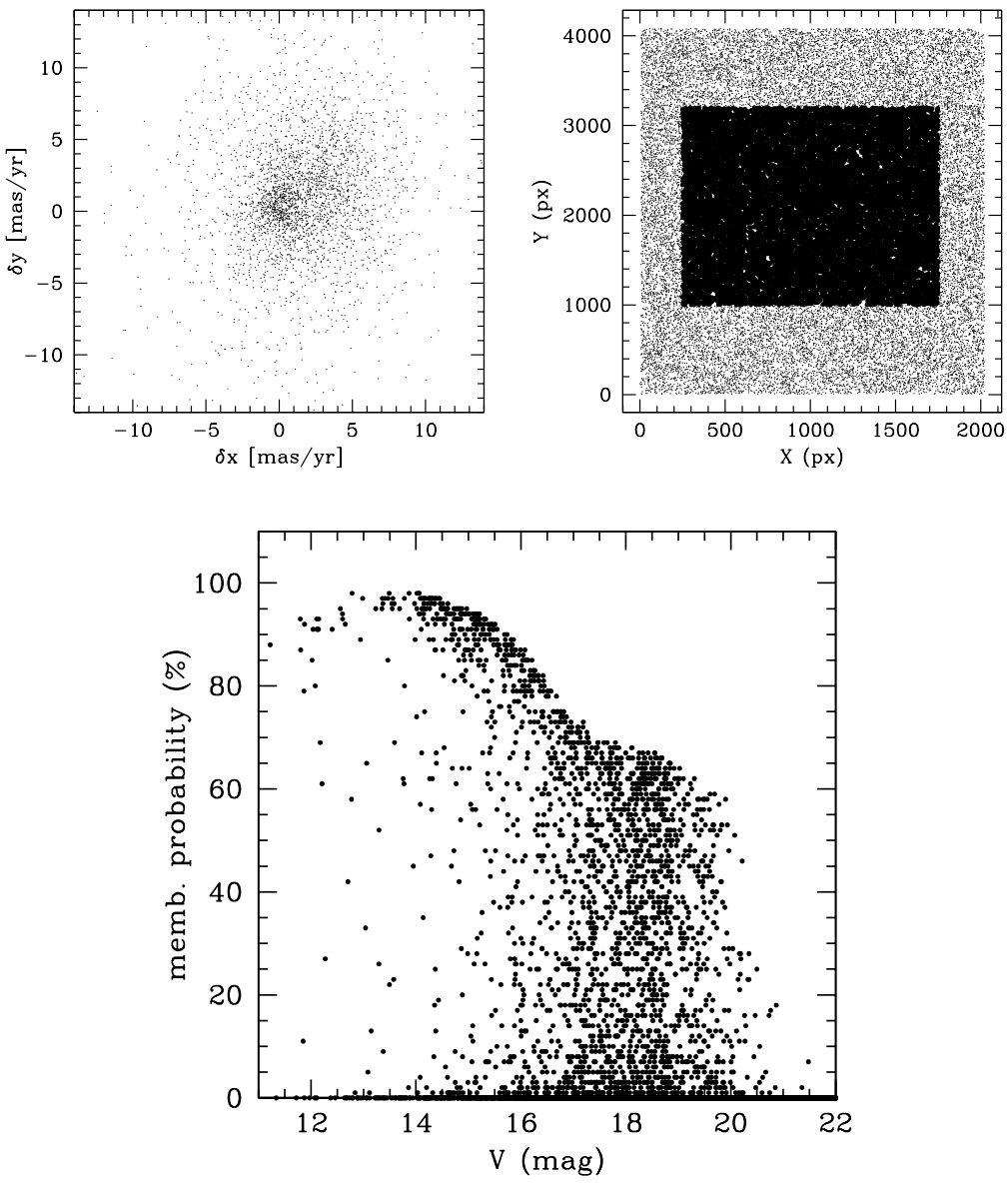

Figure 2.6: Left panel: vector point diagram for NGC 6253. Right panel: selected area where distortion effects are verified to be negligible. Bottom panel membership probabilities against visual magnitudes.

Chapter 3

Variable stars in the open cluster NGC 6791 and its surrounding field

In this chapter, adapted from De Marchi et al. (2007) [25], a high–precision variability survey in the field of the old, super metal–rich open cluster NGC 6791 is presented. The dataset relative to this cluster and the photometric reduction procedure was described in Sect. 2.1.

The main problems occurred for this database was the lack of information relative to the mean colors of the stars and to their membership.

We partially resolved this problem by cross–correlating our database with the Stetson et al. (2003) [102], hereafter S03, and Kaluzny et al. (1995) [49], hereafter K95, photometric catalogs. In this way, we obtained mean colors for about the 45% of our databases.

Regarding the other problem, preliminary membership probabilities based on proper motions analysis were kindly provided by Kyle Cudworth (private communication) for about 1800 stars (6% of the CFHT data) located at less than 6 arcmin from the center of NGC 6791. Moreover, implicit information about membership will be obtained by making a radial projected stellar density profile for our data, as described in Sect. 3.3.

Finally, for some kind of variable stars other selection criteria are possible. In particular, information about membership can be obtained using the well known Period/Luminosity relations existing for the pulsating variables, or the Period/Color/Luminosity relation given by Rucinski, (2003) [92] for contact binaries (see details in Sect. 3.3.4).

Our search allows us to discover 260 new variables and re-determine periods and amplitudes of 70 known variable stars. By means of a photometric evaluation of the membership in NGC 6791, and a preliminary membership based on the proper motions, we give a full description of the variable content of the cluster and surrounding field in the range $16 \lesssim V < 23.5$. Accurate periods can be given for the variables with $P \lesssim 4.0$ d, while for ones with longer periods the limited time–baseline hampered precise determinations. We categorized the entire sample as follows: 6 pulsating, 3 irregular, 3 cataclysmic, 89 rotational variables and 61 eclipsing systems; moreover, we detected 168 candidate variables for which we cannot give a variability class since their periods are much longer than our time baseline.

On the basis of photometric considerations, and of the positions of the stars with respect to the center of the cluster, we inferred that 11 new variable stars are likely members of the cluster, for 22 stars the membership is doubtful and 137 are likely non–members. We also detected an outburst of about 3 mag in the light curve of a very faint blue star belonging to the cluster and we suggest that this star could be a new U Gem (dwarf nova) cataclysmic variable.

3.1 Introduction

Because of its extreme characteristics (see Sect. 2.1), NGC 6791 has been the target of many photometric surveys (see Table 3.1 for a list of publications). Taking into account the fact that in four cases the same stars have two identification numbers (V15≡B7, V56≡V96, V76≡V85 and V77≡V88) and counting also the stars B4 and B8, the total number of known variable stars

Authors	Nr. of variables	IDs	Notes
Kaluzny & Rucinski (1993) [47] (KR93)	17	V1–V17	V15≡B7
Rucinski, Kaluzny & Hilditch (1996) [93] (RK96)	5	V18–V21 and B8	
Mochejska et al. (2002) [69] (M02)	47	V22–V67 and B4	B4 was previously cataloged by Kaluzny & Udalski (1992) [51] as a blue star, but not as variable.
Mochejska et al. (2003) [70] (M03)	7	V68–V74	
Kaluzny (2003) [46] (K03)	4	V75–V78	
Bruntt et al. (2003) [13] (B03)	19	V79–V100	V85≡V76; V56≡V96; V77≡V88
Mochejska et al. (2005) [72] (M05)	14	V101–V114	
Hartman et al. (2005) [41]	10	V115–V124	Plus 7 suspected variables

Table 3.1: Previous variable star searches in NGC 6791.

in the field of NGC 6791 to date was 123 (plus 7 suspected variables, proposed by Hartman et al. 2005 [41]).

The entire catalog of variable stars is reported in Appendix A.

3.2 The identification of variable stars

The intensive monitoring of NGC 6791 allowed us to obtain tens of thousands of photometric time series for stars located in, close to, and far away from the cluster center. We have analyzed 28464, 6055, and 2152 light curves obtained from the CFHT, Loiano and SPM telescopes respectively. A representation of the field of NGC 6791 is reported in Fig. 2.1 on page 24. The CFHT, Loiano and SPM time series are composed of about 250, 60 and 170 data-points, respectively. The observations, intended to detect photometric transits, were performed in the V band only.

3.2.1 The search for variable candidates

To search for variable stars, we calculated the best "sinusoid plus constant" fit for all light curves (Vanicek, 1971 [107]; Ferraz-Mello, 1981 [29]). We evaluated the goodness of the fit by calculating parameters related to the

reduction of the initial variance obtained by introducing the periodic term. These parameters are the reduction factor (Vanicek, 1971 [107]) and the coefficient of spectral correlation $S(\nu)$ (Ferraz-Mello, 1981 [29]).

Owing to the huge number of light curves, we need one or more parameters to discover the variability. Toward this goal, we considered the parameter r defined as $r = \log_{10} S_{max}$, where S_{max} is the maximum value of S (i.e., the one corresponding to the frequency of the best-fit sinusoid in the Ferraz-Mello method). If a star does not show variability the introduction of a sinusoid does not improve the fit and then S_{max} is close to zero (no variance reduction) and $r \ll 0$; on the other hand, a sine-shaped variability strongly reduces the variance (S close to 1) and hence $r = 0$. The purpose was to use the r parameter as a tracer of variability for short-period (i.e., intra-night) variability.

To search for long–period variability, we introduced a second parameter, more sensitive to the night–to–night variations. We calculated the mean magnitude V_i and the standard deviation σ_i on each night, and after that we calculated the parameter s defined as:

$$s = \log_{10} \frac{\Delta V}{\bar{\sigma}}$$

where ΔV is the peak–to–peak difference and $\bar{\sigma}$ is the mean of the σ_i over all nights.

To test the capability of the r and s parameters to detect variable stars, we prepared a sample containing two types of light curves: 7722 artificial *constant* light curves (obtained as described in Sect. 6.3.3) and 70 light curves of *already known variable stars* which are included in our CFHT field. In Fig. 3.1 we plot r vs. s for the light curves of constant stars (small points) and of variable stars (large points). The variable stars are substantially apart from the constant stars and most have $r \gtrsim -1$. The variable stars with $r \lesssim -1$ and superposed on constant stars are mostly EA–type stars or irregular stars (e.g., cataclysmic variables). Among variables (i.e., large dots in Fig. 3.1), the stars with small s have short periods ($P \leq 0.50$ d), while

stars with large s have long periods. Therefore, we can conclude that the combination of the r and s parameters is a good tracer of variability.

To detect the variable stars in our sample of $\sim$30,000 light curves we first selected in an automatic way all the stars with $r \geq -2.0$, according to the test described above. We thereby reduced the huge initial sample to $\sim$6,500 stars. After the calculation of the amplitude spectrum of their time series, we adopted as a second selection criterion a signal–to–noise ratio (S/N) greater than 4.0 around the highest peak in the amplitude spectrum. This procedure allowed us to reduce our sample to $\sim$900 stars, i.e., 3% of the whole initial sample. Further checks have been made by examining the light curves of a random sample of stars with $r < -2.0$, large s and 3.5<S/N<4.0, but we did not find any additional variables.

Our approach allowed us to detected hundreds of stars showing peaks in their power spectra at f =1.00 cd^{-1}, at f $\leq$0.05 cd^{-1}, or at f=0.6 cd^{-1}. The first two spurious periodicities are common and can be ascribed to small misalignments in the mean magnitudes from one night to the next or recurrent drifts (caused by small color effects, for example) in the intra-night light curves. We suggest that the latter one is probably a photometric artifact occurring in some particular cases of blended stars, or stars close to CCD edges, or bad pixels. They have been considered as not reliable enough to infer a physical light variability. In our opinion, only the combination of automatic procedures and visual inspection allowed us to identify the three classes (P=1.00 d, P=1.6 d, $P \gg$10 d) of spurious variables in the huge number of $\sim$82,000 light curves. In particular, we note that the identification of the whole sample of eclipsing binaries has been confirmed by the application of the box fitting technique (BLS, Kóvacs et al. 2002 [54]), used by Montalto et al. (2007) [75] to detect planetary transits.

At the end of the variable star identification, we were left with 330 cases to be characterized. Since we rejected about 2/3 of the sample selected by means of the r, s parameters, we are confident we have not applied overly strict constraints in the candidate selection.

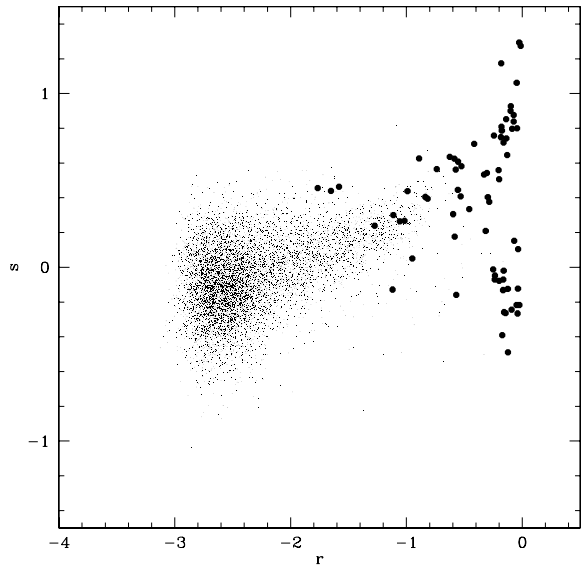

Figure 3.1: *Grey points*: r parameter vs. s parameter for constant light curves. *Black dots*: parameters derived from our light curves for the variable stars previously detected in our field.

3.2.2 The cross check with previous surveys of NGC 6791

When comparing our field of view with those of other surveys, we found that 81 known variable stars are included. The CFHT survey failed to detect 45 known variable stars: seventeen stars (V22, V24, V26, V28, V30, V35, V36, V47, V50, V57, V61, V63, V64, V102, V103, V104, V105) are outside the CFHT field of view; 4 stars (V71, V106, V113 and V120) lie between two chips; 23 stars (V1, V6, V13, V19, V33, V39, V45, V49, V54, V56≡V96, V65, V66, V67, V69, V70, V72, V73, V74, V77≡V88, V78, V81, V97 and V112) are saturated; while the data points of the light curve corresponding to V76 were too few.

Among the 81 known variable stars that we have observed, not all of them display variability in our sample: 4 stars (V10, V18, V21, V32) are previously classified as long-period detached eclipsing variables and we did not observed

eclipses. We are not able to confirm the period of 15.24 days for V68 (M03), likely because of our shorter time baseline and the small amplitude of this variable (about 0.003 mag in V–band, M03). Finally, we cannot confirm the variability of six stars (V20, V79, V84, V98, V99, V116) and of the seven suspected variables found by H05, since our data do not show any trace of variability.

Among the sample of the stars missing from the CFHT field, we identified 22 stars in the Loiano and SPM data sets (V6, V13, V19, V20, V33, V45, V54, V56≡V96, V65, V66, V67, V70, V71, V73, V74, V76≡V85, V77, V78, V81, V97, V106 and V113). However, owing to the smaller signal–to–noise ratio (S/N), the small number of data-points and (in the case of the Loiano data) the limited survey time, we could only confirm the variability of stars V56≡V96, V66 and V76≡V85.

Throughout this paper we use the existing names for the already known variables; to identify the new ones discovered in our survey we used the five–digit number assigned by the DAOPHOT package followed by the number of the chip which the star belongs to. Accurate astrometry is provided to identify the stars on the sky. Moreover, all light curves of the variables will be available on CDS.

3.3 The variable star content of NGC 6791 and its surrounding field

The CFHT measurements are quite precise, thus the light curves are generally very well defined for P <4 d. On the other hand, the periods and the shapes are uncertain for P >4 d, since the observations only covered 2.5 cycles or less. In order to evaluate the precision in the study of the variable stars, we calculated the standard deviations of the Fourier least-squares fits (truncated at the last significant term for the given star) for the 138 light curves having very good phase coverage. The precision was found to be better than 0.010 mag in 73 cases (53%), and better than 0.020 mag in

a total of 122 cases (88%), as expected for stars ranging from V ∼16.0 to V ∼22.5. The discussion based is mostly on the CFHT data, which are by far the most numerous, precise and homogeneous; however, for some variables we have used data from Loiano and SPM in a very profitable way. As an example, only the longitude spread of the three observatories allowed us to derive the periods of the eclipsing binaries 00645_10, V107, V12, V109 and of the rotational variable 03079_9.

To proceed in the definition of the variable star content of NGC 6791 and its surrounding field, we calculated the power spectra of the data for all the 330 candidate variables by using the least-squares iterative sine-wave search (Vanicek, 1971 [107]) and the Phase Dispersion Minimization (Stellingwerf, 1978 [100]) methods. Differences have been examined and resolved. The separation into different classes of variable stars has been made on the basis of the light curve parameters (period, amplitude, Fourier coefficients) and standard photometric values (V, $B-V$, $V-I$), when available. The period estimates have been refined by means of a least–squares procedure (MTRAP, Carpino, 1987 [15]) and appropriate error bars have also been calculated. At the end of the process we get six pulsating stars with $P < 0.6$ d, three irregular variables, three cataclysmic variables (CVs), 31 detached or semi–detached eclipsing binaries, 29 contact binaries, 90 rotational variables, 167 stars showing clear night-to-night variability on timescales too long for periods to be determined over our 9.2–d baseline. We adopt the Cudworth membership probabilities for 35 stars. Moreover, for three new variable stars we adopted membership probabilities based on proper motions performed by Bedin et al. (2006) [5] (hereafter B06, see Figure 3.3).

For the other stars, we consider their position in color–magnitude diagrams (CMDs), and their distance from the center of the cluster to infer whether they belong to the cluster (for EW–Type stars we also utilize the P-L-C relation of Rucinski (2003) [92].

Towards this end, we plotted the radial distribution of all stars in Fig. 3.2. We see that at a distance of ∼10' from the center of the cluster, the stellar

density becomes near constant (about 21 star/arcmin^2). Thus, we adopt the value of 10' as the external limit of the cluster and we consider "likely non-members" the variables located farther from the cluster center. With a simple calculus we estimated the number of real members of the cluster as 4900±1000 stars.

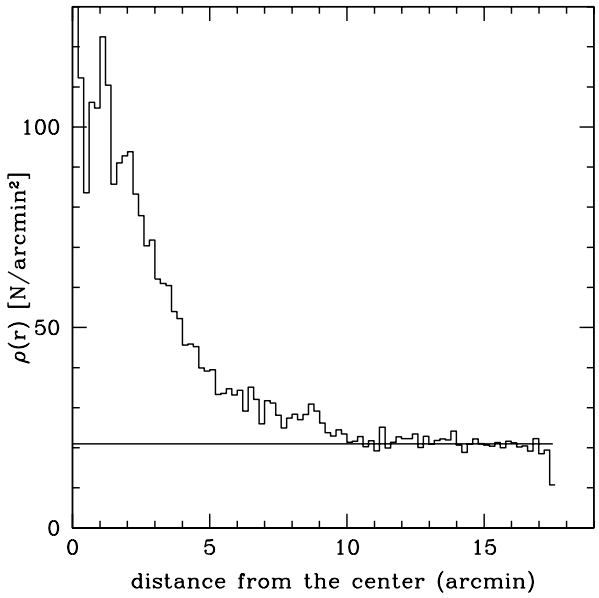

Figure 3.2: Stellar density ρ (number of stars per square arcminute) as a function of the distance from the center. The straight line represents the mean stellar density at distances greater than 10' .

3.3.1 Pulsating variables

The main characteristics of our variables are listed in Tab. 3.3.3 and their light curves are shown in Fig. 3.4. The classification as High–Amplitude Delta Sct (HADS), SX Phe, RRc or RRab stars is based on the parameters of the Fourier decomposition (Poretti, 2001 [87]). In all cases, the ϕ_{21} Fourier parameters are on the progressions described by the different classes. We note that our period for V123 is quite different from that given by H05 (0.107 d).

Error bars on the periods are in the range 1–6·10^{-5} d.

Both RR Lyr variables are too faint to belong to NGC 6791. Since they have V=17.21 (03653_3) and V=18.28 (00345_1), their distance moduli greatly exceed that of the cluster.

This is also true for the very faint and short-period stars 00311_7 (V=23.17) and 00224_10 (V=21.72); therefore, it is more likely that they are Pop. II stars. On the other hand, using the $P - L$ relation given by McNamara (2000) [67], we get distance moduli of 14.50 and 13.78, respectively, for V123 and 01497_12. These distance moduli and the distance from the cluster center (12' and 22' , respectively) suggest that they do not belong to the cluster, though they are not very far from it. Therefore, they are probably Pop. I stars and hence High Amplitude δ Scuti stars.

Moreover, there are several variables whose light curves are very similar to those of Cepheid variables; the Fourier decomposition of some light curves (in particular the large amplitude ones, i.e., 00913_5, 01659_8, V46 and 01431_10, but also 01606_11, 02285_10, 00122_4 and 03056_3) yields parameters typical for Cepheid light curves. However, most of these variables are quite faint and the Period–Luminosity relation for Cepheids (Tammann et al. 2003 [105]) yields distances in the range 39-171 Kpc. It is difficult to say whether these stars are nearby rotational variables (see below) in the Milky Way or very distant pulsating variables. For our present purposes, these stars have been included among the rotational variables listed in the Appendix. The puzzling nature of all these apparently distant stars (i.e., the Cepheid-like ones, the RR Lyr and the faint SX Phe variables discussed above) deserves further investigation by means of spectroscopic and/or kinematic data.

3.3.2 Irregular variables

Table 3.3.3 also lists three irregular variables: these stars lie on the middle Main Sequence and are all located less than 3' from the cluster center; thus we suggest that they belong to the cluster. V92 and V83 were previously defined as "periodic variables" by B03. Indeed, we noticed fast variability in

our light curves (Fig. 3.5), but, more noticeably, the mean magnitude is also changing from night to night. The long periods given by M03 are not able to explain either the short- or the longer-timescale variability; actually, we could not detect any periodic term. We also detected no trace of periodicity in V93 (Fig. 3.5); we suspect that the periods given by M05 and B03 are spurious, since they are close to 1.0 d (0.99 and 0.94 d, respectively) and they could be produced by the irregular fluctuations.

We can conjecture that these variables are eruptive variables observed in a quiescent phase, in which rapid and/or slow changes with smaller amplitude can be observed; they resemble the case of V15 (see Sect. 3.3.3). We have no reliable indications about the membership probabilities.

3.3.3 Cataclysmic variables

As regards V15: M03 and M05 detected variability over the range of 3 mag and observed outbursts of about 0.5-1.0 mag; from our side, we could see a 0.15–mag variability in our light curves (Fig. 3.5), corresponding to the quiescent phase. V15 is very probably a NGC 6971 member, since the Cudworth proper-motion membership probability is very high (98%).

Both the position of the faint blue star 06289_9 in the two-color diagram and the shape of its light curve (Figure 3.6) strongly suggest that this star could be a new cataclysmic variable (U Gem-type, dwarf nova). Moreover, we know that this object is a cluster member (see Figure 3.3). The star shows an outburst of about 3 mag and, though we did not observe the entire brightening, we would highlight that the magnitude was still increasing on the first night; thus we are able to say that the maximum brightness was reached immediately after.

A magnification of the region of the sky obtained by HST on which is located 06289_9 (see Figure 3.3) reveals no particular features typical of U Gem stars (as accretion discs).

We can estimate the orbital period, P_{orb}, and the recurrence time, T_n, from the decay time, $\tau_d = \Delta t / \Delta m$ [days mag^{-1}] and the amplitude, Δm

(Warner, 1995 [108], equations 3.5, 3.1, respectively). Assuming for Δt and Δm the values 3.33±0.50 d and 2.87±0.31 mag respectively, we find P_{orb}= 2.54±1.41 h and T_n=13.9±10.6 d. However, our light curve (Fig. 3.6) seems to rule out T_n values shorter than 8 d.

The variable B8 shows a large-amplitude light curve (Fig. 3.6) over a quite short 7 d time span. The cataclysmic nature of B8 has been confirmed spectroscopically by Kaluzny et al. (1997) [50] who also notes that B8 exhibits red $V - I$ color while in a low state.

Following the same procedure used for 06289_9 and assuming τ_d=1.3±0.3 [d mag^{-1}] for B8, we find P_{orb}=2.97±1.63 h and T_n=11.4±8.5 d. The T_n value is compatible with the 7 d periodicity (Fig. 3.6). A membership probability is not available for B8. However, using the equations 3.3 and 3.4 after Warner (1995) [108], we obtain M_{Vmin}=8.06±0.68 mag and M_{Vmax}=4.97±0.42 mag. In turn, these values give two estimates for the distance modulus of B8, i.e., 13.82 ± 0.68 mag and 14.20 ± 0.42 mag. We note that the first is in agreement with the distance modulus of the cluster. Kaluzny et al. (1997) [50] assumed that B8 belongs to the cluster, finding M_{Vmax}=5.2 mag and M_{Vmin}=7.6, i.e., values very similar to ours. B8 is located at 4' from the center, and we can only conclude that the membership of this star is very probable.

3.3.4 Contact binaries

The simplest cases of eclipsing systems are the contact binaries (also named W UMa systems); they show short periods and continuous variability and therefore can be easily recognized and classified. We detected 29 of these variable stars; they have P <0.40 days and very well defined light curves. The complete list and the light curves are reported in the Appendix. Tab. 3.3.4 lists the stars likely belonging to NGC 6791 (see above); their light curves are shown in Fig. 3.7. The very short periods and the secondary minima occurring at $\phi \approx 0.5$ indicate binaries with circular orbits, as is also the case for stars with small amplitudes (in 7 cases we have amplitudes less than

Star	Type	α_{2000}	δ_{2000}	V [mag]	$< B-V >$ [mag]	$< V-I >$ [mag]	Ref.	T_0 [HJD–2452400]	Period [d]	Ampl. [mag]
				Pulsating variables						
V123	HADS	19.362064	37.666034	17.08	0.45		k	59.559	0.06026	0.14
01497_12	HADS	19.379083	37.812419	16.06				59.528	0.07227	0.40
00311_7	SXPhe	19.324628	37.716768	23.17				59.605	0.10443	0.10
00224_10	SXPhe	19.353639	37.710163	21.72	0.71	1.06	s	59.801	0.12261	0.20
03653_3	RRc	19.347147	37.992413	17.21	0.57	0.58	k	59.937	0.32654	0.39
00345_1	RRab	19.325082	37.964170	18.28				60.151	0.57866	0.72
				Irregular variables						
V92	IRR	19.350754	37.766876	18.10	0.91		k			0.10
V83	IRR	19.346220	37.737232	19.10	1.02	1.05	k			0.07
V93	IRR	19.351452	37.785687	18.12	0.98	1.03	s			0.04
				Cataclysmic variables						
V15(=B7)	CV	19.352057	37.799019	18.26	0.20		k			0.06
B8	CV	19.343262	37.747833	20.64	–0.23	0.78	k			2.27
06289_9	CV (?)	19.348976	37.770355	22.80	0.25	0.88	s			3.10

Table 3.2: Pulsating, irregular and cataclysmic variables. V is the minimum brightness for CVs and irregular, the mean brightness for pulsating variables. T_0 is the time of maximum brightness for pulsating stars. Hereafter, the labels "k" and "s" indicate that the $B-V$ color index is taken from Kaluzny & Rucinski (1995) [49] or Stetson et al. (2003) [102], respectively.

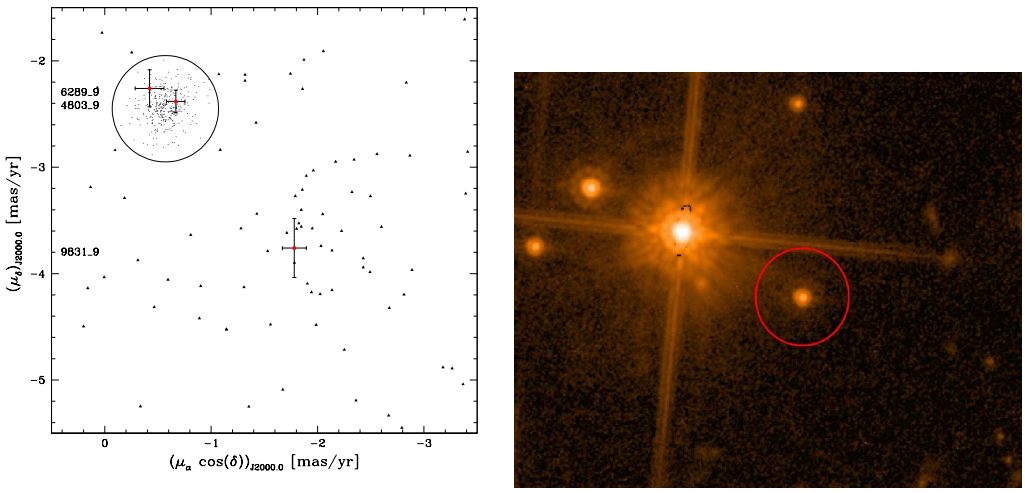

Figure 3.3: *Left*: proper-motion vector-point diagram for the inner region of NGC 6791. The circle (centered on the absolute proper motion of the cluster) represents a safe limit corresponding to 0.5 mas/yr. Triangles represent non–members, points with error bars are the new variables 06289_9, 04803_9 and 09831_9 *Right*: magnification of the region surrounding 06289_9 (highlighted with a red circle). No features as accretion disc are visible around the object. Both images were kindly provided by Luigi Bedin.

0.20 mag: V3, V4, V5, V8, V23, V40 and 01441_8). The average error bar on the period estimates is of the order of 4–5$\cdot 10^{-5}$ d.

However, we note that the stellar surfaces are not homogeneous since the maxima are often at different heights. Therefore, binarity and activity are probably combined here. In particular, the shape of the light curves of V4 (comparing RK96, M02 and our data) and V7 (comparing K93 and our data) have changed a lot; we suppose that stellar spots strongly modify the light curves. Proximity effects are also responsible for the large amplitudes observed for 01434_3 (Fig. 3.7, last panel) and 00766_5. We also found different periods for V118 (0.306321 d) and V124 (0.320143 d) compared to H05.

As for membership, the probabilities provided by Cudworth are 78%, 98% and 98% for V3, V4 and V5, respectively. Indeed, they are very close to the cluster center (4.5', 2.1' and 2.8', respectively).

We suggest that 01441_8, V118, V8, V117 and V7 are also contact binaries

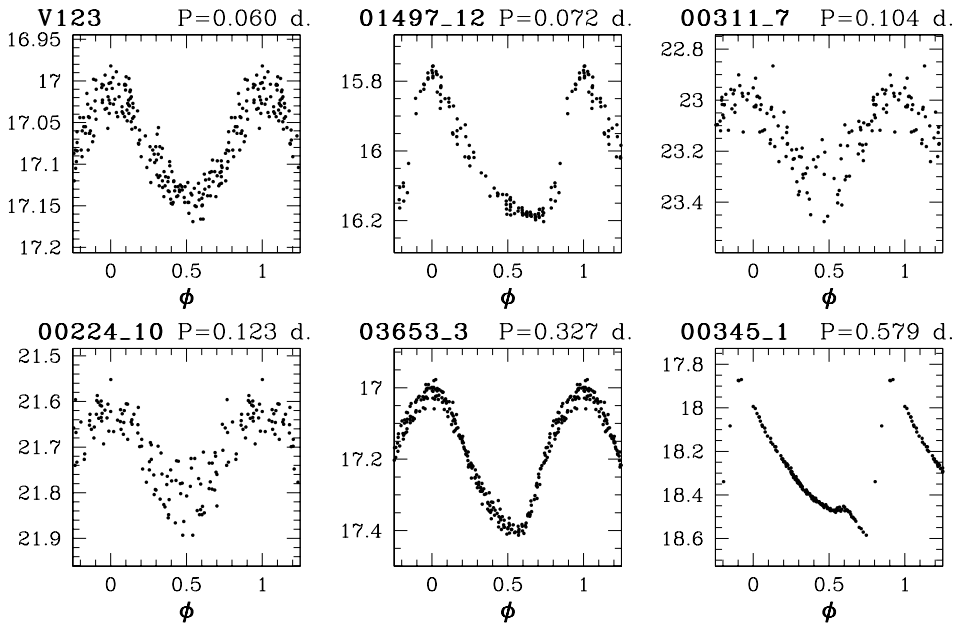

Figure 3.4: Light curves of pulsating variables. V123 and 01497_12 are probably HADS stars, 00311_7 and 00224_10 are SX Phe stars, 03653_3 and 00345_1 are RR Lyr stars.

belonging to NGC 6791. To further verify this hint, we calculated their distance by using the *P-L-C* relation given by Rucinski (2003) [92].

This relation is essentially based on the hypothesis that two contact stars have quite similar temperatures, thus the total luminosity of the system can be written as $L \propto ST_{eff}^4$ where S is the surface of the system. We can assume $S = sa^2$ where a is the semi-major axis of the orbit and s a numerical factor. It was demonstrated that s is slightly dependent from the mass ratio q and the degree of contact (Mochnacki, 1984 [73] and 1985 [74]) and for our purposes it can be considered constant. Therefore, using the third Kepler's law, we have $L \propto P^{4/3}T_{eff}^4$. The value of T_{eff} is related to the color of the system, then we can rewrite the previous equation for the absolute magnitude M_V:

$$M_V = A \cdot color + B \log P + C$$

where A, B and C are calibration constants.

The final relations that we utilize are:

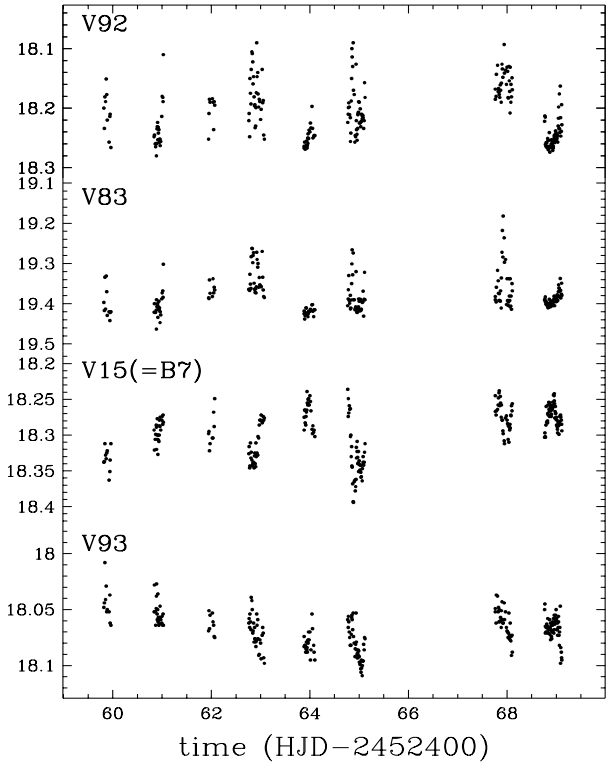

Figure 3.5: Variable stars showing irregular fluctuations.

$$M_V = -4.44 \log P + 3.02(B-V)_0 + 0.12 \tag{3.1}$$

or, alternatively, using the $V-I$ color:

$$M_V = -4.43 \log P + 3.63(V-I)_0 - 0.31 \tag{3.2}$$

the resulting distance moduli for our stars (obtained using Equation 3.1) are 13.28, 13.28, 13.48, 13.28 and 13.18, respectively; very similar to that of the cluster (13.35).

Moreover, these stars are located at similar angular distances from the cluster center (6.2', 7.2', 7.1', 7.2' and 6.3', respectively). Figure 3.8 shows how the distance modulus of the cluster is in better agreement with those of the stars we proposed as cluster members than with those of the previously

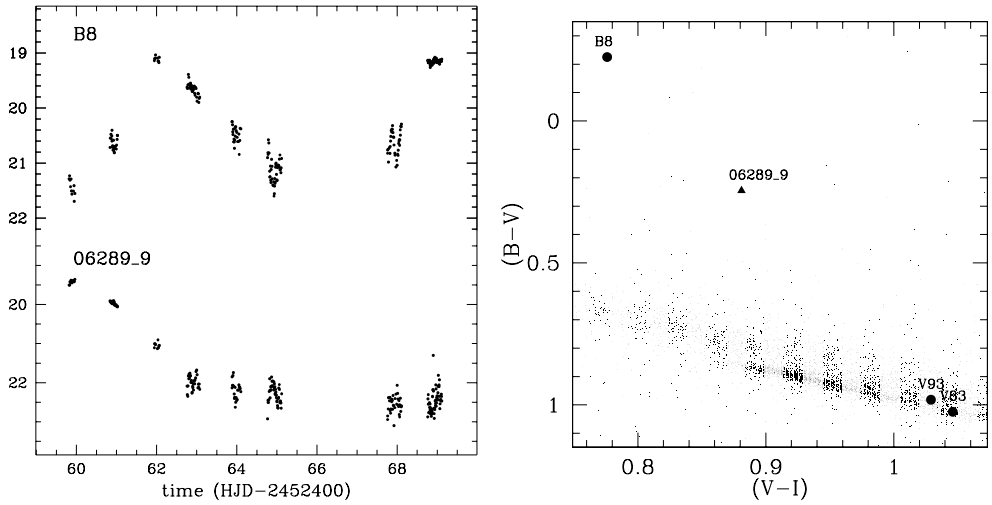

Figure 3.6: *Top*: Light curves of B8 (CV star) and 06289_9 (candidate CV). *Bottom*: positions in the two–color diagram for two irregular stars (V83 and V93), for the cataclysmic variable B8 when in a low state, and for the new variable candidate 06289_9.

known members. Their positions in the CMDs (Fig. 3.9, filled circles) are similar to those of stars in the sample with V <7.5 whose parallaxes have been determined by HIPPARCOS (Rucinski, 2003 [92]. We also note that most of the cluster members are near the turnoff point.

Taking into account also the other surveys, we try now to estimate the frequency of eclipsing contact binaries. Using the results of the *P–C–L* relations and the Cudworth's proper motion membership. We found that, *up to now* the number of EW-Type variables discovered in NGC 6791 and that are real members are.18-23. For 5 stars there are not information available about membership. Assuming that NGC 6791 has about 4900±1000 members (see above), we find a frequency of (0.4±0.1)%. This is in accordion with the value given by Kaluzny & Rucinski (1993) [48] for the same cluster, and it is about an order of magnitude lower than that relative to 47 Tuc (1.7×10^{-4}), Weldrake et al. 2004 [109]). Other globular clusters such M 71 and M 5 have intermediate frequencies (Yan & Mateo, 1994 [114], Yan & Reid 1996 [115]).

In general, the frequency is related to the richness of the cluster, in fact,

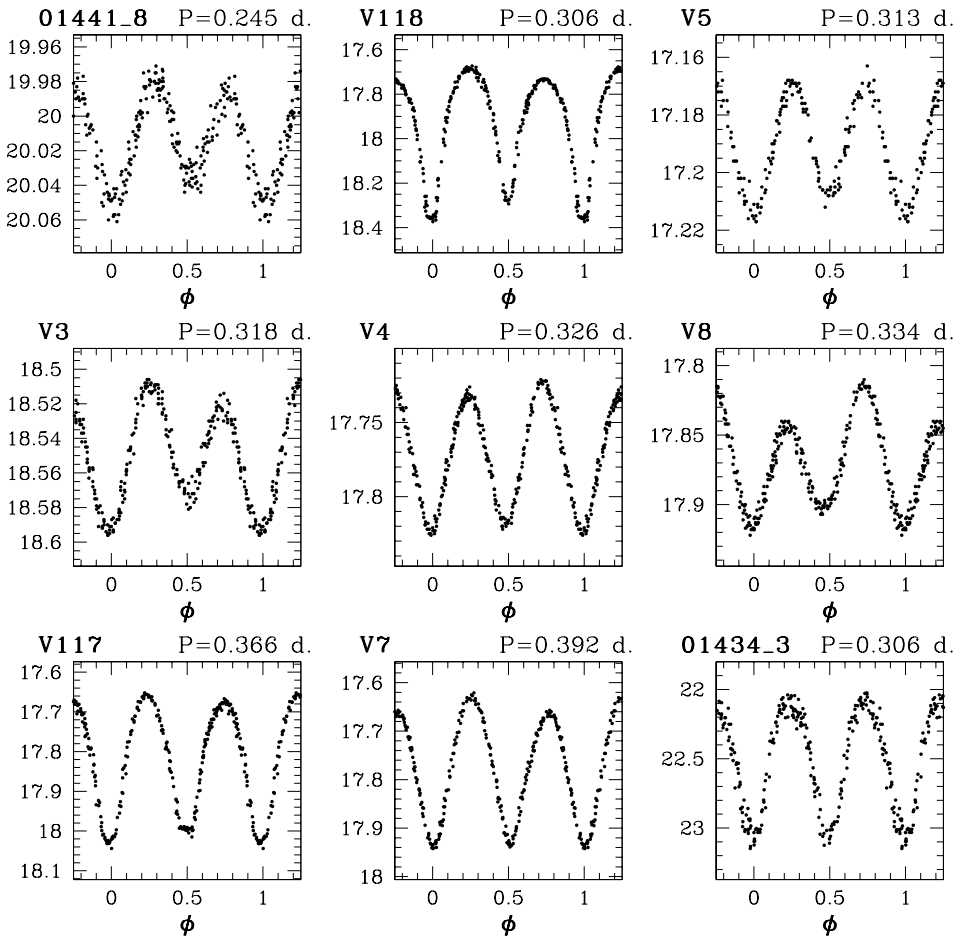

Figure 3.7: The light curves of the contact binaries that are likely members of NGC 6791. The case of 01434_3 (amplitude much larger than 0.75 mag) is also shown in the last panel.

it was observed that the frequency of contact binaries in old open cluster is anti-correlated with the richness of the host clusters (Kaluzny & Rucinski 1993 [48]) In particular, the frequency of EW-Type variables in NGC 6791 is lower with respect that of other old cluster (Kaluzny & Rucinski 1993 [48], K95). This is probably due to the stellar evaporation: during the lifetime of a cluster, the observed binary frequencies is modified by the process of mass stripping, and stars with lower masses are more susceptible to this process Henon (1969) [42]. For this reason, binaries have larger probability to survive

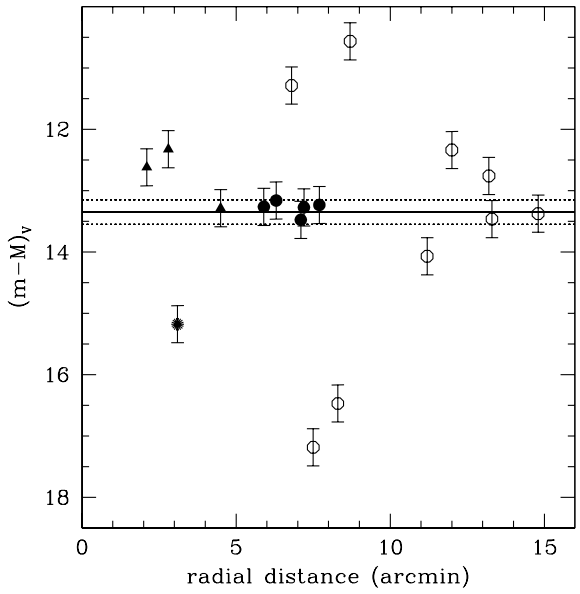

Figure 3.8: The $m - M$ values calculated for contact binaries by means of the Rucinski (2003) [92] *P-L-C* relation plotted against the distance from the cluster center. Triangles indicate the stars whose membership has been proposed by M03, the filled circles the stars whose membership has been proposed by us, and the open circles the stars that we suggest do not belong to NGC 6791. The starred point indicates the star 09891_9 which does not belong to the cluster on the basis of the proper motion (B06). The $(m - M)_V$ value for the cluster (solid line) with an error bar of ± 0.20 mag (dashed lines) is also shown.

as cluster members than single stars. Since evaporation affect especially the low-mass clusters, for the more massive ones the frequency of binaries does not increase.

3.3.5 Eclipsing variables

In the cases of detached or semi–detached eclipsing binaries the classification and membership tasks are different from the case of contact binaries. Tab. 3.3.5 lists the systems for which we could determine periods; their light curves are shown in Fig. 3.10. We still have short-period cases where we can reconstruct the complete light curve, as for the classical examples of β Lyr variables (V29, 01558_5 and 00331_3). V9 is a more complicated β Lyr

Star	α_{2000}	δ_{2000}	V [mag]	$< B-V >$ [mag]	$< V-I >$ [mag]	Ref.	T_0 [HJD–2452400]	Period [d]	Ampl. [mag]	Notes
01441_8	19.339422	37.778118	19.98	1.38		k	63.073	0.24544	0.07	likely memb.
V118	19.347500	37.651222	17.68	0.75	1.01	s	59.912	0.30623	0.70	likely memb.
V5	19.346258	37.813354	17.19	0.90	0.95	k	60.221	0.31274	0.05	member (98%)
V3	19.354380	37.769349	18.51	1.05	1.06	k	59.798	0.31764	0.09	member (78%)
V4	19.348396	37.806652	17.72	1.01		k	59.591	0.32568	0.10	member (98%)
V8	19.341938	37.865810	17.81	0.79	0.88	k	59.896	0.33406	0.10	likely memb.
V117	19.343433	37.665848	17.66	0.87	0.90	k	59.987	0.36644	0.38	likely memb.
V7	19.340271	37.821892	17.63	0.93	0.86	k	59.820	0.39174	0.31	likely memb.

Table 3.3: Coordinates and light curve parameters of the contact binaries (W UMa systems, EW) belonging to NGC 6791. V is the brightness at maximum and T_0 is the time of the primary minimum.

system in which spots produce maxima with different heights. Indeed, it has been classified as an RS CVn variable by M05 and B03; they also observed a "shift of the modulation wave" from 1995 to 2002.

We note that our period for V119 is quite different from that given by H05 (0.1133 days); the new period makes this star an intermediate case between semi–detached and contact systems. Error bars on the periods in Tab. 3.3.5 are $\sim 10^{-4}$ d for P <1.0 d, $\sim 10^{-3}$ d for 1.0 < P <2.0 d and a bit larger for P >3.0 d.

Some variables show very sharp eclipses and out-of-eclipse variability due to different levels of stellar activity (05736_9, 00645_10, V109, 01393_1, V11 and V107; for the period of the latter star we prefer the longer of the two values given by M05).

In many cases we observed one eclipse only and we cannot give any value for the period, unless it has been given in the previous studies, as for the cluster member V80 (86% on the basis of the Cudworth membership probability). We also note that the amplitude we observed in V80 is much larger than that reported by B03.

To establish the membership of these eclipsing systems is not an easy task, since binary effects should be taken into account when considering colors and magnitudes. However, on the basis of the distance from the cluster

center and their position in the CMDs, we can argue that V60, 02461_8 (both single-event eclipsing binaries), 05736_9, V29 and 00645_10 are very probable members. This hint is corroborated by the membership probabilities for V60 and 02461_8, which are 91% and 88% respectively.

The special cases of V9 and B4 deserve attention. V9 is the binary closest to the center and its membership probability is 82%. However, it looks a very evolved object in the CMD; its period (3.2 d) and activity (see above) are also more typical for a Main Sequence star. Therefore, its membership is very doubtful.

The Cudworth membership probability for B4 is only 40%, but in the CMDs B4 belongs to a little "clump" of very blue stars. This location is in agreement with the results of Liebert et al. (1994) [55] and therefore B4 is likely a blue extended horizontal–branch star belonging to NGC 6791. The star is classified by M02 and M03 (who consider it a non–member) as an eclipsing binary, but we note that the light curve could also result from a rotational modulation.

Other possible members are: V107, 00331_3, V109 and V11, considering that they are within 6.4' radius from the cluster center. The location in the CMDs of the eclipsing binaries belonging to NGC 6791 is shown in Fig. 3.9 (triangles).

3.3.6 Rotational variables

We found 89 variables whose light curves are characterized by small amplitude (usually less than 0.10 mag) and continuous variability. It is difficult to ascribe such variability to contact binaries undergoing grazing eclipses, since they should be less numerous than those having partial eclipses, since grazing eclipses occur only for a particular orientation of the orbital plane. Our hypothesis is that in most cases this variability results from spots carried by the stellar rotation; under this hypothesis, a large variety of light curves can be produced. Of course, we cannot rule out that a small fraction of these light curves might be actually generated by grazing eclipses.

Star	Type	α_{2000}	δ_{2000}	V [mag]	$< B-V >$ [mag]	$< V-I >$ [mag]	Ref.	T_0 [HJD–2452400]	Period [d]	Ampl. [mag]	Notes
V119	EB	19.351961	37.916328	18.15	1.13	1.33	k	59.879	0.30197	0.15	member ?
V29	EB	19.354796	37.751386	20.00	1.23	1.61	k	69.012	0.43662	0.22	likely memb.
01558_5	EB	19.372697	37.953469	19.15				69.028	0.52910	0.28	likely non–memb.
01393_1	EA	19.329588	37.970392	21.23				59.326	0.58998	0.56	likely non–memb.
00331_3	EB	19.352367	37.864391	19.73	1.20	1.36	k	68.815	0.7347	0.13	member ?
V11	EA	19.342575	37.804802	19.38	0.96	1.22	k	67.875	0.8833	0.48	member ?
05736_9	EA	19.348484	37.721855	20.20	1.21		k	68.333	1.210	0.29	likely memb.
V12	EB	19.345259	37.849083	17.52	0.96		k	64.103	1.524	0.06	member (96%)
00645_10	EA	19.354692	37.710104	20.60	1.33	1.46	k	60.893	1.451	0.20	likely memb.
V9	EB	19.346634	37.777035	17.15	1.23	1.38	k	63.873:	3.2	>0.2	member (82%)
V107	EA	19.355068	37.761553	17.97	0.93	1.00	k	64.433	3.27	0.24	member ?
V109	EA	19.342716	37.793961	20.73	1.46	1.60	k	69.021	3.70	0.86	member ?

Table 3.4: Eclipsing variables with well defined light curves. EA stands for a β Per system, EB for a β Lyr one. V is the brightness at maximum and T_0 is the time of the primary minimum. Also B4, V60 and 02461_8, whose parameters are reported in the Appendix, are possible cluster members. The last column shows the Cudworth membership probability (when available).

The complete list of the rotational variables and their light curves is given in the Appendix. Here we discuss some examples. If the inclination of the rotational axis causes the progressive disappearance of the largest spots, the light curve displays continuous variation, which could be sine shaped in the simplest cases (a fraction of the spots is always visible; it can also produce Cepheid–like variability, as in the 001606_1 case, Fig. 3.11), or with a standstill (the hot or cold spots totally disappear; 00513_2 in Fig. 3.11) or, more commonly, it can be distorted by other spots besides the largest ones (00471_12 in Fig. 3.11). In cases of very active stars, a secondary wave also occurs (01175_5 in Fig. 3.11). Since the second wave often covers less than half of the period, these rotational variables can be distinguished from eclipsing binaries; we also note that the amplitude ratio between the first and second waves can be very different.

Also in the three cases in which the full amplitude is larger than 0.10 mag (V2, 02006_1 and 07483_9) rotational effects explain the observed features better than eclipses. For example, the light curves of V2 (P=0.273 d) and 01298_5 (P=0.586 d; see Fig. 3.11) show typical eclipsing binary behaviour,

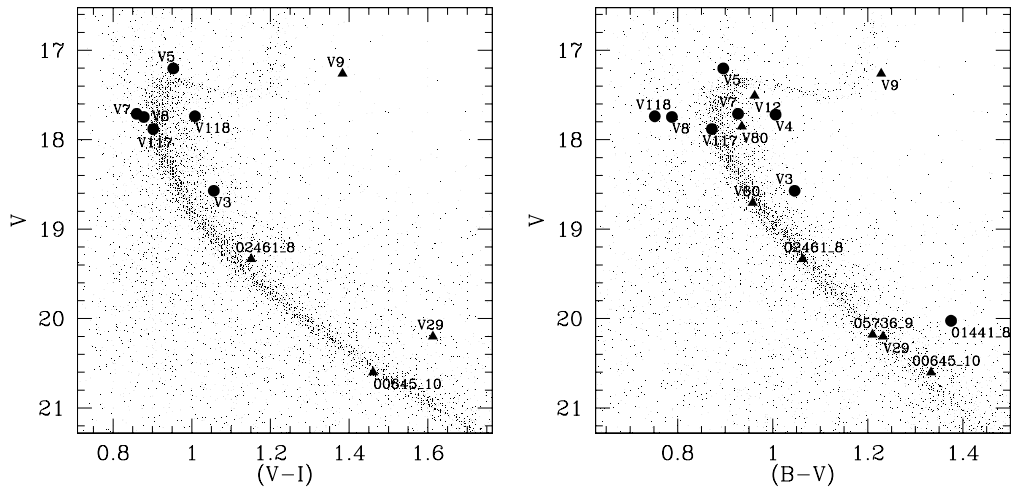

Figure 3.9: The CMDs for the binary systems belonging to NGC 6791. Filled circles are contact binaries (W UMa stars), triangles are detached or semi–detached systems (β Per or β Lyr systems).

but the amplitudes, the periods, and, mainly, the asymmetries are more typical of a rotational effect. The case of 02270_11 is different (Fig. 3.11). Its light curve is very similar to that of a contact binary, but it does not repeat exactly, and unusual scatter is observed through the cycle. We also note that this non-repetitive behaviour of the light curves, due to the spot activity, is the reason why several variables stars show residual standard deviations higher than expected.

Our periods for V34, V37 and V38 are approximately half of those given by M02, since these authors classified these variables as ellipsoidal ones; the large amplitudes (0.18, 0.06 and 0.13 mag) are more in favor of a variability resulting from large spots, rather than the purely geometrical effect of tidally distorted stars. We also note that V37 did not show any flare activity similar to that reported by M02 during our survey. We have also revised the classification of V16, considered an eclipsing binary by M02 and M03.

We count 33 rotational variables in the 10' –circle (i.e., 0.105 star/arcmin^2) centered on the cluster, while we have 56 variables in the remaining 924–arcmin^2 area (i.e., 0.061 star/arcmin^2). We have color indices ($B-V$ and/or

$V - I$) for 48 stars; 33 of them have a radial distance less than 10' from the cluster center. We can confirm the membership for 6 stars having proper motion membership: V16, V38, V42, V48, V53 and 03079_9. We have no photometric indices for V41; however, it is at only 2' from the cluster center and its Cudworth probability membership is 77%. Therefore, we consider V41 a member. For V14 we have the opposite situation because this star is at 1' from the cluster center and its positions in the CMDs agree very well with a membership, but the proper motion measurements rule out that it can be a cluster member (0%) (see Figure 3.12, V14 is displayed as a starred dot). As mentioned by M03, the positions of V17 in the CMDs are unusual. Other variables located below the subgiant branch like V17 were found in the open cluster M67 (Mathieu et al. 2003 [61]) and in the globular cluster 47 Tuc (Albrow et al. 2001 [2]). Probably these objects (named "red stragglers" or "sub-subgiant branch stars") are the result of some kind of mass exchange between the members of a binary system.

Putting the rotational variables without proper motion measurements on the CMDs we could infer that 8 stars are located on or close to the MS (represented with filled circles in Fig. 3.12); thus we suggest that these 8 stars belong to the cluster as well. Among the variables at greater distances, for three stars (01149_2, 01122_4 and 00513_2, all located between 11' and 13') the membership is doubtful, since their position in the CMDs is unclear. The other stars show apparent magnitudes and/or color indices too discrepant to be considered active MS stars belonging to NGC 6791.

When considering the variables without color indices, only two (V41 and 01874_2) are at less than 10' from the cluster center. We know that V41 is a probable cluster member (membership probability 77%), but, at the moment, we have no valid reason to consider the other star as a member.

Table 3.3.6 lists the rotational variables we suggest as cluster members. The error bars on the period are $\sim 10^{-4}$ d for P <1.0 d, $\sim 10^{-3}$ d for 1.0< P <2.0 d, $\sim 10^{-2}$ d for 2.0< P <5.0 d; periods longer than 5.0 d are tentative. Figure 3.12 shows the CMDs with the rotational variables

Star	Type	α_{2000}	δ_{2000}	V [mag]	$< B-V >$ [mag]	$< V-I >$ [mag]	Ref.	T_0 [HJD–2452400]	Period [d]	Ampl. [mag]	Notes
04803_9	RO1	19.347698	37.796043	21.81	1.33	1.84	s	61.799	1.1034	0.17	member (B06)
V82	RO1	19.344366	37.793381	19.01	1.00	1.02	k	56.481	1.1568	0.04	likely memb.
06553_9	RO1	19.349134	37.672577	19.26	1.04	1.13	s	61.421	1.3485	0.08	likely memb.
01724_9	RO1	19.344957	37.785362	20.73	1.29	1.69	s	64.410	1.6130	0.17	likely memb.
V38	RO1	19.351021	37.768288	18.82	0.96		k	55.630	1.96	0.13	member (92%)
03079_9	RO1	19.346190	37.754753	19.23	1.14	1.26	k	66.630	2.640	0.07	member (93%)
V14	RO1	19.347687	37.756874	18.58	0.93	1.05	k	55.933	5.45	0.05	non–member (0%)
V48	RO1	19.352076	37.718506	17.51	0.88		k	65.223	5.65	0.09	member (96%)
V17	RO1	19.344135	37.817928	17.92	1.20	1.28	k	63.211	6.523	0.04	member (88%)
V51	RO1	19.353382	37.748795	19.94	1.22	1.21	k	63.624	6.72	0.09	likely memb.
V52	RO1	19.355795	37.771935	17.49	0.88	0.88	k	64.345	7.06	0.03	likely memb.
V53	RO1	19.350233	37.743187	18.72	0.89	0.93	k	69.294	7.47	0.04	member (86%)
00436_3	RO2	19.352205	37.878635	18.92	0.92	1.08	k	60.018	0.26601	0.04	likely memb.
07483_9	RO2	19.349997	37.746311	21.28	1.32	1.70	s	60.465	0.4375	0.17	likely memb.
V41	RO2	19.347492	37.806892	19.09				60.000	0.4798	0.07	member (77%)
V42	RO2	19.350058	37.714867	19.51	1.05	1.16	k	60.323	0.5068	0.10	member (92%)
V16	RO2	19.352108	37.802662	17.79	0.93	1.01	k	67.713	2.182	0.03	member (96%)

Table 3.5: Rotational variables belonging to the cluster. V is the mean brightness value. T_0 indicates the time of the maximum brightness. The last column shows the membership probability (when available) or our photometric membership. The two uncertain cases (V41 and V14) are also listed (see text).

belonging to the cluster (Tab. 3.3.6) clearly indicated. We rejected as cluster members 16 stars out of 32 located within 10' from the cluster center; i.e., we considered them to be stars of the Galactic field. We note that the resulting density of the Galactic field (0.051 star/arcmin^2) superimposed on the cluster is in good agreement with that of the surrounding galactic disk field (0.061 star/arcmin^2, see above), especially considering that Poisson statistics supply uncertainties around $\pm$0.01 on the density values.

The stellar rotation and the activity level are both expected to be small for single stars as old as NGC 6791. Therefore we suggest that the rotational variables belonging to the cluster are likely short–period binaries, whose rotational velocity and activity level have been enhanced by the tidal synchronization.

3.3.7 Long-period variables

We detected numerous stars having different mean magnitudes on the different nights. Their behaviours are more diversified than those of the stars we considered as spurious on the basis of their close similarities. The resulting power spectra are dominated by terms at very low frequencies, corresponding to periods often much longer than 10 d. These periods cannot be evaluated in a precise way, being comparable or, more frequently, longer than our time baseline. Therefore, we can only argue that these stars are variables, either in a periodic or in an irregular way. Since we detected many spotted stars, it is quite obvious to think that most of these long-period variables are spotted stars having a rotational periods longer than 10 d. The mean amplitude of these stars is about 0.02 mag, except for 5 stars whose amplitude exceeds 0.1 mag.

Among the long-period variables, we used the Cudworth probabilities to establish the membership of 18 stars. In order to roughly estimate the membership of the remaining long-period variables we checked their locations in the CMDs, in the cases where at least one color is available. We suggest that 5 stars are likely members of NGC 6791: 02138_8, 01610_9, 04392_3, V75 and 02268_10 (see Figure 3.13). They lie along the MS or the red-giant branch and, furthermore, they are all located at distances smaller than 8.5', from the cluster center. Looking at the position of the variable V76 $\equiv$ V85 (memberships: 97%) in both CMDs, we suggest that this star could be similar to the "sub-subgiant branch" star V17. In Figure 3.14 we show its light curve and those of the 5 stars that we suspect to belong to the cluster. Table 3.3.7 lists the long-period variables we suggest as cluster members; the entire sample is listed in the Appendix.

3.4 Conclusions

Our wide-field survey in the direction of the Galactic open cluster NGC 6791 for the planetary-transit search allowed us to discover 260 new variable stars.

Star	α_{2000}	δ_{2000}	V [mag]	$< B-V >$ [mag]	$< V-I >$ [mag]	Ref.	Ampl. [mag]	Notes	Distance arcmin
02138_8	19.341864	37.749653	19.68	1.12	1.18	k	0.06	likely memb.	4.6
02444_8	19.342766	37.810604	18.34	0.93	1.00	k	0.02	member (78%)	4.4
00510_9	19.343704	37.796719	18.67	0.94	0.98	k	0.03	member (83%)	3.4
01610_9	19.344818	37.740486	19.09	1.01	1.05	k	0.02	likely memb.	3.0
V94	19.345139	37.743549	17.54	0.88	0.92	k	0.03	member (90%)	2.7
V95	19.345295	37.792412	19.16	1.03	1.10	k	0.07	member (93%)	2.3
V56(=V96)	19.345908	37.763525	17.01	0.95	0.97	k	0.04	member (98%)	1.6
04392_3	19.345982	37.870571	17.90	0.88	0.92	k	0.02	likely memb.	6.1
V75	19.346651	37.766308	17.38	0.94	0.98	s	0.01	likely memb.	1.0
04133_9	19.347109	37.777020	18.47	0.94	0.98	k	0.04	member (98%)	0.7
V76(=V85)	19.347192	37.764169	18.19	1.03	1.15	k	0.11	member (97%)	0.8
V86	19.347258	37.808815	19.44	1.06	1.14	k	0.03	member (83%)	2.3
V87	19.347996	37.749668	18.12	0.91	0.93	k	0.03	member (98%)	1.3
05740_9	19.348534	37.808022	17.96	0.93		k	0.03	member (95%)	2.2
06725_9	19.349329	37.724495	17.77	0.91		k	0.02	member (91%)	3.0
06796_9	19.349415	37.769268	18.46	0.92	1.04	k	0.03	member (92%)	1.0
V90	19.349686	37.746449	18.11	0.86	0.94	k	0.01	member (94%)	1.9
07680_9	19.350193	37.718224	18.32	0.89	0.97	k	0.03	member (98%)	3.5
V31	19.350683	37.785912	17.12	1.00	1.02	k	0.01	member (97%)	2.1
09376_9	19.351952	37.831886	18.21	1.00	1.02	k	0.01	member (92%)	4.6
09611_9	19.352139	37.773365	17.97	0.85	0.91	k	0.01	member (76%)	2.9
V58	19.354042	37.801240	17.52	0.89	0.94	k	0.05	member (87%)	4.6
02268_10	19.359475	37.731544	18.59	0.95	0.99	k	0.02	likely memb.	8.5

Table 3.6: Long period variable stars that are likely members of NGC 6791 (ordered by increasing right ascension). The column 9 shows the membership probability (when available) or our photometric membership.

When considering the membership probabilities given by Cudworth and B06, 13 of them belong to the cluster and one star (09831_9) is not member. On the basis of the distances from the cluster center and the positions in the CMDs, we suggest that another 11 stars are likely members, for 22 stars the membership is doubtful, and 137 stars are likely non-members. No photometric or kinematic data are available for 76 stars.

The variable star content of the cluster is very similar to that of the surrounding Galactic environment: in both samples we find rotational variables, contact and eclipsing systems. Contact binaries and rotational variables belonging to the cluster have the same characteristics as those located in the surrounding Galactic field. No evidence of pulsating variables has been found in NGC 6791, but this is not surprising, since it is a very evolved cluster and stars located in the instability strip or hotter pulsators have already left the MS.

The discovery of the new cataclysmic variable 06289_9 in addition to B8 and V15 adds another peculiarity to NGC 6791, making it unusual among the open clusters.

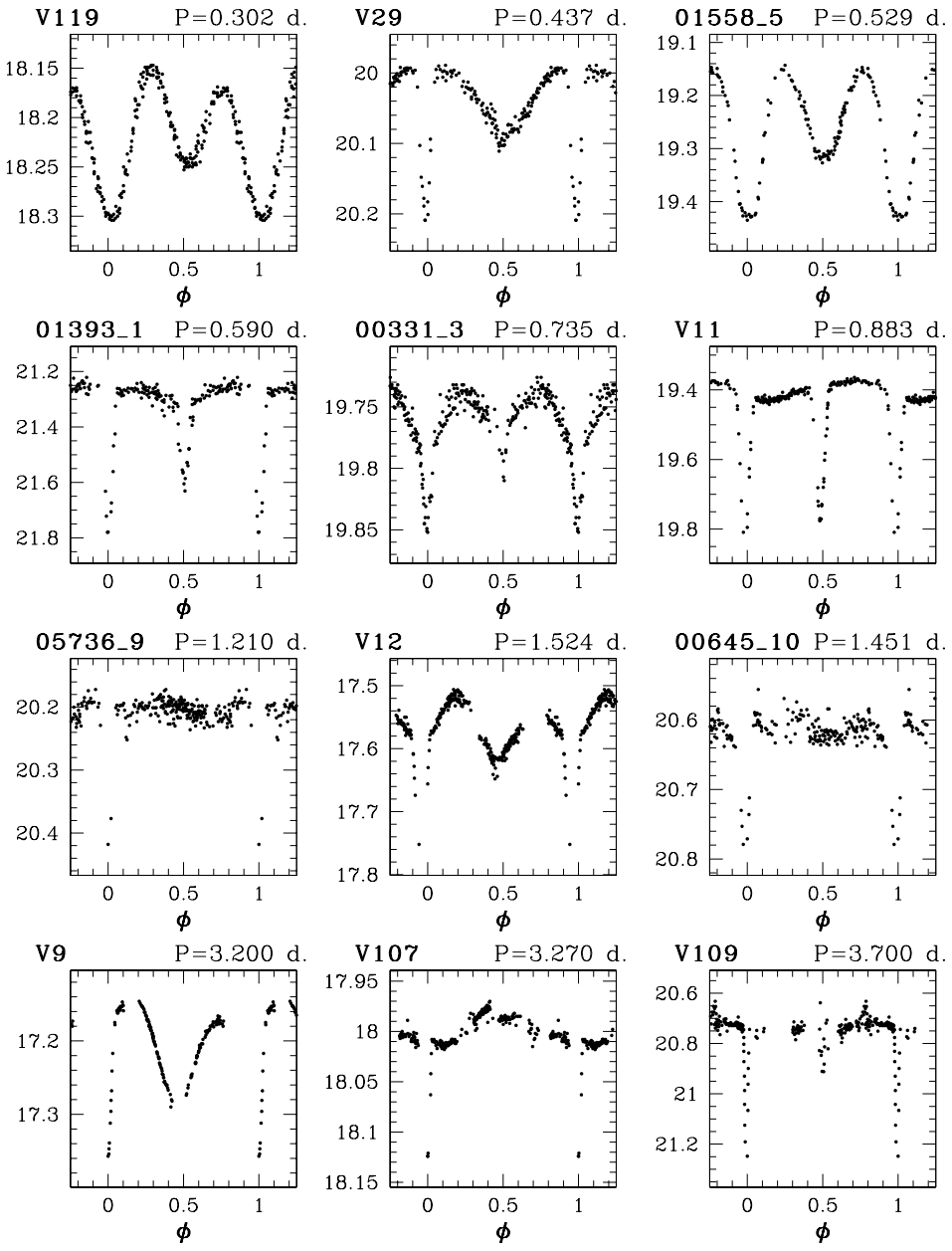

Figure 3.10: The light curves of short–period detached or semi–detached eclipsing binaries.

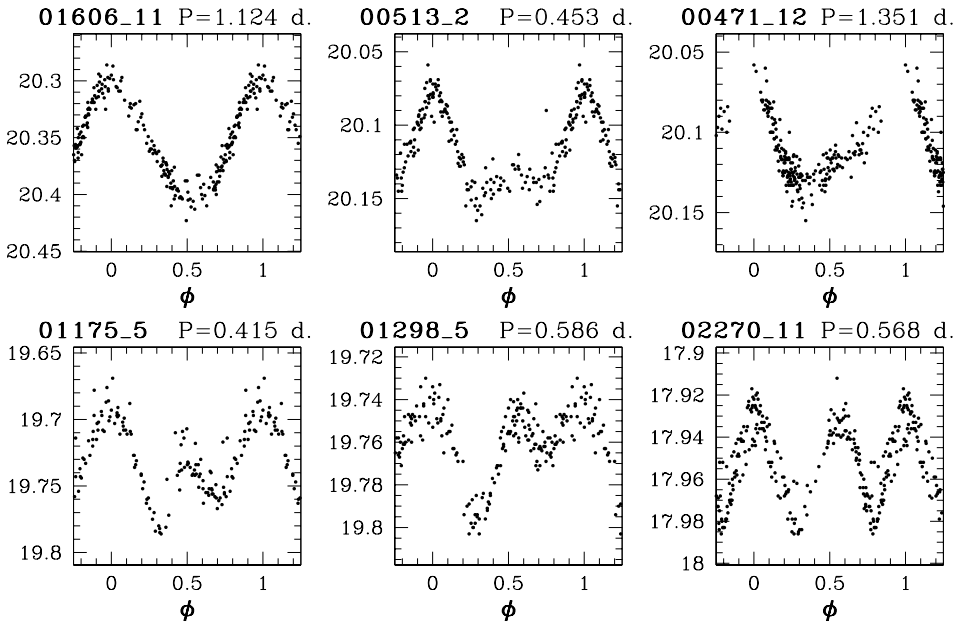

Figure 3.11: The light curves of a small sample of rotational variables, illustrating the growing importance of the second wave.

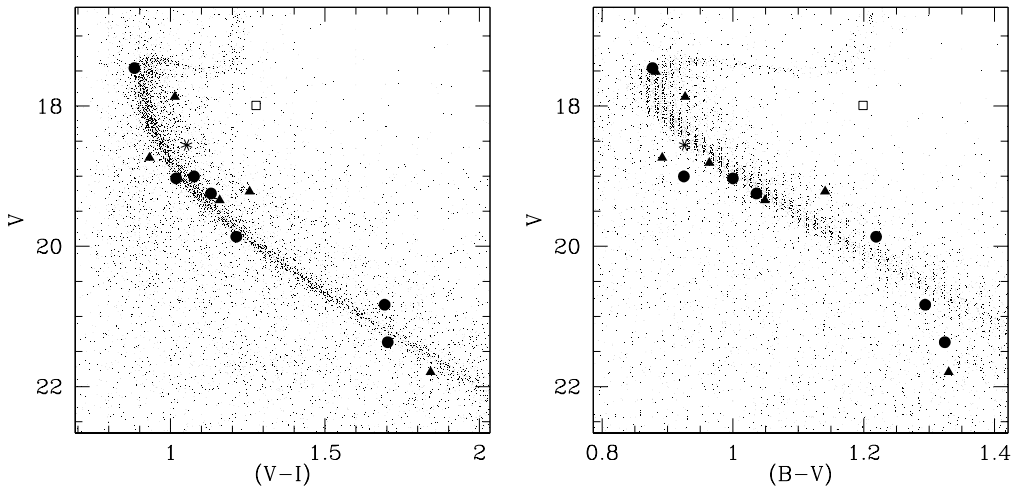

Figure 3.12: $(V-I)-V$ and $(B-V)-V$ diagrams for NGC 6791. The rotational variables that we suggest may belong to the cluster are indicated with filled circles. *Triangles*: stars belonging to the cluster according to the Cudworth's membership; *starred point*: V14, *open square*: V17 (see text for details about these stars).

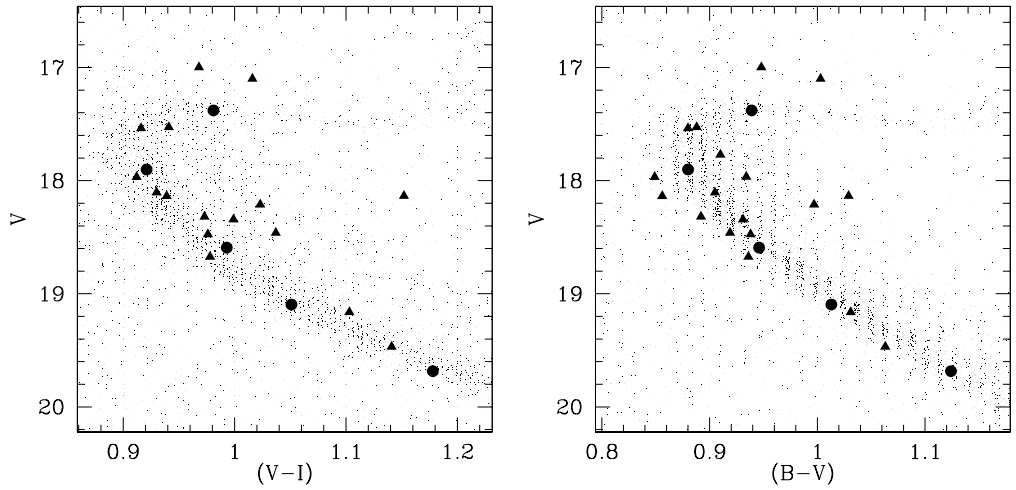

Figure 3.13: $(B-V)-V$ and $(V-I)-V$ diagrams for NGC 6791. *Filled circles*: long–period variables that we suggest belong to the cluster. *Filled triangles*: long–period variables that belong to the cluster (membership probability higher than 76%.)

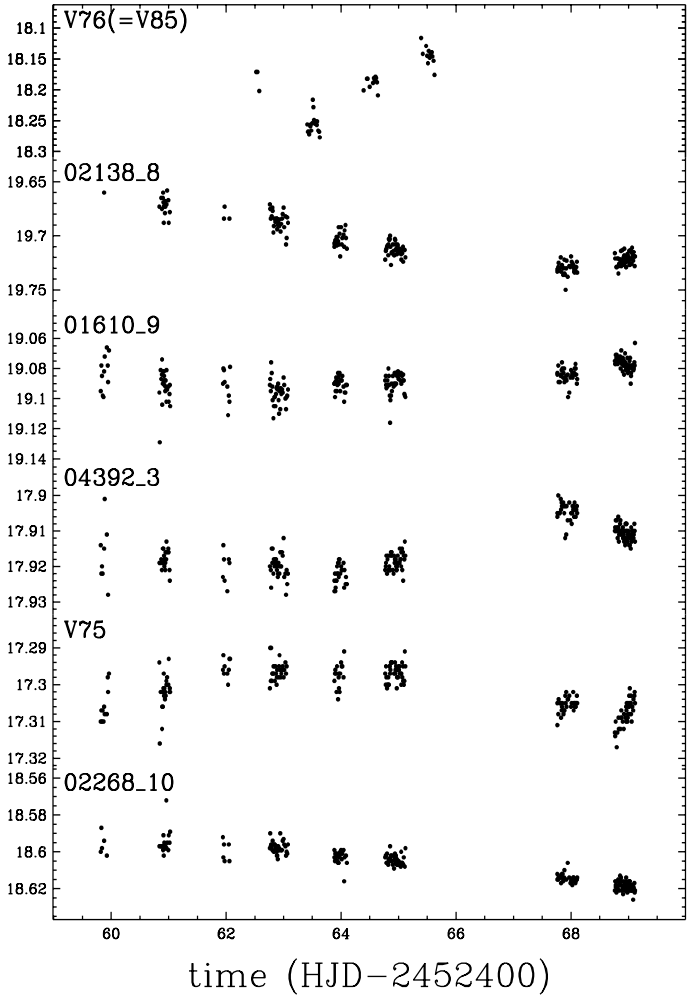

Figure 3.14: Light curve of the suspect "red straggler" V76 ≡ V85 and the five stars that we suggest may belong to the cluster.

Chapter 4

Variable stars content among the Blue and Yellow stragglers of NGC 6791

Here, we will describe the search for the variability among the Blue and Yellow Stragglers stars (BSS–YSS) into the open cluster NGC 6791. This study is an extension of the results obtained in Chapter 3, but, in order to complement our data (mostly due to saturation, because we are studying stars above the turn off), we also used the information available in literature (see Table 3.1).

4.1 Introduction

BSSs are stars significantly bluer and brighter than the turn–off point of a CMD. They appear as a spread population on the prolongation of the Main Sequence (MS). The formation of BSSs is thought to occur following two different channels: stellar collisions between single stars or binary systems (Benz & Hills, 1987 [8], Lombardi et al. 1996 [58]) or evolution of primordial binary systems via mass transfer or merging; (McCrea, 1964 [64]; Eggen & Iben, 1989 [27], Mateo et al. 1990 [60]; Preston & Sneden, 2000 [88]; Davies

et al. 2004 [23]).

Actually, in old stellar populations two sorts of variable BSSs are known: pulsating BSSs and eclipsing BSSs. It is well known that some class of main sequence stars pulsate due to their location within the low luminosity extension of the Cepheids instability strip.

The study of variability of BSSs contributes to our understanding of their properties and origins; for example, stars that fall in the IS are expected to be pulsating variables, but not all BSSs located in the instability strip pulsate. It is likely that if BSSs are formed via mergers or collisions, they will be fast rotators and thereby inhibit pulsation.

Pulsating BSSs as δ Scuti or SX Phe were found in some OCs (e.g.: M67: Gilliland & Brown, 1992 [35]; Bruntt et al. 2007 [14]) and in several globular clusters (e.g: NGC 6397, Kaluzny & Thompson, 2003 [46]; 47 Tuc: Gilliland et al. 1995 [36], Bruntt et al. 2001 [12]).

Moreover, variability due to eclipses is often observed in both globular and open clusters.

It will be shown that, in the case of NGC 6791, the IS crosses the MS well above (i.e.: about 2 mag) the turn–off point (see Figure 4.2).

The definition of Yellow and Red Stragglers is ambiguous. Kaluzny (2003) [46] (hereafter K03) defines the YSSs as those objects located between BSSs and the RGB stars, in a CMD diagram. Instead, RSSs are stars located redward of the MS and RGB of the parent cluster. Binary systems near the MS are excluded because RSSs are defined also as stars whose positions on the CMD can not be obtained combining the light of two MS stars.

Clark & Sandquist (2004) [21] define both Red and Yellow Stragglers as stars located between the BSSs and the RGB regions of a CMD (that corresponds to the YSSs region in K03). Stars located into this region are expected to be evolved BSS, binary systems, or blended unassociated stars.

Another definition of YSS is given by Edmonds et al. (2003) [26]: stars located below the subgiant branch of the parent cluster (also know as sub-subgiant stars).

In this paper we adopt the definition given by K03.

As described in Sect. 2.1, all light curves of the CFHT sample are in V band only. Mean $B-V$ colors for the 45% of the entire sample were obtained by two cross–correlations: the first with the Stetson et al. (2003) [102] (hereafter S03); photometric catalog, while the remaining stars were cross-correlated with the database of Kaluzny et al. (1995) [49] (hereafter K95)

In order to establish what the merging of two different photometric catalogs implies, we started selecting a sample of 1575 stars located into the region on the CMD on which or studies are focused: $0 \leq (B-V) \leq 2$ and $10 \leq V \leq 18$ (i.e.: the BSS/YSS/IS region). In Figure 4.1 we report the differences among the mean B and V magnitudes for the stars in common to the two catalogs, small offsets are visible, therefore we shifted the data from K95 in order to uniform our catalog to those of S03 (the proportions between the S03 and K95 data in our merged catalog are 65% and 35% respectively).

Among the sample of 385 known variables into the NGC 6791 area, mean colors are available for 239 of them.

4.2 Selection criteria for BSSs–YSSs candidates

Following the definition of K03, we started by drawing an area on the CMD of the cluster where Blue and Yellow Stragglers lie (see Fig. 4.2). The BSSs region was selected following the same criterium of De Marchi et al. (2006) [24]; while the adopted YSSs area is simply an elaboration of the BSSs location towards the RGB. We highlight also the region of the classical IS for pulsating variables, translated by reddening and distance modulus relative to NGC 6791.

Looking at the CMD of NGC 6791, a severe field contamination it is evident. For this reason, we started adopting as fiducial edge of the cluster a circle of 10'–radius from the center of the cluster. In Sect. 3.3 it was shown

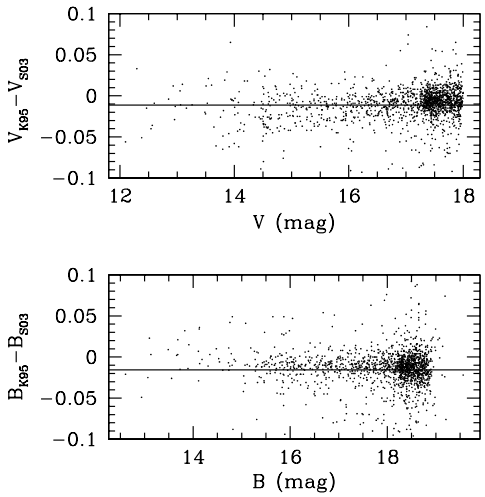

Figure 4.1: Differences between K95 and S03 mean V (*top*) and B (*bottom*) magnitudes for each star as a function of mean V and B. The horizontal lines represent the mean of the differences between the magnitudes. The zero point offsets are estimated to be ΔB=-0.0113 mag and ΔV=-0.0157 mag. The entire sample represented contains 1575 stars.

that at this distance, the stellar density becomes similar to the field one. A similar result (9.3') was obtained by K92. In Fig. 4.2, in the top–right panel, only the stars external to the fiducial 10' circle are reproduced, and there is no evidence of cluster populations.

Thus, with this criterion, we will exclude *a priori* all stars located at $r > 10'$, as non–members.

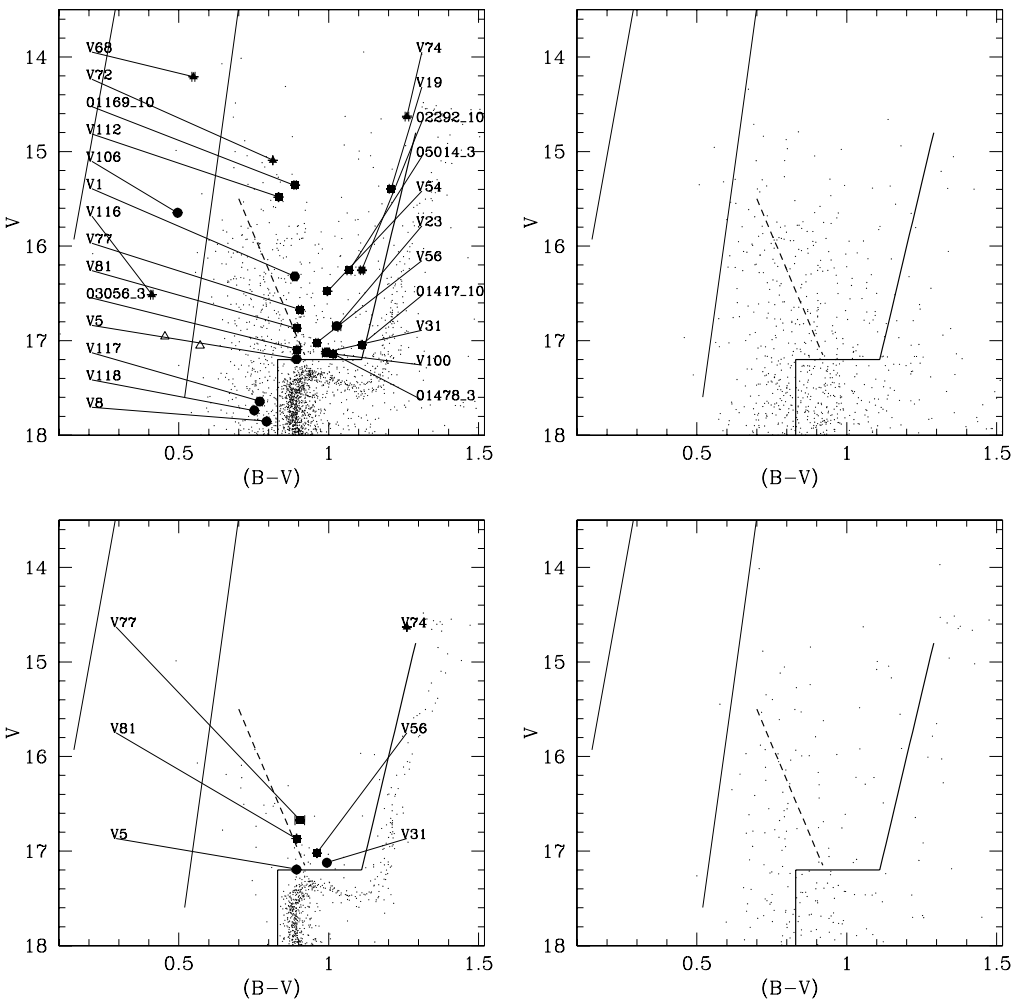

Figure 4.2: CMDs of NGC 6791. *Top left*: stars located into the 10' radius. *Top right*: stars located farther than 10' radius. *Bottom left*: proper motion members. *Bottom right*: proper motion non–members. For each figure the straight lines on the up–left individuate the approximate edges of the IS, other lines are the boundary of the BSSs–YSSs region. Dashed line represents the indicative separation between BSSs and YSSs. *Filled circles*: eclipsing binaries. *Filled squares* rotational or long–period variables. *Filled triangles* irregular or pulsating variables. *Open triangles* pulsating variables 03653_3 and V123 (likely non members).

4.3 Cumulated radial distributions

Once we have selected the BSSs and YSSs samples, we considered also other five stellar populations: MS stars , Subgiant Branch (SGB) stars , RGB stars, and Horizontal Branch (HB) stars.

We will take into account MPs (when available) and we will compare the cumulate distributions for BSSs, YSSs with that of the selected stellar populations. We consider as members all stars with MPs greater than 80% in order to have at the same time both relatively high probabilities and samples of stars not too scarce. The numbers of selected objects with MPs> $C80\%$ are 651, 143, 71 and 9 stars for MS, SGB, RGB and HB respectively. In Figure 4.3 we plotted the normalized cumulate radial distributions for the BSSs and YSSs samples with solid lines, and the MS, SGB, RGB populations (dotted lines). We not consider the HB stars because the small number.

One can see that the concentration of YSSs is greater than that of all stellar populations selected for the comparisons, clearly, at least part of the YSSs are the results of blends, which are expected to be more frequent towards the cluster center.

Kolmogorov–Smirnov tests were applied to these populations; they give no decisive results regarding the concentration of the different groups of stars: the probability that BSSs and RGB stars are taken from the same population is 45% (69% between BSSs and MS stars and 44% between BSSs and SGB stars). The same comparisons, using YSSs, yield 3%, 5% and 2% respectively. A comparison between BSSs and YSSs give a 56% of confidence.

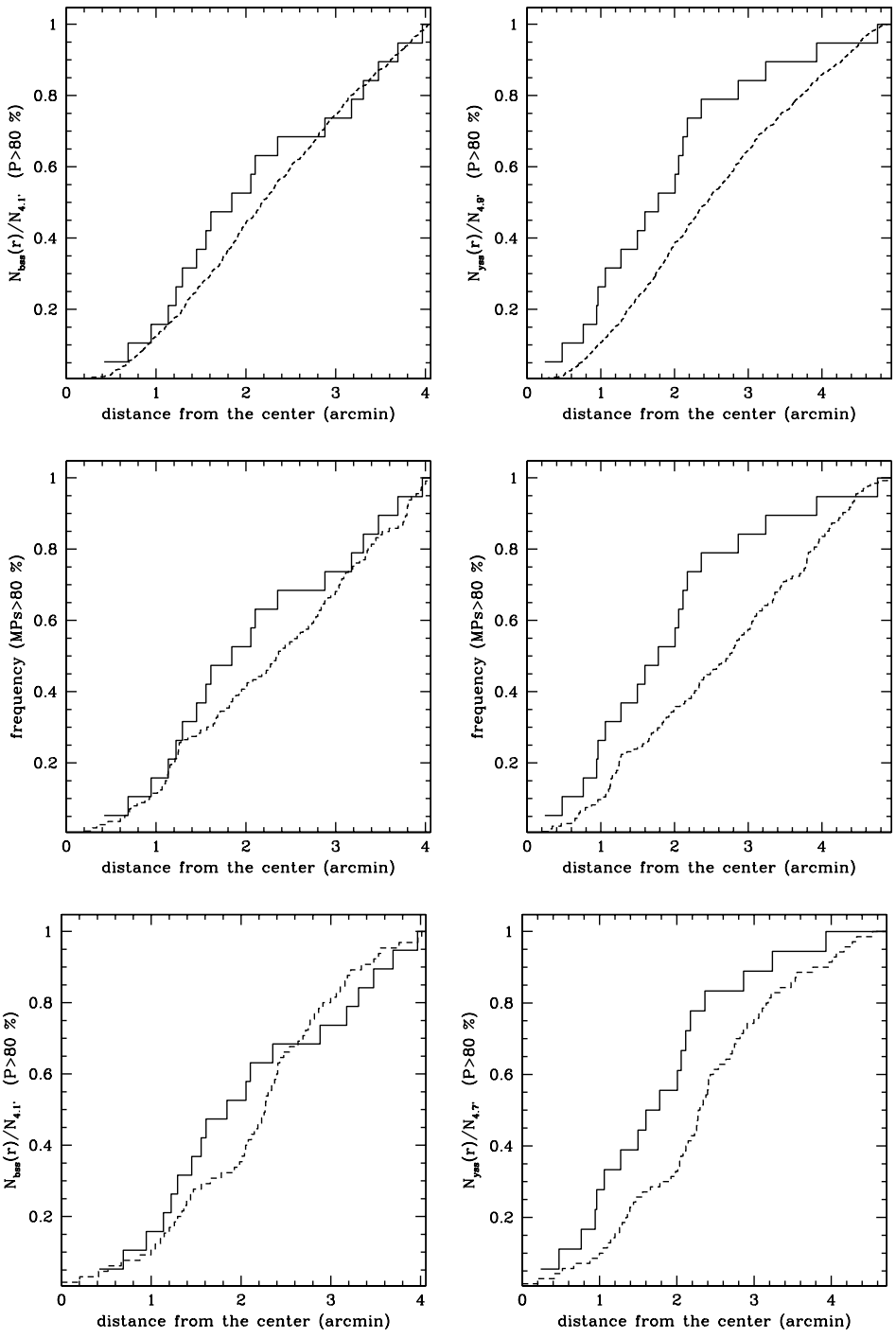

Figure 4.3: Comparison between the radial cumulate distribution of BSSs (left column) and YSS (right column) with MS stars (top), SGB stars (middle), RGB stars (bottom). BSSs and YSSs are indicated with solid lines, while dotted lines are used for MS stars, SGB stars and RGB stars.

4.4 Variable stars into the BSSs, YSSs and IS regions

4.4.1 Blue Stragglers

The total number of object within our field of view located into the BSSs region (N_{BSS}) is 590, among these, 363 are located at less than 10' from the center ($N_{BSS<10}$). Field contamination is certainly significant, thus, we make now some statistical consideration in order to estimate the expected number of real members of the cluster. Considering as field stars all BSSs located at more than 10' from the center, we evaluate a field density ρ_{field} equal to 0.63±0.06 stars into the BSSs region over square arcminute. The expected BSSs population for NGC 6791 can then be simply evaluated with:

$$N_{memb.} = N_{BSS<10} - \rho_{field} \times \pi \times 10'^2$$

we estimate a BSSs population for NGC 6791 composed by 160±27 stars (i.e.: the 45±10% of the BSSs candidates at less than 10' from the center) Only six variables are located into the BSSs region, at less than 10' from the center. Four of them are contact binaries: V6, V8, V117 and V118. V6 is a non member (M03), while the last three objects are likely members, as was found in Sect. 3.3.4 (page 51). The other two variables, V110 and 03056_3 are respectively a long period and a rotational single–wave variable, see Sect. 3.3.1 (page 46).

We exclude V110 as non–member (MP=25%), while the last object, 03056_3, with P=6.7 d and amplitude equal to 0.07 mag on the CMD is located at about 0.2 mag above the turn–off and on the equal–mass binary sequence.

Its MP is unknown, but, if member, 03056_3 could be a rotational variable. Its position into the CMD suggests the possibility that this star is a binary system. In that case this star could belongs to the RS–CVn class of stars, for which the variability is due to rotating chromospheric spots, and the

ID	Type	RA (J2000) [hrs]	DEC (J2000) [deg]	V [mag]	$B-V$ [mag]	Memb. %
V8	EW	19.3419380	37.8658100	17.855	0.793	m
V117	EW	19.3434310	37.6656950	17.644	0.770	m
V118	EW	19.3475000	37.6512220	17.738	0.752	m
03056_3	RO1	19.3479790	37.8694310	17.095	0.895	?

Table 4.1: List of variables into the BSSs region.

surface activity is induced by a close (non-eclipsing, in this case) companion.

One can notice that into the CMD V8, V117 and V118 are located on the left of the main sequence. Following Kaluzny & Udalski (1992) [51], these stars could be called "faint stragglers". The values of the mean $B-V$ colors and V magnitudes that we adopt for these stars are all taken from the S03 catalog. We firstly verify that the standard errors of the mean for the $B-V$ colors and V magnitudes of these variables are significantly smaller than the "gap" between V8, V117 and V118 and the MS (i.e. 0.1-0.15 mag). For the three variables $\sigma(B-V)$ values are always smaller than 0.04 mag, while σV magnitudes are smaller than 0.03 mag; moreover, the number of images from which each mean $B-V$ color and V magnitude was obtained, are between 4 and 11.

We noticed also that, in the $V, V-I$ CMD (obtained using the S03 catalog), these stars are all located in the middle of the high MS. In this case, we cannot conclude that V8, V117 and V118 are really BSSs because the data are in disagreement; we retain that the observed excess of blue color for the three contact binaries is due to some phenomena typical of this kind of objects.

The characteristics of V8, V117, V118 and 03056_3 are listed in Table 4.4.1.

While for several stars in the BSSs region the membership determinations

are unknown, and the classification itself of some variables as true BSSs is questionable, it is not possible to derive conclusively the fraction of BSSs in NGC 6791 that show photometric variability. Nevertheless, the data allow us to put some significant constraint.

To this goal we followed two different approaches: the first is to scale the number of variables in the BSSs region using the ratio members expected over number of stars (i.e. 45±10%, see above). This goes $2.7^{+1.9}_{-1.4}$ variable BSSs within a sample of 160±27 BSSs and then a frequency of (2±1)%.

The second approach is to consider only the BSSs with confirmed proper motion membership, but none of them is variable, and the resulting frequency is zero.

4.4.2 Yellow Stragglers

We selected a sample of 213 stars located into the YSSs region and included into the 10' radius , among these, the variables are 17 . The characteristics of the YSSs sample are reported in Table 4.4.2.

How many are the expected real members among the YSS ? We can apply the same statistical considerations performed in the previous section obtaining that only 21±12% of the YSSs candidates into the 10' radius are probable members, that means 45±23 stars.

Among the 17 variable stars located into the YSSs region (see Fig.4.2 and 4.4.2 and Tab. 4.4.2), the proper motion members are 5:

V81 is a periodic variable (P=7 d or 16 d, B03 and M05) with small amplitude (0.008 and 0.005 mag in V, B03 and M05); CFHT database does not contain it because of the saturation limit. This object seems similar to 03056_3: it lies about 0.5 mag above the turn–off, on the equal–mass binary main sequence. the variability can be interpreted as due to rotational modulation caused by starspot/magnetic activity probably induced by the presence of an uneclipsing variable.

V56 is another periodic variable, P=12 d, ampl=0.017 mag; M02). The

ID	Type	RA(J2000) hrs	DEC(J2000) deg	V mag	$(B-V)$ mag	Period days	A_V mag	Memb. (%)
V81	LON	19.3471370	37.8024600	16.868	0.893	7–16	<0.01	99
V56	LON	19.3459130	37.7635620	17.022	0.961	12	0.017	98
V31	EB	19.3506900	37.7858990	17.123	0.994	1.54–3.34	0.015	97
V77	LON	19.3480390	37.7769680	16.673	0.904	7–8	0.004	80
V74	IRR	19.3520020	37.7429970	14.631	1.261	-	0.03–0.04	91
V19	LON/IRR	19.347878	37.764137	15.395	1.208	>25 ?	0.25	?
V100	LON	19.3505080	37.7616530	17.127	0.991	>10	0.1	?
01478_3	RO1	19.3505270	37.8624280	17.139	1.015	∼8	0.07	?
05014_3	LON	19.345045	37.876141	16.256	1.068	>8	0.03	?
01417_10	LON	19.3569340	37.7568280	17.044	1.111	≫8	0.02	?
V1	EW	19.3465610	37.7421900	16.321	0.887	0.268	0.30	nm
V23	EW	19.3386140	37.7877810	16.846	1.027	0.272	0.07	nm
V72	IRR	19.3517000	37.6943810	15.093	0.814	-	0.045	?
02292_10	RO1	19.3595350	37.7102070	16.255	1.111	0.46371	0.06	?
V54	LON	19.355194	37.726807	16.477	0.996	8.4	0,01	?
V112	LON	19.334492	37.809277	15.482	0.833	8.8	0.002	?
01169_10	LON	19.3560780	37.6349360	15.355	0.888	>8	∼0.1	?

Table 4.2: List of variables within the YSSs region. The label 'nm' means that the variables (contact binaries) are non–members basing on the P–L–C relations.

sine–shape light curve (M02) give no indications about the type of variability, but is quite probable that V56 is another uneclipsing binary system as V81 and 03056_3.

V31 is an EB–Type or ellipsoidal variables (M02) with P=1.54 d (or the double, B03), This star was cataloged in Sect. 3 as a generic "long period variable", but, looking our light curve, we could also suppose that the short–period variability is not evident because of an incompatibility between the period of the variable and our observative window. We analyze also the light curve from the M02/M05 database, but we found not new periodicities. The phased light curve (with P=1.53 d) is plotted in Figure 4.4.2; we retain that because of the relatively long period and, especially, that the secondary minimum falls not at ϕ=0.5, this star is more probably a rotational double-wave variable.

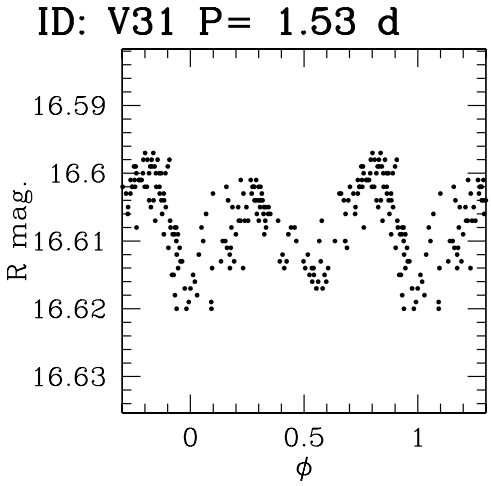

Figure 4.4: Phased light curves of V31 (from M02).

V77 was cataloged as a YSS by K03 (P=8 d), the variability is likely due to the presence of spots on the surface. As was for V81 and 03056_3, also V77 is located on the binary sequence.

V74 our data are heavily saturated, M03 founded irregular variations with amplitude $\simeq$ 0.04 mag). The fact that V74 is located quite near to the

red clump star, together with its variability type, suggests that it belongs to another class of objects.

The stars with unknown MPs are:

V19 and **V72** are stars that show irregular variabilities (M03) and from the light curve of V72 given by RKH96, we could infer a period near 25–30 d; this star is located about 2 mag over the turn–off. V19 is located near the RGB; and exhibits sudden "flares" of 0.1–0.2 mag (M03).

V100 from CFHT data we can only say that its period is greater than 8–10 d, while its amplitude is $\simeq$0.1 mag. The variability is likely due to rotational effects, even if the shape of the light curve could remember the Cepheids. This object is probably a BY Dra type variable located between the cluster and the Sun or an uneclipsing binary system member of the cluster (see Sect. 4.6).

Our sample contains also two EW–Type stars: V1 and V23, for which periods are P=0.2676758 d and P=0.2718 (M03 and M02, respectively). Applying the *P-L-C* relation, M03 shown that V1 is a non–member and the same calculus for V23 gives a comparable result (periods and colors of these tho stars are similar). V1 and V23 must be located closer than the cluster (both from 1.4 to 2 kpc from the Sun).

Also for the remaining stars (V54, V112, 01169_10, 01417_10, 01478_3, 02292_10 and 05014_3), the light curves suggest rotational variability.

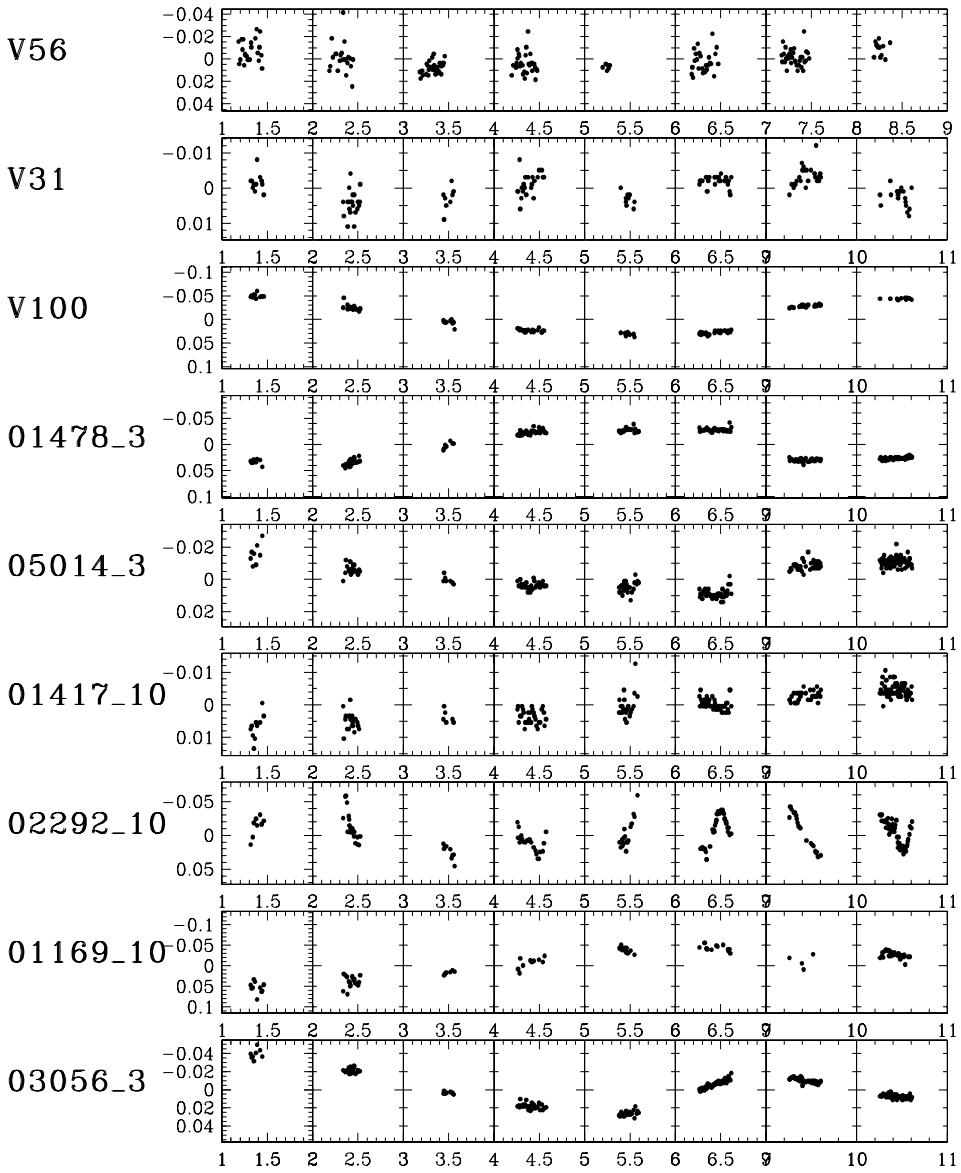

Figure 4.5: Long–period variables into the YSSs region (CFHT data). We added also the light curve of 03056_3.

ID	ID_var	RA (J2000) [hrs]	DEC (J2000) [deg]	V [mag]	$B-V$ [mag]	Memb. %
03907_9	blue–HB (?)	19.3499130	37.7744180	16.069	0.562	97
03965_9	blue–HB	19.3499920	37.7676420	14.989	0.491	83
V116	HADS	19.3361680	37.7200200	16.514	0.410	nm
V68	RV Tau (?)	19.3418770	37.8489650	14.210	0.549	nm?
05672_3	-	19.3440490	37.8894840	14.072	0.644	?
02573_10	-	19.3604470	37.7496000	16.278	0.556	?
V106	EB(?)	19.352976	37.758778	15.648	0.496	?
V123	HADS	19.3620640	37.6660340	16.967	0.458	nm
03653_3	RRc	19.3471470	37.9924130	17.064	0.575	nm

Table 4.3: List of stars into the IS.

As was made for the BSSs sample, we estimate the expected number of real members among the variables. Following the same procedures, we found: $3.6^{+3.4}_{-2.4}$ (making simply the multiplication) and The first determination agrees with the number of confirmed proper motions members (5–7 stars). The corresponding frequency of variable YSSs is $8^{+17}_{-5}\%$, and the same calculus made using the proper motion members (26 YSSs have MPs greater than 50%) yields $19^{+15}_{-10}\%$.

4.4.3 Instability strip

The IS for intermediate age OCs generally crosses the BSSs region, but, in the CMD of NGC 6791 we can see that the red edge of the IS is more luminous and bluer than the clump of bright and blue stars over the turn–off (Figure 4.2). This is due to the age of the cluster and its high metallicity that shifts the CMD towards the red. For this reason in our analysis, we preferred to consider the pulsating variables region relative to NGC 6791 separately from the BSSs one.

We noticed that 7 stars are located into the IS relative to NGC 6791,

three of them are variables (unfortunately, our data show no trends for two of them: V68 and V116, because the saturation limit, while the last star, V106 does not belong to the CFHT sample).

The characteristics of these stars are listed into Table 4.4.3.

We start considering the two only objects likely members of the cluster and that lie into the IS: 03965_9 and 03907_9 (MPs are respectively 83% and 97%). The CFHT light curves of both stars show no variability. The first star, 03965_9, was the target of a study on the heavy–element abundances of NGC 6791 by Peterson et al. (1998) [82]. They conclude that this object is likely a blue–HB star that serendipitously falls into the hydrogen-burning IS, not a pulsating variable.

We cannot advance hypothesis about 03907_9 (our light curve could be saturated), but, knowing that it is a member, it is quite probable that this star has similar characteristics as 03965_9.

V116 was classified by H05 as a δ Scuti pulsating variable with a period of 0.049967 d, The membership for this star, located at 9' from the center, is unknown.

We adopted the P–L relation for HADS star given by McNamara (1997 [65], 2000 [66]) and Petersen & Christensen–Dalsgaard (1999) [80] in order to give an estimation of the distance modulus, assuming that the period give by H05 corresponds to the fundamental–mode.

The resulting distance modulus (14.2 mag) puts V116 slight behind the cluster, at a distance of about 5–6 kpc from the Sun. However, the adopted period could be inadequate (we assumed that the period adopted corresponds to the fundamental mode period) and we cannot rule out that V116 could be a pulsating BSS of NGC 6791.

V68 is likely another pulsating star into the BSSs region: it was classified by M03 as probable RV Tau variable with P$\simeq$15 d and a very small amplitude (0.003 mag in V–band, M03). If the classification is correct, this star must be located behind the cluster, at least at 6 kpc from the Sun. Unfortunately, even in this case we cannot detect any coherent variability for this

star because of the saturation limit.

V106 is discussed in Sect. 4.7

The light curves of 05672_3 and 02573_10 are constant; if members, they are probably other two blue–HB stars. Otherwise (more probably) they are simply field stars.

To conclude, we briefly consider also two pulsational variables: V123 and 03653_3, located i our field but slightly external to the 10' radius (indicated with open triangles in Fig. 4.2). For these object (HADS and RRc, respectively) the P–L relation (McNamara; 1997 [65], 2000 [66] and Petersen & Christensen–Dalsgaard, 1999 [80]) gives a distance modulus for V123 similar to that of V116: 14.5 mag. Finally, as regard 03653_3, it must be located about 3 mag beyond the cluster; the light curves of these stars are plotted in Fig. 4.4.3.

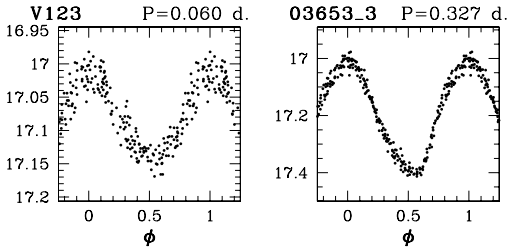

Figure 4.6: Phased light curves of V123 and 03653_3, HADS and RRc stars

4.5 Artificial binary systems

In general, the origin of the YSSs is uncertain; one can suppose that YSSs are BSSs in SGB phase, but the time interval spent by a star into the "Hertzsprung gap" is so short with respect to the MS life duration that, even with a a population of at least 140 BSSs, we expect that no more than some YSSs could be a slightly evolved BSS. Therefore, the most of the YSSs must have another origin. Our results about the variability of the YSSs together with a strong concentration towards the center of the cluster, are

compatible with non–eclipsing binarity for many of them. In order to clarify this point, we made a simple simulation to individuate the positions occupied by binary stars into the CMD diagram; then we compare it with the locations of YSSs. We proceeded as follows.

We selected on the CMD MS stars, SGB stars, RGB stars and HB stars; and, for each of them, knowing its $B-V$ color and V mag, we randomly selected a star companion among the same sample and we evaluate the resulting color and magnitude of the binary system composed by the two stars.

In Fig. 4.7 we plotted the fiducial isochrone for NGC 6791 (taken from Girardi et al. 2002 [38]) with the following parameters: age: 8.9 Gyr, Z=0.040, $E(B-V)$=0.12 mag and $(m-M)_V$=13.35 mag. With small points, we indicate the positions of the "artificial" binary systems; moreover, we represented with black points the positions of BSSs and YSSs that are confirmed members of the cluster.

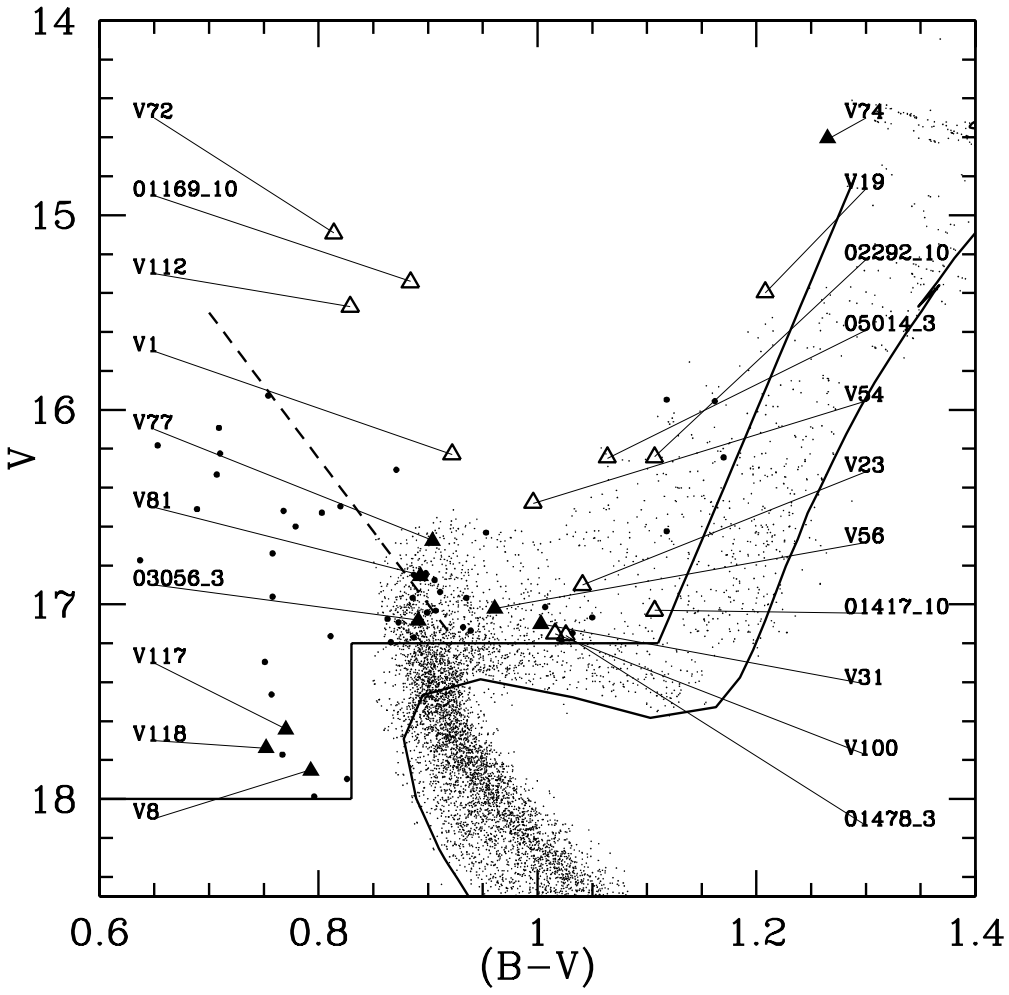

Figure 4.7: Simulated binary systems in the CMD diagram of NGC 6791. The solid line represents the fiducial isochrone for the cluster, the smallest points are the resulting positions obtained by randomly coupling pairs of stars from the selected population of MS, SGB, RGB and HB stars. Intermediate–sized points are constant stars members of the cluster. Close triangles are variables confirmed members, while open triangles are stars with unknown MPs.

We can see that no one of the BSSs could be a binary system composed by a pair of MS/SGB/RGB/HB stars; instead, the positions of most of YSSs that are real members (black points) is well represented by binary systems (real or perspective) as MS+MS, MS+SGB, SGB+SGB stars. In particular, the little clump of YSSs at V=17 and $(B-V)$=0.95. is compatible only with binary systems composed by two similar MS stars.

On the CMD it is evident a lack of objects on an ideal oblique line that goes approximatively (in $B-V$,V coordinates) from the point (1.05,16.6) to (1.20,17.4). The region on the right/left of this line is relative to the positions of the binaries with/without a RGB star, respectively. We can see that this lack of objects is also well reproduced by the YSSs confirmed members

V $\sim$The lack of object at V $\sim$17 and $(B-V)$ $\sim$1.15 that corresponds to binaries with or without a RGB star (on the right or the left of the gap, respectively) is also qualitatively reproduced.

RS CVn–type stars seem to be the ideal candidates to explain the variables YSSs in NGC 6791, for a summary description, see Sect. 1.2 at page 13.

Binarity and, in particular, RS–CVn type variability, can explain 9 over 10 variable YSSs located into the CMD region occupied by binary systems. Eight of them are likely as MS+SGB or SGB+SGB non-eclipsing RS–CVn variables, while the other two stars are V31 (EB–Type system, member) and V23, an EW-Type system, confirmed non–member). All these variables, except the last two, have a period greater than 7–8 d

Among the remaining stars, only 4 stars over 8 can be classified as "rotational": V112 and 01169_10, but they are located both at 9.9' from the center of the cluster and they are likely field stars, moreover, 02292_10 and 05014_3 could be binary systems where at least one component is a RGB star, or alternatively field stars (this hypothesis is quite probable for 02292_10 because of its short period). The other stars are a contact binary (non member) and 3 irregular variables.

Even if our sample contains few objects, we retain that a 8/10 incidence of YSSs rotational (and long–period) variables in the same region of the CMD

(occupied by MS+SGB or SGB+SGB systems) is significant.

We conclude that a scenario where the most of the YSSs are composed by unresolved binary systems composed by stars in the cluster MS, SGB, and RGB, is fully compatible with our observative data and our simulation. Moreover, we cannot rule out the fact that non variable YSSs could be binary systems with periods too long to induce chromospheric activity.

4.6 Models for some variable YSSs

In this section we tried to estimate the values of masses, radii and effective temperatures for the rotational YSSs that lies in the "binary region" as represented in Fig. 4.7. Therefore, from the sample of YSSs rotational variables we excluded 01169_10 V112, V74, V19 05014_3.and V54 because they belong not to the binary region and then we know *a priori* that no solutions are possible. We implicitly assume that 01417_10, V100, 03056_3 and 01478_3 are members of NGC 6791. For each YSSs, we adopt its V magnitude and $B-V$ color taken from our catalog and, with the constraints that one component must lie on the fiducial isochrone (drawn with solid lines, in Fig. 4.6), and that the resulting magnitude and color are fixed, we evaluate the corresponding position of the star companion (dotted lines).

For each YSSs, we assumed as solution the most likely scenario: both stars on the isochrone (represented by the two points in common between solid and dotted lines). In most cases we found, as expected, a slightly evolved primary and a secondary on the MS. In all cases masses and temperatures, derived by the isochrone, are quite similar, while the radius of the secondary is near twice the radius of the primary.

Errors relative to our parameters are mainly due to the incertitudes on distance modulus and reddening (photometric errors are about 5$\sim$10 times smaller) and we estimate them as follows: first, we assumed that the best estimates for the parameters are those obtained adopting $(m-M)_V$=13.35 mag and $E(B-V)$=0.12 mag. Then, we performed 4 simulations, each time we

shifted the distance modulus and the reddening adding or subtracting their respective errors. Finally, using the four determinations of each parameter obtained in this way, from its best estimate we calculate the standard deviation and we adopt this value for the error relative to the parameter itself.

on the red edge of the region corresponding to binary systems composed by at least RGB star (see Figure 4.7) The physical parameters that we found are reported in Table 4.6

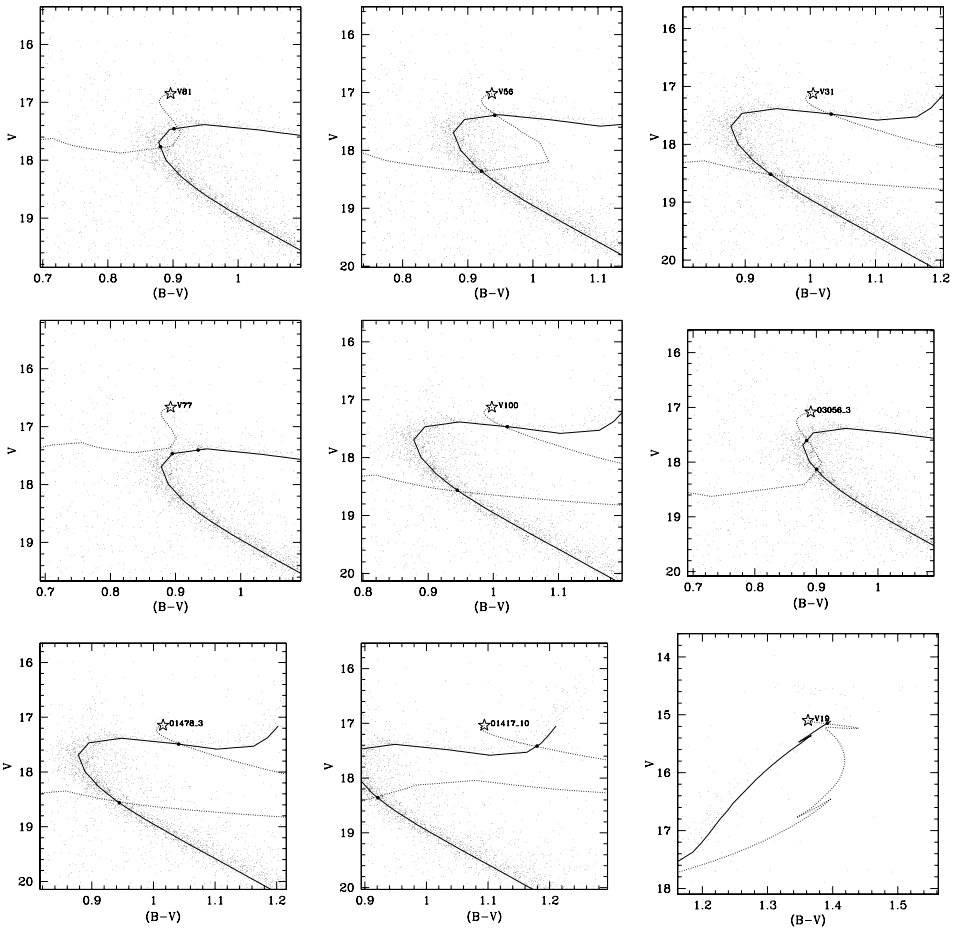

Figure 4.8: Models for some YSSs that could be binary systems. Black points represents the most probable configuration for the two components. The solid lines individuate a fiducial unevolved isochrone for NGC 6791 The dotted line represents the possible positions, for the companion, after fixing the $B-V$ and V of the system (starred point).

Star ID		$M/M_{\odot}$	$R/R_{\odot}$	Temp. (K)	Notes
V77	secondary	1.05 ± 0.01	1.54± 0.13	5522± 112	two turn–off
	primary	1.06 ± 0.01	1.67± 0.16	5410± 149	stars
V56	secondary	0.98 ± 0.04	1.14± 0.12	5507± 95	MS star and
	primary	1.05 ± 0.02	1.54± 0.29	5522± 350	SGB star
V31	secondary	0.92 ± 0.05	0.98± 0.13	5346± 180	MS star and
	primary	1.07 ± 0.01	1.75± 0.32	5314± 427	SGB star
V81	secondary	1.03 ± 0.02	1.35± 0.08	5573± 17	two turn–off
	primary	1.05 ± 0.02	1.51± 0.30	5528± 293	stars
V100	secondary	0.92 ± 0.06	0.96± 0.14	5317 ± 207	MS and
	primary	1.07 ± 0.01	1.73± 0.27	5343 ± 414	SGB star
01417_10	secondary	0.99 ± 0.07	1.16± 0.18	5520 ± 191	MS star and
	primary	1.08 ± 0.00	2.24± 0.39	4790 ± 94	SGB/RGB star
01478_3	secondary	0.92 ± 0.05	0.97± 0.11	5324 ± 178	MS star and
	primary	1.07 ± 0.01	1.77± 0.34	5285 ± 417	SGB star
03056_3	secondary	1.00 ± 0.07	1.21± 0.21	5544 ± 183	two turn–off
	primary	1.03 ± 0.04	1.35± 0.33	5573 ± 179	stars
02292_10	secondary	1.05 ± 0.05	1.54± 0.22	5522 ± 143	turn off star and
	primary	1.09 ± 0.06	3.99± 0.71	4620 ± 345	a RGB star

Table 4.4: Physical parameters for the rotational YSSs whose locations on the CMD are compatible with the binarity.

4.7 The eclipsing system V106

W106 is an object that deserves a special discussion. It was cataloged by M05 as EW–Type system, with a very long period (P=1.4464 d) and a relatively small amplitude (0.022 mag in V band); As mentioned above, the variable is within the IS and well above the turn–off of the cluster, its membership is unknown.

The light curve in R-band (kindly provided by B. Mochejska) is plotted in Figure 4.7. The shape of the light modulation suggests that the components of V106 are probably in contact, in this case, the relatively long period indicates that these must have large radii. Moreover, the small amplitude could be due to the inclination of the orbital plane or to a small masses ratio; the maxima are slightly unequal, probably because of surface activity. From the light curve we can derive the ratio between the temperatures of the components: $J_p/J_s = (T_p/T_s)^{1/4}$, where J_p and J_s are the depth of the eclipses expressed in flux units. We obtain that the ratio between the temperatures of the two components is about 0.9.

The shape of the light curve (even if noisy) remember that of contact binaries, therefore we apply the usual P-L-C relation (Equation 3.1) and we obtain M_V=0.53‘mag that corresponds to a distance modulus 1.7 mag greater than that of the cluster. However, we cannot exclude that V106 could be a semi-detached system and, in this case, the P-L-C is not applicable. If V106 is a member of NGC 6791, the shape of its light curve and its very long period imply that the two components, or, at least one, are stars more massive than the turn-off stars; moreover the position on the CMD of V106 is incompatible with that of a binary system composed by MS/SGB/RGB/HB stars.

As we made for the YSSs, we developed another rough model for the components of V106 (assuming that it belongs to NGC 6791). The position on the CMD of V106 (as is for all BSS, see Fig.. 4.7) is incompatible with unresolved binary systems. Therefore, we assume that one of the components lies on an unevolved isochrone.

Star ID		$M/M_\odot$	$R/R_\odot$	Temp. (K)	Notes
V106	primary	1.69	1.678	7291	Blue Straggler
	secondary	1.25	1.196	6037	Blue Straggler
		1.027	1.336	5570	turn–off star

Table 4.5: Physical parameters for V106.

There are several possibilities: the primary could be a massive BSSs and the secondary a late MS star, or, we can have two BSSs (represented by the intersections between the solid and dotted line in Figure 4.7, right panel), or, finally a BSSs and a turn-off star. In each case, at least a massive single star is necessary in order to obtain the brightness of V106. The numerical results of our simulation are listed in Table 4.7, for the case BSSs plus BSS and BSS plus turn-off star.

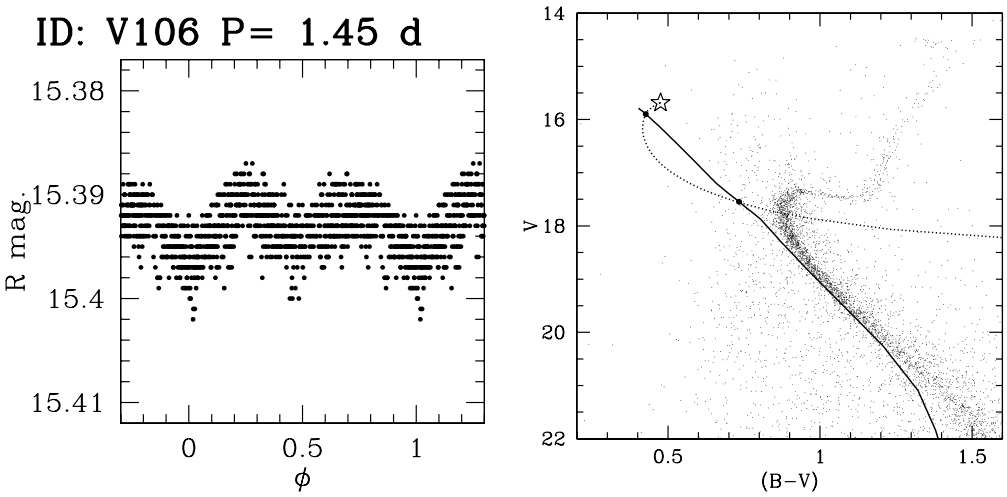

Figure 4.9: Phased light curves of V106 (left panel, data were obtained by M05). Right panel: model for the parameters of the components of V106 performed using an unevolved isochrone (solid line). Black points represent the positions of the two components (see text for details).

It must be remarked that the solutions of our model for V106 are much more arbitrary than performed in Sect. 4.6 for the rotational YSSs. This is due to more than one reason: first, the BSSs region is not so well defined as the MS or the SGB and V106 could be also composed by a massive BSS and a late–type MS star, moreover fitting a single-star isochrone to the components of a close binary system. it is not appropriate because interactions as, for example, mass transfer, modifies masses and radii. Anyway, even if the values for each single component are probably wrong, we can adopt equally our results in order to have a qualitative estimate of the *total* mass of the system that results to be nearby 3 $M_{\odot}$.

Finally, we want to highlight that, even if the results are only indicative, this model demonstrates that, if V106 is a member of the cluster, one of its components must be a BSS.

4.8 Conclusions

NGC 6791 contains several stars into the BSSs/YSSs regions. By means of statistical considerations we estimate 130–190 real members among the BSSs and 40–80 among the YSSs. The IS region contains only 9 stars (listed in Table 4.4.3), but only two of them are confirmed members, while 3 are very probable non–members). We shown that the incidence of the variability among the BSSs is quite low: we found only 4 variables (three contact binaries and a rotational variable) all located very near to the MS or to the turn–off points. Instead, in the $V-I, V$ plane, the contact binaries appear to be on the MS; therefore, we retain that their blue excess could be due to some phenomena typical of close binaries. For the last star, 03056_3, if member, it is probably a close binary non-eclipsing system; otherwise, a single rotating spotted star (BY Dra type), located between the Sun and the cluster. The position of this star into the CMD, and its of variability, so similar to that we found in several YSSs suggest to consider it as a YSS rather than a BSS. The CFHT light curves of all other BSSs show no coherent fluctuations;

Cluster	age (Gyr)	N_{BSSs}	N_{var}	N_{bin}	N_{pul}	N_{other}	Ref.
NGC 2158	2.5	30-40	6	1	5	0	Mochejska et al. (2004) [71]
Melotte 66	2.8	5-10	1	1	0	0	Zloczewski et al. (2007) [117]
NGC 188	4.3	20-30	1	1	0	0	Zhang et al. (2004) [116]
M 67	4.3	10-15	2	0	2	0	Simoda (1991) [99]
Berkeley 39	7.9	30-40	4	3	0	1 (rot.?)	Kaluzny et al. (1993) [44]
Collinder 261	8.9	40-50	4-10	4-10	0	0	Mazur et al. (1995) [62]
NGC 7789	9.2	20-30	1-2	1 (?)	1	0	Mochejska et al. (1999) [68]
47 Tucanae	10-12	40-50	13	8	5	0	Weldrake et al. (2004) [109]

Table 4.6: Frequencies of variable stars among the BSSs in some open cluster and in the globular cluster 47 Tuc.

moreover, no pulsational variables are found among the BSS. The binary system V106 that we sampled into the IS group, could also be considered as a BSS candidate. With the hypothesis (to be confirmed) that V106 is a member, its very blue color suggests that almost one of the two components must be a massive BSS of about 1.7 $M_{\odot}$.

This object, if member, could be similar to the semidetached Algol system V228 (period: 1.15 d) in the globular cluster 47 Tuc described by Kaluzny & Thompson (2007) [52] that is composed by a 1.5 $M_{\odot}$ BSS and a 0.2 $M_{\odot}$ secondary (a turn off star). However, further information about membership and eventually a spectroscopic analysis are needed to explain the real nature of V106.

To conclude, we compare our results with the data available in literature; we focused on intermediate–age and old open clusters as M67 (4.3 Gyr) , Melotte 66 (2.8 Gyr), Collinder 261 (8.9 Gyr), NGC 188 (4.3 Gyr), Berkeley 39 (7.9 Gyr) and NGC 2158 (2.5 Gyr). Results are listed in Table 4.8.

Our results about the variability among BSSs (no more than 2 candidates: 03056_3 and V8 among $\sim$140 estimated BSSs members) are in agreement with our previsions (2.7$\pm$1.2). This corresponds to a frequency of $\sim$ 1–3% , inferior to the values found into the clusters listed above, in particular the oldest ones. This is unlikely do to the age of NGC 6791 (slightly superior to

that of NGC 7789, but inferior to that of 47'Tuc), we rather retain that this is due to the incompleteness of our database relatively to the brightest stars because of the saturation limit. indeed, for the study of a discrete number of bright variable stars described in this Chapter, it was necessary to recur at the data available in literature.

To conclude, we retain that the frequency of variable stars among the BSSs that we found is underestimated because of the incompleteness of our database relatively to bright objects.

Regarding the YSS, we statistically estimated 40–80 real members; we identified 17 variables, but likely no more than 8–9 are real member (5 stars are confirmed members). We observed that several YSSs are crowded into the CMD region corresponding to MS+SGB or SGB+SGB binary systems; moreover, 9 over 10 variables into the same region are rotational "spotted" variables with long periods (more than 7–8 d).

For the remaining variable YSSs, the incidence of the same kind of variables is only 4/8. We retain that the most of stars located into this region are very probably binary systems; but only few of them are so close to produce chromospheric activity of the RS–CVn type. The incidence of variables among members is 8%–17%; higher than that evaluated for the BSSs sample (i.e.: 1%–3%). This discrepancy, could indicate that BSSs and YSSs are two independent populations.

We also consider the IS region relative to the cluster; we identified a blue–HB object (maybe two), some pulsating variables that seem all located beyond the cluster, three constant stars and a binary system, V106 (discussed above). As for the pulsating variables, only V116 could belong to the cluster (we know not if the period given by H05 is appropriate for the P–L relation that we used). The small number of pulsating variables in NGC 6791 (at most one star, V116), is compatible with those of the clusters listed in Table 4.8, for which the pulsating BSSs are at most 5 and in some cases are absent.

Into the IS region (that corresponds to the brighter area of the BSSs region) we found an interesting binary system, V106, that, if member of

NGC 6791, it must be composed by at least a BSSs. Further spectroscopic and photometric analysis are needed to estimate its membership probability and resolve this question.

Chapter 5

Variable stars in the open cluster NGC 6253

5.1 Introduction

In this chapter we describe our preliminary results about the variable stars in NGC 6253. This is the first search for variable stars performed in this cluster, therefore the results obtained cannot be compared with other works. I followed a procedure similar to that adopted for NGC 6791 and described in details in Chapter 3.

For NGC 6253 we have the advantage that mean colors were obtained during our own survey (see Sect. 2.3.1), therefore, cross-correlations with other photometric catalogs are not necessary. Colors in $(B-V)$,$(V-I)$ bands are available for $\sim$81% of the stars of chip 2, while, regarding the other 7 chips, actually the reduction process is still in progress. For the same reason, R.A. and DEC. determinations are available only for chips 2 and 3.

Accurate proper motions were evaluated by M. Montalto for each star of the chip on which the cluster was imaged (i.e. chip 2); however, the values obtained for MPs are reliable only for the stars with V <17.5 mag because of increasing errors of proper motion measurements at fainter magnitudes (see Sect. 2.3.3, where the procedure followed to obtain the membership

probabilities (MPs) is described in details).

The radius of the cluster was reported to be 2.5 arcmin (Lang, 1992) [56], but Bragaglia et al. (1997) [11] reported that at distances from the cluster center between 2.5' and 8' it is possible to find cluster members. For the coordinates of the center of NGC 6253 we adopted the values given by Piatti et al. (1998) [83]. A representation of the coordinates of all stars into chip 2 is reported in Fig. 2.3 and the $\sim$150 stars with MPs greater than 90%. were highlighted with black points. The distribution of these stars suggests that some members of the cluster are contained also in chip 1 and chip 3 (the width of each chip is equal to 8'), however an estimate of the number of star belonging the outer chips should be necessarily imprecise.

The study that here is presented is necesarily not as complete as that for NGC 6791, and the lack of colors implies that the preliminary analysis relative to the variables found in outer chips (i.e. nr. 1, 3, 4, 5, 6, 7 and 8) is only qualitative. In any case, accurate determinations for periods and amplitudes, and preliminary classifications for the most of them are possible. Tables containing all our results and light curves are reported in Appendix B.

Only the variables belonging to chip 2 will be discussed here. Among them, we will discuss in details the characteristics of those for which MPs are greater than 50%, while, for the others, memberships will be estimated from their location on the $B-V, V$ and $V-I, V$ color-magnitude diagrams (CMDs).

Moreover, for pulsating variables and EW-Type binaries with membership unknown, our conclusions will be based on the applications of the usual P–L and P–L–C relations.

5.2 The variable stars content of NGC 6253

5.2.1 Variability search and spurious effects

The search for variable stars among the light curves was performed following the same method described in Sect. 3.2.1. The distribution of best-fit periods

for all light curves are plotted in Figure 5.1. The situation is quite similar to that of NGC 6791 (see pag. 41): we found peaks corresponding to 1, 1.6, and 10 d in near all chips; also in this case, after visual inspections of the light curves with these periods, we deduced that they are not reliable.

We observed also evidence of spurious effects, for example, in many light curves the data taken at night nr 2 shown often a significant decrease of the brightness that, for some eclipsing variables, it could be confused with an eclipse. Therefore, if a variable was affected by this trend, we rejected the data corresponding to the entire night in order to better determine period and amplitude. Some examples of light curves of variable stars that show this effect during the 2^{nd} night are plotted in Figure 5.2.

Moreover, during nights nr. 4 and nr. 8 all light curves have few and often misaligned points and therefore we rejected these data from all variables.

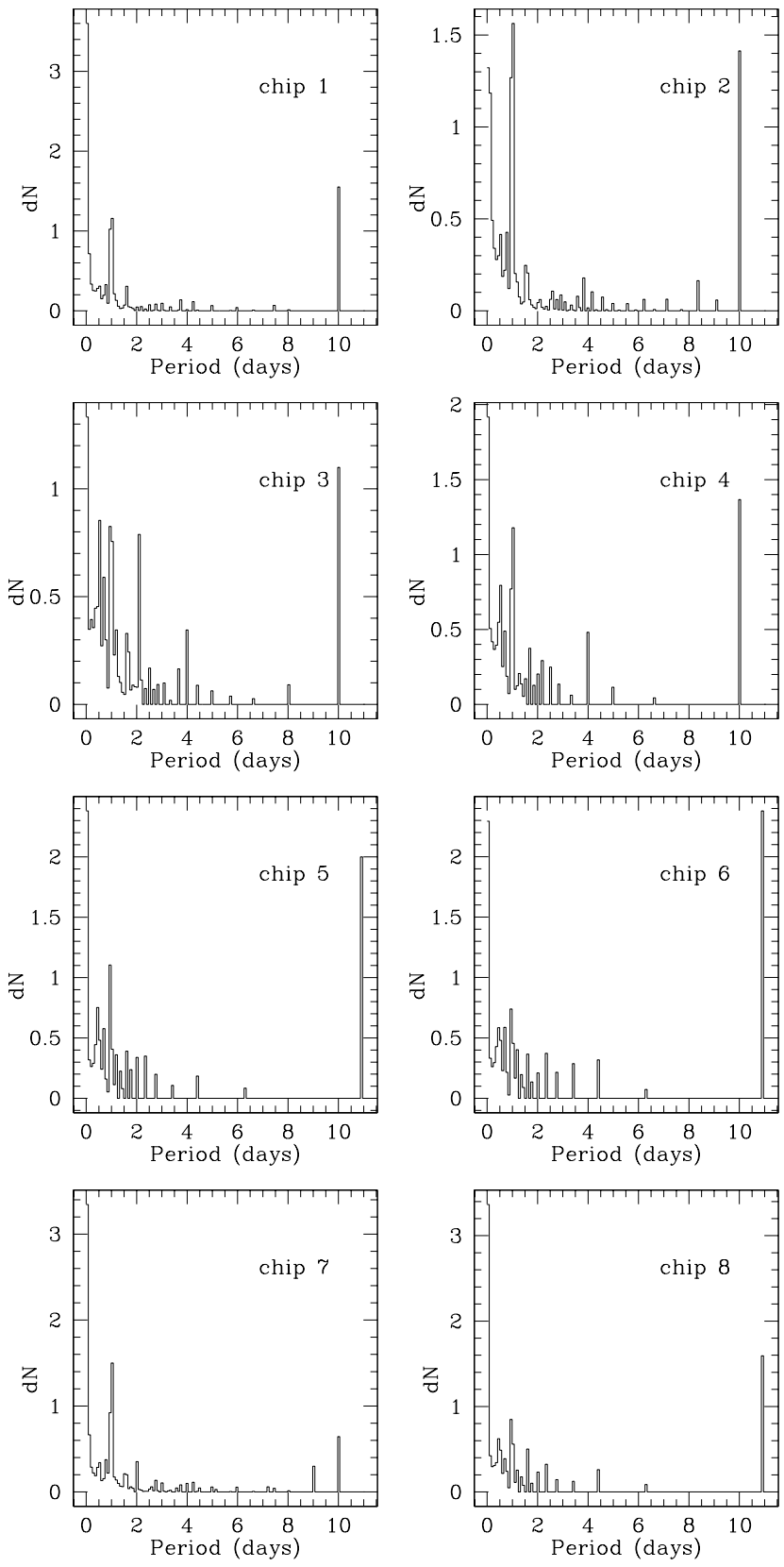

Figure 5.1: Period distribution for all light curves of each chip. Periods were obtained using the "sinusoidal plus constant" best fit (see text for details).

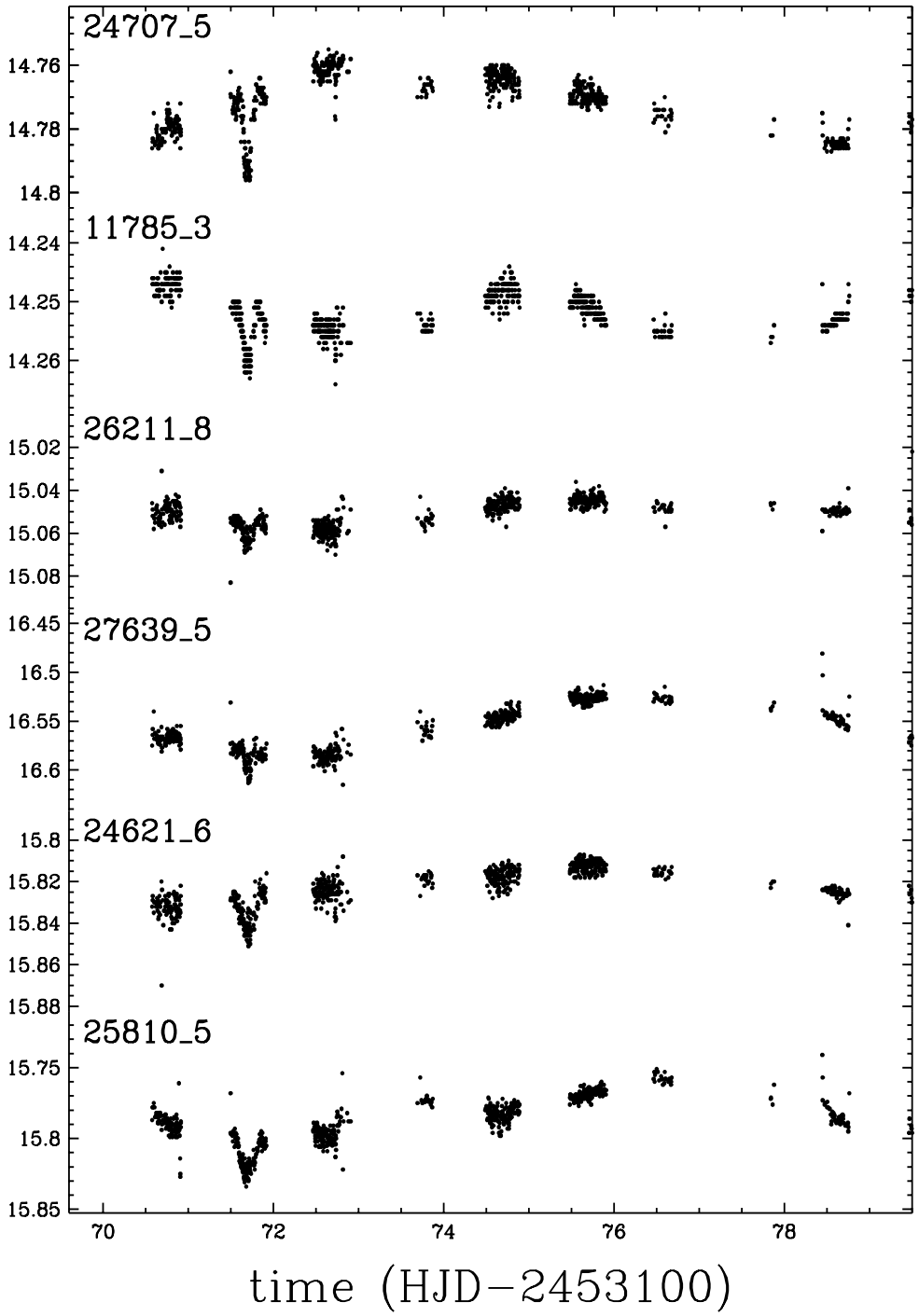

Figure 5.2: Spurious effects during the 2^{nd} night for some long period variables.

Type	Nr. of variables	
	all chips	chip 2
δ Scuti	11	0
HADS	4	0
RR Lyrae	4	1
Cepheids	1	0
EW-type	238	37
EB-Type	13	3
EA-Type	60	16
RS CVn	18	5
U Geminorum	1(?)	1(?)
Rotational	72	16
Long period	173	29
Planetary transits	1(?)	1(?)

Table 5.1: Summary of variables found into NGC 6253 and its surrounding area.

The total number of variables found is 597. 110 of them belong to the chip 2 and a summary classification of the entire sample is reported into Table 5.1

5.2.2 Pulsating variables

The only pulsating variable into chip 2 is a RRab star: 10540_2; but it is clear that it is too faint (and also too reddened) to belong to the cluster.

Its period is P=0.4303 d; applying the Equation 6 by McNamara (2000) [66] we can obtain the intrinsic color $< V - I >_0$=0.431 mag. Therefore, the reddening is $E(V - I)$=0.764 mag. and its distance modulus is $\sim$16'mag. Assuming A_V=3.2$\dot{E}(B - V)$ we found a distance of about 5 Kpc. The light curve of this star is reported in Fig. 5.2.3 and its parameters are reported in Appendix (Table B.1).

5.2.3 Binary systems

Contact binaries We start considering *all* contact binaries found in chip 2; both $(B - V)$ and $(V - I)$ colors are available for 32 over 37 stars, while for

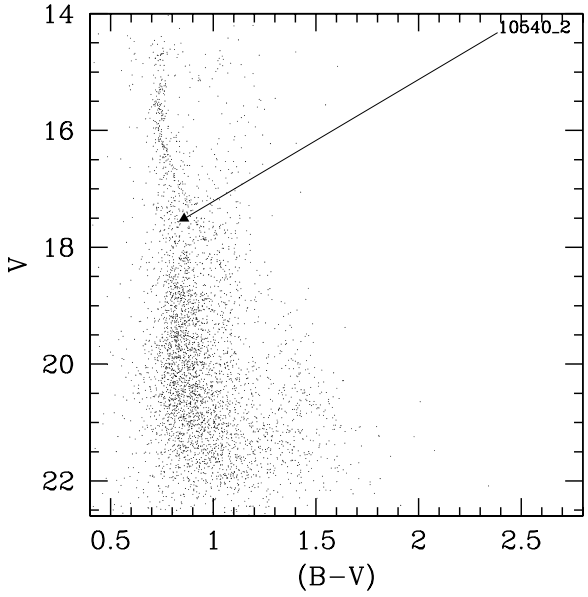

Figure 5.3: Positions on the CMDs of the RRab field star 10540_2.

three of them we have only the $(V - I)$ colors.

On these samples it is possible to apply the *P-L-C* relations (Equations 3.1 and 3.2 on page 52) given by Rucinski (2003) [92] and compare the resulting distance moduli with that of the cluster, obtained by isochrone fitting (Montalto et al. 2008 in preparation).

For the distance modulus and reddening we adopt a weighted mean of the determinations available in literature and our owns. The adopted distance modulus and reddening of NGC 6253 for this calculus are $(m - M)_V$=11.68±0.43 mag, $E(B-V)$=0.24±0.04 mag while we estimate $E(V - I)$=0.32±0.08 mag assuming $E(V - I)/E(B - V)$=1.35±0.10 mag (Sagar, Munari & de Boer, 2001 [94]).

It must be taken into account that, being our light curves in R band, we cannot know the exact value V_{max} of the magnitude at the maximum brightness required by Equations 3.1 and 3.2, therefore, because usually EW-Type variables have amplitudes generally $\lesssim$ 0.7 mag, we associate an additional error ΔV=0.3‘mag to the distance modulus that becomes $(m -$

$M)_V$=1.68±0.52 mag

Moreover, we noticed that the mean colors obtained from our survey show an offset with respect the ones of Bragaglia et al. (1997) [11] . Actually we don't know the reason of this discrepancy, but, in order to apply the *P-L-C* relations, we decided to evaluate it. We compare the mean $(B-V)$ colors of our contact binaries with that of the same stars from the Bragaglia et al. (1997) [11] catalog, and, from this comparison (10 contact binaries are in common between the two catalogs) we estimate $\Delta(B-V)$=0.18 mag and $\Delta(V-I)$=0.10 mag.

These values were used in the calculus of the errors on the distance moduli (errorbars in Fig. 5.2.3). The comparison among the estimated distance moduli for the EW-type stars and that of the cluster are plotted in Fig 5.2.3.

The calculated distance moduli are listed in Table 5.2.3.

ID	$< V >$	$< B-V >$	$< V-I >$	$(m-M)_1$	$(m-M)_2$	radius	Memb (%)
09268_2	16.360	1.073	1.364	11.194	10.370	1.2	87
13288_2	15.560	1.205	0.933	11.082	12.219	1.2	3
00145_2	17.340	1.141	1.186	12.119	12.147	1.9	0
23188_2	15.040	0.682	0.917	12.236	11.851	2.0	87
10853_2	17.040	0.968	1.186	12.357	11.862	2.1	78
01015_2	16.080	0.799	1.029	12.442	12.005	2.2	22
19024_2	16.740	0.801	0.894	13.136	13.195	3.0	0
14996_2	21.290	-	1.791	-	13.512	3.6	–
20779_2	20.130	-	1.307	-	13.575	3.7	–
17194_2	18.280	0.897	1.248	13.815	12.881	4.1	–
25539_2	18.180	0.750	1.061	14.002	13.303	4.5	–
24765_2	21.580	-	1.705	-	14.196	4.9	–
04477_2	18.810	0.843	1.144	14.398	13.678	5.4	–
06387_2	16.590	0.860	1.126	14.441	13.833	5.5	85
04611_2	19.240	0.969	1.350	14.477	13.390	5.6	–
15389_2	19.930	1.109	1.058	14.578	14.974	5.8	–
15046_2	18.260	0.856	1.034	14.546	14.263	5.8	–
06503_2	19.070	0.910	1.237	14.835	13.979	6.6	–
03734_2	19.580	1.071	0.650	15.020	16.780	7.2	–
19284_2	16.500	0.489	1.166	15.133	13.259	7.5	0
08822_2	18.870	0.816	1.064	15.160	14.648	7.6	–
18198_2	19.350	0.899	0.754	15.292	16.156	8.1	–
02366_2	18.100	0.451	1.265	15.391	13.047	8.5	–
00208_2	20.280	1.112	0.934	15.536	16.389	9.1	–
18759_2	19.680	0.887	1.105	15.731	15.284	9.9	–
04843_2	18.940	0.599	1.067	15.768	14.589	10.1	–
11470_2	20.560	0.978	0.959	15.885	16.243	10.7	–
00564_2	20.850	1.020	1.139	15.971	15.804	11.1	–
10805_2	18.840	0.484	1.631	16.071	12.497	11.6	–
10609_2	18.180	0.647	0.935	16.475	15.917	14.0	–
13453_2	19.510	0.478	1.191	16.653	14.659	15.2	–
24135_2	21.390	1.166	1.335	16.677	16.238	15.4	–
15649_2	21.540	0.995	1.084	17.197	17.153	19.5	–
16373_2	20.080	0.500	0.958	17.286	16.204	20.3	–
02948_2	20.370	0.115	1.712	18.418	13.437	30.8	–

Table 5.2: Results for the P–L–C relations: for all variables we report in columns 5 and 6 the calculated distance moduli using $(B-V)$ and $(V-I)$ colors, respectively (errorbars are $\sim$0.7 mag and $\sim$0.6 mag). Our proper motions MPs are reported in the last column. The variables are listed in increasing distance from the center order.

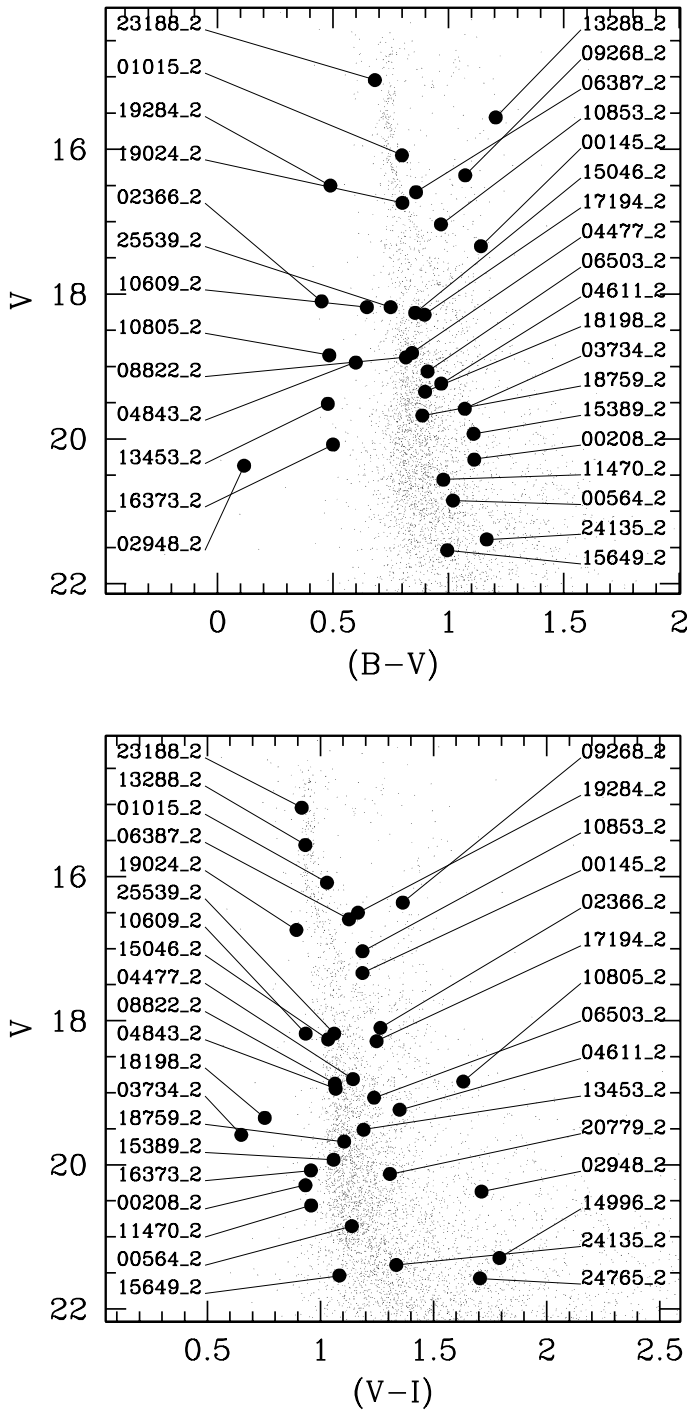

Figure 5.4: $B-V, V$ and $V-I, V$ diagrams of NGC 6253 with highlighted the contact binaries.

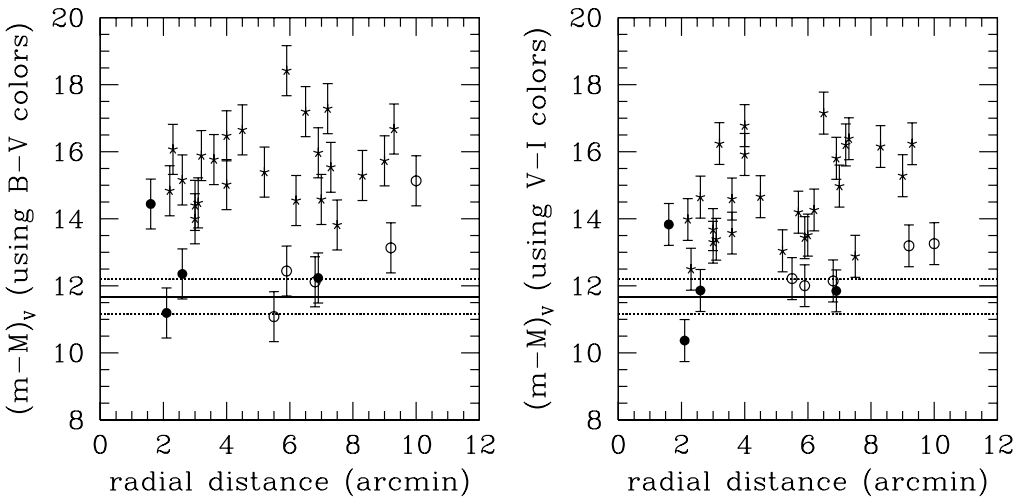

Figure 5.5: Distance moduli of all contact binaries found in chip 2 obtained using the *P-L-C* relations. We utilize both $(B-V)$ (left panel) and $(V-I)$ colors (right panel). The horizontal line represents the distance modulus of the cluster resulting from isochrone fitting. With filled circles we plotted the binaries with MPs>50%; open circles are stars with MPs<50%, starred points are bnaries with unknown membership. The errorbars are the errors associated with the M_V calculation and include errors in the colors determinations.

Information about membership can be obtained using the CMDs, the proper motion MPs and the two *P-L-C* relations. Results are not ever in agreement, therefore, in order to individuate the candidate members we summarize in Table 5.2.3 our results.

We retain the first four stars as members of NGC 6253, despite the last two ones have small MPs. The other cases will be discussed briefly one by one:

13288_2: wrong $(B-V)$?

06387_2: interesting case. The resulting distance moduli are too large because of the period of this star (P=0.92‘d). The light curve (see Figure 5.2.3) shows maxima at different heights. This variable could be a semi-detached system.

10805_2: wrong $(B-V)$?

17194_2: wrong $(B-V)$?

09268_2: this variable is probably located between us and the cluster.
19024_2: wrong $(B-V)$? It could be an EB-Type system (see Fig. 5.2.3).
19284_2: wrong $(V-I)$?
02366_2: wrong $(V-I)$?
We retain that the number of eclipsing contact binaries that belong to NGC 6253 is *at most* 12 objects (the number of missed EW-Type members into chip 1 and chip 3 is likely partially compensated by the number of doubtful cases in Table 5.2.3). Our estimate implies the (32±15)% of the EW–Type stars into the chip 2 are real members. Assuming that NGC 6253 has about 500-1000 members (Montalto et al. 2008, in preparation), this implies a frequency of a contact binary that range from 0.7% to 6%, with a mean value equals to 1.6%. Even if the uncertainties are large, our estimate is greater the that found for NGC 6791 (i.e.: 0.4±0.1%, see pag. 3.3.4); as explained in Chapter 3, the anti-correlation of the number of binaries with the richness, is probably due to the evaporation process of the lighter stars.

ID	Memb. (%)	CMD_{BV}	CMD_{VI}	PLC_{BV}	PLC_{VI}
23188_2	87	y	y	y	y
10853_2	78	y	y	y	y
01015_2	22	y	y	y	y
00145_2	0	y	y	y	y
13288_2	3	n	y	y	y
06387_2	85	y	y	n	n
10805_2	–	n	y	n	y
17194_2	–	n	y	n	n?
09268_2	87	n	n	y	n
19024_2	0	y	n	n	n
19284_2	0	n	y	n	n
02366_2	–	n	y	n	n

Table 5.3: List of contact binaries candidate members of NGC 6253. Columns are: ID, proper motions MPs, membership basing on the position on the $B-V, V$ CMD, on the $V-I, V$ CMD, and basing on the two *P–C–L* relations (using $(B-V)$ and $(V-I)$ colors respectively). The labels "y" or "n" indicate if a certain variable is a candidate member, or not.

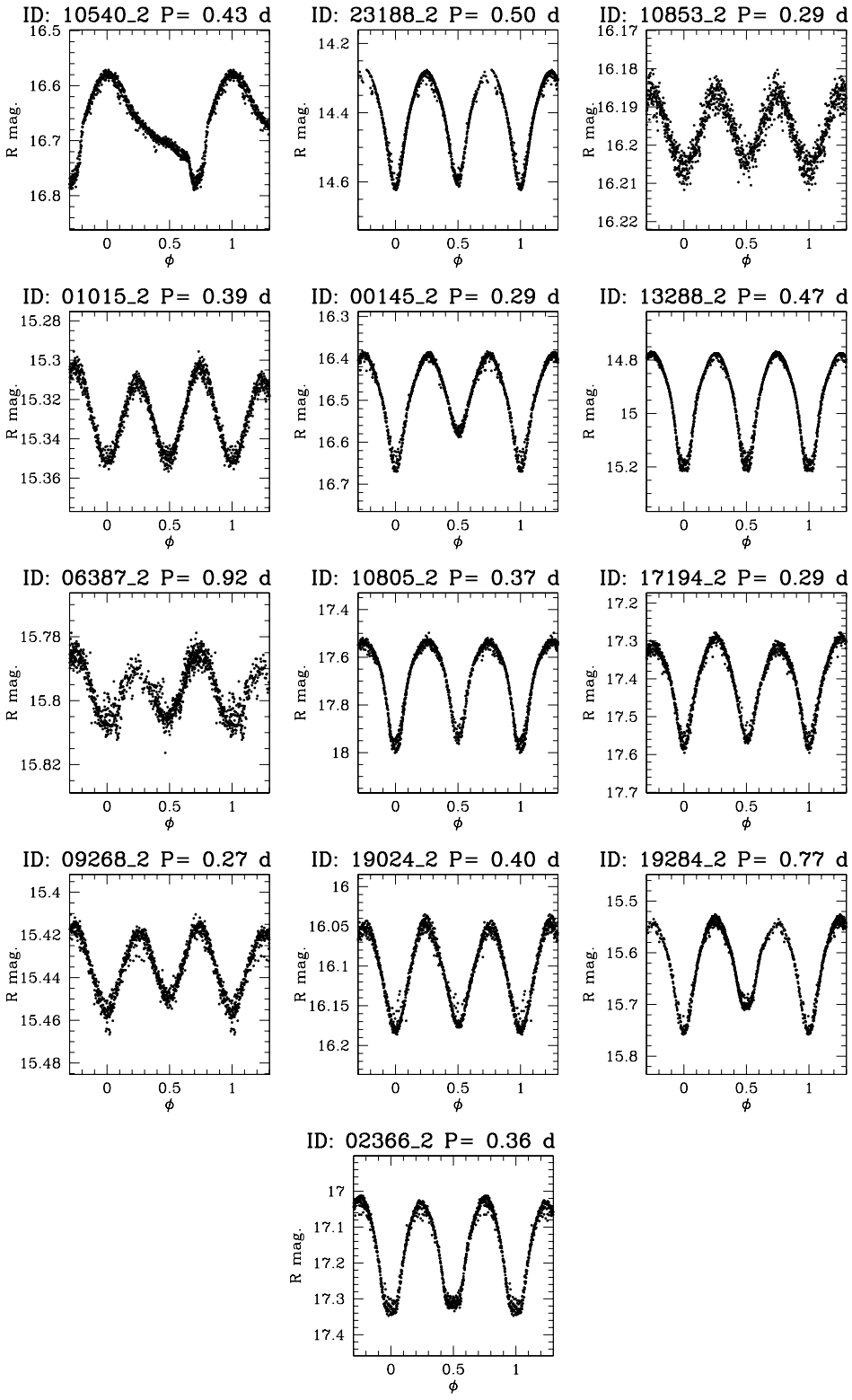

Figure 5.6: Phased light curves of the RRab star 10540_2 and of the contact binaries discussed in the text.

Table 5.4: List of eclipsing binaries.located near the MS T_0 is the time of minimum brightness.

Star	Type	α_{2000}	δ_{2000}	V	$< B-V >$	$< V-I >$	T_0	Period	Ampl.	Distance	Memb.
		[hrs]	[deg]	[mag]	[mag]	[mag]	[HJD-253100]	[d]	[mag]	arcmin	%
06539_2	EA	16.976877	-52.728415	18.891	1.039	1.480	70.727	0.68	0.19	4.4	–
16725_2	EA	16.984213	-52.590126	20.034	1.120	1.415	70.945	0.61	0.31	7.1	–
18853_2	EA	16.988134	-52.561751	21.330	1.371	2.092	72.613	2.65	0.75	9.0	–
01866_2	EA	16.976933	-52.793779	16.460	0.778	0.882	70.883	0.85	0.53	6.7	0
10340_2	EA	16.980457	-52.676389	16.514	0.844	1.099	72.051	1.82	0.02	3.0	38
19258_2	EA	16.979872	-52.556585	16.822	0.804	1.062	71.152	0.66	0.01	9.5	0
13573_2	EA	16.987514	-52.633374	17.120	0.798	1.022	71.039	2.30	0.34	4.7	8
02944_2	EB	16.990040	-52.778304	15.196	0.592	0.829	70.766	0.42730	0.37	5.1	0
00447_2	EB	16.979506	-52.814296	17.669	0.837	0.903	70.777	0.92	0.38	7.0	–
08123_2	EB	16.985958	-52.705800	21.108	1.287	2.288	70.883	0.31903	0.15	0.7	–
17502_2	EA	16.983360	-52.579913	22.146	–	2.563	70.855	0.55	0.44	7.7	–
01907_2	RSCVn	16.981108	-52.793187	17.388	0.934	1.260	71.352	1.34	0.15	5.5	0
26902_2	RSCVn	16.984060	-52.738899	15.198	0.768	1.019	72.090	2.18	0.05	1.9	90
25070_2	RSCVn	16.987598	-52.738510	19.335	–	1.507	71.953	1.46	0.06	2.4	–

Semi-detached and detached systems The field on which NGC 6253 is projected is heavily contaminated, therefore at fainter magnitudes (where MPs are not reliable) the identification of the MS is not easy. Here we take into account the EA/EB/RS-CVn variables: 10 of them are near the MS in both CMDs. They are: 26902_2 (MP=90%), 10340_2 (MP=38%), 13573_2 (MP=8%), 19258_2 (MP=0%), 01907_2 (MP=0%), 02944_2 (MP=0%), 06539_2, 08123_2 and 18853_2.

Other 5 variables are near the MS of only one CMD. They are listed in Table 5.4 together with the previous 10. For two of them, $(B-V)$ colors are not available. Their light curves are shown in Figure 5.2.3

The most part of them are non members, despite their position on the CMD.

16725_2 is a classical EA-type system with a period is 0.61 d. Despite its faintness (V=22.65 mag at the maximum brightness) its light curve is very well defined (see Fig 5.2.3) and shows clearly a secondary eclipse with an amplitude of about 0.04 mag. Its color could seem unusually blue (see Fig 5.7 but this is likely because of its associated error (the star is very faint) together with the intrinsic variability of the color.

The other EA-Type binary, 26902_2 is very likely an RS CVn-type star, its light curve shows clearly a narrow eclipse and a very complicated surface activity. It is located on the high binary sequence.

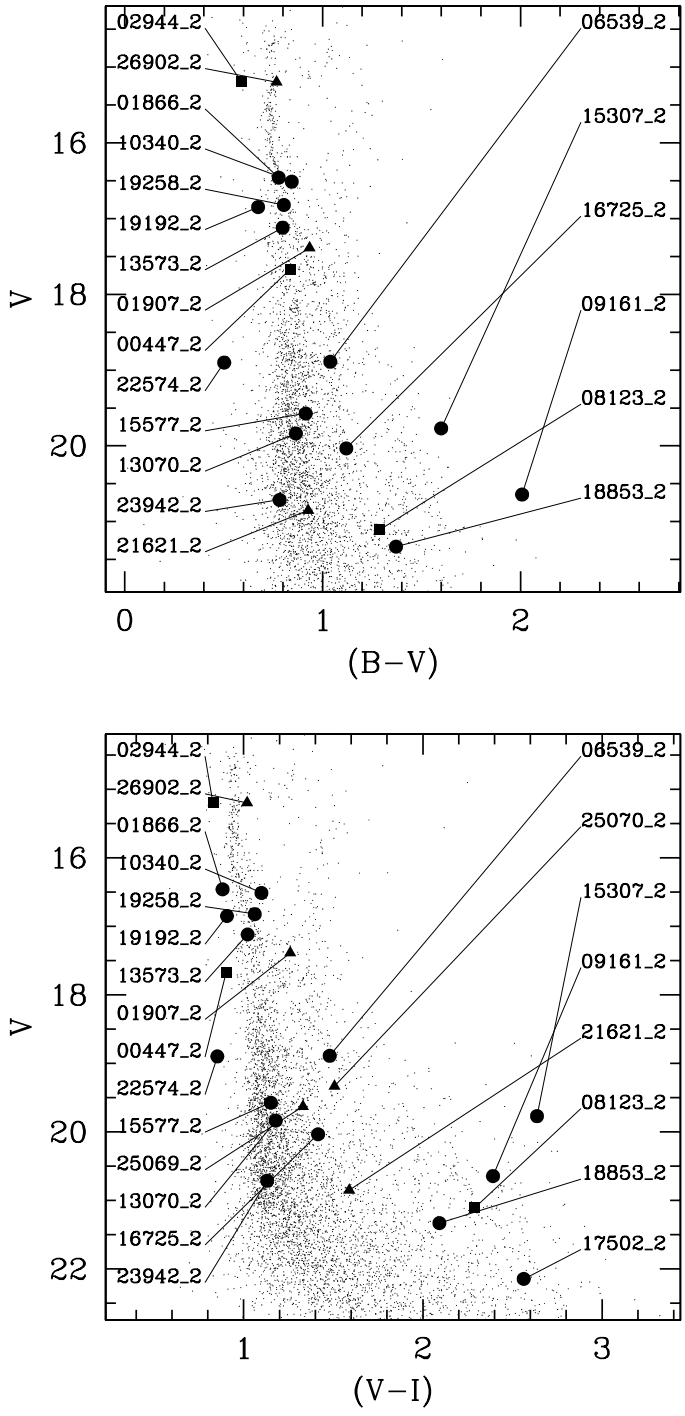

Figure 5.7: CMDs of NGC 6253 with highlighted the EA (circles), EB (squares), RS-CVn (triangles) variables.

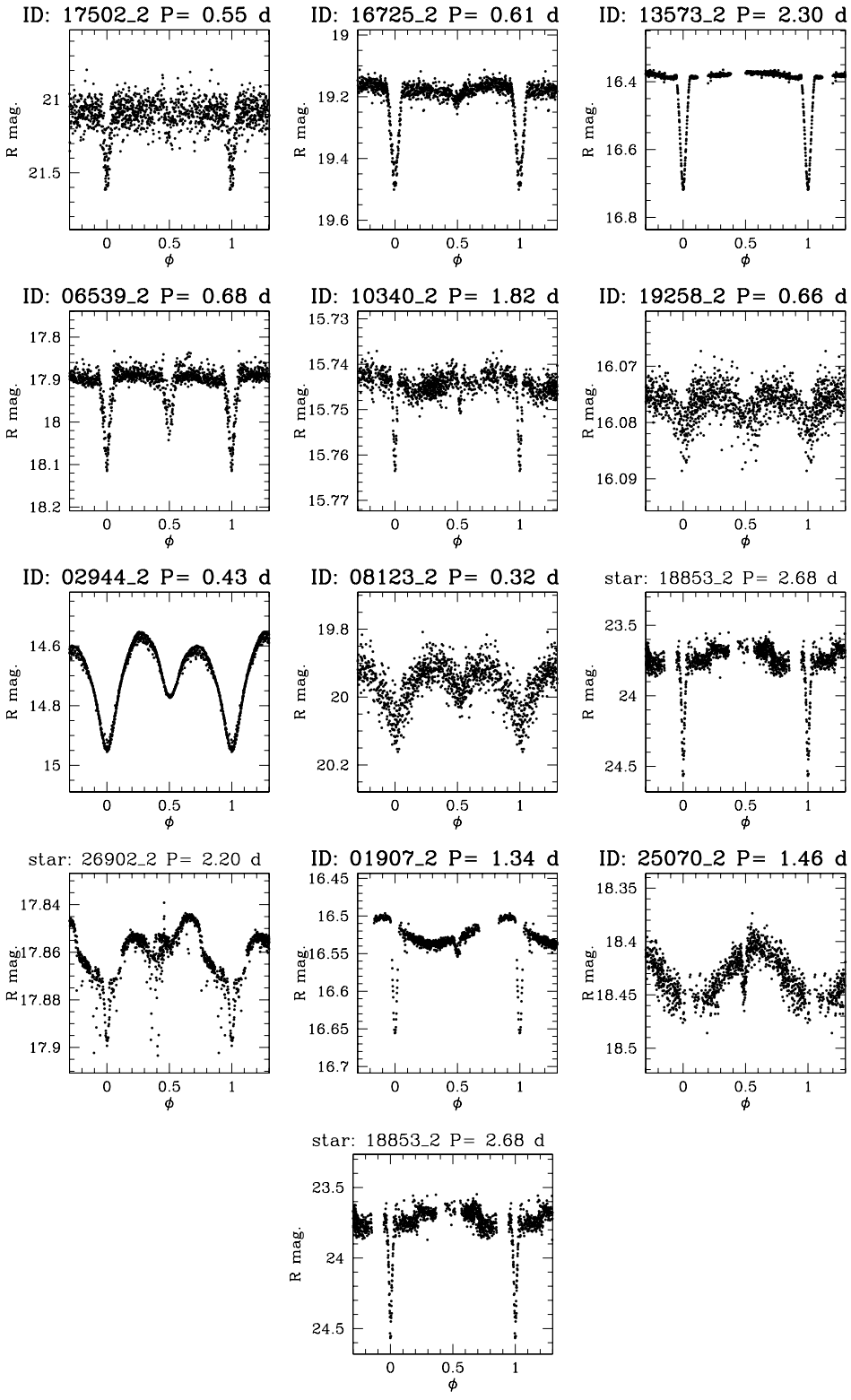

Figure 5.8: Phased light curves of the semi-detached and detached eclipsing binaries in NGC 6253.

Star	Type	α_{2000}	δ_{2000}	V	$< B-V >$	$< V-I >$	T_0	Period	Ampl.	Distance	Memb.
		[hrs]	[deg]	[mag]	[mag]	[mag]	[HJD-253100]	[d]	[mag]	arcmin	%
08284_2	RO1	16.983198	-52.703842	16.406	0.761	1.032	70.609	2.39	0.05	0.9	0
10042_2	RO2	16.984837	-52.679586	16.496	0.797	1.025	71.445	3.1	0.07	1.7	87
11077_2	RO2	16.990780	-52.666229	17.397	0.900	1.192	70.801	5.1	0.06	4.2	71
06932_2	RO2	16.987518	-52.722460	18.267	0.990	1.349	70.688	0.90	0.05	1.7	–
09775_2	RO2	16.990065	-52.683311	18.298	1.033	1.489	72.156	2.14	0.02	3.3	–
10372_2	RO1	16.978662	-52.675731	18.433	0.996	1.463	72.957	2.74	0.04	3.8	–
00455_2	RO2	16.985790	-52.814033	20.030	1.398	1.875	70.949	1.21	0.07	6.4	–
22278_2	RO2	16.976639	-52.665819	20.556	1.501	2.044	70.988	0.86	0.07	5.1	–
09901_2	RO2	16.982153	-52.681548	18.364	0.955	1.355	72.668	3.4	0.08	2.1	–
14911_2	RO1	16.981436	-52.615434	18.415	0.972	1.207	70.902	1.58	0.05	5.9	–
15993_2	RO1	16.989754	-52.600491	19.857	1.365	1.858	71.766	3.2	0.03	7.0	–

Table 5.5: Rotational variables located near to the MS. T_0 represents the time of the maximum brightness.

5.2.4 Rotational variables

Among the stars with MP$\geq$50% we classified as rotational variables 2 stars.

On both the CMDs of the cluster there are 6 rotational variables, while the remaining 4 are located on the MS of only one off the CMDs. Only two over 10 stars have MPs>50% 10042_2 11077_2 , both show non-sinusoidal light curves (see Fig. 5.2.4). CMDs with highlighted the positions of all rotational variables belonging to the chip 2 are plotted in Figure 5.9.

09901_2 shows three minima if phased with a period of P=3.36 d, we retain that it could be due to a complicate distributions of the spots on the surface.

The most part of these stars are probably non-member. The high level of fore/background contamination on NGC 6253 makes not improbable that several field variables lie serendipitously on the Main Sequence (MS) of the cluster.

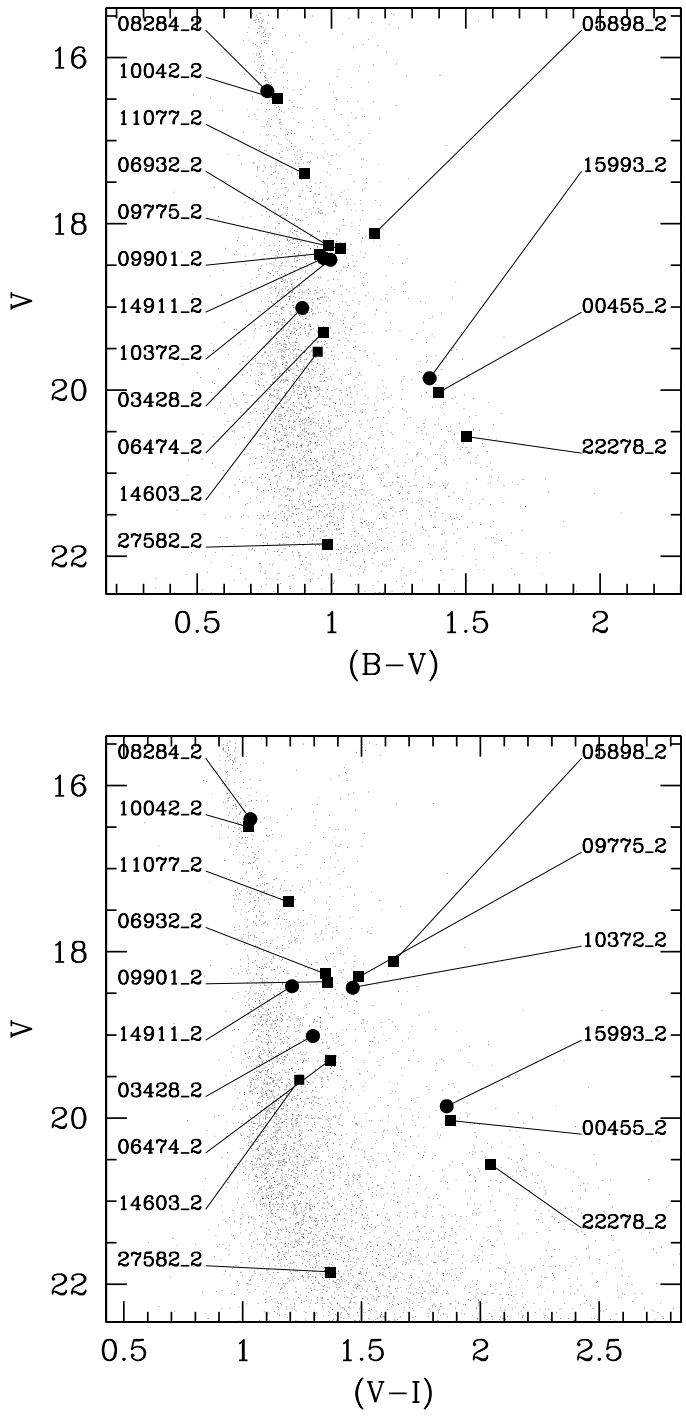

Figure 5.9: CMDs of NGC 6253 with highlighted the rotational single-wave (circles), and double-wave (squares) variables.

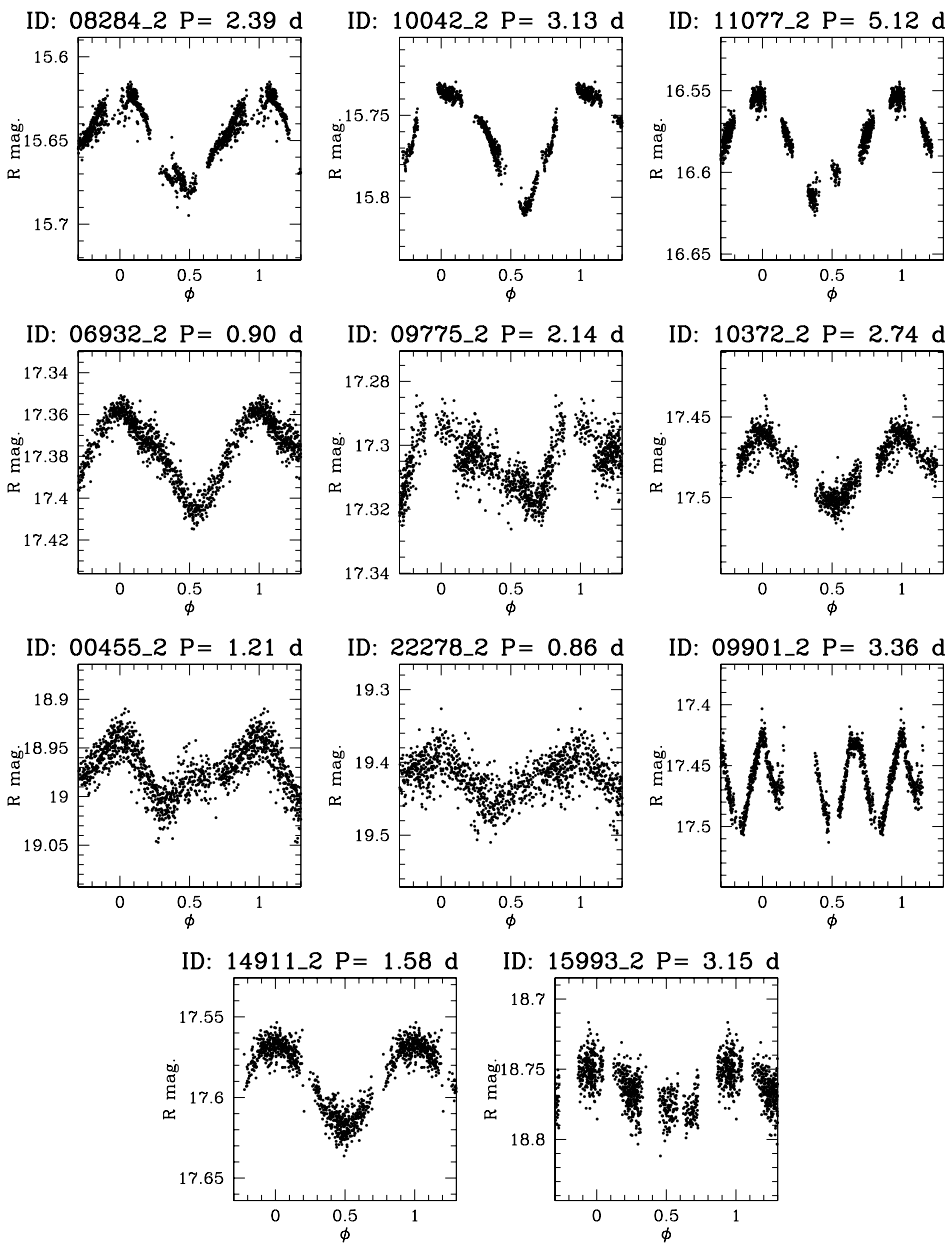

Figure 5.10: Phased light curves of the rotational variables located near to the MS. 10042_2 and 11077_2 are very likely members.

5.3 Peculiar objects

5.3.1 A possible candidate transit in the NGC 6253 field

Among the selected candidates variable stars, I found an interesting object 00434_2. Its light curve shows two well defined decreases in magnitude that remember planetary eclipses. The light curve is shown in Fig. 5.11, while its position on the CMD is plotted in Figure 5.12. The star is located slightly

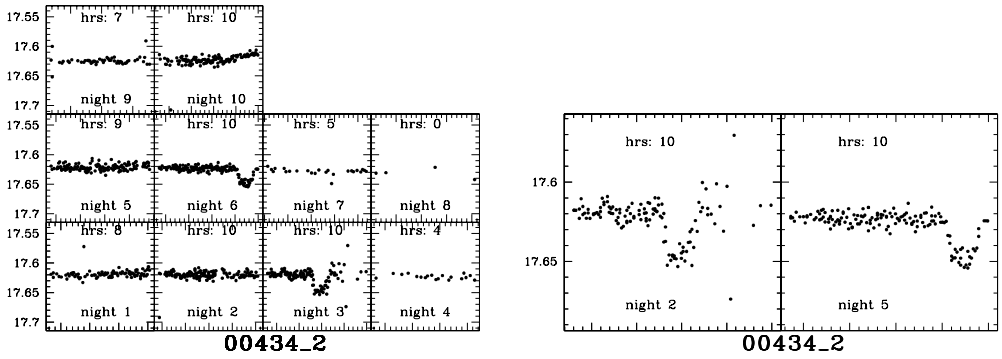

Figure 5.11: Light curve of the candidate transiting planet.

below the MS of the cluster and, for this reason, it was excluded by the sample of stars initially analyzed by M. Montalto with the BLS algorithm.

Successive application of the BLS algorithm to the whole dataset confirm the detection of this candidate at high significance level, and also identify additional candidates in the other chips, likely unrelated to NGC 6253. 00434_2 is located at 6.4 arcmin from the center of NGC 6253.

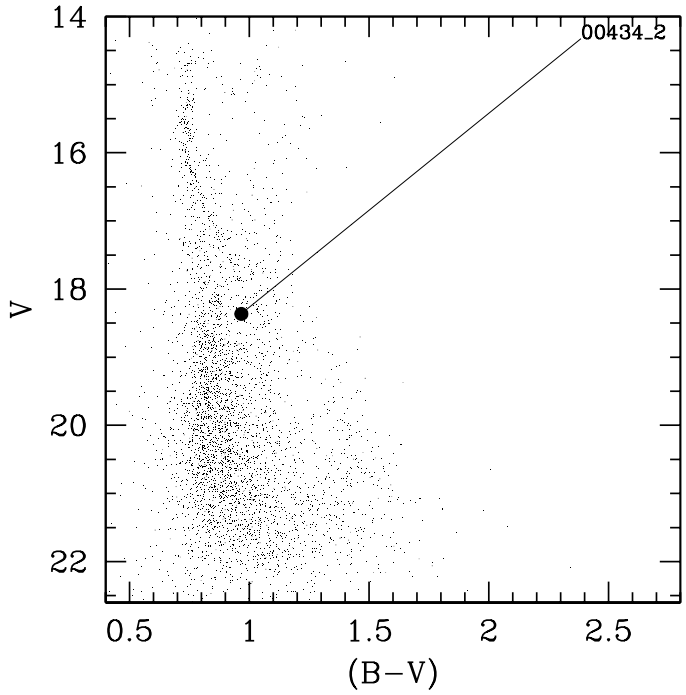

Figure 5.12: Position on the CMD of the candidate.

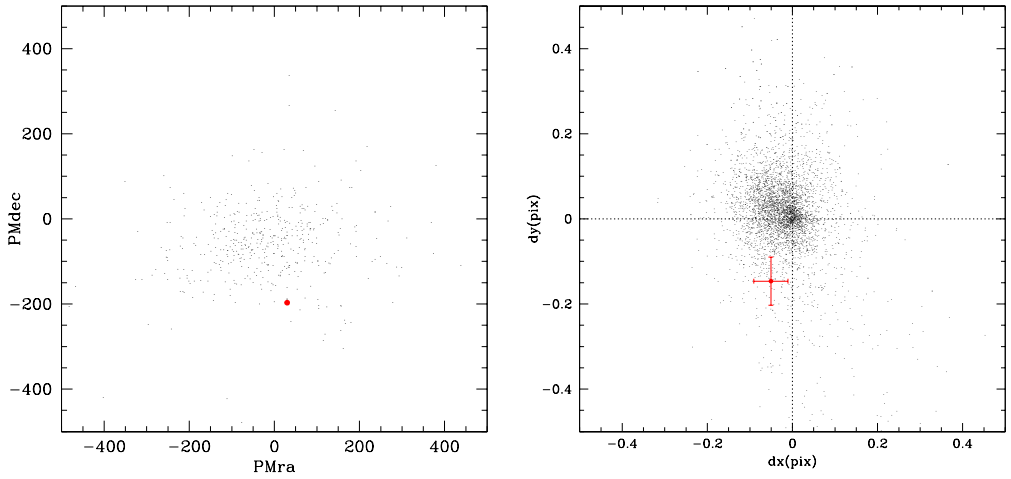

Figure 5.13: Light curve of the candidate transiting planet.

5.3.2 A candidate cataclysmic variable

Among our sample of variables there is another interesting object that could remember the U Geminorum 06289_9 described in Sect. 3.3.3. For this star,

15877_2.1, belonging to into chip 2 we know only its V mean magnitude (equals to 18.62 mag); its membership is unknown. The light curve is plotted in Fig. 5.14

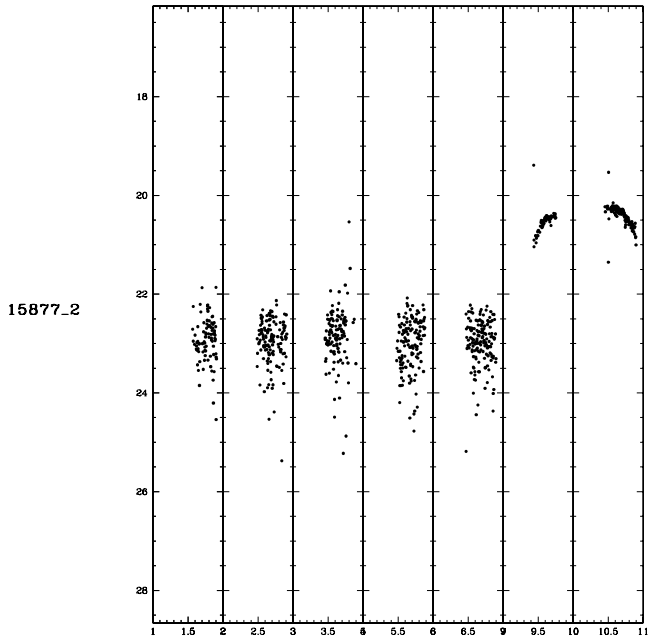

Figure 5.14: Light curve of the candidate U Gem cataclysmic variable.

The light curve present a nearby constant (and noisy) light curve during the first 8 days. During the two last days of the survey., its brightness in R-band increases of about 2.5 mag. The exact instant of the peak is not observed because it falls between the 9 and 10 nights.

Actually, a preliminary analysis of the light curve before the outburst, in order to find eventual oscillations, gave null results.

5.4 Discussion and conclusions

In this Chapter we described the first study about the variable stars content of NGC 6253. Few variables are members of the cluster. This is due to both

the small size of NGC 6253 and to the fact that our proper motion MPs are not reliable under the 18^{th} magnitude. Unfortunately, because of the saturation limit, we found no variable stars with V <15 mag (the turn-off is at V=14.5 mag), therefore, an analysis similar to that accomplished for NGC 6791 (Chapter 4) about the Blue and Yellow Stragglers is impossible using this database.

We discussed the variables that could be members basing on their position on $B-V, V$ and $V-I, V$ CMDs and on MPs (when available).

For the contact binaries we applied the usual P-L-C relations and we compare our results about membership with the ones obtained using proper motions. We found in general a good agreement: the most of the binaries with MPs<50% have also distance moduli uncompatible with that of the cluster.

The star 06387_2 is an interesting object: its MP is 85%, and it is located on the binary sequence, but, basing on the P-L-C relations, the resulting distance modulus (14.8 mag) is significantly greater than that of the cluster (11.7 mag) This excess is due to the period, significantly greater than that of other EW-type stars that belong to the cluster. Our hypothesis is that 06387_2 is a detached or semi-detached binary system and its components have different temperatures. Among the other variables, the only peculiar object is probably the RS CVn-type star 26902_2; it shows a peculiar profile of surface activity that suggests a complex distribution of spots.

We must remember that this survey is necessarily incomplete for two reasons: first, because probably a small number of members belong to the chip 1 and chip 3, as discussed at the beginning of this Chapter; on the other hand, there is a lack of information about variables located over the turn-off, due to the saturation limit. However, we retain that no more than some variables are undetected, among these there are surely pulsating variables, located into the BSS region.

We estimate that the number of EW-Type systems in NGC 6253 is at most one tenth of stars, that implies an incidence from 0.7% to 6% while for

NGC 6791, the same estimation gave (0.4±0.1)% (see Sect. 3.3.4). This is in accordion with the results found by K95 about the anti-correlation between binary stars frequencies and richness of the host clusters.

We retain that the number of eclipsing variables undetected because the incompleteness of the survey in NGC 6253 don't affect significantly our estimation.

It should be interesting to have information about the variables into the BSSs/YSSs region of NGC 6253; a comparison with the results found in NGC 6791 (see Sect. 4.4.2) could be useful to better know the nature of these stars.

Regarding the candidate transiting planet and the candidate cataclysmic variable, spectroscopic follow-up observations are planned using FLAMES at VLT: all the variables possible members and several other will be observed. Radial velocity and spectral classification will allow to refine the membership and better define the properties of the variables.

Chapter 6

Transits Simulations

There are several factors that influence the detection rates of extrasolar planets using the transits method: the geometrical probability that the transit will occur, the duration of the observations compared to transit duration and orbital period, and the photometric precision of the measurements.

In this chapter I will describe the transit simulator code that has been my specific contribution to the project on the search for planetary transits in NGC 6791 and NGC 6253 (Montalto et al. 2007 [75] and Montalto et al. 2008, in preparation). The transit simulator code has been used to:

- estimate the number of expected transit candidates;
- evaluate the transit detection efficiency (TDE) of the transit search algorithm
- investigate how the number of transiting planets variates for surveys of different number of observative nights and/or number of observative hours per night.

This code was applied to both NGC 6791 and NGC 6253 surveys.

6.1 The transit method: basic concepts

An occultation is the temporary diminution of the apparent brightness of a star that happens when another object transits in front of its disk, as viewed by the observer. This phenomenon has been longly observed for the planets of the Solar System and for eclipsing binary systems (see Sect. 1.2). The idea of detecting planets around other stars was discussed in the mid of the last century (Sturve, 1952 [103]), but was seriously taken into consideration after the detailed quantification of its possibilities by Rosenblatt (1971) [90] and Borucki & Summers (1984) [10].

The transiting planet is much cooler than its host star, this means that, differently to what happens to two stars eclipsing each others, for which primary and secondary occultations can be seen, only the dip caused by the transit of the small, cool planet in front of the parent star can be detectable.

The relative variation of the star brightness during the transit is proportional to the fraction of stellar surface subtended by the transiting object, and thus on the relative dimensions of the star and of the planet. The photometric measurement of the transit deepness leads ultimately to the knowledge of the size of the transiting object.

The transit duration, instead, depends on the stellar radius as long as on the orbital semi-major axis and inclination (see the next Section for the calculus that lead to this results). Once the star's physical properties have been characterized, accurate measurements of the transit duration and period provide a measure of the orbital period and of the inclination of the orbital plane.

Larger planets in closer orbits are much more easier to detect by means of the transit technique than planets with other characteristics. This because they cause deeper eclipses and more frequent transits. Typically, ground based transit surveys are targeted towards Hot-Jupiter planets (called also 51-Peg type objects or CGEPs, Close in Extra Solar Giant Planets), that are Jovian planets with orbital periods of a few days.

The amplitude of the photometric signal places a lower limit on the ratio

R_p/R_star of the planetary radius to stellar radius, while the duration of the event places a lower limit on the orbital period P and thus on the orbital radius a as well. If the inclination i is known, these lower limits become measurements. In principle it could be determined by fitting the wings of the transit profile in different wavebands using the known limb-darkening of the star, but in practice this will probably prove too difficult. Instead, multiple transits will be required to time the transits and thus measure the period P of the planet, from which the inclination can be determined from the known transit duration (Eq. 6.4). This makes the transit method most appropriate for large planets orbiting their parent stars at (relatively) small orbital radii a.

Transit surveys are complementary to the very successful radial velocity surveys, (which detects planets by means of the Doppler shifts in the spectra stellar lines caused by the motion of the star around the barycenter of the star-planet system), in the sense that it is possible to monitor thousands of stars simultaneously and at fainter magnitudes than what done spectroscopically acquiring informations on planetary processes also on distant environments. Planetary transits permit to determine the physical characteristics of planets such as the radius, the mass, (joining the $M\dot{\sin}i$ coming from radial velocities), and thus to derive the planet density. This allows to study the internal structure of planets and to better understand all the processes associated with planet formation and evolution

6.2 Mathematical background about planetary transits

In this section we will describe the simple model of planetary system, that we developed into the transit simulator code.

6.2.1 Transit duration

Let us consider a star of radius $R_\star$ and a planet of radius R_{pl} orbiting around it at a distance a. Our time baseline (about 10 d), coupled with the decreasing geometric probability of observing a transit, make nearby impossible to detect planetary systems with periods longer than this time coverage. The orbit of a planet with a period shorter than 10 d is likely circularized by tidal forces, thus in our model we will assume circular orbits. Moreover, by the fact that $\mathrm{M}_\star \gg \mathrm{M}_{pl}$, we will assume that the center of mass of the star–planet system is coincident with the center of the star. Finally, we consider only stars with a single planet.

We can parametrize the orbit of the planet with:

$$\begin{aligned} x &= a\cos\omega t \\ y &= a\sin\omega t \\ z &= 0 \end{aligned}$$

where ω is $2\pi/P$.

Let us calculate the same orbit, as could be seen by an observer at $\theta = (\pi/2 - i)$ degrees over the orbital plane.

We can write the rotation as:

$$\mathcal{R} = \begin{pmatrix} \cos\theta & 0 & \sin\theta \\ 0 & 1 & 0 \\ -\sin\theta & 0 & \cos\theta \end{pmatrix}$$

and the result is:

$$\begin{aligned} x' &= a\cos\omega t\sin i \\ y' &= a\sin\omega t \\ z' &= -a\cos\omega t\cos i \end{aligned}$$

We are interested only by y' and z' because the $y'z'$ plane is tangent to the celestial sphere and x' represents the direction of the line of sight. The orbit appears to us as an ellipse with semi–axes equal to a and $a\cos i$.

At each instant t, we can define a phase ϕ as:

$$\phi = \omega t = \phi_0 + \frac{2\pi\, s}{P} t \tag{6.1}$$

where ϕ_0 is arbitrary.

We now define $d(\phi)$ and p as:

$$d(\phi) = \frac{y'^2 + z'^2}{R_\star} = \frac{a}{R_\star}\sqrt{1 - \cos^2\phi \sin^2 i} \qquad p = R_{pl}/R_\star \tag{6.2}$$

$d(\phi)$ represents the projected star–planet distance normalized to the star radius (see Fig. 6.1).

The instants when a transit begins (or ends) correspond to $d = 1+p$, with the constraint that x' must be positive (otherwise we have an occultation of the planet by the star). The condition $d = 1 - p$ instead corresponds to the begin (or end) of the "flat" phase of a transit. This happens when the planet disc is entirely contained into the stellar disc, and , if we consider this latter as an uniform brightness source, we have that during this phase, the amount of brightness remains constant.

The transit duration is given by:

$$\Delta T = \frac{P}{2\pi}(\phi_2 - \phi_1)$$

where $\phi_{1,2}$ are given by the condition $d = 1 \pm p$:

$$\cos^2\phi_{1,2} = \frac{1 - \left[\dfrac{R_\star \pm R_{pl}}{a}\right]^2}{\sin^2 i} \tag{6.3}$$

Taking into account that the condition $x' > 0$ implies $\cos\phi > 0$, we have:

$$\Delta T = \frac{P}{\pi} \arccos\left[\frac{\sqrt{1 - \dfrac{(R_\star \pm R_p)^2}{a^2}}}{\sin i}\right] \qquad \text{with } \cos i \leq \frac{R_\star \pm R_{pl}}{a} \tag{6.4}$$

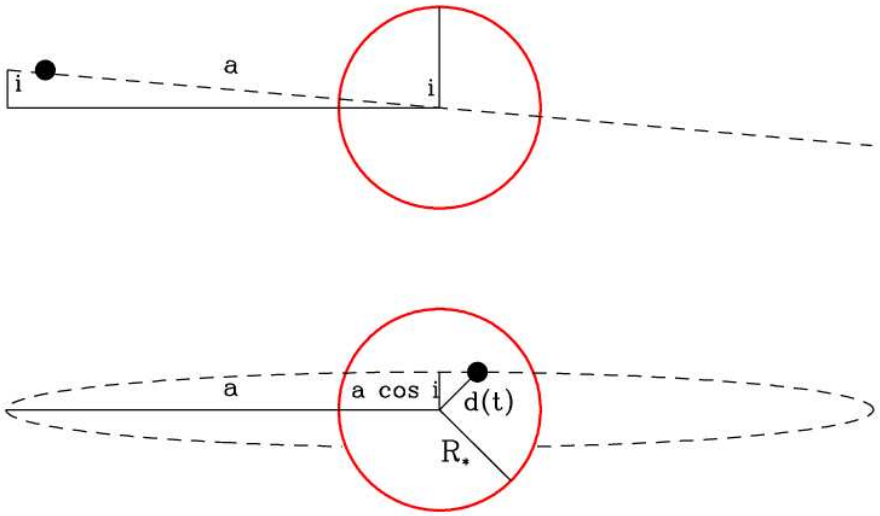

Figure 6.1: Representation of the model

The "$\pm$" notation is referred to the entire transit duration (taking the plus sign) or the "flat" phase duration (taking the minus sign).

6.2.2 Shape of the eclipses

Let us calculate the shape of the eclipse: we define $I(x)$ the specific intensity of the star disc, where $x = r/R_\star$ goes from 0 (center) to 1 (edge).

The depth of the eclipse at each instant is:

$$\Delta V = -2.5 \lg_{10} \left[1 - \frac{F_p}{F_\star} \right] \tag{6.5}$$

where

$$F_p = \int I(x) dA \qquad F_\star = 2\pi \int_0^1 I(x)\, dx \tag{6.6}$$

and the first integral is evaluated over the star's obscured area (that depends by $d(\phi)$).

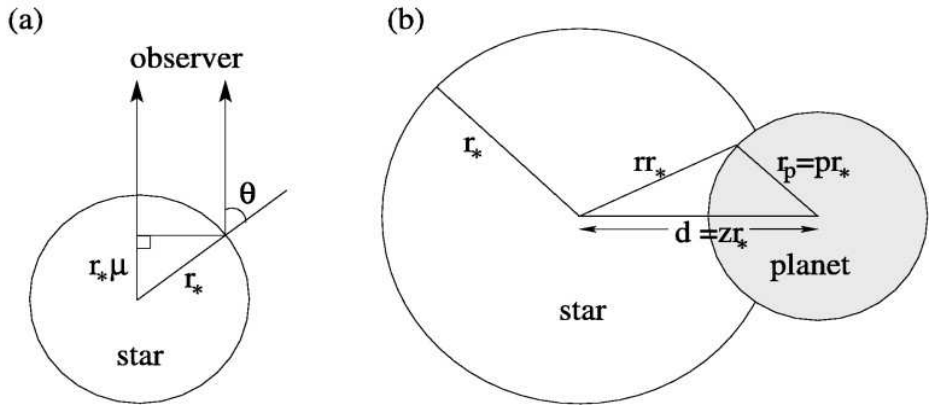

Figure 6.2: *a)* Geometry of the limb–darkening and *b)* geometry of a star–planet system as seen by the observer. Figure taken from Mandel & Agol (2002) [59].

Uniform brightness star disc

If we consider the star as an uniform brightness source ($I(x)$ equals to a constant) , in this case, the obscuration as a function of $d(\phi)$ can be evaluated by means of geometrical considerations (see Fig. 6.2).

The results are:

$$\begin{cases} \dfrac{F_p}{F_\star} = 0 & d(\phi) > 1+p \\ \dfrac{F_p}{F_\star} = \dfrac{p^2}{\pi}\arccos\left[\dfrac{p^2+d(\phi)^2-1}{2pd(\phi)}\right] + \dfrac{1}{\pi}\arccos\left[\dfrac{1-p^2+d^2(\phi)}{2d(\phi)}\right] + & \\ -\dfrac{1}{2\pi}\sqrt{4d^2(\phi)-(1+d^2(\phi)-p^2)^2} & |1-p| < d(\phi) \leq 1+p \\ \dfrac{F_p}{F_\star} = p^2 & d(\phi) \leq 1-p \end{cases} \tag{6.7}$$

where $d(\phi)$ and p were defined in Equation 6.2. The first equation does not modifies the light curve (no transit), the second is referred to the "grazing" phase and the last is relative to the "flat" phase.

Limb Darkening

A "real" stellar disc shows no uniform brightness, this is due to the fact that the light that we observe at the center of the disc comes from hotter regions of the star than the light that come from the edges. This effect is commonly known as "limb–darkening" (LD).

For our purposes, it is necessary to create artificial transits the more realistic as possible, and we take into account the LD effect.

Several models for the LD were developed, we adopted the non–linear, four–parameters empirical model of Claret et al. (2000) [20] that assumes

$$\frac{I(\mu)}{I(1)} = 1 - \sum_{1}^{4} a_k \, (1-\mu)^{k/2} \tag{6.8}$$

where $\mu = \cos\theta$ is the cosine of the angle between the normal to the stellar surface and the line of sight of the observer (see Fig. 6.2, and a_k are numerical coefficients that depend upon V_{turb} (micro–turbulent velocity), metallicity, T_{eff}, and the spectral band. The coefficients are available at CDS from the ATLAS calculations.

LD influences the shape of a transit in this way: when a planet transits over the edge regions of the star disc, the loss of light is modest with respect the uniform brightness case. Instead, when the planets covers the central regions of the disc, the flux decrease is more conspicuous. An example is represented in Fig. 6.3 where we consider a Jupiter–like planet around a Sun–like star with a period of 3 d. We put i=90 degrees (left panel) and i=83 degrees (right panel, grazing eclipse). The brightness variations were evaluated by means of Equations 6.7 (dotted lines), and numerically considering the LD effect (Equations 6.5, 6.6 and 6.8; solid lines).

6.3 Transits simulator code

In this section we will describe in details the procedure that we follow in order to estimate the number of transiting planets into the observing window, the

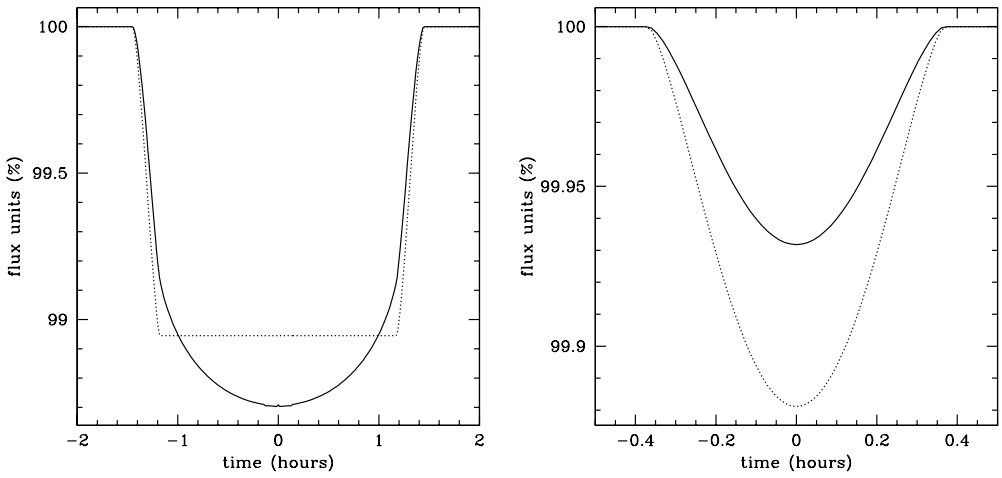

Figure 6.3: Representation of two transits: central (left panel) and and grazing (right panel), in both cases we consider the LD (solid line) or the uniform brightness disc case ($I(x)$ constant, dotted line). The adopted parameters are $M_\star$=$M_\odot$, $R_\star$=$R_\odot$, M_{pl}=M_J, R_{pl}=R_J, P=3 d.. The inclinations are i=90 degrees (central) and i=83 degrees (grazing).

Transit Detection Efficiency (TDE) for the transit search algorithm, and the level of confidence of our final results.

6.3.1 Basic assumptions

To estimate the number of planetary transits expected in our survey, it is mandatory to include in the simulations appropriate estimate for planet frequency, distributions of planetary parameters (mass, period, radius) and realistic stellar masses and radii. As the main goal of the survey is to look for possible effects on the occurrence of planets caused by the cluster environment, the natural choice is to adopt the distributions resulting from field stars. In the following we describe how our fiducial parameters and distribution are derived from literature data.

For the transit search in both clusters we worked on two samples of light curves:

- **Artificial light curves**, obtained as described in in Sect 6.3.3; into

these light curves we will insert artificial planetary transits. For NGC 6791 this sample is composed by 7722 light curves, while for NGC 6253 the stars are 2000.

- **Real light curves**: our search is limited to the main sequence stars only , therefore, for NGC 6791, 24 bins of 0.2 magnitudes were considered in the interval 17.3< V <V=22.1 mag. Inside each bin,a robust mean of all of the $(B-V)$ colors was calculated, and we consider only the stars with colors $(B-V)-<B-V>$<0.06 mag. The selected stars were 3311. Regarding NGC 6253, the selected stars (using our own proper motions membership probabilities) were 671.

At the end of the procedure, all results obtained working on the first sample, were calibrated to the reference number of Main Sequence Stars (second sample) in order to compare the simulations with the transit search.

Frequency of planets

The frequency of planets in radial velocity surveys results strongly correlated to the metallicity of the host stars (FV05). The best-fit found by FV05 is:

$$P = 0.03 \times 10^{2.0[Fe/H]} \qquad \text{with } -0.5 < [Fe/H] < 0.5 \tag{6.9}$$

and it is represented graphically in Figure 6.4 (taken from FV05).
where P is the probability of formation of giant planets with orbital period shorter than 4 yr and radial velocity semi-amplitude $K > 30$ ms^{-1}.around solar-type stars.

The number of stars with a giant planet with $P < 9$ d can be estimated considering the ratio between the number of the planets with $P < 9$ d and the total number of planets from Table 3 of FV05 (850 stars with uniform planet detectability). The result is $0.22^{+0.12}_{-0.09}$. Therefore, taking into account Equation 6.9 and its correction, the fraction of stars with a planets with P <9 d in our target clusters (assuming [Fe/H] ranging from +0.39 to +0.47) is expected to be between 3.5% and 5.7%.

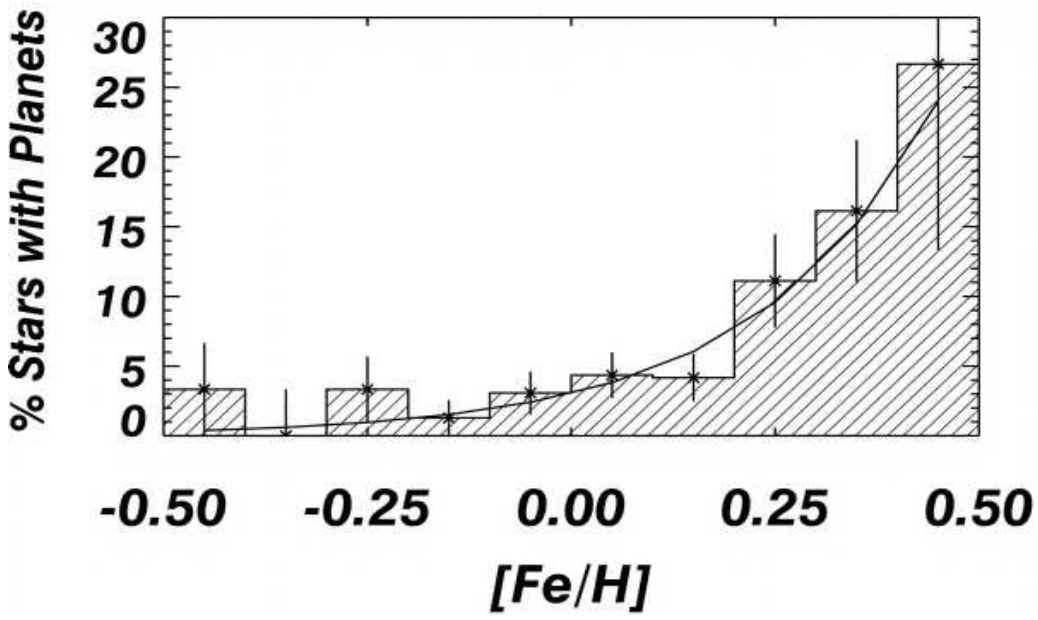

Figure 6.4: Probability that a star has a planet as a function of its metallicity, the continuous curve represents the Equation. 6.9 (Figure taken from FV05.

This is significantly larger than that resulting from unbiased samples (∼0.7%), confirming the motivation of surveying metal-rich open clusters to explore the environment effect on planet formation.

The metallicity of our target has still significant uncertainly, then, for NGC 6791 we considered three different values for the metallicity: low ([Fe/H]=+0.19); intermediate ([Fe/H]=+0.39, Carraro et al. 2006 [16]) and high ([Fe/H]=+0.47, Taylor, 2001 [104] Gratton et al., 2006 [39]); making three independent simulations.

For NGC 6253 we considered two cases: [Fe/H]=+0.36 (Sestito et al. 2007 [97]; Carretta et al. 2000 [17]) and [Fe/H]=+0.46 (Carretta et al. 2007 [18]).

Planetary parameters

To estimate the physical planetary parameters (mass, radius, period) we used the information obtained by previous planetary surveys.

- **Radius** The actual distribution of planetary radii has a very strong impact on the transit depth and therefore on the number of planetary transits we expect to be able to detect.

  Gaudi (2005) [33] suggests for the close-in giant planets a mean radius R_p=1.03 with a dispersion of 0.2 R_J. We have considered three cases:

  1. R_{pl}=(0.7±0.1) R_J: (HD 149026b, R=0.72±0.03 R_J; Sato et al. 2005 [96]).
  2. R_{pl}=(1.0±0.2) R_J best estimation (Gaudi, 2005 [33]).
  3. R_{pl}=(1.4±0.1) R_J (HD 209458b, R=1.35±0.07 R_J Wittenmyrer et al. 2005 [111]).

  assuming a Gaussian distribution for R_{pl}.

- **Mass** Regarding the planetary masses, we simply adopt M_{pl}=1 M_J because the effect of planet mass on transit depth or duration is negligible.

- **Period** The periods distribution was taken from the data for planets discovered by radial velocity surveys, reported in the Extrasolar Planets Encyclopedia[1]. We selected the planets discovered by radial velocity surveys with mass $0.3M_J \leq M_{pl} \sin i \leq 10M_J$ (the upper limit was fixed to exclude brown dwarfs; the lower limit to ensure reasonable completeness of RV surveys and to exclude Hot Neptunes that might have radii much smaller than giant planets, Baraffe et al. 2005) and periods $1 \leq P \leq 9$ d. We assumed that the period distribution of RV planets is unbiased in this period range. We then fitted the observed period distribution with a positive power law for the Very Hot Jupiters (VHJ, $1 \leq P \leq 3$ d.) and a negative power law for the Hot Jupiters (HJ, $3 < P \leq 9$ d).. As constraint we assume the ratio $r_{12}=N_{VHJ}/N_{HJ}$ equal to 0.07 as suggested by Gaudi et al. (2005) [34]. Our fiducial best–fit is shown in Fig. 6.5.

[1] `http://exoplanet.eu/index.php`

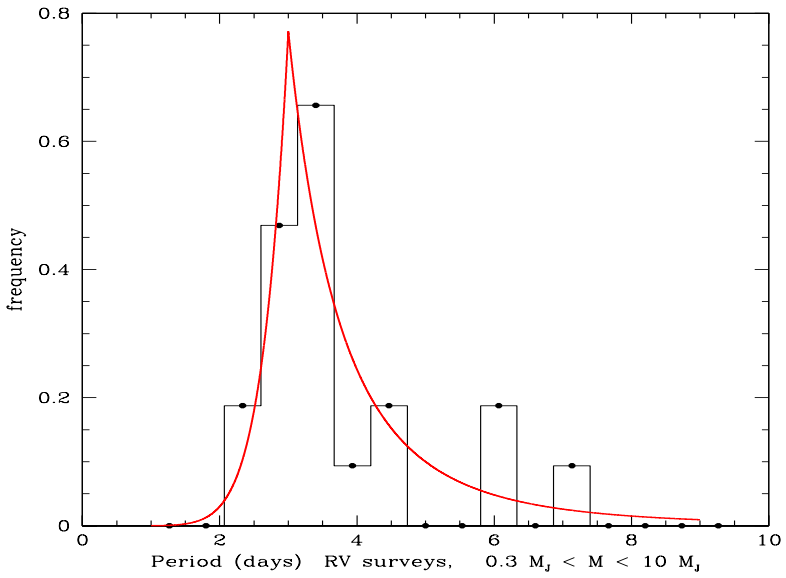

Figure 6.5: Continuous line: adopted distribution for planet periods. Histogram: RV surveys data (from the Extrasolar Planets Encyclopedia).

Stellar parameters

We started selecting a subsample among the artificial light curves, accordingly to the luminosity function of the main sequence of both clusters. The luminosity function of the MS of NGC 6791 is reported in Figure 6.6), while, for NGC 6253 the distribution in magnitudes of the MS stars was nearby constant in the range considered.

Now, we need to know for each star an estimate of its mass and radius; this was made by fitting theoretical isochrones from Girardi et al. (2002) [38] to the observed color magnitude diagram of both clusters.

For NGC 6791 we referred to the photometric catalog of Stetson et al. (2003) [102] and our best fit parameters are (see Fig. 6.7): age=10.0 Gyr, $(m-M)_V$=13.30 mag, $E(B-V)$=0.12 mag and Z=0.040 corresponding to [Fe/H]=+0.18

The value adopted for the metallicity could be too low, but, making other best–fits with different values of Z, we noticed that the discrepancies among

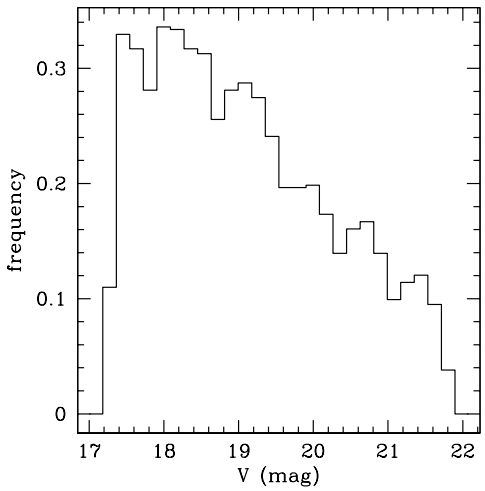

Figure 6.6: Luminosity function (V band) of the MS of NGC 6791

.

the resulting masses and radii were scarcely dependent from this parameter with respect to others (e.g. age and distance modulus), therefore, we adopt this value.

For NGC 6253 we fitted our own data with these parameters: age=2.3 Gyr $(m-M)_R$=12.4 mag, $E(V-R)$=0.30 mag, and Z=0.040 (see Fig. 6.8).

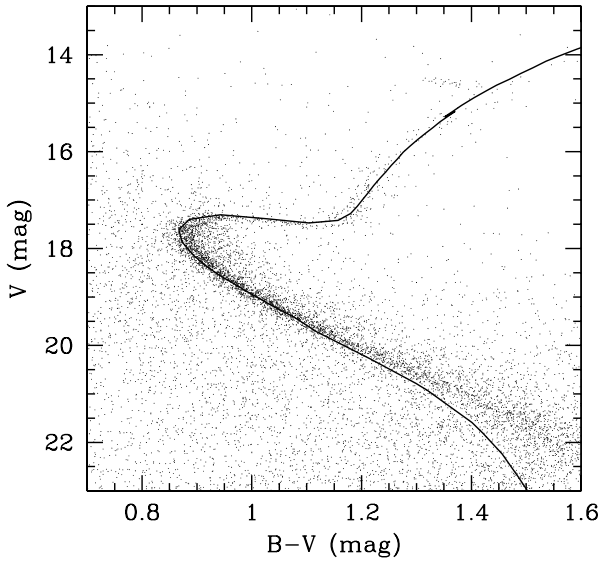

Figure 6.7: Padova stellar isochrones superimposed to the $V, B-V$ CMD diagram of NGC 6791.

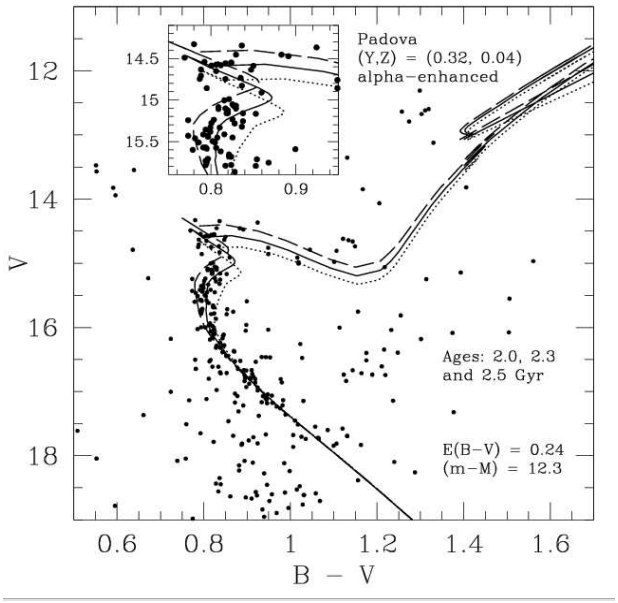

Figure 6.8: Padova stellar isochrones superimposed to the $V, B-V$ CMD diagram of NGC 6253.

From the best–fit isochrone, for each star, we obtained values for mass and radius (with the hypothesis that each of them belongs to the cluster) as a function of its visual magnitude for NGC 6791 and for R magnitude [2] for NGC 6253. The trends of mass and radius as a function of the apparent magnitudes for both clusters are plotted in Fig. 6.9). the mass range explored on NGC 6253 is larger than that of NGC 6791 because of younger age.

6.3.2 Number of expected transiting planetary systems

We started considering the sample of artificial light curves representative of the MS. Assuming that the probability P (given by equation 6.9) that a star have a planet is independent from its mass or radius, we randomly selected a number of stars corresponding to the fraction given by the relation of FV05 (Equation 6.9) weighted by the factor 0.22 (see Sect. 6.3.1).

Now, we must select the planetary systems with an inclination angle i compatible with detectable transit events, therefore we assign to each object of this subsample a planet with mass, radius and period randomly selected from the distributions described above. Moreover, we assign an inclination angle i randomly chosen with $0 < \cos i < 1$, with a uniform distribution in $\cos i$.

We consider only these systems for which

$$\cos i \leq \frac{R_\star + R_{pl}}{a}$$

is verified (transiting systems). The selected subsample (about 10% of the previous subsample) represents the object of our interest. Now, we must estimate how many transits fall into the observative window. With this purpose, at each star of them we assigned an initial phase ϕ_0 randomly

[2] We would point out that, interpolating a main sequence, one can obtain masses and radii from only the magnitude (or the color). In our case, using the magnitude, the values for reddening adopted are ininfluent for our results.

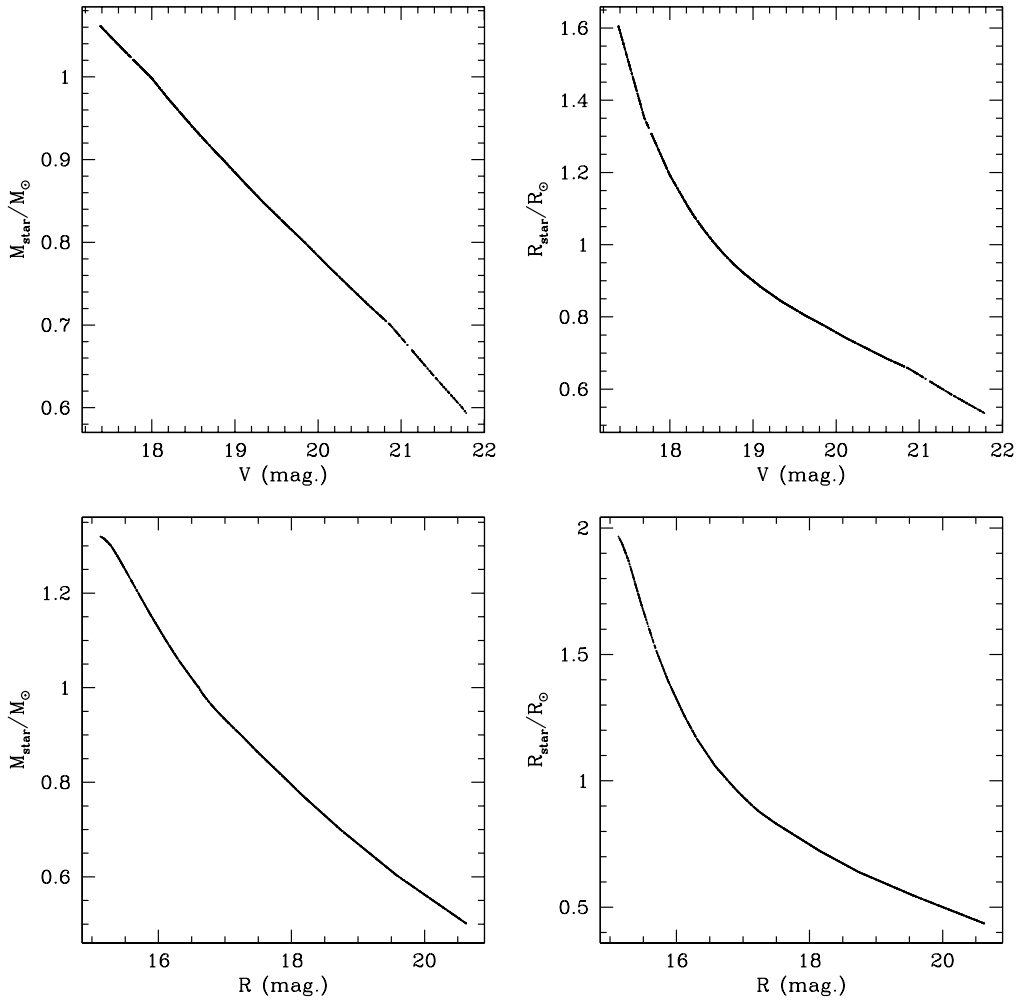

Figure 6.9: *Left*: $M_\star/M_\odot$ vs. apparent magnitude. *Right*: $R_\star/R_\odot$ vs. apparent magnitude for the MS stars of NGC 6791 (top) and NGC 6253 (bottom).

chosen from 0 to 2π rad and a random direction of orbital revolution (equals to ± 1, clockwise or counter-clockwise). Having fixed the planet parameters (P, i,ϕ_0, M_p, R_p, a), the star's parameters ($M_\star$, $R_\star$), for a given artificial light curve (t_i , V_i) it is now possible to derive the position of the planet with respect to the star at each instant from the relation

$$\Phi_i = \phi_0 + \frac{2\pi}{P} t_i$$

where ϕ_i is the angle between the star–planet radius and the line of sight. The positions were calculated at all times t_i for each star. When the planet is transiting the star (i.e.: when $d(\phi) < (R_{pl} + R_\star)$), the light curve is modified, by calculating the corresponding brightness variation $\Delta V(t_i)$, as explained in Sect. 6.2.2.

Thus, being now interested only to statistical numbers (number of planets that *make* transits into the observing window), the shape of a transit is inessential, and to speed up the routine, in this case we consider not the LD and we applied directly Equations 6.7.

Once transits where inserted, we evaluate the following quantities:

- number of planets that make transits (thanks to their inclination angles): N_{geom};
- number of planets that make one or more transits in the observing window: N1+
- number of planets that make one single transit in the observing window: N1;
- number of planets that make at least two transits in the observing window: N2+;

and so on, with N3, N3+, etc.

Transits were considered only if at least the 50% of their duration was included into an observative night.

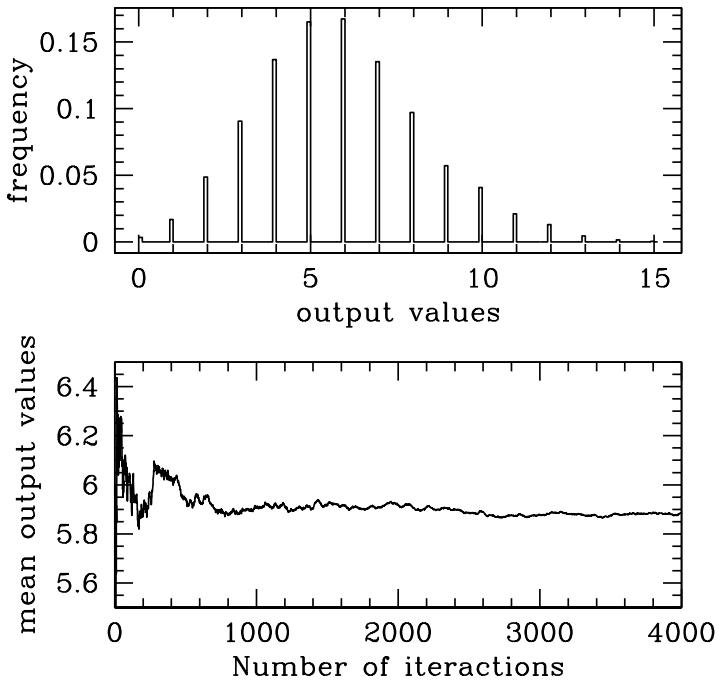

Figure 6.10: *Top* Frequency for different results for N1+ (uncalibrated) the distribution is a Poissonian, here quite similar to a Gaussian because the relatively high value of <N1+>. *Bottom*: Mean value of N1+ (uncalibrated) as a function of the number of iteractions.

We iterate this procedure N times (with N greater than 3000, see below), and we evaluated the mean values of N_{geom}; N1+, N1, N2+..

Finally, the results of our simulations were calibrated to the reference values of 3311 stars and 671 stars (for NGC 6791 and NGC 6253 respectively, see above).

In Figure 6.10 we show, as an example, the mean value of N1+ (uncalibrated) as a function of the number of iteractions (bottom), and the distribution of the expected value over all iteractions (top). Other parameters have a similar trend. As regard the number of iteractions, we can see that for $N \gtrsim 3000$ the mean value becomes stable.

6.3.3 Calculating the TDE

To detect transits in our light curves we adopted the BLS algorithm by Kovács et al. (2002) [54]. This technique is based on the fitting of a box shaped transit model to the data. It assumes that the value of the magnitude outside the transit region is constant. It is applied to the phase folded light curve of each star spanning range of possible orbital periods for the transiting object, (see Table 4). Chi-squared minimization is used to obtain the best model solution.

The TDE is a measure of the probability that an algorithm correctly identifies a transit in a light curve, and the False Alarm Rate (FAR) is a measure of the probability that an algorithm identifies a feature in a light curve that does not represent a transit, but rather a spurious photometric effect.

In order to evaluate the FAR, artificial stars with constant magnitude were added to each image, according to an equally-spaced grid of 2× PSFRADIUS+1, (where the PSFRADIUS was the region over which the Point Spread Function of the stars was calculated. This procedure was applied to the images of both clusters.

We took into account the photometric zero-point differences among the images, and the coordinate transformations from one image to another. 7722 and 2000 stars were added on the images relative to NGC 6791 and NGC 6253, respectively. In order to assure the homogeneity of these simulations, the artificial stars were added exactly in the same positions, (relative to the real stars in the field), for the other sites. The entire set of images was then reduced again with the procedure described in Sect. 2.2. This way we got a set of constant light curves which is completely representative of many of the spurious artifacts that could have been introduced by the photometry procedure. We then applied the algorithm to the constant light curves of both clusters. This simulation yielded a FAR of 0.10%.for both clusters. An error of 0.04% associated to the FAR was estimated by repeating the whole procedure 4 times and slightly shifting the positions of the artificial

stars. Running the transit search procedure on the 3311 and 671 selected main sequence stars, we expect 3.3±1.3 and 0.7 ± 0.3 false candidates (for NGC 6791 and NGC 6253 respectively).

Simulations

The procedure followed to determine the TDE is near identical to the one shown in Sect. 6.3.1

The differences are three:

- we need of a conspicuous number of light curves with artificial transits added, therefore we put two simply constraint at the very beginning of the procedure: P=100% (all stars have a planet), and $0 < \cos i < 0.1$ (with uniform distribution in $\cos i$) in order to obtain that about 85% of the stars can make transits;
- the transits must be realistic: variations of the flux due to the transits were calculated taking into account the LD effect as described in Sect. 6.2.2;
- only one iteration is necessary.

We report some examples of the simulations; in Fig. 6.11 we show a portion of a light curve before (top) and after (bottom) the insertion of a transit.

In Fig. 6.12 we plotted the distributions of transit durations and depths as regard the planetary radii; we assumed $R_{pl} = (1.0 \pm 0.2)\ R_J$) with gaussian distribution.

We show also $R_\star$ as a function of the transits depths (in this case we putted $R_{pl} = 1.0\ R_J$ without dispersion), the points located on bottom–left of the figure represent grazing eclipses.

Having the sample of light curves with transits added, we selected only the ones for which there was at least a half transit inside an observing night and applied our transit detection algorithm. We considered the number of light curves that exceeded the thresholds, and also determined for how many

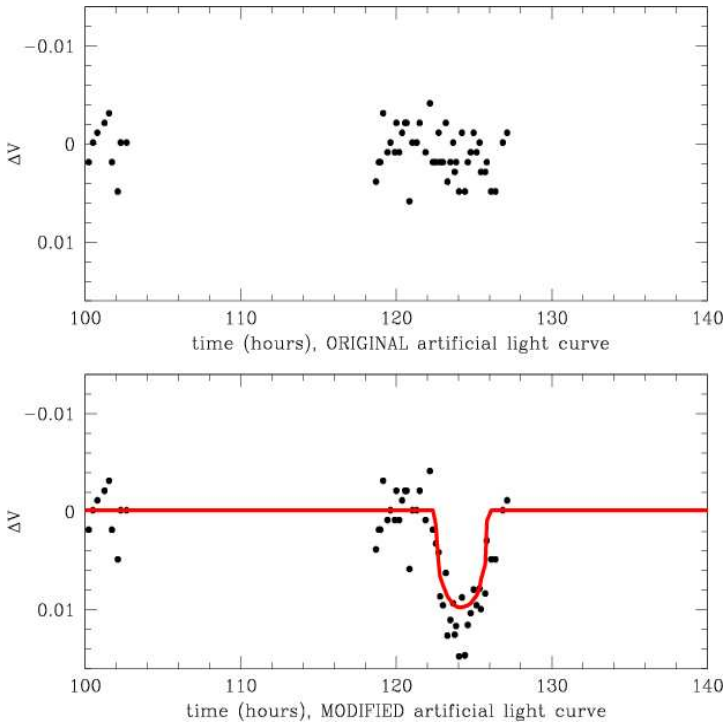

Figure 6.11: *Top*: original light curve. *Bottom*: the light curve after insertion of a transit. The solid line represents the transit model

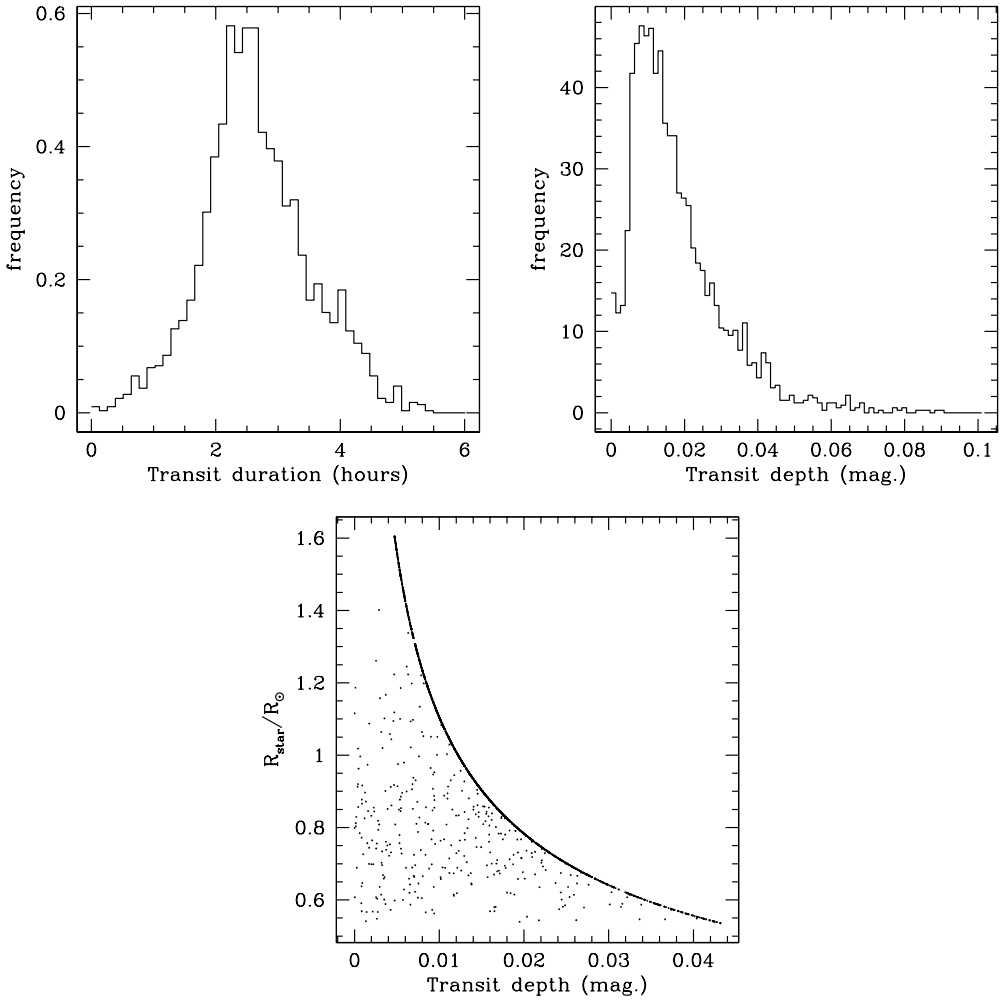

Figure 6.12: Distribution of the transit durations and depths for a set of light curves. Transit depth as a function of the stellar radius (assuming R_{pl}=R_J)

of these the transit instants were correctly identified on the unfolded light curves.

We isolated three different outputs (see M07, Sect. 7.4 for details):

- Missed candidates: the light curves for which the algorithm did individuate no transits, or if it did, the epochs of the transits were not correctly recovered;

- Partially recovered transit candidates: the algorithm identify at least one of the transits that fell in the observing window.

- Totally recovered transit candidates: All the transits that were present into a light curve were correctly recovered by the algorithm.

The TDE was calculated as the sum of the totally and partially recovered transit candidates relative to the whole number of stars with transiting planets. We show the trend of the TDE as a function of magnitude (for NGC 6791) in Fig. 6.13. The TDE decreases with increasing magnitude because the lower photometric precision at fainter magnitudes is not fully compensated by the larger transit depth. The TDE depends strongly also on the assumptions concerning the planetary radii, and on the inclusion of the LD effect.

6.4 Results

Here we show how the procedure above described was applied to the real data relative to NGC 6701 and NGC 6253 and the results obtained.

6.4.1 Two different approaches for NGC 6791

The data we have acquired on NGC 6791 came from four different sites and involved telescopes with different diameters and instrumentations.

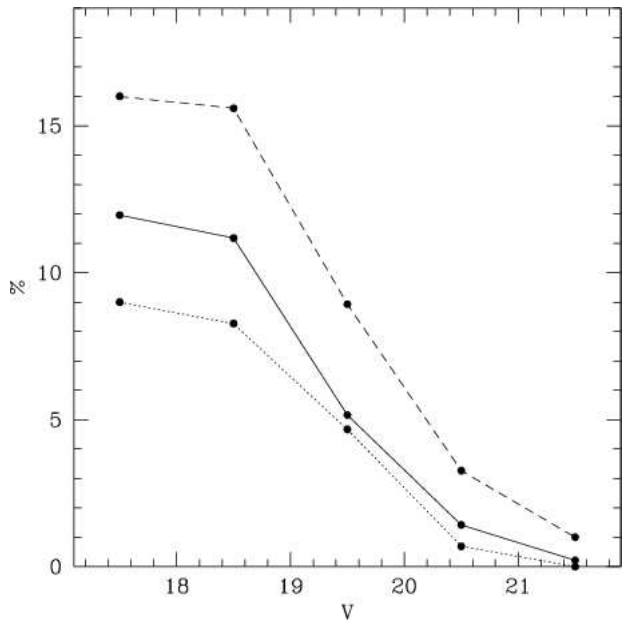

Figure 6.13: TDE for the NGC 6791 database as a function of the stellar magnitude for various assumptions on planetary radii distribution. From the top to the bottom: 1) Dashed line, R = (1.4 ± 0.1) R_J; 2) Solid line, R = (1.0 ± 0.2) R_J; 3) Dotted line, R = (0.7 ± 0.1) R_J. The normalization is respect to the whole number of transiting planets.

[Fe/H]	<R>=0.7 R_J	<R>=1.03 R_J	<R>=1.4 R_J
+0.17	0.2 ± 0.5	0.4 ± 0.7	0.6 ± 0.8
+0.39	1.6 ± 1.3	2.3 ± 1.6	2.6 ± 1.7
+0.47	2.5 ± 1.7	3.4 ± 2.0	4.0 ± 2.1
+0.17	0.0 ± 0.0	0.0 ± 0.0	1.8 ± 0.9
+0.39	0.1 ± 0.1	1.9 ± 0.8	3.6 ± 1.8
+0.47	0.2 ± 0.3	3.2 ± 1.9	5.4 ± 1.8

Table 6.1: Expected number of detectable transiting planets for NGC 6791 inside our observing window, for the three assumed planetary radii distributions and the three determinations of the metallicity. The first three rows are the results relative to the only CFHT data, the other are relative to the all–sites data.

Moreover, the observing window of each site was clearly different with respect to the others as well as observing conditions like seeing, exposure times, etc.

Considering only the stars in common with all sites, would reduce the number of candidates from 3311 to 1093 which means a reduction of about 60% of the targets.

We decided to follow two approaches:

- Consider only the CFHT data.
- Put together the observations coming from all the different telescopes, taking into account that some stars were measured only in a subset of the sites. Another set of 7722 artificial light curves was created, taking into account the "multi–sites stars".

All results given by the transit simulator code are reported in Tables C.1 and C.1, for the CFHT only case and for the all–sites case, respectively.

Final values, after applying the transit search algorithm) are reported in Table 6.1

A comparison between data in Table 6.1 reveals that, in general, except for the largest planetary radii distribution, the number of expected detections

is not increasing considering all the sites together instead of the CFH only. Moreover, for the cases of [Fe/H]=(+0.39, +0.47) dex, and the R=(0.7± 0.1) R_J radii distribution, we obtained significantly better results considering only the CFHT data than putting together all the data-sets. We interpreted this result as the evidence that the transit signal is, in general, lower than the total scatter in the composite light curves and this didn't allow the algorithm to take advantage of the increased observing window giving, for the cases of major interest, R=(1.0±0.2)R_J and [Fe/H]= (+0.39, +0.47 dex), comparable results.

Comparison with real data

On real data, considering all–sites dataset, 4 real candidates were obtained (see M07, Sect. 9); considering only CFHT data, the number of candidates is 3. Their number agrees with the expected number of false candidates coming from the simulations (3.3 ± 1.3, see Sect. 6.3.3). Assuming the most likely planetary radii distribution R= (1.0 ± 0.2) R_J and the high metallicity resulting from recent high dispersion studies (Carraro et al. 2006 [16]; Gratton et al. 2006 [39]), we expected to be able to detect 2-3 planets that exhibit at least one detectable transit in our observing window.

Therefore, this study reveals a lack of transit detections. What is the probability that our survey resulted in no transiting planets just by chance? To answer this question we perform another set of simulations: we follow the procedure described in Sect. 6.3.3, to create light curves with added transits to be analyzed, but we adopt *realistic* values of P, $\cos i$ and we iterate the procedure N times, with $N \sim$ 500–1000.

The output consists in N little samples of constant light curves with added transits. We apply the search algorithm on this dataset and we evaluated the ratio of the number of simulations for which we were not able to detect any planet, relative to the total number N of simulations performed. The resulting probabilities to obtain no transiting planets were respectively around 10% and 3% for the metallicities of Carraro et al. (2006) [16] and

[Fe/H]	<R>=0.7 R_J	<R>=1.03 R_J	<R>=1.4 R_J
+0.36	0.3 ± 0.1	0.4 ± 0.2	0.4 ± 0.2
+0.46	0.5 ± 0.1	0.6 ± 0.3	0.7 ± 0.4

Table 6.2: Expected number of detectable transiting planets in NGC 6253 inside our observing window, for the three assumed planetary radii distributions and the two determinations of the metallicity..

Gratton et al. (2006) [39] considered above.

6.4.2 Results for NGC 6253

In the case of NGC 6253, the selection of the MS stars candidates was accomplished in two steps: first, 110 main sequence stars were identified by means of proper motions, with magnitude between V=14.5 and V=17. and after, 561 stars at fainter magnitudes (where proper motions errors are too large to allow meaningful membership determination) were selected on the basis of the only photometry. The total range of magnitudes for the 671 stars sample goes from V=14.5 to V=20. In this range of magnitudes, the photometric precision was fully adequate for the search for transits for the La Silla telescope.

We performed the same simulations described above assuming the metallicity of Carretta et al. (2000) [17] and of Gratton et al. (private communication), corresponding to [Fe/H]=+0.36 and +0.46 respectively. We expected 0.6±0.3 detectable transiting planets inside our observing window, as reported in Table 6.2.

From the real light curves, the BLS algorithm found one candidate, that doesn't show any planetary transit feature (it is an eclipsing binary with eclipse depths around 0.1 mag, and period of around 4 days).

This is in agreement with the FAR (evaluated as explained in Sect. 6.3.3), from which we expect (0.7 ± 0.3) candidates, and the probability that this result is simply due to chance, calculated as explained in Sect. 6.4.1 is comprised between 50% and 70%, referred to [Fe/H]=+0.36 and +0.46 respec-

tively.

Taking into account field contamination on the fainter stars and binarity, the significance of the result further decrease.

Despite the fact that this cluster is one of the most metal rich open clusters in the Galaxy, the small number of cluster stars we were able to identify was the most important limitation in this work, and being the number of expected transiting planets lower than 1, no conclusions can be drawn about the planetary frequency on this cluster.

As was made for NGC 6791, all results given by the transit simulator code applied to NGC 6253 data are reported in Tables C.2.

6.4.3 Discussion of the results

NGC 6791

Different hypothesis can be invoked to explain the lack of observed transits in NGC 6791:

1. The discrepancy could be due to a lower frequency of close–in planets in clusters compared to the field stars of similar metallicity.

2. Guillot et al. (2006) [40] suggested that the masses of heavy elements in planets was proportional to the metallicities of their parent star. This correlation remains to be confirmed, being still consistent with a no–correlation hypothesis at the 1/3 level in the least favorable case. A consequence of this would be a smaller radius for close–in planets orbiting super–metal rich stars. This would have important implications for transit detectability.

3. While we exploited the best available results to estimate the expected number of transiting planets, it is possible that some of our assumptions are not completely realistic, or not fully applicable to our sample.

4. The probability that our null result was simply due to chance was comprised between 3% and 10%, depending on the metallicity assumed

for the cluster. This is a rather small, but not negligible probability, and other efforts must be undertaken to reach a firmer conclusion.

The small number of stars in the high metallicity range in the Fischer & Valenti sample makes the estimate of the expected planetary frequency for the most metallic stars quite uncertain. For this reason, the planetary frequency might no longer increases above a given metallicity.

Another possibility concerns systematic differences between the stellar sample studied by FV05 and the present one. One relevant point is represented by binary systems. The sample of Fischer & Valenti has some biases against binaries, in particular close binaries. As the frequency of planets in close binaries appears to be lower than that of planets orbiting single stars and wide binaries (Bonavita & Desidera, 2007 [9]), the frequency of planets in the Fischer & Valenti sample should be larger than that resulting in an unbiased sample. On the other hand, our selection of cluster stars excludes the stars in the binary sequence, partially compensating this effect.

Another possible effect is that of stellar mass: the cluster's stars searched for transits have mass between 0.5 to 1.1 $M\odot$, on the other hand, the stars in the FV sample have masses between 0.8 to 1.6 $M\odot$. The comparison between the two distribution is plotted in Figure 6.14.

If the frequency of giant planets depends on stellar mass, the results by FV05 might not be directly applicable to our sample.

Furthermore, some non-member contaminations is certainly present. As discussed in Sect. 6.3.1, the selection of cluster members was done photometrically around a fiducial main sequence line.

NGC 6253

It must be said that we are still refining the proper motion calculation presented in this Chapter, and thus these are preliminary results. Moreover, the estimated number of expected planets in this cluster can be certainly increased including other observations of this cluster. The EXPLORE group

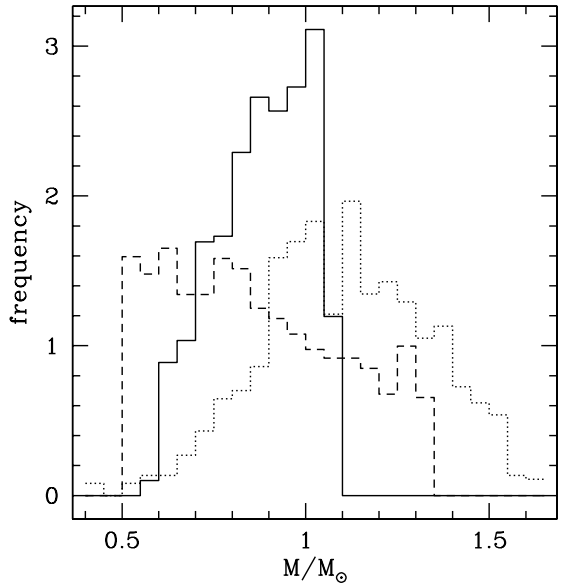

Figure 6.14: Distributions of the masses for the Main Sequence selected stars in NGC 6791 and NGC 6253 (solid and short-dashed lines, respectively), and that of the FV05 sample (∼850 stars, dotted line).

observed NGC 6253 in June 2004, dedicating 18 nights on it, probably partially overlapped with our own ten observing nights. Moreover Carraro, (private communication), has observed the cluster in 2005 for other 5 nights at the Cerro Tololo Observatory, in order to search for variability. Hence, significant improvements on the results presented here could be obtained considering these datasets all together.

6.5 Transit simulations applied to other surveys

The possibilty to detect periodic signals strongly depends to the observative window. In this section we describe another application of our code in order to investigate the efficiency of a generic hypothetical surveys to capture planetary transits. The main goal of this study is to evaluate the observing

time required to push at high significance level (>99%) the lack of transits detections in NGC 6791.

There results were used for the preparation of a new proposal for observations on NGC 6791 at INT (Canary island), that resulted in time allocation next summer.

These simulations are also needful in the general contest of other transit search programs on going or planned by our group (RATS,ΩTRANS). We made six simulations, where the free parameters were:

- number of observative night;
- number of hours per night.

We could also consider the number of images per night, but this parameter is near ininfluent to our purposes, and we adopted a frequency of one image over 15 minutes for each night in all cases.

The procedure is quite similar to the one described in Sect. 6.3.2 used to calculate the number of transiting planets into our *specific* observing window.

Given the two parameters listed above, accordingly with the luminosity function of the MS of NGC 6791, we create a big sample of light curves with V_i equals to a constant and t_i sampled as required the free parameters.

We run our procedure N times (with $N \gtrsim 3000$) and we compared our results.

We performed six cases (5, 10,15,20,25 and 30 nights) and for each one we evaluated the expected number of transiting planets considering each subcases from 1 to 23 observing hours per night, with bins of 1 hour. Obviously, multisite campaign are needed to obtain more than 6–7 observative hours per night.

The results of this simulations are shown in Tables C.4, C.5, C.6, C.7, C.8 and C.9, and plotted in Fig. 6.15 and Fig. 6.16.

For simplicity, the output data will be normalized to N_{geom} that represents our ideal target.

We can see that, for example, with a 5 night campaign, the "efficiency" of the observative window is greater than 50% only for more than 8–9 observative hours per night. Instead, with 20 nights, and 8–9 hours we are able to detect more than 80% of the transiting planets and the most of them makes 2 transits. Our survey in NGC 6791 is well represented by the case corresponding to 10 nights and 5 hours per night.

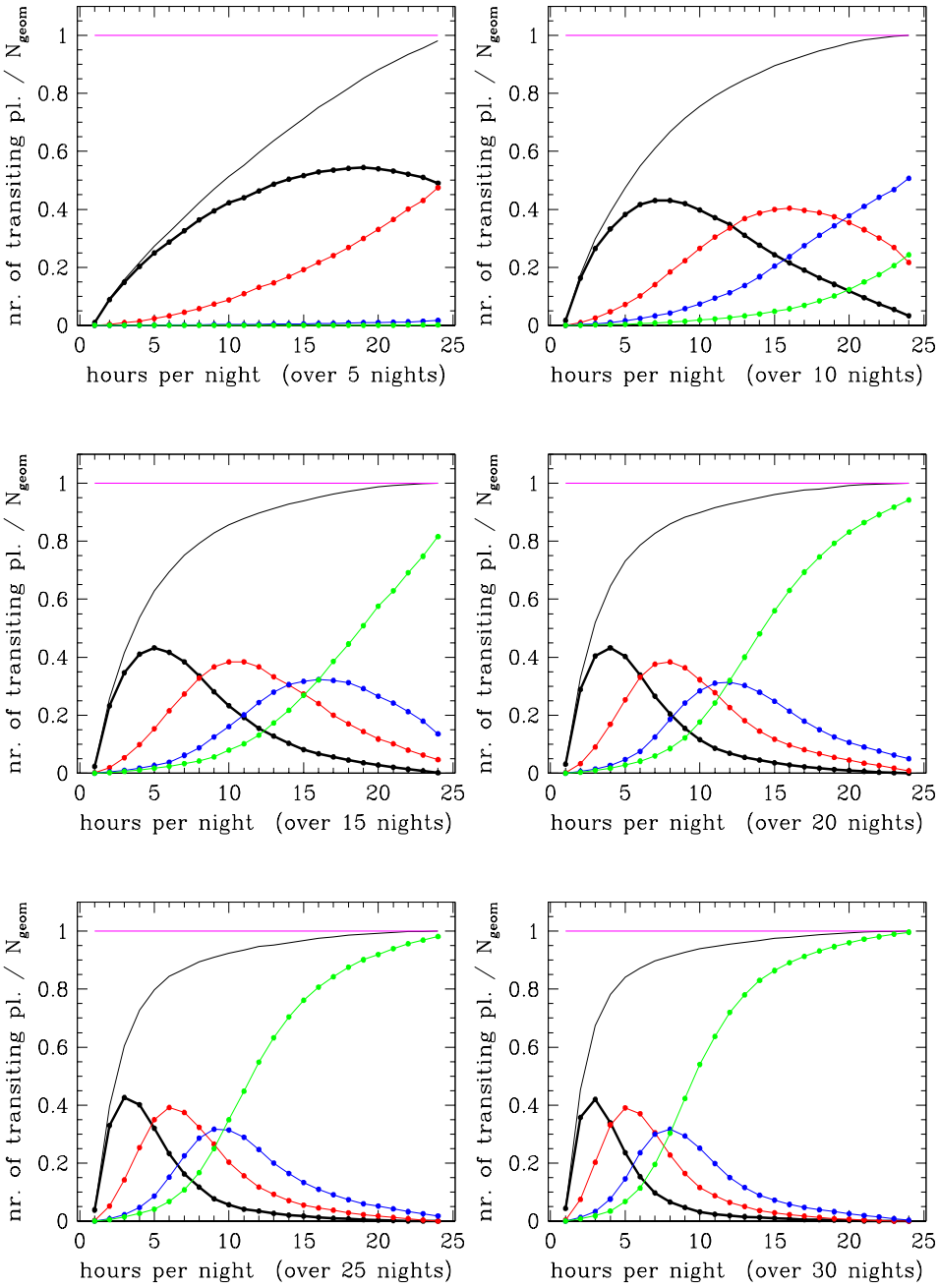

Figure 6.15: Number of transiting planets into the observing window as a function of the number of hours per night (for 5, 10, 15, 20, 25 and 30 nights surveys). Black lines: N1 (see text for details), red lines: N2, blue lines : N3, green lines: N4+. The tiny black lines is N1+ (equals to N1 plus N2 plus N3 plus N4+).

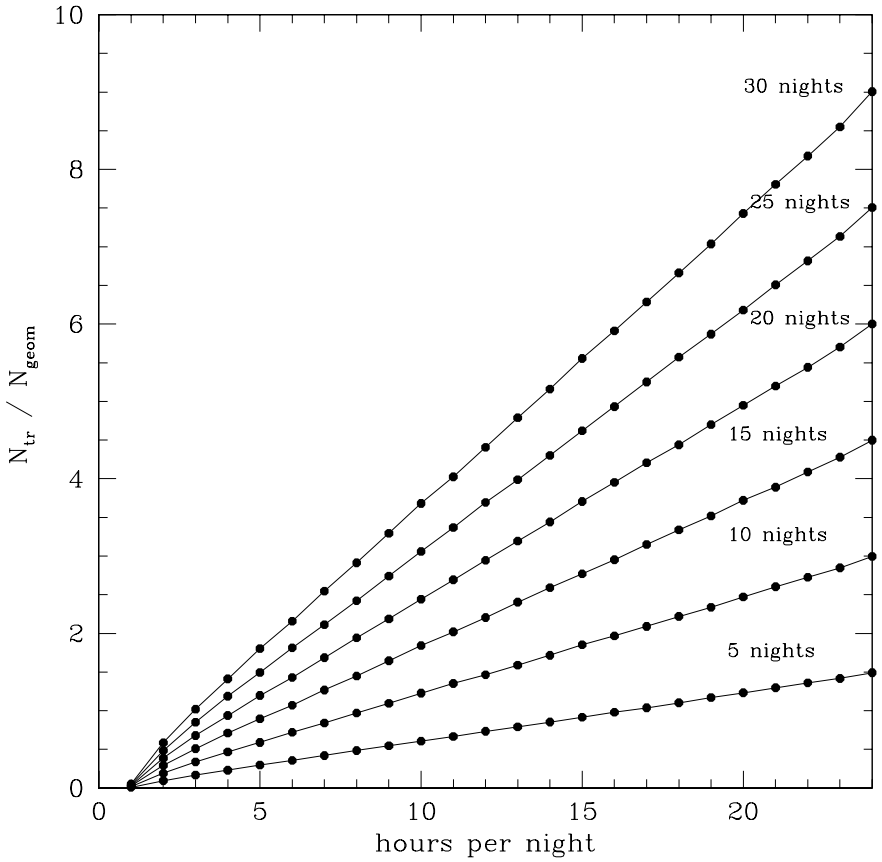

Figure 6.16: Number of transit detected as a function of the number of hours per night for different time baselines.

Appendix A

List of identified variables in NGC 6791

This Appendix includes the full list of the identified variables, separated according to our classification:

1. Pulsating, irregular and cataclysmic variables: Table: A.1, Figures A.1, A.2, A.3.
2. EW–Type stars: Table A.2, Figure A.4.
3. EA/EB–type stars: Table A.3, Figures A.5, A.6, and A.7.
4. Single–wave rotational variables: Tables A.4, A.5, Figures A.8, A.9, A.10.
5. Double–wave rotational variables: Table A.6, Figure A.11.
6. Long–period variables: Table A.7.

Into the tables, for each star we give the name (a five–digit number followed by the chip number which the star belongs), coordinates, photometric data (always the V mag, $B-V$ color when available), information about the variability (T_0, period, amplitude), distance from the center (in arcmin)

Table A.1: Pulsating, irregular and cataclysmic variables. V is the minimum brightness for CVs and irregular, the mean brightness for pulsating variables. T_0 is the time of maximum brightness for pulsating stars.

Star	Type	α_{2000}	δ_{2000}	V [mag]	$< B-V >$ [mag]	$< V-I >$ [mag]	Ref.	T_0 [HJD–2452400]	Period [d]	Ampl. [mag]	Memb.	Distance [arcmin]
V123	HADS	19.362064	37.666034	17.08	0.45		k	59.559	0.06026	0.14	nm	11.8
01497_12	HADS	19.379083	37.812419	16.06				59.528	0.07227	0.40	nd2	22.2
00311_7	SXPhe	19.324628	37.716768	23.17				59.605	0.10443	0.10	nd2	17.0
00224_10	SXPhe	19.353639	37.710163	21.72	0.71	1.06	s	59.801	0.12261	0.20	nm	5.4
03653_3	RRc	19.347147	37.992413	17.21	0.57	0.58	k	59.937	0.32654	0.39	nm	13.3
00345_1	RRab	19.325082	37.964170	18.28				60.151	0.57866	0.72	nd2	20.0
V92	IRR	19.350754	37.766876	18.10	0.91		k			0.10	m	1.9
V83	IRR	19.346220	37.737232	19.10	1.02	1.05	k			0.07	m	2.4
V93	IRR	19.351452	37.785687	18.12	0.98	1.03	s			0.04	m	2.6
V15(=B7)	CV	19.352057	37.799019	18.26	0.20		k			0.06	98	3.3
B8	CV	19.343262	37.747833	20.64	–0.23	0.78	k			2.27	m	3.7
06289_9	CV	19.348976	37.770355	22.80	0.25	0.88	s			3.10	m (B06)	0.7

and finally the numerical value of the Cudworth's membership probability (reported in the column 'Memb.').

In most cases, when membership probabilities were not available, in the same column the label "m" means that we retain the star belonging to the cluster, while 'm?' and "nm" mean "uncertain membership" and "likely non–member" respectively. The label "nd1" means that no photometric data are available to advance hypothesis about the membership, but the star is located nearer than 10' from the center of the cluster. Finally "nd2" means that no photometric data are available and the star is located further than 10' from the center; in this case we strongly suggest that the star does not belongs to the cluster (see Sect. 3.3).

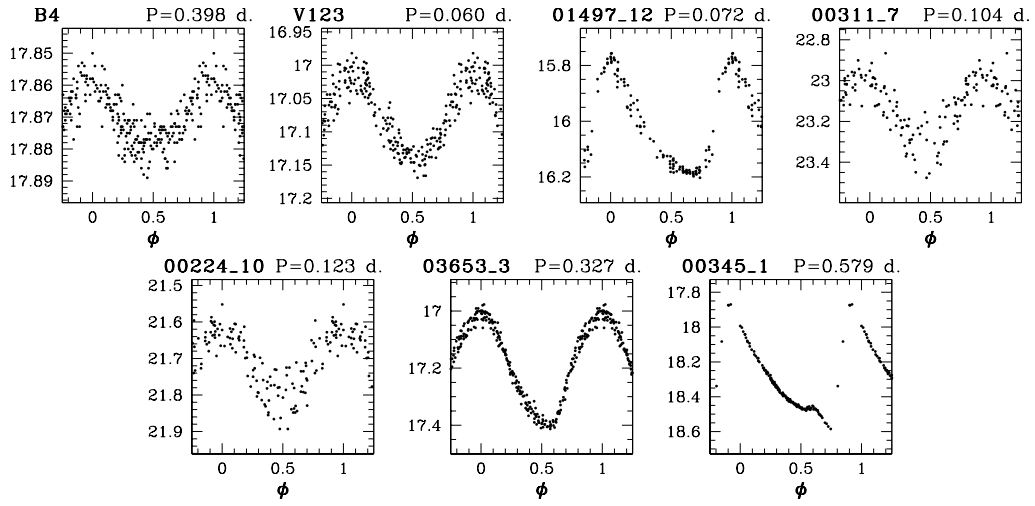

Figure A.1: Light curves of pulsating variables. V123 and 01497_12 are probably HADS stars, 00311_7 and 00224_10 are SX Phe stars, 03653_3 and 00345_1 are RR Lyr stars.

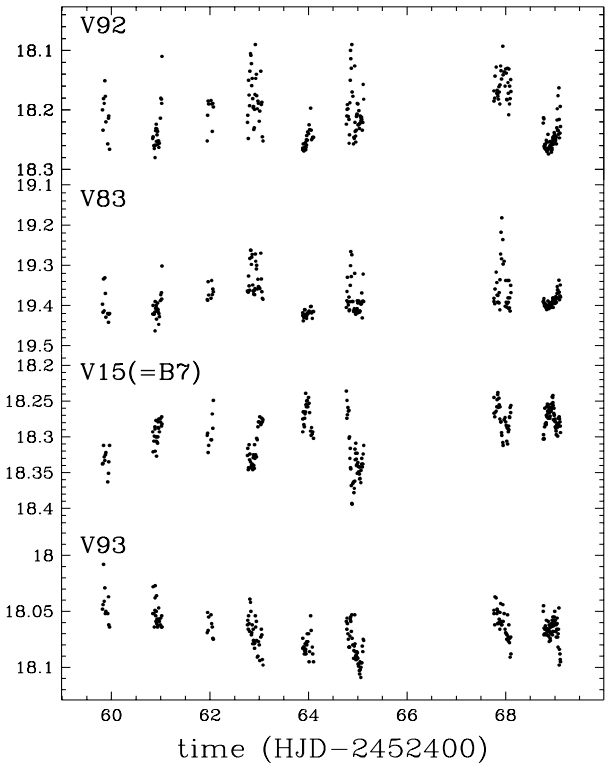

Figure A.2: Variable stars showing irregular fluctuations.

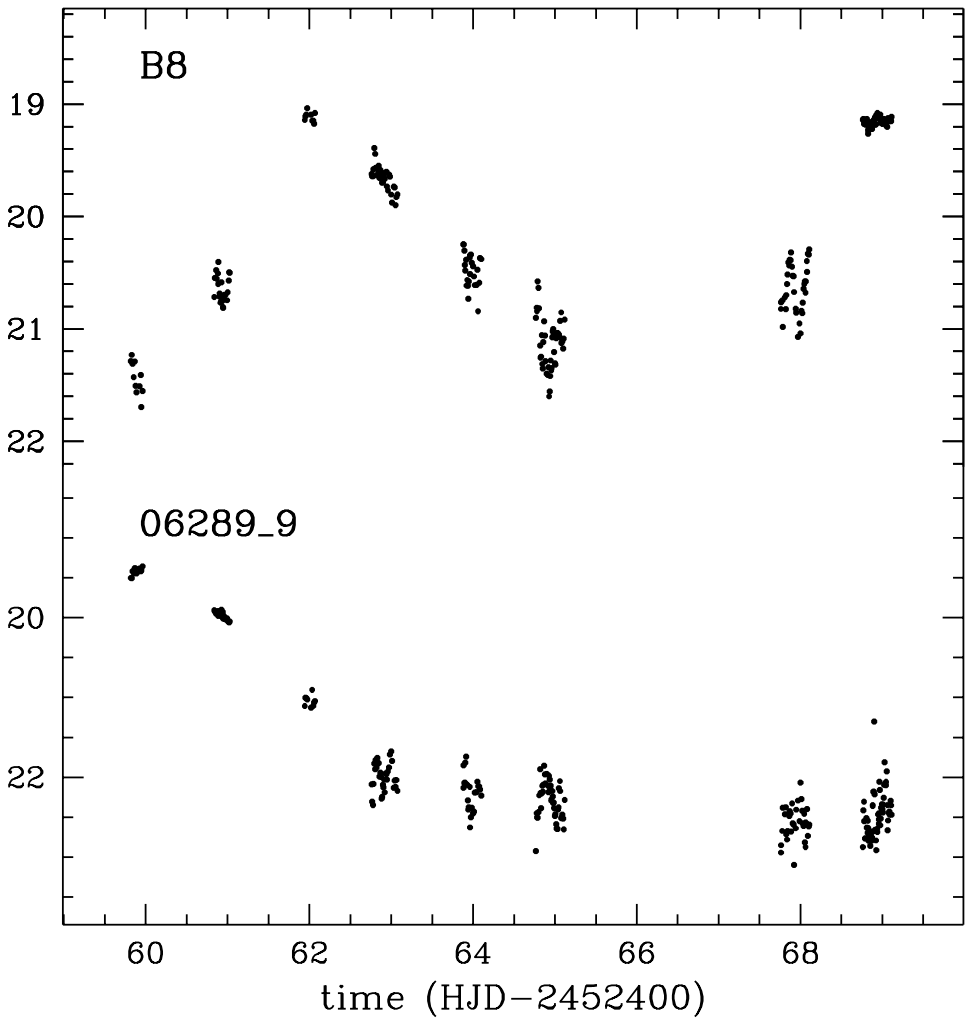

Figure A.3: Cataclysmic variables: B8 (top) and 06289_9 (bottom).

Table A.2: Contact binaries; V is the brightness at maximum and T_0 is the time of the primary minimum.

Star	α_{2000}	δ_{2000}	V [mag]	$< B-V >$ [mag]	$< V-I >$ [mag]	Ref.	T_0 [HJD–2452400]	Period [d]	Ampl. [mag]	Memb.	Distance [arcmin]
V122	19.360729	37.641436	20.92				59.614	0.22883	0.58	nd2	11.9
V115	19.330646	37.975902	20.70				59.473	0.23636	0.24	nd2	17.4
01407_8	19.339256	37.701576	21.52	0.64	1.25	k	59.447	0.24155	0.82	nm	7.5
01150_4	19.357227	37.962177	18.58	1.07	0.93	k	59.455	0.24510	0.27	nm	13.2
01441_8	19.339422	37.778118	19.98	1.38		k	63.073	0.24544	0.07	m	6.2
00144_2	19.334044	38.030701	19.19				59.457	0.24780	0.77	nd2	18.5
01670_10	19.357625	37.681442	16.64	1.14	1.24	k	59.729	0.25807	0.49	nm	8.7
V121	19.358063	37.932346	17.24	0.81	0.84	k	59.619	0.26742	0.71	nm	12.0
02291_11	19.371624	37.795464	19.15				59.582	0.26774	0.29	nd2	16.8
V23	19.338614	37.787781	16.92	1.04	1.23	k	59.915	0.27180	0.07	nm	6.8
V25	19.328426	37.713237	18.50				59.772	0.27730	0.56	nd2	14.4
00665_12	19.375697	37.713244	18.89				59.472	0.28369	0.41	nd2	20.0
09831_9	19.352356	37.780907	20.55	1.09	1.19	s	59.662	0.29488	0.3	nm (B06)	3.1
01434_3	19.350643	37.985512	22.10				59.831	0.30581	0.97	nd2	13.0
V118	19.347500	37.651222	17.68	0.75	1.01	s	59.912	0.30623	0.70	m	7.2
00721_11	19.365737	37.713858	15.53				59.491	0.31008	0.26	nd2	13.1
01701_2	19.341944	38.017998	18.72				59.534	0.31201	0.51	nd2	15.4
V5	19.346258	37.813354	17.19	0.90	0.95	k	60.221	0.31274	0.05	98	2.8
V3	19.354380	37.769349	18.51	1.05	1.06	k	59.798	0.31764	0.09	78	4.5
02030_4	19.353487	38.009422	19.04	1.19	1.42	k	59.614	0.31797	0.33	nm	14.8
V124	19.365150	37.681544	17.62	0.70	1.07	k	59.855	0.32014	0.58	nm	13.3
00766_5	19.367585	37.943904	22.31				59.466	0.32363	0.78	nd2	17.3
V4	19.348396	37.806652	17.72	1.01		k	59.591	0.32568	0.10	98	2.1
V27	19.336275	37.648720	18.47	0.82	1.29	k	59.763	0.33170	0.84	nm	11.2
V8	19.341938	37.865810	17.81	0.79	0.88	k	59.896	0.33406	0.10	m	7.1
V101	19.351563	37.640388	19.94	0.56		k	59.798	0.33480	0.29	nm	8.3
V117	19.343433	37.665848	17.66	0.87	0.90	k	59.987	0.36644	0.38	m	7.2
V7	19.340271	37.821892	17.63	0.93	0.86	k	59.820	0.39174	0.31	m	6.3
V40	19.327495	37.616839	19.67				60.101	0.39750	0.16	nd2	17.3

Table A.3: Eclipsing variables. V is the brightness at maximum and T_0 is the time of the primary minimum.

Star	Type	α_{2000}	δ_{2000}	V [mag]	$< B-V >$ [mag]	$< V-I >$ [mag]	Ref.	T_0 [HJD−2452400]	Period [d]	Ampl. [mag]	Memb.	Distance [arcmin]	Notes
V119	EB	19.351961	37.916328	18.15	1.13	1.33	k	59.879	0.30197	0.15	m?	9.1	
B4	E:	19.353589	37.764290	17.87	−0.13	−0.15	k	54.788	0.39841	0.02	40	4.0	
V29	EB	19.354796	37.751386	20.00	1.23	1.61	k	69.012	0.43662	0.22	m	4.9	Light curve distortion at maximum light
01558_5	EB	19.372697	37.953469	19.15				69.028	0.52910	0.28	nd2	20.6	
01393_1	EA	19.329588	37.970392	21.23				59.326	0.58998	0.56	nd2	17.7	
00331_3	EB	19.352367	37.864391	19.73	1.20	1.36	k	68.815	0.7347	0.13	m?	6.4	
V11	EA	19.342575	37.804802	19.38	0.96	1.22	k	67.875	0.8833	0.48	m?	4.4	
05736_9	EA	19.348484	37.721855	20.20	1.21		k	68.333	1.210	0.29	m	3.0	
V12	EB	19.345259	37.849083	17.52	0.96		k	64.103	1.524	0.06	96	5.1	
00645_10	EA	19.354692	37.710104	20.60	1.33	1.46	k	60.893	1.451	0.20	m	6.0	
V9	EB	19.346634	37.777035	17.15	1.23	1.38	k	63.873	3.2	0.20	82	1.1	
V107	EA	19.355068	37.761553	17.97	0.93	1.00	k	64.433	3.27	0.24	m?	5.0	Minima at the very beginning of the night.
V109	EA	19.342716	37.793961	20.73	1.46	1.60	k	69.021	3.70	0.86	m?	4.0	
00219_11	EA	19.364048	37.827507	17.94	0.92	0.87	k	67.913		0.52	nm	11.9	
00663_4	EA	19.359652	37.894062	17.49	0.79	0.83	k	65.003		0.49	nm	11.0	
00671_2	EA	19.336983	37.903919	18.46	0.70	0.91	k	64.968		0.07	nm	11.2	
00828_5	EA	19.367917	37.885330	21.28				64.979		0.38	nd2	15.7	
00938_2	EA	19.338285	37.861633	20.57	1.20	1.80	k	67.867		0.60	nm	8.8	
00997_10	EA	19.355692	37.799655	19.58	0.76	0.83	k	68.020		0.20	nm	5.7	
01709_1	EA	19.330890	37.932268	18.04				64.818		0.32	nd2	15.5	
01731_10	EA	19.357813	37.672819	19.27	0.67	0.80	k	64.783		0.34	nm	9.1	Minimum at the very beginning of the night.
01780_8	EA	19.340677	37.655354	22.19		2.25	k	68.969		0.66	nm	8.7	
02461_8	EA	19.342779	37.741798	19.34	1.06	1.15	k	60.968		0.11	88	4.2	
01740_7	EA	19.330623	37.638774	21.30				69.007		0.33	nd2	14.8	Maybe another minimum at 64.40
02045_12	EA	19.381420	37.712211	17.16				68.030		0.26	nd2	24.0	Other minimum at 63.39
02241_11	EA	19.371472	37.827819	19.21				68.823		0.53	nd2	17.0	Maybe another minimum at 63.50
00346_5	EA	19.365356	37.929481	20.16				65.014		0.17	nd2	15.5	Other minimum at at 68.410. Short in time.
00631_12	EA	19.375473	37.649140	17.92				68.753		0.30	nd2	20.9	Minimum at the very beginning of the night.
01511_10	EA	19.357145	37.689907	19.74	1.45	1.86	k			0.50	nm	8.1	Two Minima at night extrema.
V60	EA	19.350189	37.762493	18.68	0.96		k	67.951		0.39	91	1.6	
V80	EA	19.351799	37.791061	17.90	0.94		k	67.607	4.631	0.10	86	2.9	Shallow eclipse ?
V108	EA	19.352606	37.823467	21.15	1.27	1.90	k	69.080		0.86	nm	4.5	

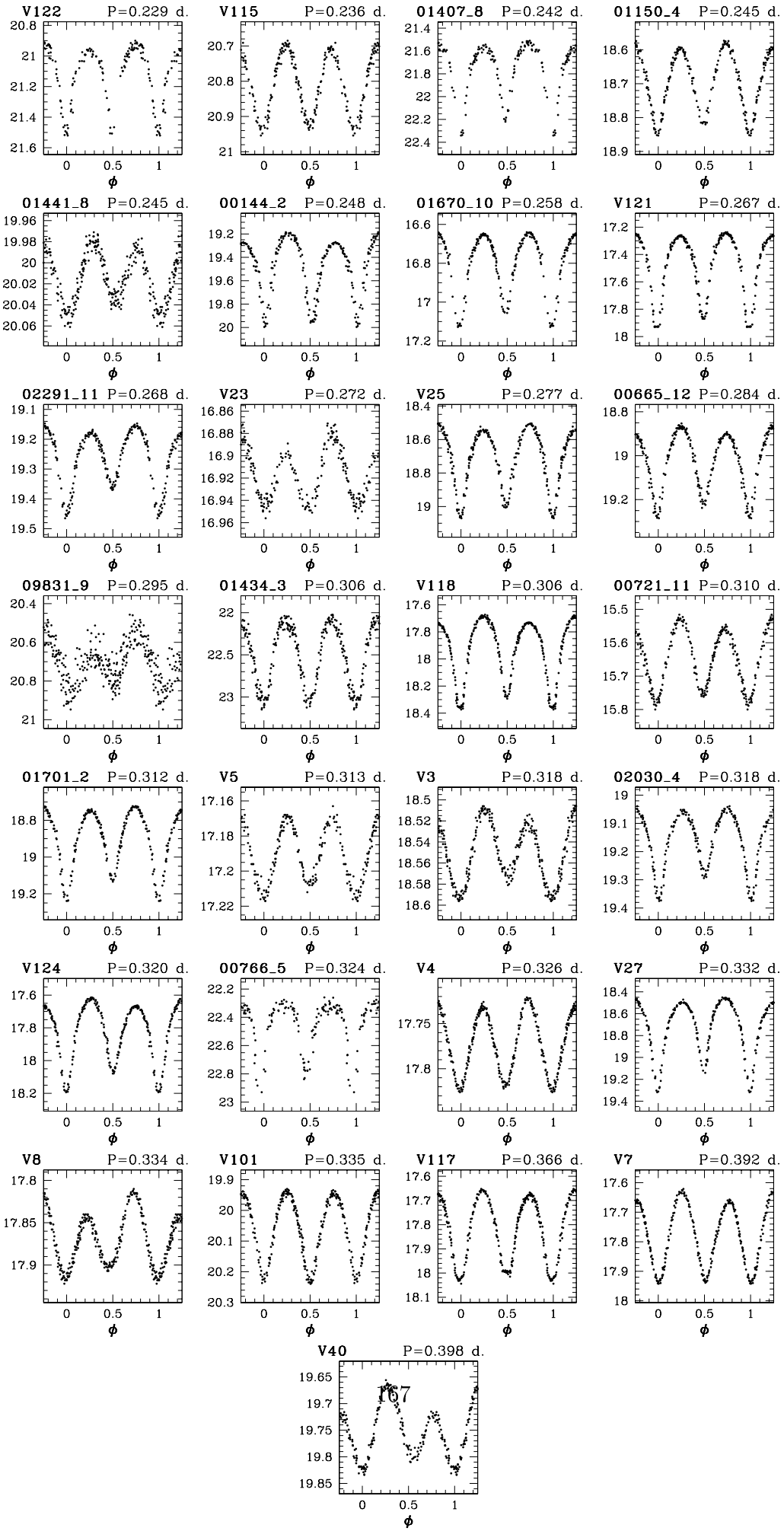

Figure A.4: Contact variables.

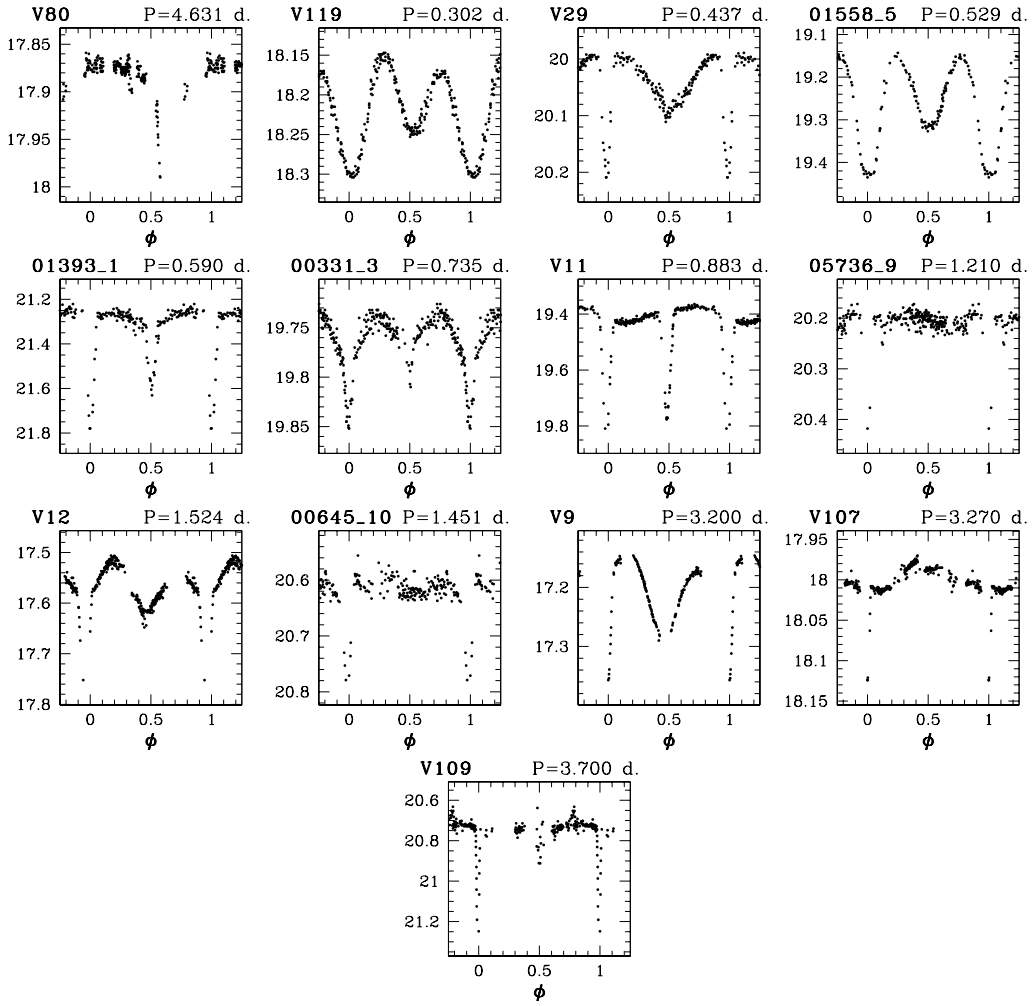

Figure A.5: Light curves of short–period detached or semi–detached eclipsing binaries.

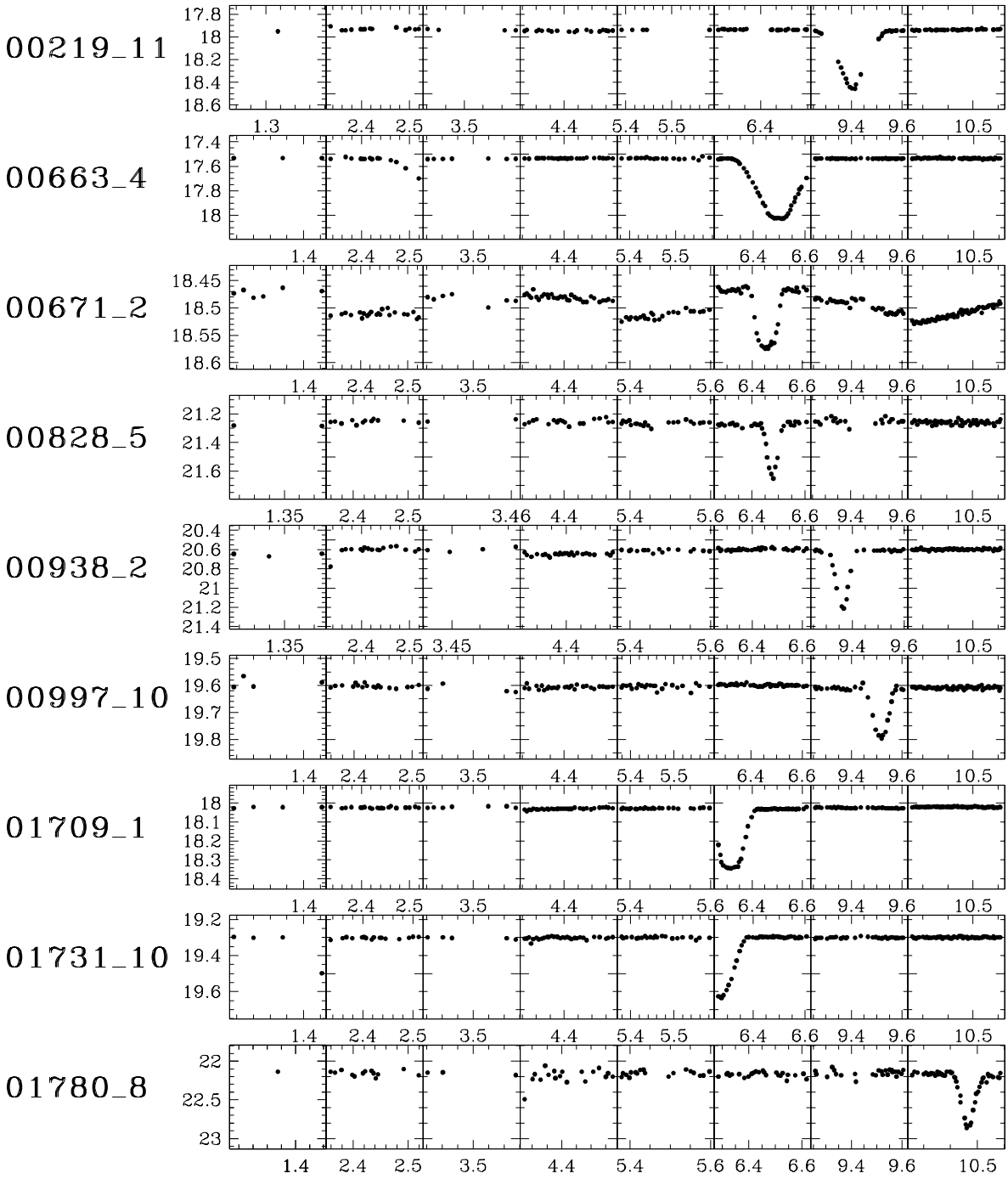

Figure A.6: .Detached systems with undetermined periods.

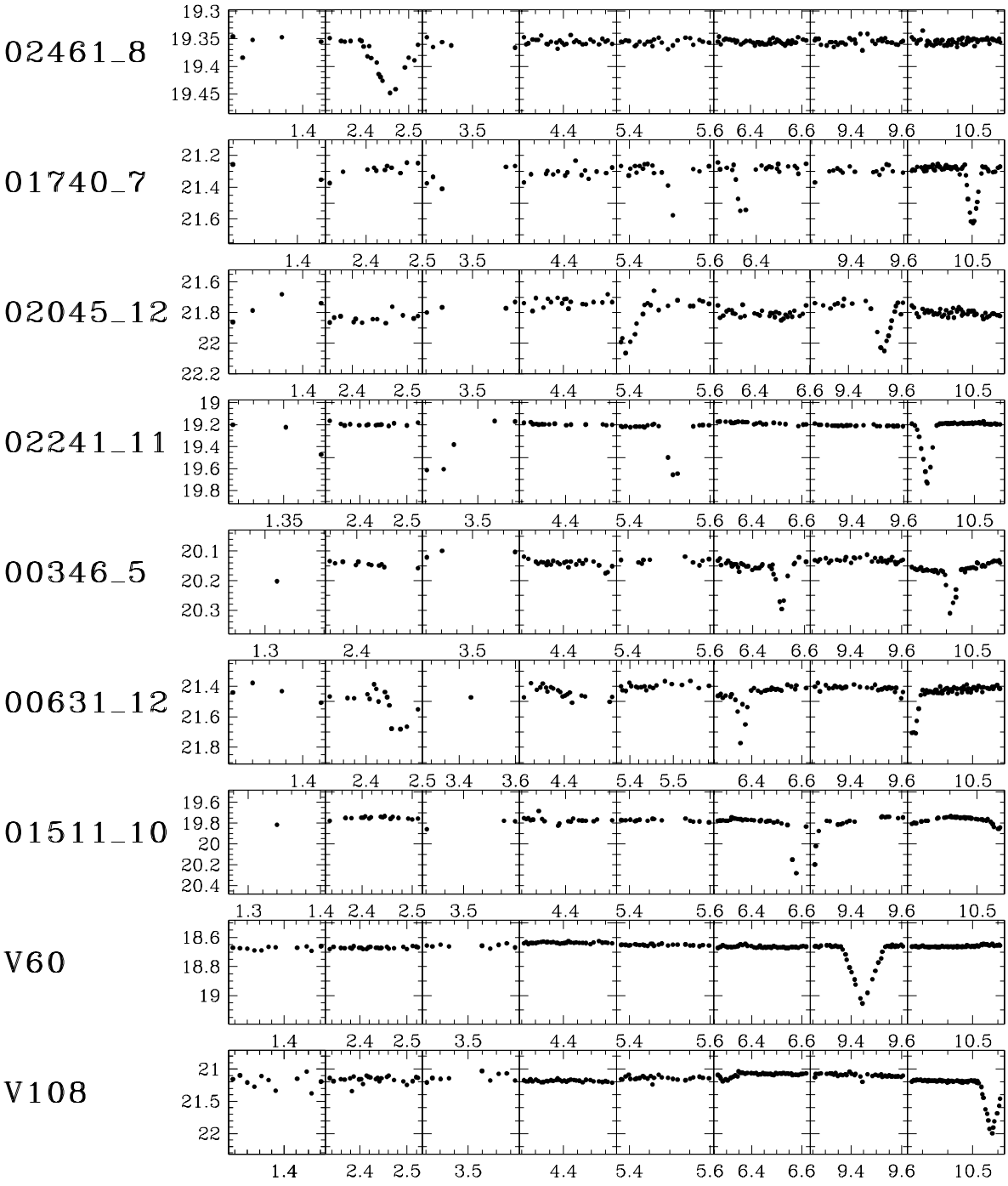

Figure A.7: Detached systems with undetermined periods.

Table A.4: Rotational variables with a single–wave light curve. V is the mean brightness value. T_0 indicates the time of the maximum brightness.

Star	α_{2000}	δ_{2000}	V	$< B-V >$	$< V-I >$	Ref.	T_0	Period	Ampl.	Memb.	Distance
			[mag]	[mag]	[mag]		[HJD–2452400]	[d]	[mag]		[arcmin]
02268_12	19.382495	37.798839	17.42				60.323	0.30910	0.02	nd2	24.6
02418_3	19.349085	38.016541	21.68				59.901	0.36498	0.12	nd2	14.7
00513_2	19.336012	37.940765	20.12	1.18	1.51	k	60.786	0.45272	0.08	m?	13.3
02292_10	19.359535	37.710207	16.24	1.11	1.25	k	61.298	0.46371	0.06	nm	9.0
01497_11	19.368601	37.770512	18.58				61.737	0.56508	0.01	nd2	14.6
01776_4	19.354509	37.935883	19.70	0.99	1.16	k	61.154	0.68029	0.06	nm	10.9
00301_5	19.365041	37.906284	22.10				62.833	0.70170	0.21	nd2	14.5
00088_8	19.333437	37.744888	21.92				65.464	0.70594	0.11	nd2	10.5
V43	19.344337	37.641777	19.58	1.62	2.97	k	55.976	0.75759	0.08	nm	8.2
00554_8	19.335732	37.664570	21.32	1.22	1.48	k	65.543	0.821	0.13	nm	10.9
00612_10	19.354604	37.729215	22.97	0.79	2.42	s	68.050	0.91581	0.24	m?	5.3
01105_12	19.377359	37.737573	19.31				62.539	0.91746	0.04	nd2	21.0
00913_5	19.368442	37.859339	20.89				62.405	1.06386	0.24	nd2	15.4
04803_9	19.347698	37.796043	21.81	1.33	1.84	s	61.799	1.1034	0.17	m (B06)	1.5
01606_11	19.368978	37.736585	20.36				62.390	1.12360	0.10	nd2	15.0
V82	19.344366	37.793381	19.01	1.00	1.02	k	56.481	1.1568	0.04	m	2.9
V34	19.335878	37.736183	19.30	1.16	1.41	k	54.955	1.20486	0.18	nm	8.9
05302_3	19.344669	37.968491	18.90				63.224	1.3334	0.15	nd2	12.1
06553_9	19.349134	37.672577	19.26	1.04	1.13	s	61.421	1.3485	0.08	m	6.0
00471_12	19.374883	37.674950	19.35				61.900	1.3513	0.06	nd2	20.0
00110_5	19.363887	38.001389	21.69				62.103	1.4085	0.08	nd2	17.8
01874_2	19.342730	37.912987	21.96				64.944	1.5503	0.14	nd1	9.3
V111	19.346970	37.812141	20.67	1.46	1.66	s	61.673	1.5626	0.15	nm	2.5
V37	19.355072	37.852001	19.58	1.65	2.48	k	55.721	1.6130	0.06	nm	6.9
01724_9	19.344957	37.785362	20.73	1.29	1.69	s	64.410	1.6130	0.17	m	2.4
02285_10	19.359424	37.607155	19.26	1.34	1.57	k	63.495	1.6668	0.08	nm	12.8
01189_11	19.367513	37.809413	20.46				64.500	1.7242	0.10	nd2	14.0
00016_5	19.363396	37.997513	18.68	1.54	2.52	k	63.157	1.7858	0.07	nm	17.4
00732_12	19.375889	37.717569	19.39				61.992	1.852	0.04	nd2	20.1
00771_11	19.365949	37.766208	19.52				62.492	1.852	0.09	nd2	12.7
00676_1	19.326459	37.929277	20.54				65.481	1.887	0.11	nd2	18.0
V38	19.351021	37.768288	18.82	0.96		k	55.630	1.96	0.13	92	2.1
02103_7	19.332028	37.696796	19.57	1.65		k	60.891	2.041	0.05	nm	12.3
00575_12	19.375449	37.792459	19.63				65.359	2.214	0.02	nd2	19.5
01914_1	19.331830	37.878855	17.71	0.73		k	62.358	2.222	0.03	nm	13.2
03838_3	19.346848	37.964615	19.45	0.91	1.05	k	64.159	2.261	0.04	nm	11.6
V44	19.326970	37.694771	18.38				58.310	2.285	0.02	nd2	15.7
00321_1	19.324957	37.905996	19.49				65.394	2.326	0.04	nd2	18.3
00810_5	19.367793	37.865903	18.17				67.424	2.564	0.05	nd2	15.1
03079_9	19.346190	37.754753	19.23	1.14	1.26	k	66.630	2.640	0.07	93	1.7
01821_12	19.380347	37.604033	20.13				70.829	2.647	0.06	nd2	25.1
01309_11	19.367871	37.748052	20.81				61.125	2.692	0.05	nd2	14.2
01956_12	19.380972	37.626492	21.39				63.833	2.699	0.06	nd2	25.0
00815_1	19.327108	37.861623	19.75				63.358	2.836	0.05	nd2	15.8
01659_8	19.340244	37.694355	21.27	1.51	1.85	k	64.446	2.840	0.17	nm	7.2
00293_11	19.364252	37.703417	15.82	0.80	0.88	k	63.606	2.941	0.05	nm	12.2
00215_5	19.364447	37.898928	22.26				65.340	3.15	0.14	nd2	13.9
03209_10	19.362653	37.732028	18.61	1.54	2.57	k	66.016	3.17	0.06	nm	10.7
01313_1	19.329261	38.025661	21.27				62.466	3.704	0.10	nd2	20.3
00277_8	19.334366	37.776566	19.52	1.54	2.68	k	60.691	4.167	0.05	nm	9.7
00179_5	19.364283	38.002234	17.18	0.91	0.90	k	64.764	4.323	0.04	nm	18.0
03039_10	19.362130	37.815850	16.58	0.79	0.87	k	65.634	4.423	0.02	nm	10.4
01555_4	19.355373	37.961205	21.22				69.673	4.546	0.09	nd2	12.5
02614_11	19.372592	37.625244	17.22				70.152	4.763	0.04	nd2	19.6
01149_2	19.339287	37.966995	17.80	0.90	0.93	k	67.803	5.0	0.04	m?	13.3
02815_3	19.348427	37.967987	19.87	1.68	2.40	k	60.828	5.0	0.05	nm	11.8
V46	19.355272	37.798869	18.65	1.18	1.36	k	56.886	5.2	0.14	nm	5.4
00357_5	19.365449	37.996214	20.91				63.108	5.3	0.07	nd2	18.3
01484_7	19.329583	37.791249	20.30	1.63		k	67.924	5.3	0.03	nm	13.2
V14	19.347687	37.756874	18.58	0.93	1.05	k	55.933	5.45	0.05	0	0.9
V48	19.352076	37.718506	17.51	0.88		k	65.223	5.65	0.09	96	4.3

Continue ...

Table A.5: Continue from Table A.4: other rotational variables with a single–wave light curve. V is the mean brightness value. T_0 indicates (one of) the times of maximum brightness.

Star	α_{2000}	δ_{2000}	V [mag]	$< B-V >$ [mag]	$< V-I >$ [mag]	Ref.	T_0 [HJD–2452400]	Period [d]	Ampl. [mag]	Memb.	Distance [arcmin]
00615_7	19.325908	37.753712	20.59				59.885	5.882	0.14	nd2	15.8
V89	19.349068	37.776783	18.75	0.88	1.20	s	63.447	5.884	0.05	nm	0.8
00188_12	19.373720	37.632076	21.78				67.253	6.25	0.06	nd2	20.1
V17	19.344135	37.817928	17.92	1.20	1.28	k	63.211	6.523	0.04	88	3.9
01122_4	19.357346	37.914520	18.84	1.03	1.12	k	65.843	6.69	0.11	m?	10.8
03056_3	19.347979	37.869431	17.10	0.89	0.97	k	66.673	6.70	0.07	nm	5.9
V51	19.353382	37.748795	19.94	1.22	1.21	k	63.624	6.72	0.09	m	4.0
00640_10	19.354585	37.604724	17.97	0.68	0.77	k	66.173	6.8	0.03	nm	11.0
V52	19.355795	37.771935	17.49	0.88	0.88	k	64.345	7.06	0.03	m	5.5
V53	19.350233	37.743187	18.72	0.89	0.93	k	69.294	7.47	0.04	86	2.3
01431_10	19.357001	37.763810	17.72	1.33	1.45	k	67.953	7.64	0.26	nm	6.4
01616_11	19.369060	37.767818	17.26				69.157	7.70	0.05	nd2	14.9
01478_3	19.350523	37.862484	17.15	1.03	1.11	k	72.123	7.96	0.07	nm	5.7
05877_9	19.348616	37.767616	20.22	1.32	1.49	k	64.272	8.0	0.12	nm	0.5

Table A.6: Rotational variables with a double–wave light curve. V is the mean brightness value.T_0 indicates (one of) the times of maximum brightness.

Star	α_{2000}	δ_{2000}	V [mag]	$< B-V >$ [mag]	$< V-I >$ [mag]	Ref.	T_0 [HJD–2452400]	Period [d]	Ampl. [mag]	Memb.	Distance [arcmin]
00436_3	19.352205	37.878635	18.92	0.92	1.08	k	60.018	0.26601	0.04	m	7.1
V2	19.354875	37.766689	19.74	0.93	1.21	k	59.712	0.27344	0.17	nm	4.9
02006_1	19.332258	38.043080	21.54				60.448	0.37500	0.19	nd2	19.8
01175_5	19.370209	37.998342	19.73				59.918	0.41481	0.09	nd2	20.8
00536_11	19.365067	37.716529	19.13				60.460	0.43740	0.03	nd2	12.6
07483_9	19.349997	37.746311	21.28	1.32	1.70	s	60.465	0.4375	0.17	m	2.1
V41	19.347492	37.806892	19.09				60.000	0.4798	0.07	77	2.2
V42	19.350058	37.714867	19.51	1.05	1.16	k	60.323	0.5068	0.10	92	3.7
01362_7	19.329000	37.662097	20.53				60.502	0.5560	0.08	nd2	15.1
02270_11	19.371548	37.794338	17.95				60.525	0.5679	0.05	nd2	16.8
01298_5	19.371044	38.002255	19.76				60.402	0.5859	0.06	nd2	21.4
V16	19.352108	37.802662	17.79	0.93	1.01	k	67.713	2.182	0.03	96	3.4
00568_2	19.336329	37.881542	18.52				60.007	2.704	0.08	nd2	10.6
00019_7	19.323382	37.710172	18.95				65.473	5.882	0.12	nd2	17.9

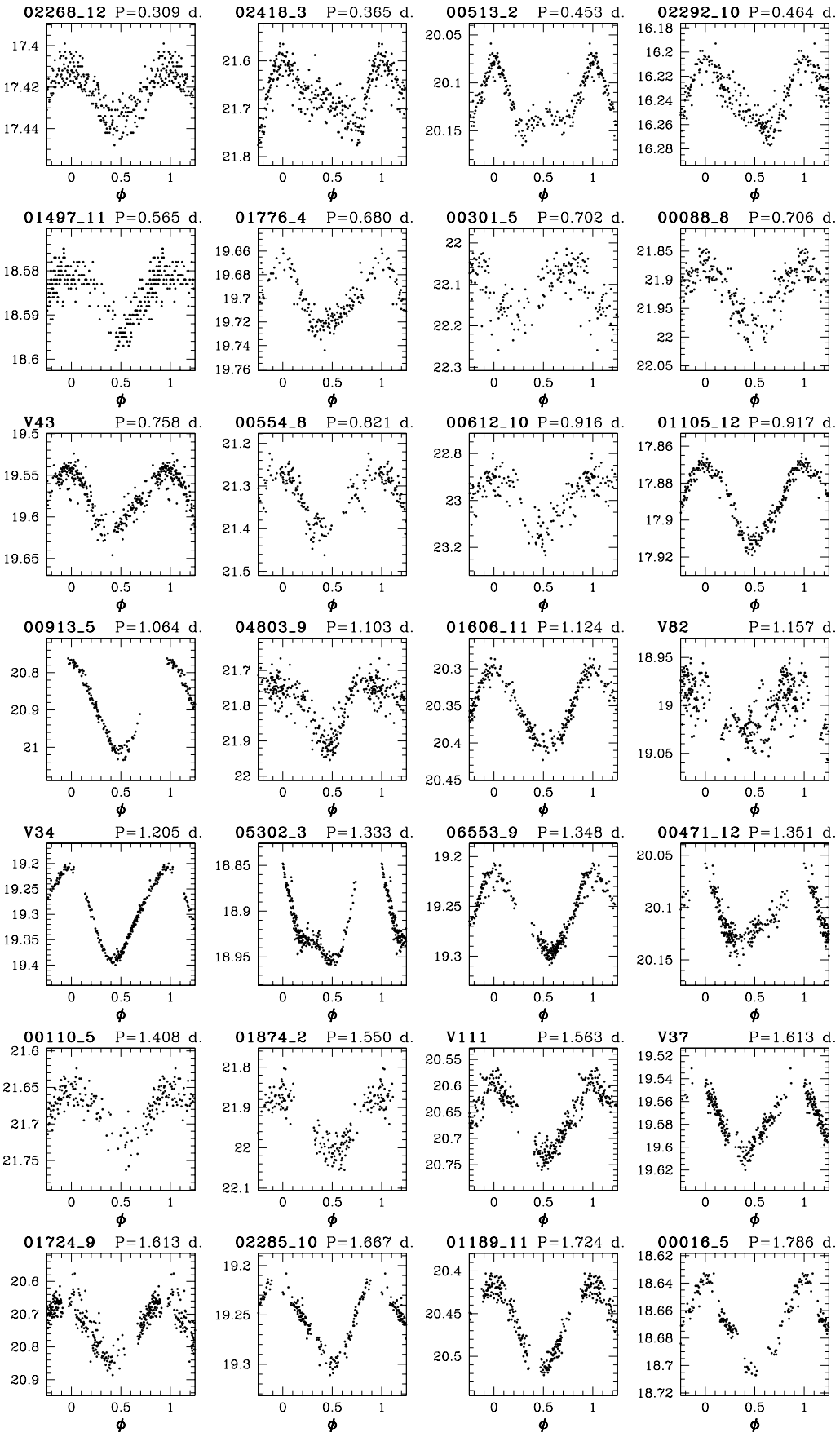

Figure A.8: Rotational variables with a single–wave light curve, in some cases very distorted (Fig. 1/3).

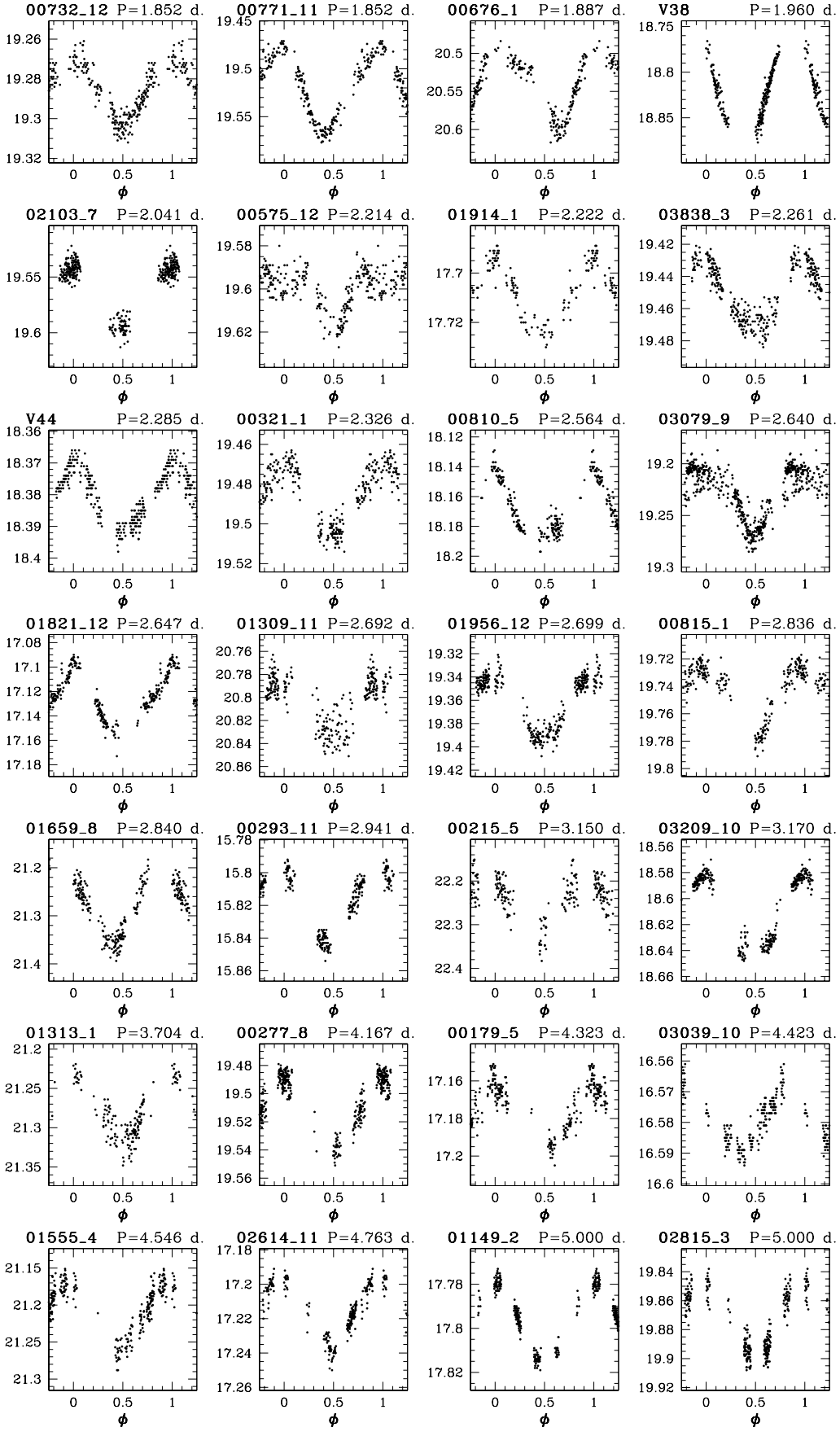

Figure A.9: Rotational variables with a single–wave light curve, in some cases very distorted (Fig. 2/3).

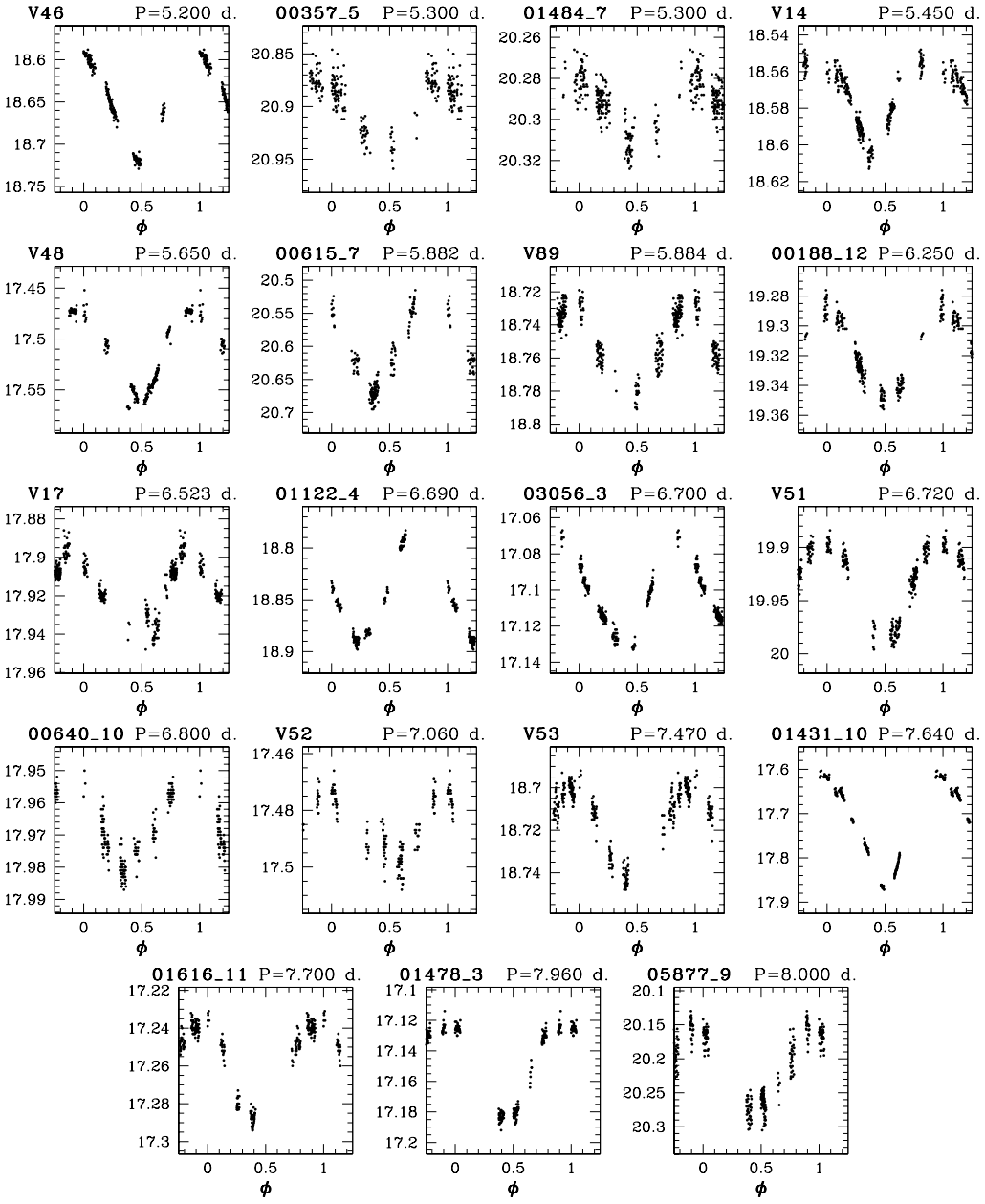

Figure A.10: Rotational variables with a single–wave light curve, in some cases very distorted (Fig. 3/3).

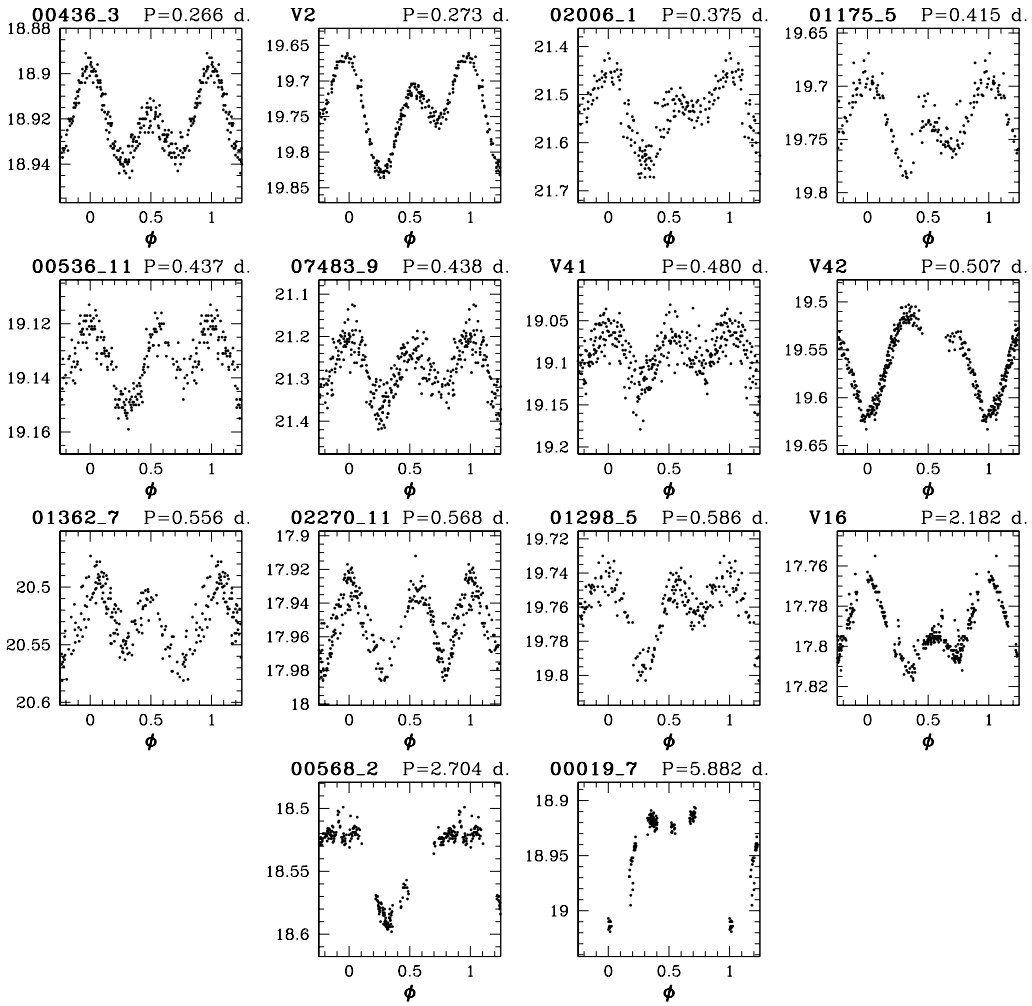

Figure A.11: Rotational variables with a double–wave light curve.

Table A.7: Long period variable stars (ordered by increasing right ascension).

Star	α_{2000}	δ_{2000}	V [mag]	$< B-V >$ [mag]	$< V-I >$ [mag]	Ref.	Memb.	Distance [arcmin]	Star	α_{2000}	δ_{2000}	V [mag]	$< B-V >$ [mag]	$< V-I >$ [mag]	Ref.	Memb.	Distance [arcmin]
00091_1	19.323698	37.943716	19,16				nd2	20.2	V90	19.349686	37.746449	18,11	0,86	0,94	k	94	1,9
00143_1	19.323947	37.927971	20.11				nd2	19.5	02011_3	19.349693	37.958382	19.50	1.19	1.16	k	nm	11.3
00250_7	19.324384	37.779393	18.32				nd2	16.8	01908_3	19.349867	37.947132	19.29	1.05	1.09	k	m?	10.6
00326_7	19.324675	37.719342	17.99				nd2	16.9	V91	19.350151	37.811325	18.07	0.83	0.91	k	m?	2.8
00364_7	19.324832	37.798606	20.17				nd2	16.6	07680_9	19.350193	37.718224	18.32	0.89	0.97	k	98	3.5
00377_1	19.325260	38.018518	18.72				nd2	21.9	07914_9	19.350483	37.822048	18.64	1.12	1.27	s	m?	3.5
00466_7	19.325296	37.809032	14.65				nd2	16.3	V100	19.350498	37.761631	17.13	1.02		k	m?	1.8
00435_1	19.325525	37.990790	16,89				nd2	20.7	V31	19,350683	37.785912	17,12	1,00	1,02	k	97	2,1
00537_1	19.325956	38.059293	18.33				nd2	23.3	01344_3	19.350784	37.970558	18.17	1.33	1.48	k	nm	12.1
00552_1	19.325972	37.941670	18.10				nd2	18.7	V62	19,350847	37.731068	19,45	1,02	1,07	k	m?	3,1
00651_7	19.326084	37.647564	16,89				nd2	17.3	01252_3	19,350937	37.911869	19,85	1,55	2.66	k	nm	8,7
00819_7	19.326732	37.764538	18,02				nd2	15.2	08747_9	19,351194	37.651299	21,32	1,50	1,71	s	nm	7.6
00836_7	19.326803	37.684309	19,78				nd2	16.0	00990_3	19,351418	38.014648	17.29				nd2	14,8
00804_1	19.327102	38.039468	21,14				nd2	21,9	V110	19,351603	37.741802	17.75	0,71	0,76	k	25	3,1
00814_1	19.327140	38.035436	20,78				nd2	21.7	09376_9	19,351952	37.831886	18,21	1,00	1,02	k	92	4.6
00973_1	19.327784	37.996820	19.17				nd2	19.7	09611_9	19.352139	37.773365	17.97	0.85	0.91	k	76	2.9
01095_7	19.327905	37.726883	15.41				nd2	14.6	V66	19.352339	37.748669	15.95	1.29	1.39	k	m?	3.3
01145_1	19.328562	38.051636	20.12				nd2	21.8	00038_3	19.352835	37.851254	19.06	0.88	0.97	k	m?	5.9
01382_7	19.329091	37.812623	18.99				nd2	13.7	00176_10	19.353423	37.611797	17.90	1.39	1.59	k	nm	10.3
01536_7	19.329780	37.640689	17.85	0.91		k	nm	15.2	V58	19.354042	37.801240	17.52	0.89	0.94	k	87	4.6
01513_1	19.330106	37.876259	17.18	0.70		k	nm	14.2	00630_10	19.354660	37.738732	18.98	1.27	1.29	k	m?	5.1
01746_7	19.330667	37.812027	18.84	1.08		k	nm	12.6	00670_10	19.354823	37.806999	23.18	-0.40	0.54	s	m?	5.3
01829_7	19.330990	37.707912	15.20	1.31		k	nm	12.7	01536_4	19.355383	37.882149	17.21	1.18	1.29	k	nm	8.4
01873_1	19.331671	37.912256	19,41	0,98		k	nm	14.4	01415_4	19,355972	38.000843	17,60	1,50	1,92	k	nm	14,9
02096_7	19.332013	37.776243	16,79	1,05		k	nm	11.4	01169_10	19.356078	37.634936	15.34	0,88	1,02	k	nm	10,0
02126_7	19.332109	37.673400	19,20	1,38		k	nm	12,8	V55	19.356228	37.841698	16,12	1,48	1,88	k	nm	7.2
02004_1	19.332252	38.055218	19,85				nd2	20.4	01232_10	19.356296	37.664158	19,31	1.41	1.64	k	nm	8,7
02262_7	19.332626	37.658640	17,99	0,77		k	nm	12,9	01225_10	19.356349	37.770012	21,02		2,91	k	nm	5.9
V114	19.333338	37.812103	17,60	1,10	1,15	k	m?	10,7	01279_10	19.356519	37.757845	20.83	1,00	1,22	k	nm	6.1
00285_2	19.334742	38.038967	19.13				nd2	18.6	01210_4	19.356915	37.957123	17.69	0.75	0.86	k	nm	12.8
00404_8	19.335062	37.790737	18,68	0,69		k	nm	9.3	01417_10	19.356934	37.756828	17.03	1,11	1,17	k	nm	6.4
00386_2	19.335152	37.960213	21.51				nd2	14.6	01101_4	19.357428	37.882973	18.25	1.02	1.11	k	nm	9.4
00620_8	19.335981	37.656742	18.99	1.61	2.08	k	nm	11.0	01082_4	19.357555	37.938122	20.49	1.24	1.10	k	nm	12.1
00791_2	19.337513	38.014545	18.01				nd2	16.4	01070_4	19.357592	37.913498	17.53	1.49	2.15	k	nm	10.9
00907_2	19.338146	38.041290	15.62				nd2	17.6	01682_10	19.357705	37.729503	18.40	0.93	0.98	k	m?	7.3
01212_8	19.338499	37.721958	18.45	0.99	1.10	s	nm	7.4	01807_10	19.358104	37.721153	18.17	1.49	2.02	k	nm	7.8
01222_8	19.338552	37.737770	18.26	1.12	1.18	k	nm	7.1	00920_4	19.358349	37.962833	17.65	0.98	1.00	k	nm	13.6
01126_2	19.339148	37.937424	16,93				nd2	11,8	01885_10	19,358407	37.824782	19,23	0,83	0,88	k	nm	8,0
01122_2	19.339149	38.031670	18.55				nd2	16.8	02145_10	19.359033	37.664901	16.66	1.24	1.36	k	nm	10.1
01406_8	19.339247	37.695103	19,03	1,22	1,37	k	nm	7,8	02165_10	19.359100	37.668317	19,60	1,54	2,31	k	nm	10,0
V59	19.339304	37.806061	17.96	1,30	1,42	k	nm	6.6	02250_10	19.359370	37.663215	18,71	0,99	1,12	k	nm	10,4
01179_2	19.339432	37.995293	19,66				nd2	14,7	00717_4	19.359394	37.895435	18,02	1,28	1,42	k	nm	11,0
01622_8	19.340046	37.629841	18,09	1,42	1,64	k	nm	10,2	00718_4	19.359436	37.961086	20,26	1,44	1,67	k	nm	13,9
02022_8	19.341475	37.682644	18,58	1,27	1,44	k	nm	7,1	02268_10	19.359475	37.731544	18,59	0,95	0,99	k	m	8,5
02108_8	19.341743	37.645943	19.50	0.97	1.12	k	nm	8.8	00598_4	19.360041	37.997711	16.73	0.90	1.05	k	nm	16.0
02138_8	19.341864	37.749653	19.68	1.12	1.18	k	m	4.6	00569_4	19.360079	37.848969	19.88	1.23	1.28	k	nm	9.7
02444_8	19.342766	37.810604	18.34	0.93	1.00	k	78	4.4	00538_4	19.360250	37.932350	17.58	0.96	0.99	k	nm	13.0
06098_3	19.343510	38.050224	18.50				nd2	17.0	00422_4	19.360813	37.962696	18.18	1.00	1.12	k	nm	14.6
05998_3	19.343616	37.956688	19.21	1.39	1.52	k	nm	11.5	00381_4	19.360947	37.864788	19.81	1.62	2.35	k	nm	10.7
05951_3	19.343662	37.927708	18.06				nd1	9.9	00313_4	19.361338	37.894558	18.56	0.72	0.79	k	nm	12.0
05938_3	19.343676	37.927959	18.19				nd1	9.9	02898_10	19.361434	37.604020	22.56				nd2	13.9
00510_9	19.343704	37.796719	18.67	0.94	0.98	k	83	3.4	02924_10	19.361641	37.711676	18.04	1.47	1.82	k	nm	10.3
05870_3	19.343727	37.882679	21.96				nd1	7.3	00092_11	19.363431	37.702573	18.52	1.63	1.95	k	nm	11.7
00835_9	19.344023	37.766895	20.02	1.21	1.25	k	m?	2.9	00097_5	19.363811	37.998650	19.70	0.97	0.99	k	nm	17.6
05677_3	19.344053	37.908951	18.83	1.50	1.81	k	nm	8.7	00473_11	19.364836	37.670896	19.83	0.75	0.91	k	nm	13.4
05524_3	19.344362	38.041668	20.16				nd2	16.4	00297_5	19.365023	37.926561	22.15				nd2	15.2
01610_9	19.344818	37.740486	19.09	1.01	1.05	k	m	3.0	00553_11	19.365157	37.749285	16.26	0.92	1.02	k	nm	12.2
05014_3	19.345045	37.876141	16.24	1.06	1.17	k	m?	6.6	00448_5	19.365911	37.852960	17.32				nd2	13.6
V94	19.345139	37.743549	17.54	0.88	0.92	k	90	2.7	00819_11	19.366089	37.737134	18.77				nd2	13.0
V95	19.345295	37.792412	19.16	1.03	1.10	k	93	2.3	00521_5	19.366291	37.911656	17.26				nd2	15.4
04768_3	19.345497	37.987465	19.83	1.16	1.22	k	m?	13.1	00601_5	19.366800	37.992387	17.91				nd2	18.8
04666_3	19.345663	38.023544	15.83				nd2	15.2	01021_11	19.366890	37.806929	17.40				nd2	13.6
02716_9	19.345829	37.651981	17.69	1.45	1.73	k	nm	7.4	00793_5	19.367687	37.917070	18.32				nd2	16.5
V56(=V96)	19.345908	37.763525	17.01	0.95	0.97	k	98	1.6	01304_11	19.367749	37.637939	18.65				nd2	16.2
04392_3	19.345982	37.870571	17.90	0.88	0.92	k	m	6.1	00922_5	19.368542	37.950158	18.62				nd2	18.1
04368_3	19.346024	37.882671	19.62	1.13	1.12	k	m?	6.8	01525_11	19.368695	37.773095	18.81				nd2	14.7
04293_3	19.346100	37.838703	19,46				nd1	4.3	01695_11	19.369359	37.789309	17.96				nd2	15.2
04298_3	19.346115	37.886810	18.35	0,78	0,92	k	nm	7,0	01785_11	19.369770	37.820589	17.13				nd2	15.7
04160_3	19.346313	37.864944	17.34	1,06	1,11	k	m?	5.7	02010_11	19.370466	37.700018	19.73				nd2	16.5
03987_3	19.346600	37.910511	19,17	1,04	1,10	k	m?	8.4	01245_5	19.370613	37.897333	18.30				nd2	17.7
V75	19.346651	37.766308	17.38	0,94	0,98	s	m	1,0	02401_11	19.371975	37.721131	16.62				nd2	17.3
03687_9	19.346727	37.787651	20.13	1,07	1,45	k	m?	1.3	02419_11	19.371994	37.662943	17.30				nd2	18.2
03859_3	19.346788	37.889477	20.95	1.11	1.85	k	nm	7.1	02550_11	19.372438	37.653960	21.54				nd2	18.7
04133_9	19.347109	37.777020	18,47	0,94	0,98	k	98	0,7	00941_12	19.376714	37.722466	17.77				nd2	20.6
V76(=V85)	19.347192	37.764169	18.19	1.03	1.15	k	97	0.8	01041_12	19.376987	37.656970	17.89				nd2	21.7
V86	19.347258	37.808815	19.44	1.06	1.14	k	83	2.3	01038_12	19.377120	37.779197	20.33				nd2	20.7
V87	19.347996	37.749668	18.12	0.91	0.93	k	98	1.3	01150_12	19.377457	37.669195	17.18				nd2	21.8
05487_9	19.348234	37.677147	18.53	0.93	1.01	k	m?	5.7	01275_12	19.378092	37.727700	20.16				nd2	21.5
05673_9	19.348469	37.793930	20.61	1.29	1.62	k	m?	1.4	01807_12	19.380555	37.832929	18.99				nd2	23.4
05740_9	19.348534	37.808022	17.96	0.93		k	95	2.2	01915_12	19.381010	37.826766	20.20				nd2	23.7
06509_9	19.349110	37.684639	20.79	1.37	1.79	k	m?	5.3	02001_12	19.381172	37.629091	20.49				nd2	25.1
06532_9	19.349180	37.785137	18.01	0.91	0.95	s	m?	1.1	01961_12	19.381188	37.780646	17.87				nd2	23.6
06725_9	19.349329	37.724495	17.77	0.91		k	91	3.0	01968_12	19.381265	37.804920	18.71				nd2	23.7
06796_9	19.349415	37.769268	18.46	0.92	1.04	k	92	1.0	02176_12	19.381966	37.690587	19.60				nd2	24.6

Appendix B

List of identified variables in NGC 6253

This Appendix includes the full list of the identified variables, separated according to our classification:

1. Pulsating variables: Table: B.1, Figures: B.
2. EW–Type variables: Tables: B.2, B.3, B.4, B.5, B.6. Figures: B.2, B.3, B.4, B.5, B.6, B.7, B.8, B.9.
3. EA–type variables: Tables: B.7, B.8, Figures: B.10, B.11, B.12.
4. EB–type variables: Table: B.9, Figure: B.13.
5. RS-CVn variables: Table: B.10, Figure: B.14, B.15, B.16.
6. Rotational single-wave variables: Table: B.11, Figures: B.17, B.18.
7. Rotational double-wave variables: Table: B.12, Figures: B.19, B.20.

The value T_0 is referred to the time of maximum brightness for: pulsating and rotational variables; to the minimum for eclipsing binaries.

Table B.1: Pulsating variables.

Star	Type	α_{2000}	δ_{2000}	V	$< B-V >$	$< V-I >$	T_0	Period	Ampl.	Distance	Memb.
		[hrs]	[deg]	[mag]	[mag]	[mag]	[HJD-253100]	[d]	[mag]	arcmin	%
16334_6	DSCT	–	–	–	–	–	70.605	0.03065	0.02	–	–
11353_4	DSCT	–	–	–	–	–	70.586	0.03818	0.04	–	–
04756_6	DSCT	–	–	–	–	–	70.586	0.04065	0.04	–	–
22953_1	DSCT	–	–	–	–	–	70.613	0.04182	0.02	–	–
03523_3	DSCT	16.964172	-52.719109	–	–	–	70.582	0.04970	0.01	12.0	–
16076_4	DSCT	–	–	–	–	–	70.586	0.05494	0.06	–	–
08420_6	DSCT	–	–	–	–	–	70.629	0.05611	0.02	–	–
22047_5	DSCT	–	–	–	–	–	70.586	0.05823	0.03	–	–
04942_4	DSCT	–	–	–	–	–	70.617	0.06244	0.04	–	–
08514_6	DSCT	–	–	–	–	–	70.590	0.06752	0.01	–	–
08103_4	DSCT	–	–	–	–	–	70.625	0.09455	0.01	–	–
09747_6	HADS	–	–	–	–	–	70.586	0.06248	0.09	–	–
15098_6	HADS	–	–	–	–	–	70.648	0.08412	0.09	–	–
26414_6	HADS	–	–	–	–	–	70.602	0.09374	0.43	–	–
04116_6	HADS	–	–	–	–	–	70.648	0.09771	0.24	–	–
04180_4	RR	–	–	–	–	–	70.594	0.31073	0.27	–	–
10540_2	RR	16.986982	-52.673369	17.509	0.858	1.195	70.965	0.43030	0.20	2.4	72
15578_7	RR	–	–	–	–	–	71.051	0.51	0.58	–	–
03814_4	RR	–	–	–	–	–	71.066	0.54	0.68	–	–
02729_4	CEP	–	–	–	–	–	71.434	1.40	0.07	–	–

Table B.2: Contact binaries.

Star	α_{2000}	δ_{2000}	V	$< B-V >$	$< V-I >$	T_0	Period	Ampl.	Distance	Memb.
	[hrs]	[deg]	[mag]	[mag]	[mag]	[HJD-253100]	[d]	[mag]	arcmin	%
20779_2	16.980289	-52.752025	20.126	–	1.307	70.617	0.18018	0.06	3.6	0
12912_3	16.968906	-52.784447	–	–	–	70.691	0.20639	0.07	10.1	–
00441_4	–	–	–	–	–	70.586	0.21002	0.38	–	–
12192_1	–	–	–	–	–	70.664	0.22407	0.33	–	–
10086_5	–	–	–	–	–	70.766	0.22423	0.53	–	–
05190_4	–	–	–	–	–	70.715	0.23070	0.36	–	–
16081_3	16.972849	-52.627533	–	–	–	70.727	0.23203	0.62	9.3	–
00114_5	–	–	–	–	–	70.785	0.23280	0.09	–	–
02456_8	–	–	–	–	–	70.773	0.23753	0.12	–	–
14996_2	16.988190	-52.614256	21.294	–	1.791	70.609	0.23792	0.27	6.0	0
20865_3	16.966557	-52.646332	–	–	–	70.711	0.23934	0.11	11.6	–
27129_8	–	–	–	–	–	70.777	0.24018	0.15	–	–
22710_1	–	–	–	–	–	70.605	0.24073	0.62	–	–
21930_7	–	–	–	–	–	70.633	0.24190	0.44	–	–
14717_5	–	–	–	–	–	70.668	0.24230	0.16	–	–
23722_8	–	–	–	–	–	70.797	0.24369	0.16	–	–
24765_2	16.977797	-52.778822	21.576	–	1.705	70.797	0.24825	0.15	5.7	0
26486_8	–	–	–	–	–	70.582	0.25020	0.18	–	–
21314_8	–	–	–	–	–	70.582	0.25022	0.10	–	–
12315_5	–	–	–	–	–	70.719	0.25155	0.53	–	–
24956_4	–	–	–	–	–	70.605	0.25528	0.16	–	–
11889_8	–	–	–	–	–	70.723	0.25613	0.35	–	–
15389_2	16.977903	-52.609304	19.929	1.109	1.058	70.582	0.25870	0.32	7.0	0
07718_6	–	–	–	–	–	70.773	0.25921	0.46	–	–
18192_4	–	–	–	–	–	70.727	0.25922	0.16	–	–
15124_4	–	–	–	–	–	70.766	0.26079	0.06	–	–
20347_5	–	–	–	–	–	70.672	0.26120	0.16	–	–
09939_3	16.971869	-52.659145	–	–	–	70.703	0.26154	0.53	8.7	–
23514_6	–	–	–	–	–	70.734	0.26185	0.71	–	–
03026_5	–	–	–	–	–	70.730	0.26267	0.45	–	–
09894_8	–	–	–	–	–	70.645	0.26627	0.22	–	–
26159_6	–	–	–	–	–	70.824	0.26690	0.42	–	–
16934_3	16.971523	-52.718536	–	–	–	70.664	0.26867	0.04	8.0	–
09268_2	16.981396	-52.690234	16.361	1.073	1.364	70.637	0.26920	0.04	2.1	87
06219_6	–	–	–	–	–	70.773	0.26973	0.28	–	–
10521_1	–	–	–	–	–	70.832	0.27082	0.21	–	–
28959_2	–	–	–	–	–	70.688	0.27090	0.07	–	–
25539_2	16.980309	-52.677632	18.180	0.750	1.061	70.676	0.27100	0.01	3.0	0
27971_5	–	–	–	–	–	70.801	0.27217	0.31	–	–
08990_4	–	–	–	–	–	70.777	0.27235	0.10	–	–
07630_4	–	–	–	–	–	70.727	0.27260	0.50	–	–
27757_1	–	–	–	–	–	70.848	0.27310	0.30	–	–
14165_4	–	–	–	–	–	70.781	0.27445	0.43	–	–
26461_4	–	–	–	–	–	70.785	0.27468	0.18	–	–
25579_5	–	–	–	–	–	70.633	0.27468	0.10	–	–
22858_8	–	–	–	–	–	70.613	0.27522	0.46	–	–
04767_5	–	–	–	–	–	70.688	0.27588	0.43	–	–
10921_6	–	–	–	–	–	70.727	0.27660	0.38	–	–
13954_5	–	–	–	–	–	70.750	0.27690	0.31	–	–
04477_2	16.983778	-52.757125	18.812	0.843	1.144	70.625	0.27757	0.04	3.0	0

Table B.3: Contact binaries.

Star	α_{2000}	δ_{2000}	V	$< B-V >$	$< V-I >$	T_0	Period	Ampl.	Distance	Memb.
	[hrs]	[deg]	[mag]	[mag]	[mag]	[HJD-253100]	[d]	[mag]	arcmin	%
17967_4	–	–	–	–	–	70.633	0.27844	0.14	–	–
24174_8	–	–	–	–	–	70.656	0.27887	0.12	–	–
04862_5	–	–	–	–	–	70.758	0.27940	0.29	–	–
25118_8	–	–	–	–	–	70.852	0.27953	0.04	–	–
06738_7	–	–	–	–	–	70.777	0.28038	0.44	–	–
01274_3	16.973759	-52.627018	–	–	–	70.711	0.28168	0.30	8.9	–
07508_8	–	–	–	–	–	70.855	0.28180	0.39	–	–
04611_2	16.986923	-52.755080	19.237	0.969	1.350	70.684	0.28199	0.02	3.1	10
16816_7	–	–	–	–	–	70.828	0.28241	0.48	–	–
21127_7	–	–	–	–	–	70.809	0.28269	0.27	–	–
13285_5	–	–	–	–	–	70.785	0.28280	0.73	–	–
16392_8	–	–	–	–	–	70.766	0.28296	0.07	–	–
14428_7	–	–	–	–	–	70.594	0.28400	0.17	–	–
26310_1	–	–	–	–	–	70.637	0.28402	0.27	–	–
15906_5	–	–	–	–	–	70.605	0.28511	0.18	–	–
09914_1	–	–	–	–	–	70.582	0.28650	0.17	–	–
00564_2	16.979319	-52.812692	20.852	1.020	1.139	70.586	0.28755	0.07	6.9	0
00920_4	–	–	–	–	–	70.859	0.28946	0.20	–	–
20677_3	16.966167	-52.710003	–	–	–	70.605	0.28960	0.07	10.9	–
17050_5	–	–	–	–	–	70.852	0.29009	0.16	–	–
00145_2	16.982185	-52.818812	17.339	1.141	1.186	70.676	0.29110	0.26	6.8	0
10327_5	–	–	–	–	–	70.711	0.29131	0.06	–	–
17881_1	–	–	–	–	–	70.695	0.29140	0.16	–	–
08259_7	–	–	–	–	–	70.746	0.29159	0.13	–	–
10853_2	16.986719	-52.669346	17.037	0.968	1.186	70.777	0.29340	0.02	2.6	78
17587_5	–	–	–	–	–	70.730	0.29340	0.03	–	–
08783_4	–	–	–	–	–	70.684	0.29376	0.26	–	–
08784_4	–	–	–	–	–	70.828	0.29389	0.52	–	–
17194_2	16.983366	-52.583898	18.284	0.897	1.248	70.742	0.29400	0.28	7.5	0
12169_5	–	–	–	–	–	70.613	0.29880	0.18	–	–
11470_2	16.982145	-52.661319	20.564	0.978	0.959	70.836	0.29920	0.18	3.2	21
10995_3	16.970404	-52.573753	–	–	–	70.812	0.30060	0.12	12.4	–
13391_3	16.963194	-52.732098	–	–	–	70.801	0.30160	0.12	12.5	–
07912_8	–	–	–	–	–	70.746	0.30210	0.02	–	–
27652_4	–	–	–	–	–	70.637	0.30244	0.25	–	–
22508_4	–	–	–	–	–	70.648	0.30281	0.07	–	–
10725_1	–	–	–	–	–	70.863	0.30368	0.51	–	–
19339_7	–	–	–	–	–	70.867	0.30368	0.46	–	–
19340_7	–	–	–	–	–	70.867	0.30380	0.38	–	–
19697_5	–	–	–	–	–	70.617	0.30521	0.81	–	–
21383_4	–	–	–	–	–	70.707	0.30524	0.19	–	–
22513_5	–	–	–	–	–	70.883	0.30529	0.26	–	–
22157_6	–	–	–	–	–	70.598	0.30556	0.63	–	–
21382_4	–	–	–	–	–	70.695	0.30556	0.16	–	–
05440_5	–	–	–	–	–	70.707	0.30660	0.50	–	–
21824_4	–	–	–	–	–	70.734	0.30689	0.07	–	–
08066_7	–	–	–	–	–	70.703	0.30749	0.62	–	–
13423_5	–	–	–	–	–	70.695	0.30801	0.32	–	–
12151_4	–	–	–	–	–	70.695	0.30822	0.36	–	–
14807_4	–	–	–	–	–	70.785	0.30831	0.10	–	–

Table B.4: Contact binaries.

Star	α_{2000}	δ_{2000}	V	$< B-V >$	$< V-I >$	T_0	Period	Ampl.	Distance	Memb.
	[hrs]	[deg]	[mag]	[mag]	[mag]	[HJD-253100]	[d]	[mag]	arcmin	%
19512_1	–	–	–	–	–	70.844	0.30875	0.13	–	–
01798_1	–	–	–	–	–	70.812	0.30880	0.40	–	–
16316_4	–	–	–	–	–	70.785	0.30898	0.66	–	–
16315_4	–	–	–	–	–	70.785	0.30906	0.34	–	–
12190_1	–	–	–	–	–	70.742	0.30906	0.07	–	–
19951_1	–	–	–	–	–	70.645	0.31080	0.51	–	–
19810_5	–	–	–	–	–	70.727	0.31109	0.11	–	–
12499_3	16.967808	-52.572376	–	–	–	70.871	0.31130	0.20	13.5	–
04359_6	–	–	–	–	–	70.746	0.31170	0.67	–	–
09421_3	16.973892	-52.705635	–	–	–	70.656	0.31190	0.01	6.8	–
23060_4	–	–	–	–	–	70.594	0.31217	0.31	–	–
19643_6	–	–	–	–	–	70.754	0.31253	0.17	–	–
06428_3	16.974588	-52.588867	–	–	–	70.680	0.31280	0.06	10.2	–
08440_3	16.966932	-52.796467	–	–	–	70.699	0.31358	0.35	11.4	–
24391_5	–	–	–	–	–	70.586	0.31662	0.14	–	–
08362_3	16.963221	-52.803123	–	–	–	70.816	0.31708	0.08	13.4	–
22265_6	–	–	–	–	–	70.598	0.31743	0.11	–	–
06418_7	–	–	–	–	–	70.809	0.31743	0.14	–	–
02948_2	16.977133	-52.778642	20.371	0.115	1.712	70.688	0.31800	0.65	5.9	0
22465_7	–	–	–	–	–	70.656	0.31812	0.38	–	–
01441_3	16.972923	-52.819435	–	–	–	70.672	0.32030	0.03	9.2	–
09135_1	–	–	–	–	–	70.773	0.32110	0.66	–	–
26855_6	–	–	–	–	–	70.785	0.32233	0.03	–	–
27351_6	–	–	–	–	–	70.891	0.32240	0.73	–	–
12869_5	–	–	–	–	–	70.602	0.32243	0.26	–	–
30029_4	–	–	–	–	–	70.816	0.32315	2.44	–	–
24512_4	–	–	–	–	–	70.812	0.32315	0.36	–	–
07369_6	–	–	–	–	–	70.727	0.32318	0.54	–	–
18093_8	–	–	–	–	–	70.738	0.32338	0.21	–	–
22091_7	–	–	–	–	–	70.688	0.32533	0.41	–	–
04317_3	16.973907	-52.794777	–	–	–	70.656	0.32733	0.03	7.9	–
22576_6	–	–	–	–	–	70.648	0.32801	0.26	–	–
24316_8	–	–	–	–	–	70.867	0.32875	0.29	–	–
12347_4	–	–	–	–	–	70.688	0.33057	0.46	–	–
11806_5	–	–	–	–	–	70.746	0.33164	0.25	–	–
15757_3	16.966194	-52.687931	–	–	–	70.871	0.33170	0.22	11.1	–
14706_7	–	–	–	–	–	70.836	0.33554	0.08	–	–
22292_7	–	–	–	–	–	70.906	0.33626	0.02	–	–
01904_7	–	–	–	–	–	70.617	0.33660	0.03	–	–
07691_1	–	–	–	–	–	70.637	0.33720	0.40	–	–
07252_1	–	–	–	–	–	70.684	0.33760	0.21	–	–
06503_2	16.988176	-52.728719	19.069	0.910	1.237	70.816	0.33800	0.12	2.2	0
11458_7	–	–	–	–	–	70.828	0.33876	0.20	–	–
20307_3	16.965603	-52.570744	–	–	–	70.703	0.33897	0.18	14.5	–
27138_8	–	–	–	–	–	70.738	0.33925	0.06	–	–
05452_4	–	–	–	–	–	70.664	0.34242	0.48	–	–
05451_4	–	–	–	–	–	70.832	0.34260	0.18	–	–
10096_3	16.969336	-52.645462	–	–	–	70.742	0.34417	0.02	10.3	–
26137_6	–	–	–	–	–	70.652	0.34417	0.24	–	–
17155_5	–	–	–	–	–	70.895	0.34570	0.47	–	–

Table B.5: Contact binaries.

Star	α_{2000}	δ_{2000}	V	$< B-V >$	$< V-I >$	T_0	Period	Ampl.	Distance	Memb.
	[hrs]	[deg]	[mag]	[mag]	[mag]	[HJD-253100]	[d]	[mag]	arcmin	%
27768_6	–	–	–	–	–	70.863	0.34605	0.18	–	–
28186_6	–	–	–	–	–	70.863	0.34605	0.23	–	–
26985_4	–	–	–	–	–	70.645	0.34670	0.42	–	–
27919_8	–	–	–	–	–	70.715	0.34675	0.05	–	–
10974_3	16.973934	-52.576180	–	–	–	70.824	0.34737	0.12	11.1	–
03079_1	–	–	–	–	–	70.918	0.34880	0.39	–	–
11224_3	16.968777	-52.556416	–	–	–	70.773	0.35070	0.22	13.8	–
13453_2	16.983324	-52.635112	19.514	0.478	1.191	70.773	0.35110	0.37	4.5	0
05955_8	–	–	–	–	–	70.617	0.35269	0.37	–	–
11448_6	–	–	–	–	–	70.691	0.35321	0.31	–	–
11447_6	–	–	–	–	–	70.699	0.35321	0.13	–	–
09336_3	16.968647	-52.713390	–	–	–	70.656	0.35394	0.02	9.6	–
08392_4	–	–	–	–	–	70.848	0.35466	0.06	–	–
21923_3	16.966995	-52.630947	–	–	–	70.855	0.35533	0.14	11.8	–
00208_2	16.979084	-52.817910	20.285	1.112	0.934	70.828	0.35610	0.34	7.3	0
10059_1	–	–	–	–	–	70.609	0.35807	0.05	–	–
26817_4	–	–	–	–	–	70.586	0.35828	0.25	–	–
19972_6	–	–	–	–	–	70.605	0.35980	0.32	–	–
04843_2	16.980251	-52.752035	18.945	0.599	1.067	70.617	0.36040	0.06	3.6	0
26844_2	16.980255	-52.752297	100.000	–	–	70.617	0.36040	0.27	3.6	0
02366_2	16.988543	-52.786850	18.099	0.451	1.265	70.594	0.36350	0.31	5.2	35
18198_2	16.984518	-52.570556	19.348	0.899	0.754	70.746	0.36420	0.23	8.3	0
14498_3	16.969845	-52.607384	–	–	–	70.582	0.36442	0.02	11.3	–
15649_2	16.981064	-52.605374	21.536	0.995	1.084	70.770	0.36516	0.29	6.5	0
03734_2	16.981199	-52.767649	19.585	1.071	0.650	70.863	0.36742	0.37	4.0	0
09173_6	–	–	–	–	–	70.863	0.36742	0.61	–	–
11723_4	–	–	–	–	–	70.863	0.36856	0.25	–	–
11724_4	–	–	–	–	–	70.852	0.36933	0.09	–	–
10805_2	16.984692	-52.670194	18.844	0.484	1.631	70.773	0.37090	0.44	2.3	32
05435_3	16.970694	-52.682507	–	–	–	70.773	0.37428	0.19	8.8	–
18276_5	–	–	–	–	–	70.934	0.37490	0.16	–	–
16373_2	16.980406	-52.595258	20.079	0.500	0.958	70.746	0.37550	0.10	7.2	0
06644_3	16.969843	-52.571827	–	–	–	70.707	0.37692	0.25	12.7	–
18759_2	16.980450	-52.563088	19.677	0.887	1.105	70.852	0.37820	0.26	9.0	0
27434_6	–	–	–	–	–	70.582	0.38040	0.25	–	–
08031_6	–	–	–	–	–	70.836	0.38200	0.71	–	–
08822_2	16.989218	-52.696185	18.874	0.816	1.064	70.855	0.38304	0.21	2.6	50
00404_5	–	–	–	–	–	70.602	0.38541	0.34	–	–
01618_8	–	–	–	–	–	70.953	0.38574	0.06	–	–
21319_5	–	–	–	–	–	70.656	0.38660	0.19	–	–
20050_6	–	–	–	–	–	70.742	0.38670	0.07	–	–
01015_2	16.985498	-52.805851	16.085	0.799	1.029	70.637	0.38720	0.05	5.9	22
11185_6	–	–	–	–	–	70.641	0.38830	0.27	–	–
09984_6	–	–	–	–	–	70.812	0.38944	0.25	–	–
24135_2	16.976894	-52.570100	21.389	1.166	1.335	70.648	0.39393	0.14	9.3	0
25832_5	–	–	–	–	–	70.777	0.39460	0.28	–	–
19024_2	16.980335	-52.559693	16.740	0.801	0.894	70.805	0.39520	0.12	9.2	0
22442_6	–	–	–	–	–	70.859	0.39560	0.17	–	–
26667_1	–	–	–	–	–	70.867	0.39570	0.58	–	–
09705_5	–	–	–	–	–	70.766	0.39580	0.20	–	–

Table B.6: Contact binaries.

Star	α_{2000}	δ_{2000}	V	$< B-V >$	$< V-I >$	T_0	Period	Ampl.	Distance	Memb.
	[hrs]	[deg]	[mag]	[mag]	[mag]	[HJD-253100]	[d]	[mag]	arcmin	%
19141_1	–	–	–	–	–	70.867	0.39600	0.12	–	–
16340_3	16.965069	-52.582767	–	–	–	70.602	0.39879	0.02	14.3	–
25157_4	–	–	–	–	–	70.910	0.40259	0.39	–	–
21625_5	–	–	–	–	–	70.840	0.40460	0.02	–	–
15046_2	16.979944	-52.613787	18.258	0.856	1.034	70.867	0.40700	0.05	6.2	26
17494_8	–	–	–	–	–	70.934	0.40941	0.27	–	–
17495_8	–	–	–	–	–	70.934	0.40941	0.28	–	–
22996_7	–	–	–	–	–	70.582	0.41208	0.11	–	–
19322_4	–	–	–	–	–	70.734	0.41902	0.22	–	–
09623_5	–	–	–	–	–	70.887	0.43070	0.39	–	–
05189_3	16.970667	-52.708267	–	–	–	70.926	0.43174	0.02	8.5	–
13354_5	–	–	–	–	–	70.730	0.43294	0.42	–	–
17580_7	–	–	–	–	–	70.887	0.43654	0.35	–	–
25202_5	–	–	–	–	–	70.715	0.44165	0.15	–	–
20160_4	–	–	–	–	–	70.781	0.44334	0.26	–	–
04424_1	–	–	–	–	–	70.758	0.44540	0.13	–	–
03930_4	–	–	–	–	–	70.781	0.45089	0.39	–	–
16369_6	–	–	–	–	–	71.000	0.46310	0.04	–	–
13288_2	16.978201	-52.637555	15.561	1.205	0.933	70.867	0.47290	0.44	5.5	3
26552_1	–	–	–	–	–	70.613	0.48143	0.02	–	–
22792_3	16.974094	-52.580025	–	–	–	70.715	0.48331	0.02	10.8	–
20282_5	–	–	–	–	–	70.637	0.48500	0.32	–	–
23188_2	16.977079	-52.616197	15.044	0.682	0.917	70.594	0.49680	0.32	6.9	87
08194_3	16.961536	-52.819134	–	–	–	70.895	0.53	0.04	14.6	–
22683_1	–	–	–	–	–	70.855	0.55	0.23	–	–
13392_6	–	–	–	–	–	70.715	0.57	0.11	–	–
11558_6	–	–	–	–	–	70.746	0.59	0.14	–	–
09620_1	–	–	–	–	–	70.668	0.61	0.10	–	–
21660_4	–	–	–	–	–	71.215	0.64	0.31	–	–
00188_1	–	–	–	–	–	71.051	0.64	0.09	–	–
04892_3	16.966537	-52.735474	–	–	–	71.023	0.65	0.06	10.7	–
03430_1	–	–	–	–	–	71.098	0.72	0.30	–	–
19284_2	16.977144	-52.556237	16.502	0.489	1.166	70.746	0.77	0.21	10.0	0
10609_2	16.990829	-52.672464	18.180	0.647	0.935	70.828	0.83	0.14	4.0	58
15261_1	–	–	–	–	–	70.695	0.88	0.04	–	–
06387_2	16.986212	-52.730394	16.592	0.860	1.126	71.191	0.92	0.02	1.6	85
28423_8	–	–	–	–	–	70.805	2.14	0.06	–	–
15861_1	–	–	–	–	–	72.582	2.36	0.05	–	–

Table B.7: EA-Type eclipsing binaries.

Star	α_{2000}	δ_{2000}	V	$< B-V >$	$< V-I >$	T_0	Period	Ampl.	Distance	Memb.
	[hrs]	[deg]	[mag]	[mag]	[mag]	[HJD-253100]	[d]	[mag]	arcmin	%
21471_1	–	–	–	–	–	70.648	0.25051	0.86	–	–
21839_2	–	–	–	–	–	70.598	0.25290	1.33	–	–
25622_1	–	–	–	–	–	70.621	0.26185	0.51	–	–
06097_8	–	–	–	–	–	70.844	0.27033	0.77	–	–
00918_4	–	–	–	–	–	70.734	0.28087	0.31	–	–
10274_1	–	–	–	–	–	70.695	0.31380	0.03	–	–
19873_1	–	–	–	–	–	70.625	0.31840	0.54	–	–
02749_1	–	–	–	–	–	70.914	0.34670	0.60	–	–
21594_4	–	–	–	–	–	70.961	0.38744	0.52	–	–
26180_4	–	–	–	–	–	70.801	0.39019	0.60	–	–
23415_5	–	–	–	–	–	70.637	0.39411	0.47	–	–
16368_8	–	–	–	–	–	70.707	0.41166	0.04	–	–
15307_2	16.988695	-52.609974	19.771	1.599	2.637	70.707	0.44900	0.27	6.3	43
05088_8	–	–	–	–	–	70.801	0.45707	0.32	–	–
16525_8	–	–	–	–	–	70.727	0.49625	0.29	–	–
09161_2	16.986677	-52.691535	20.644	2.008	2.391	70.859	0.51	0.69	1.5	0
17502_2	16.983360	-52.579913	22.146	–	2.563	70.855	0.55	0.44	7.7	0
23787_1	–	–	–	–	–	70.625	0.61	0.91	–	–
23781_1	–	–	–	–	–	70.629	0.61	0.30	–	–
16725_2	16.984213	-52.590126	20.034	1.120	1.415	70.945	0.61	0.31	7.1	51
04015_8	–	–	–	–	–	70.734	0.65	0.52	–	–
19258_2	16.979872	-52.556585	16.822	0.804	1.062	71.152	0.66	0.01	9.5	0
25809_8	–	–	–	–	–	71.086	0.66	0.11	–	–
19192_2	16.980442	-52.557440	16.849	0.674	0.907	70.816	0.67	0.01	9.4	0
22574_2	16.989311	-52.650657	18.900	0.503	0.853	70.922	0.68	0.51	4.3	40
06539_2	16.976877	-52.728415	18.891	1.039	1.480	70.727	0.68	0.19	4.4	0
23313_4	–	–	–	–	–	71.031	0.70	0.48	–	–
28980_1	–	–	–	–	–	70.891	0.73	0.39	–	–
01866_2	16.976933	-52.793779	16.460	0.778	0.882	70.883	0.85	0.53	6.7	0
11762_4	–	–	–	–	–	70.926	0.87	0.60	–	–
26784_8	–	–	–	–	–	71.309	0.91	0.18	–	–
04861_8	–	–	–	–	–	70.746	0.91	0.38	–	–
26355_8	–	–	–	–	–	71.168	0.93	0.26	–	–
05247_5	–	–	–	–	–	71.363	1.01	0.13	–	–
23942_2	16.980873	-52.579244	20.714	0.783	1.131	71.617	1.05	0.08	8.0	0
27820_8	–	–	–	–	–	70.812	1.16	0.37	–	–
07143_4	–	–	–	–	–	71.289	1.21	0.15	–	–
13070_2	16.989361	-52.640158	19.836	0.865	1.179	71.680	1.24	0.30	4.8	0
09324_4	–	–	–	–	–	71.809	1.30	0.18	–	–
18145_1	–	–	–	–	–	71.453	1.33	0.38	–	–
13414_8	–	–	–	–	–	70.734	1.35	0.15	–	–
06441_8	–	–	–	–	–	71.828	1.42	0.47	–	–
09471_8	–	–	–	–	–	71.703	1.47	0.02	–	–
25420_6	–	–	–	–	–	71.047	1.55	0.25	–	–
08541_6	–	–	–	–	–	71.004	1.59	0.02	–	–
20077_7	–	–	–	–	–	70.738	1.60	0.56	–	–
03685_4	–	–	–	–	–	71.129	1.61	0.34	–	–
04601_1	–	–	–	–	–	71.828	1.65	0.73	–	–
27270_4	–	–	–	–	–	71.449	1.67	0.54	–	–
19297_4	–	–	–	–	–	72.008	1.69	0.38	–	–

Table B.8: EA-Type eclipsing binaries.

Star	α_{2000}	δ_{2000}	V	$< B-V >$	$< V-I >$	T_0	Period	Ampl.	Distance	Memb.
	[hrs]	[deg]	[mag]	[mag]	[mag]	[HJD-253100]	[d]	[mag]	arcmin	%
09235_8	–	–	–	–	–	72.266	1.78	0.54	–	–
10340_2	16.980457	-52.676389	16.514	0.844	1.099	72.051	1.82	0.02	3.0	38
18972_5	–	–	–	–	–	71.656	1.85	0.60	–	–
16769_8	–	–	–	–	–	72.555	2.07	0.31	–	–
13573_2	16.987514	-52.633374	17.120	0.798	1.022	71.039	2.30	0.34	4.7	8
25223_5	–	–	–	–	–	72.270	2.31	0.28	–	–
18853_2	16.988134	-52.561751	21.330	1.371	2.092	72.613	2.65	0.75	9.0	0
19466_4	–	–	–	–	–	71.688	2.66	0.30	–	–
27374_8	–	–	–	–	–	72.004	3.8	0.14	–	–
15577_2	16.979782	-52.606404	19.574	0.915	1.152	72.207	3.8	0.17	6.7	0

Table B.9: EB-type systems.

Star	α_{2000}	δ_{2000}	V	$< B-V >$	$< V-I >$	T_0	Period	Ampl.	Distance	Memb.
	[hrs]	[deg]	[mag]	[mag]	[mag]	[HJD-253100]	[d]	[mag]	arcmin	%
25252_3	16.974054	-52.641083	–	–	–	70.867	0.30780	0.17	8.2	–
08123_2	16.985958	-52.705800	21.108	1.287	2.288	70.883	0.31903	0.15	0.7	0
14546_3	16.970892	-52.600807	–	–	–	70.766	0.35970	0.31	11.1	–
02944_2	16.990040	-52.778304	15.196	0.592	0.829	70.766	0.42730	0.37	5.1	0
22426_6	–	–	–	–	–	70.711	0.43650	0.33	–	–
16994_7	–	–	–	–	–	70.793	0.52	0.40	–	–
18865_6	–	–	–	–	–	70.703	0.55	0.60	–	–
11754_1	–	–	–	–	–	70.785	0.56	0.27	–	–
05980_6	–	–	–	–	–	70.785	0.63	0.12	–	–
27172_5	–	–	–	–	–	70.629	0.67	0.39	–	–
07509_4	–	–	–	–	–	71.172	0.80	0.20	–	–
00447_2	16.979506	-52.814296	17.669	0.837	0.903	70.777	0.92	0.38	7.0	0
11432_5	–	–	–	–	–	71.738	1.17	0.18	–	–

Table B.10: RS-CVn variables.

Star	α_{2000}	δ_{2000}	V	$< B-V >$	$< V-I >$	T_0	Period	Ampl.	Distance	Memb.
	[hrs]	[deg]	[mag]	[mag]	[mag]	[HJD-253100]	[d]	[mag]	arcmin	%
02582_7	–	–	–	–	–	–	–	0.08	–	–
25516_5	–	–	–	–	–	70.855	–	0.03	–	–
00503_1	–	–	–	–	–	75.906	–	0.03	–	–
20346_3	16.971287	-52.559353	–	–	–	70.844	0.47060	0.06	12.7	–
06395_3	16.965502	-52.591270	–	–	–	70.871	0.55	0.06	13.8	–
20136_7	–	–	–	–	–	70.902	0.59	0.04	–	–
21621_2	16.981159	-52.703461	20.850	0.927	1.589	70.805	0.63	0.29	2.0	0
24631_4	–	–	–	–	–	70.930	0.81	0.24	–	–
21527_6	–	–	–	–	–	70.887	1.05	0.28	–	–
01907_2	16.981108	-52.793187	17.388	0.934	1.260	71.352	1.34	0.15	5.5	0
25070_2	16.987598	-52.738510	19.335	–	1.507	71.953	1.46	0.06	2.4	0
25069_2	16.987574	-52.738541	19.631	–	1.331	71.926	1.46	0.06	2.4	0
26281_4	–	–	–	–	–	71.699	1.77	0.07	–	–
26902_2	16.984060	-52.738899	15.198	0.768	1.019	72.090	2.18	0.05	1.9	90
15961_5	–	–	–	–	–	71.711	2.20	0.13	–	–
05622_3	16.964361	-52.666779	–	–	–	71.500	2.29	0.02	12.4	–
12979_1	–	–	–	–	–	70.738	3.3	0.02	–	–
26602_8	–	–	–	–	–	71.496	5.3	0.12	–	–

Table B.11: Single-wave rotational variables

Star	α_{2000}	δ_{2000}	V	$< B-V >$	$< V-I >$	T_0	Period	Ampl.	Distance	Memb.
	[hrs]	[deg]	[mag]	[mag]	[mag]	[HJD-253100]	[d]	[mag]	arcmin	%
02849_5	–	–	–	–	–	70.805	0.34014	0.03	–	–
08107_3	16.964911	-52.562267	–	–	–	70.648	0.34119	0.01	15.1	–
07149_3	16.965294	-52.749905	–	–	–	70.965	0.52	0.01	11.5	–
25160_6	–	–	–	–	–	70.984	0.68	0.05	–	–
10203_3	16.967066	-52.637199	–	–	–	70.836	0.77	0.02	11.6	–
06026_3	16.969152	-52.625393	–	–	–	70.707	0.95	0.02	11.0	–
15047_5	–	–	–	–	–	70.984	1.12	0.02	–	–
30482_1	–	–	–	–	–	70.617	1.18	0.03	–	–
05605_3	16.966005	-52.668472	–	–	–	71.324	1.27	0.04	11.5	–
22750_5	–	–	–	–	–	71.664	1.31	0.17	–	–
13347_3	16.974161	-52.738277	–	–	–	71.086	1.42	0.06	6.6	–
14911_2	16.981436	-52.615434	18.415	0.972	1.207	70.902	1.58	0.05	5.9	63
12587_6	–	–	–	–	–	71.531	1.59	0.05	–	–
15454_8	–	–	–	–	–	70.941	1.63	0.11	–	–
17345_7	–	–	–	–	–	71.570	1.63	0.18	–	–
04644_3	16.970226	-52.760670	–	–	–	72.188	1.68	0.03	9.0	–
06406_3	16.973270	-52.588940	–	–	–	72.031	1.72	0.03	10.7	–
13548_3	16.961927	-52.714737	–	–	–	71.711	1.74	0.04	13.2	–
11977_1	–	–	–	–	–	71.188	1.84	0.01	–	–
03428_2	16.981392	-52.772055	19.014	0.891	1.295	71.148	2.08	0.05	4.2	4
17385_8	–	–	–	–	–	71.406	2.35	0.04	–	–
08284_2	16.983198	-52.703842	16.406	0.761	1.032	70.609	2.39	0.05	0.9	0
12192_3	16.974863	-52.632557	–	–	–	71.918	2.40	0.02	8.2	–
06272_6	–	–	–	–	–	71.496	2.53	0.11	–	–
15378_6	–	–	–	–	–	72.266	2.62	0.07	–	–
23010_5	–	–	–	–	–	72.203	2.69	0.04	–	–
27108_4	–	–	–	–	–	71.871	2.70	0.12	–	–
10372_2	16.978662	-52.675731	18.433	0.996	1.463	72.957	2.74	0.04	3.8	26
17835_8	–	–	–	–	–	71.543	2.78	0.04	–	–
05858_7	–	–	–	–	–	71.652	2.83	0.05	–	–
12388_4	–	–	–	–	–	71.496	2.89	0.02	–	–
07392_1	–	–	–	–	–	70.914	2.98	0.11	–	–
10199_7	–	–	–	–	–	70.738	3.0	0.04	–	–
13461_1	–	–	–	–	–	71.523	3.1	0.01	–	–
15993_2	16.989754	-52.600491	19.857	1.365	1.858	71.766	3.2	0.03	7.0	0
27870_8	–	–	–	–	–	71.664	3.2	0.05	–	–

Table B.12: Double-wave or distorted rotational variables.

Star	α_{2000}	δ_{2000}	V	$< B-V >$	$< V-I >$	T_0	Period	Ampl.	Distance	Memb.
	[hrs]	[deg]	[mag]	[mag]	[mag]	[HJD-253100]	[d]	[mag]	arcmin	%
14568_1	–	–	–	–	–	75.906	–	0.13	–	–
04796_8	–	–	–	–	–	70.605	0.19174	0.05	–	–
27582_2	16.982239	-52.598549	21.854	0.986	1.368	70.762	0.35688	0.34	6.7	0
00729_1	–	–	–	–	–	71.082	0.57	0.03	–	–
05640_1	–	–	–	–	–	70.977	0.58	0.04	–	–
07671_4	–	–	–	–	–	70.668	0.61	0.03	–	–
12434_1	–	–	–	–	–	70.945	0.64	0.11	–	–
20185_4	–	–	–	–	–	71.188	0.72	0.14	–	–
22278_2	16.976639	-52.665819	20.556	1.501	2.044	70.988	0.86	0.07	5.1	0
06932_2	16.987518	-52.722460	18.267	0.990	1.349	70.688	0.90	0.05	1.7	10
06474_2	16.983744	-52.729254	19.303	0.969	1.368	70.949	0.90	0.06	1.4	9
14557_3	16.963148	-52.600479	–	–	–	70.828	0.95	0.05	14.6	–
05167_3	16.966007	-52.710724	–	–	–	70.637	1.03	0.02	11.0	–
04913_3	16.971159	-52.735096	–	–	–	71.395	1.10	0.04	8.2	–
19467_6	–	–	–	–	–	71.176	1.12	0.08	–	–
21207_1	–	–	–	–	–	70.875	1.19	0.09	–	–
30202_1	–	–	–	–	–	70.676	1.19	0.04	–	–
00455_2	16.985790	-52.814033	20.030	1.398	1.875	70.949	1.21	0.07	6.4	0
26964_5	–	–	–	–	–	71.410	1.23	0.12	–	–
10610_4	–	–	–	–	–	71.734	1.26	0.05	–	–
05898_2	16.981155	-52.737351	18.117	1.160	1.635	71.496	1.59	0.06	2.6	53
02033_8	–	–	–	–	–	70.906	1.59	0.09	–	–
08864_1	–	–	–	–	–	70.859	1.60	0.04	–	–
06236_1	–	–	–	–	–	72.207	1.75	0.01	–	–
02131_1	–	–	–	–	–	71.059	1.83	0.16	–	–
14603_2	16.981838	-52.619528	19.541	0.949	1.237	72.031	1.91	0.07	5.6	43
15421_8	–	–	–	–	–	71.242	2.14	0.10	–	–
09775_2	16.990065	-52.683311	18.298	1.033	1.489	72.156	2.14	0.02	3.3	64
14272_8	–	–	–	–	–	72.906	2.42	0.03	–	–
15936_6	–	–	–	–	–	70.734	2.43	0.09	–	–
09463_7	–	–	–	–	–	72.711	2.77	0.07	–	–
10042_2	16.984837	-52.679586	16.496	0.797	1.025	71.445	3.1	0.07	1.7	87
19539_8	–	–	–	–	–	70.793	3.2	0.04	–	–
09901_2	16.982153	-52.681548	18.364	0.955	1.355	72.668	3.4	0.08	2.1	0
13211_7	–	–	–	–	–	71.312	3.5	0.08	–	–
11077_2	16.990780	-52.666229	17.397	0.900	1.192	70.801	5.1	0.06	4.2	71

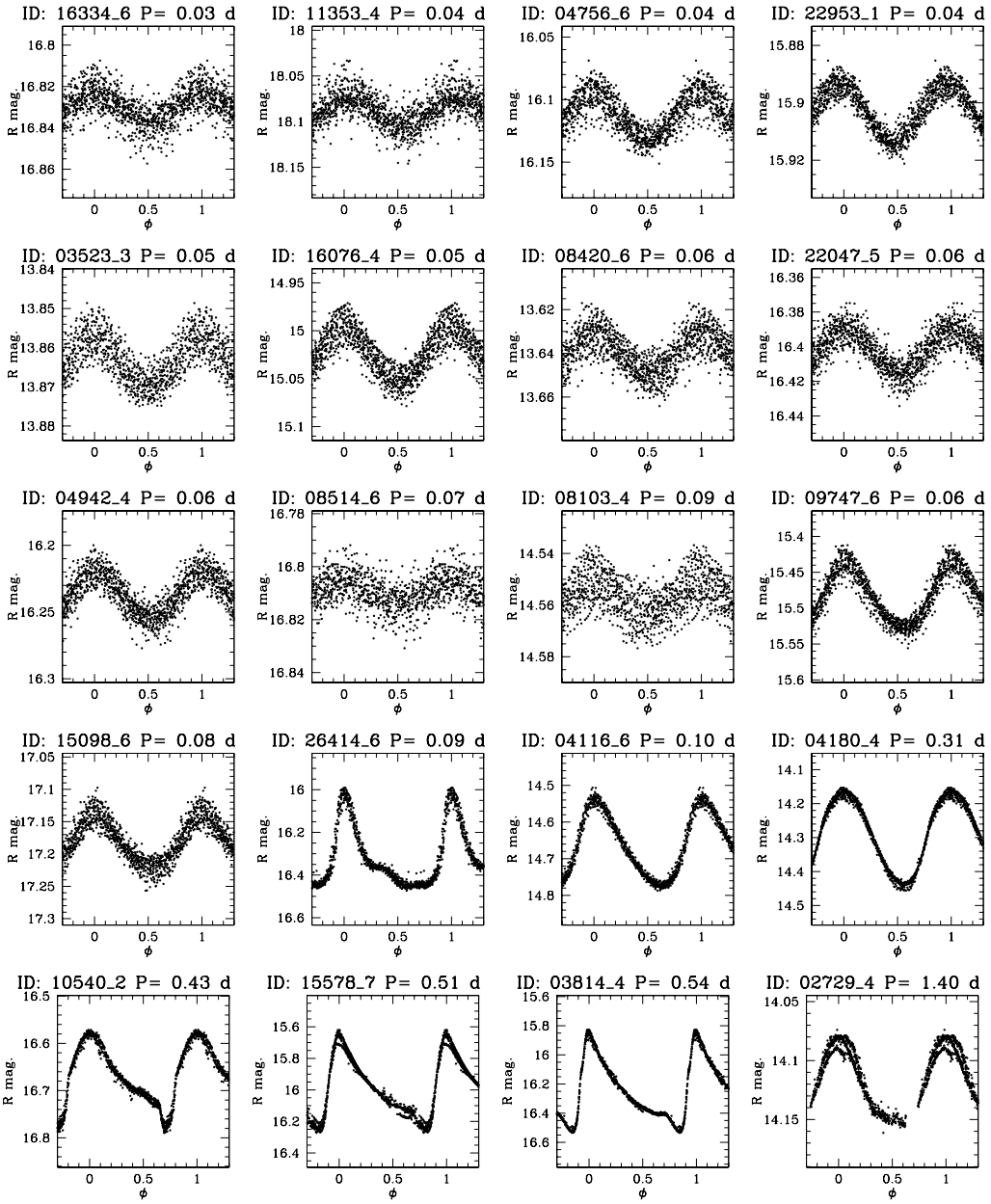

Figure B.1: Pulsating variables: δ Scuti, High Amplitude Delta Scuti, RR Lyrae and a Cepheid.

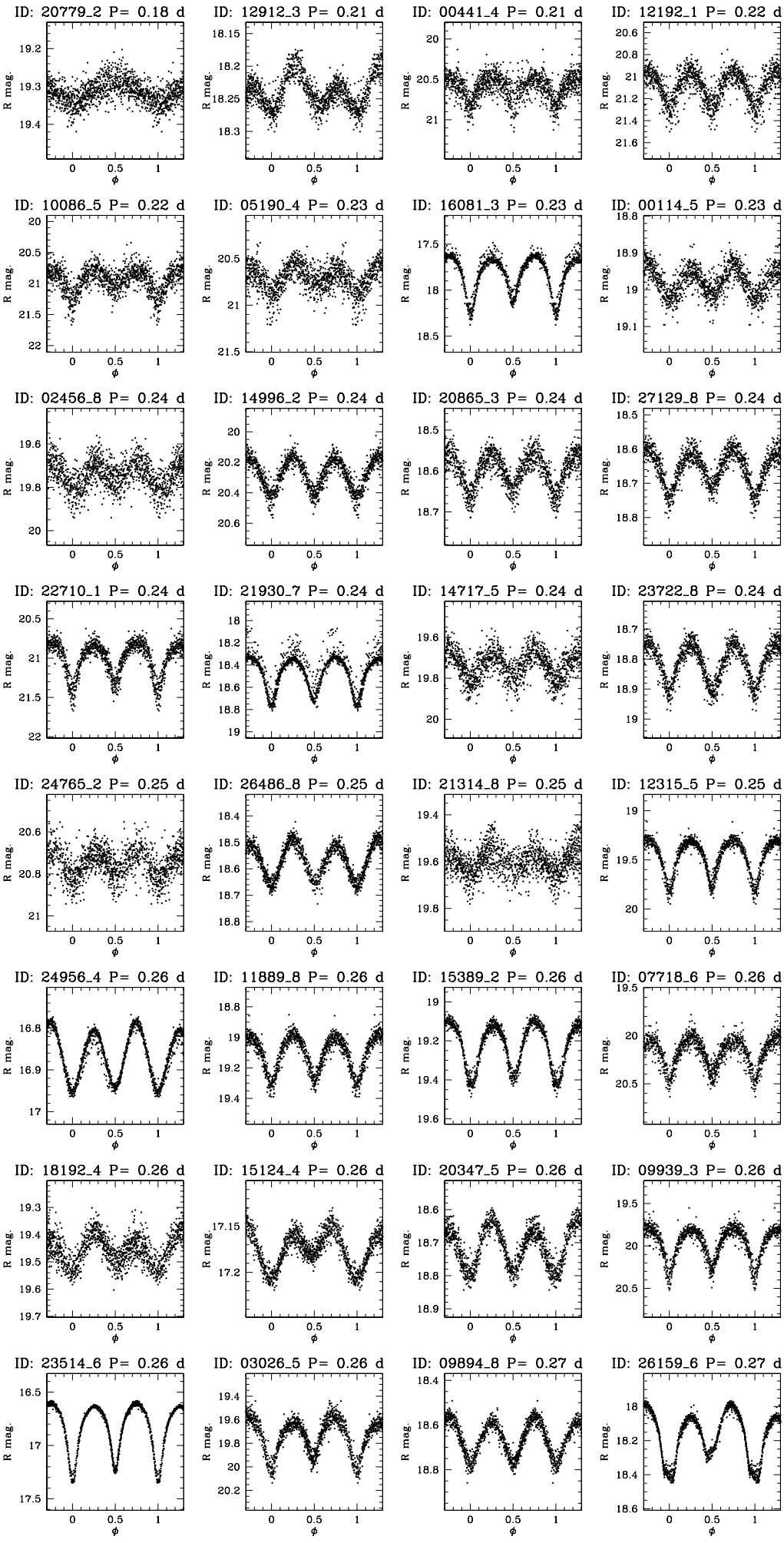
ID: 20779_2 P= 0.18 d
ID: 12912_3 P= 0.21 d
ID: 00441_4 P= 0.21 d
ID: 12192_1 P= 0.22 d
ID: 10086_5 P= 0.22 d
ID: 05190_4 P= 0.23 d
ID: 16081_3 P= 0.23 d
ID: 00114_5 P= 0.23 d
ID: 02456_8 P= 0.24 d
ID: 14996_2 P= 0.24 d
ID: 20865_3 P= 0.24 d
ID: 27129_8 P= 0.24 d
ID: 22710_1 P= 0.24 d
ID: 21930_7 P= 0.24 d
ID: 14717_5 P= 0.24 d
ID: 23722_8 P= 0.24 d
ID: 24765_2 P= 0.25 d
ID: 26486_8 P= 0.25 d
ID: 21314_8 P= 0.25 d
ID: 12315_5 P= 0.25 d
ID: 24956_4 P= 0.26 d
ID: 11889_8 P= 0.26 d
ID: 15389_2 P= 0.26 d
ID: 07718_6 P= 0.26 d
ID: 18192_4 P= 0.26 d
ID: 15124_4 P= 0.26 d
ID: 20347_5 P= 0.26 d
ID: 09939_3 P= 0.26 d
ID: 23514_6 P= 0.26 d
ID: 03026_5 P= 0.26 d
ID: 09894_8 P= 0.27 d
ID: 26159_6 P= 0.27 d
R mag.
ϕ

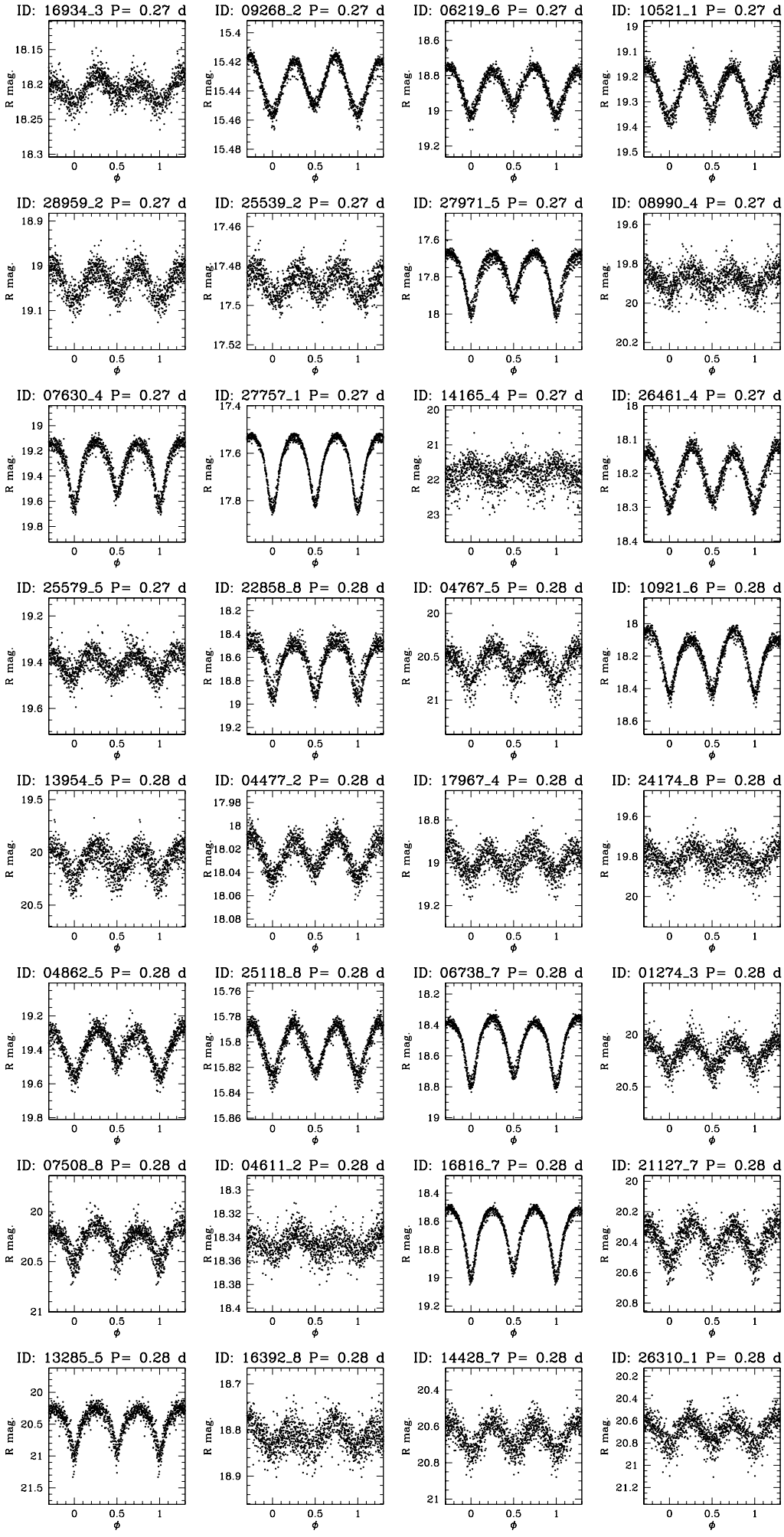
ID: 16934_3 P= 0.27 d
ID: 09268_2 P= 0.27 d
ID: 06219_6 P= 0.27 d
ID: 10521_1 P= 0.27 d
ID: 28959_2 P= 0.27 d
ID: 25539_2 P= 0.27 d
ID: 27971_5 P= 0.27 d
ID: 08990_4 P= 0.27 d
ID: 07630_4 P= 0.27 d
ID: 27757_1 P= 0.27 d
ID: 14165_4 P= 0.27 d
ID: 26461_4 P= 0.27 d
ID: 25579_5 P= 0.27 d
ID: 22858_8 P= 0.28 d
ID: 04767_5 P= 0.28 d
ID: 10921_6 P= 0.28 d
ID: 13954_5 P= 0.28 d
ID: 04477_2 P= 0.28 d
ID: 17967_4 P= 0.28 d
ID: 24174_8 P= 0.28 d
ID: 04862_5 P= 0.28 d
ID: 25118_8 P= 0.28 d
ID: 06738_7 P= 0.28 d
ID: 01274_3 P= 0.28 d
ID: 07508_8 P= 0.28 d
ID: 04611_2 P= 0.28 d
ID: 16816_7 P= 0.28 d
ID: 21127_7 P= 0.28 d
ID: 13285_5 P= 0.28 d
ID: 16392_8 P= 0.28 d
ID: 14428_7 P= 0.28 d
ID: 26310_1 P= 0.28 d
R mag.
ϕ

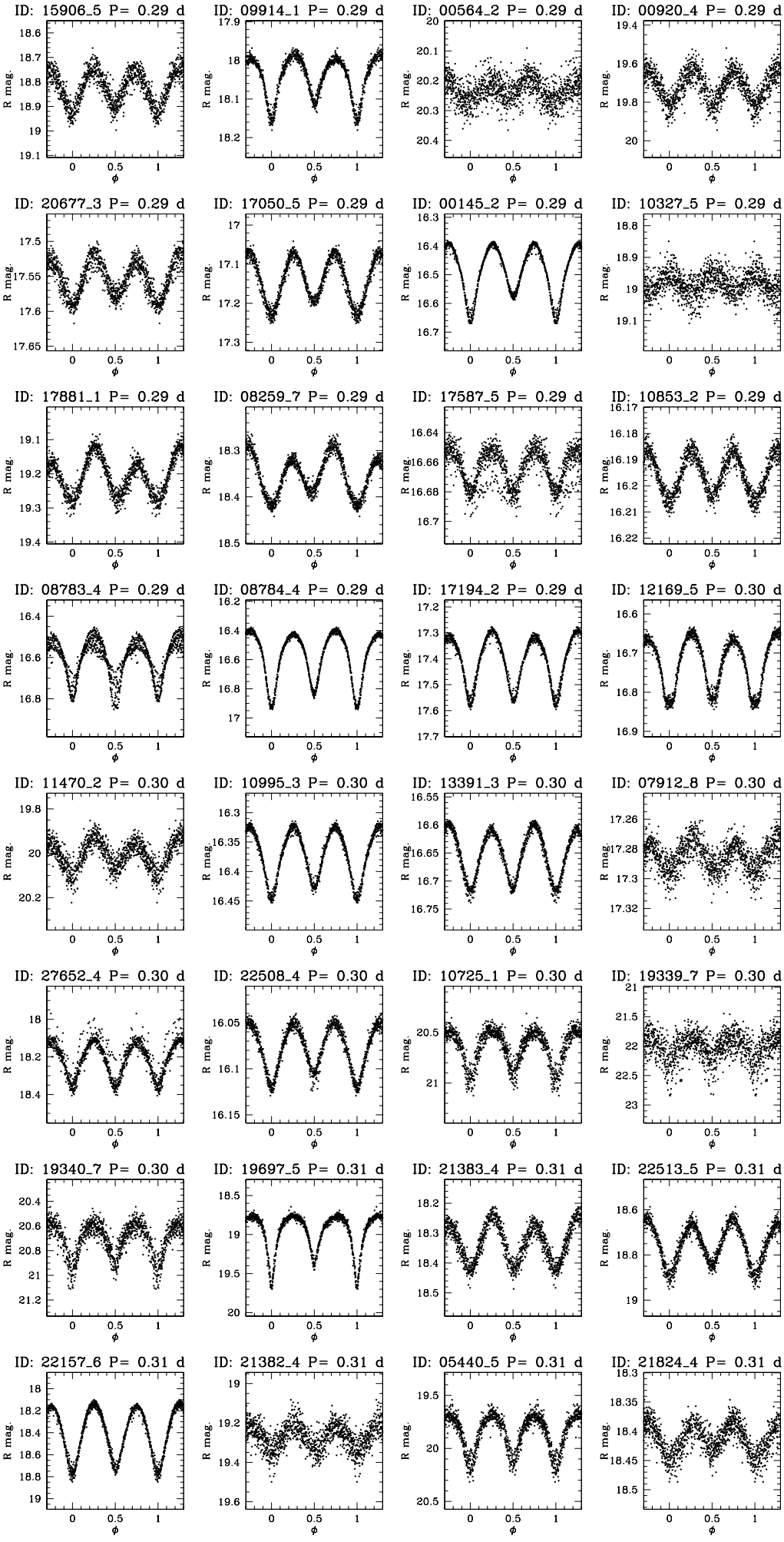
ID: 15906_5 P= 0.29 d
ID: 09914_1 P= 0.29 d
ID: 00564_2 P= 0.29 d
ID: 00920_4 P= 0.29 d
ID: 20677_3 P= 0.29 d
ID: 17050_5 P= 0.29 d
ID: 00145_2 P= 0.29 d
ID: 10327_5 P= 0.29 d
ID: 17881_1 P= 0.29 d
ID: 08259_7 P= 0.29 d
ID: 17587_5 P= 0.29 d
ID: 10853_2 P= 0.29 d
ID: 08783_4 P= 0.29 d
ID: 08784_4 P= 0.29 d
ID: 17194_2 P= 0.29 d
ID: 12169_5 P= 0.30 d
ID: 11470_2 P= 0.30 d
ID: 10995_3 P= 0.30 d
ID: 13391_3 P= 0.30 d
ID: 07912_8 P= 0.30 d
ID: 27652_4 P= 0.30 d
ID: 22508_4 P= 0.30 d
ID: 10725_1 P= 0.30 d
ID: 19339_7 P= 0.30 d
ID: 19340_7 P= 0.30 d
ID: 19697_5 P= 0.31 d
ID: 21383_4 P= 0.31 d
ID: 22513_5 P= 0.31 d
ID: 22157_6 P= 0.31 d
ID: 21382_4 P= 0.31 d
ID: 05440_5 P= 0.31 d
ID: 21824_4 P= 0.31 d
R mag.
ϕ

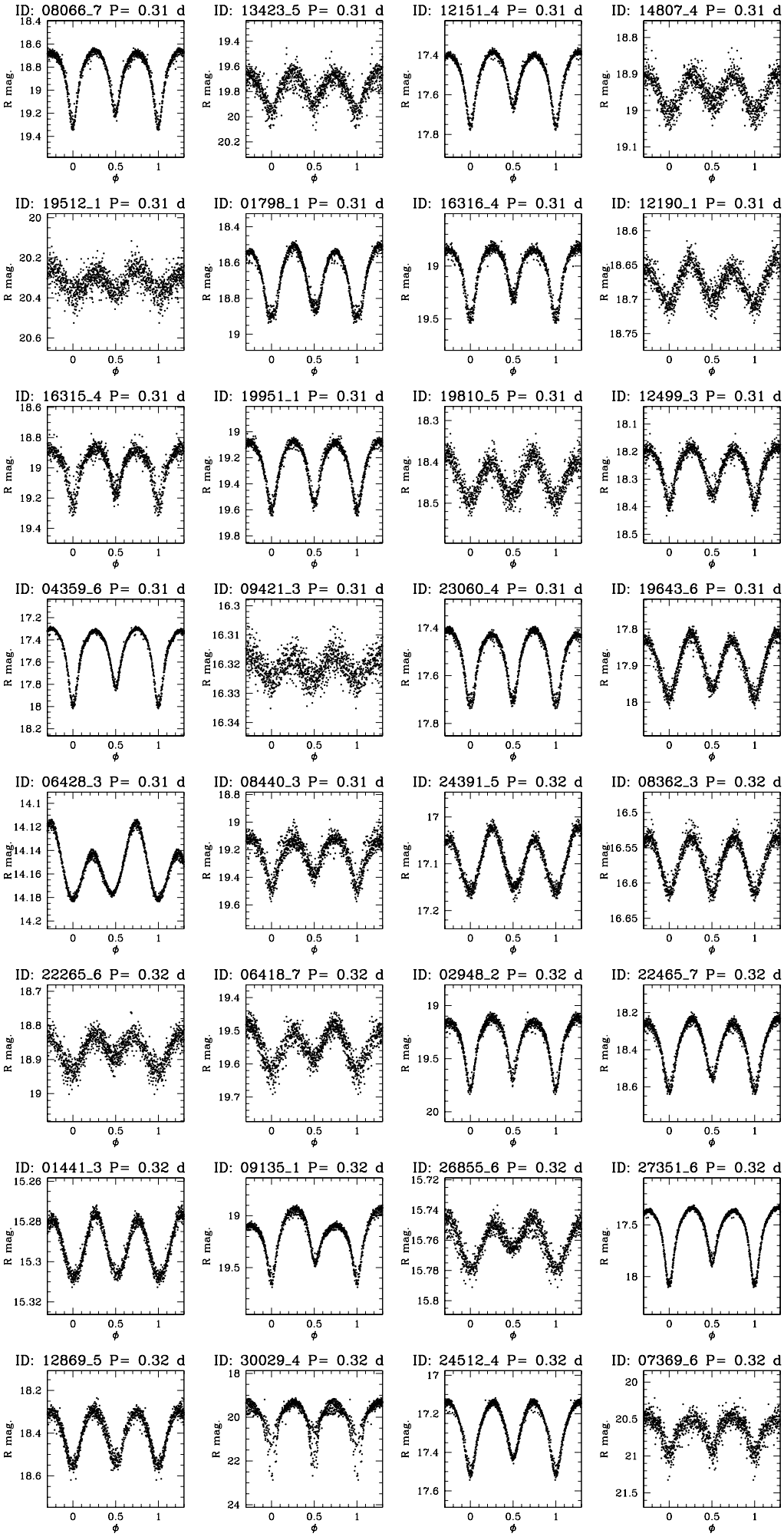
ID: 08066_7 P= 0.31 d
ID: 13423_5 P= 0.31 d
ID: 12151_4 P= 0.31 d
ID: 14807_4 P= 0.31 d
ID: 19512_1 P= 0.31 d
ID: 01798_1 P= 0.31 d
ID: 16316_4 P= 0.31 d
ID: 12190_1 P= 0.31 d
ID: 16315_4 P= 0.31 d
ID: 19951_1 P= 0.31 d
ID: 19810_5 P= 0.31 d
ID: 12499_3 P= 0.31 d
ID: 04359_6 P= 0.31 d
ID: 09421_3 P= 0.31 d
ID: 23060_4 P= 0.31 d
ID: 19643_6 P= 0.31 d
ID: 06428_3 P= 0.31 d
ID: 08440_3 P= 0.31 d
ID: 24391_5 P= 0.32 d
ID: 08362_3 P= 0.32 d
ID: 22265_6 P= 0.32 d
ID: 06418_7 P= 0.32 d
ID: 02948_2 P= 0.32 d
ID: 22465_7 P= 0.32 d
ID: 01441_3 P= 0.32 d
ID: 09135_1 P= 0.32 d
ID: 26855_6 P= 0.32 d
ID: 27351_6 P= 0.32 d
ID: 12869_5 P= 0.32 d
ID: 30029_4 P= 0.32 d
ID: 24512_4 P= 0.32 d
ID: 07369_6 P= 0.32 d
R mag.
ϕ

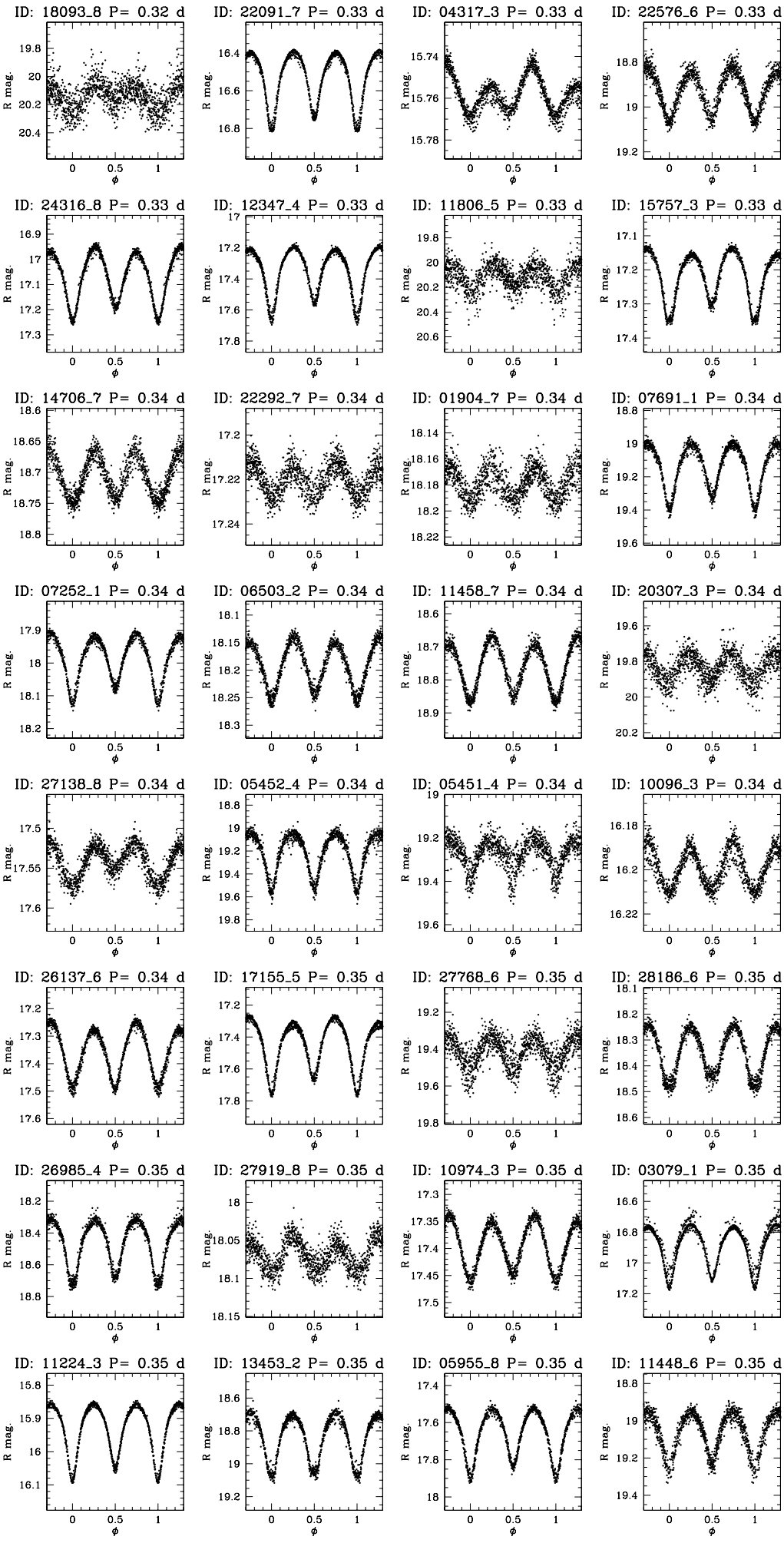
ID: 18093_8 P= 0.32 d
ID: 22091_7 P= 0.33 d
ID: 04317_3 P= 0.33 d
ID: 22576_6 P= 0.33 d
ID: 24316_8 P= 0.33 d
ID: 12347_4 P= 0.33 d
ID: 11806_5 P= 0.33 d
ID: 15757_3 P= 0.33 d
ID: 14706_7 P= 0.34 d
ID: 22292_7 P= 0.34 d
ID: 01904_7 P= 0.34 d
ID: 07691_1 P= 0.34 d
ID: 07252_1 P= 0.34 d
ID: 06503_2 P= 0.34 d
ID: 11458_7 P= 0.34 d
ID: 20307_3 P= 0.34 d
ID: 27138_8 P= 0.34 d
ID: 05452_4 P= 0.34 d
ID: 05451_4 P= 0.34 d
ID: 10096_3 P= 0.34 d
ID: 26137_6 P= 0.34 d
ID: 17155_5 P= 0.35 d
ID: 27768_6 P= 0.35 d
ID: 28186_6 P= 0.35 d
ID: 26985_4 P= 0.35 d
ID: 27919_8 P= 0.35 d
ID: 10974_3 P= 0.35 d
ID: 03079_1 P= 0.35 d
ID: 11224_3 P= 0.35 d
ID: 13453_2 P= 0.35 d
ID: 05955_8 P= 0.35 d
ID: 11448_6 P= 0.35 d
R mag.
φ

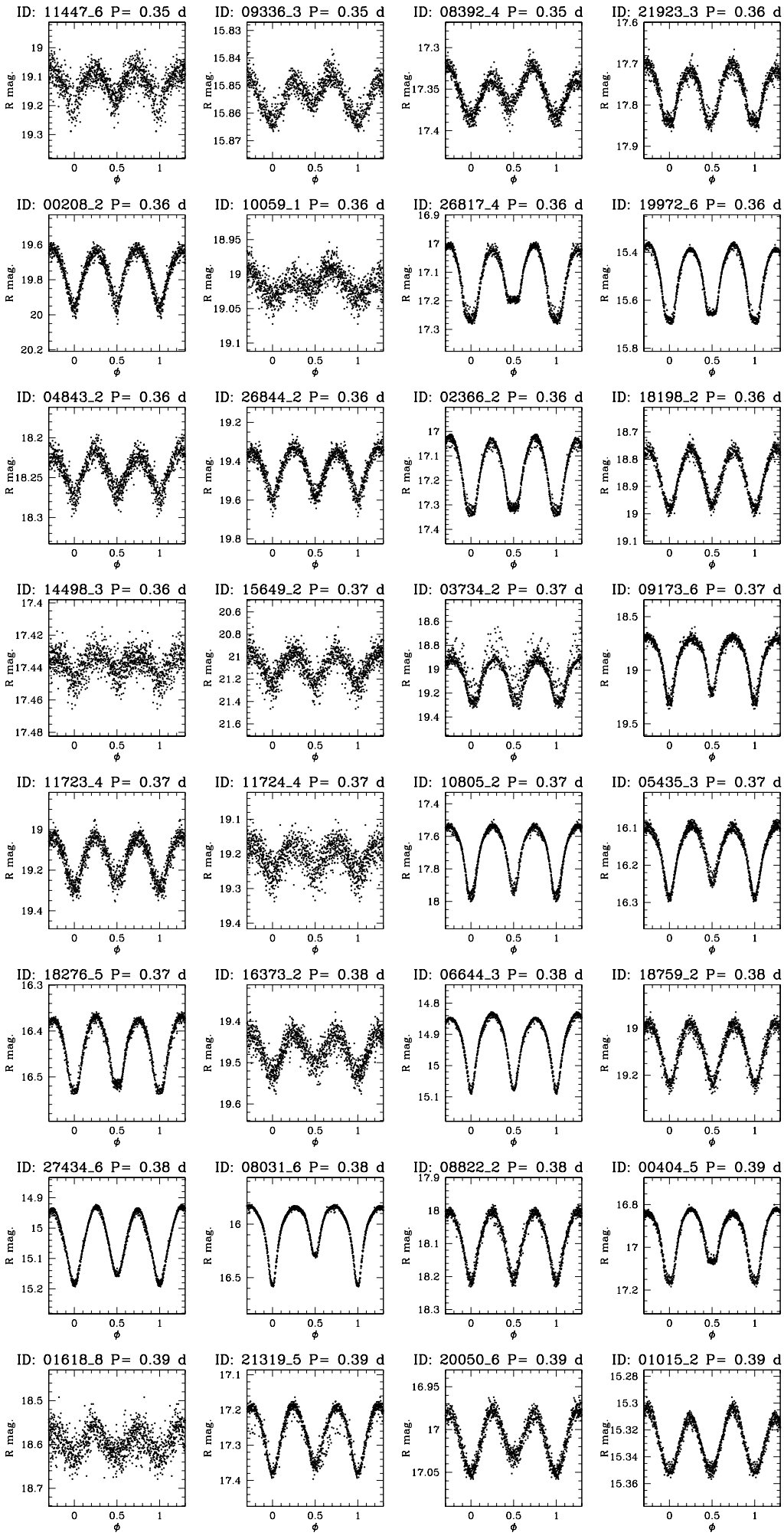
ID: 11447_6 P= 0.35 d
ID: 09336_3 P= 0.35 d
ID: 08392_4 P= 0.35 d
ID: 21923_3 P= 0.36 d
ID: 00208_2 P= 0.36 d
ID: 10059_1 P= 0.36 d
ID: 26817_4 P= 0.36 d
ID: 19972_6 P= 0.36 d
ID: 04843_2 P= 0.36 d
ID: 26844_2 P= 0.36 d
ID: 02366_2 P= 0.36 d
ID: 18198_2 P= 0.36 d
ID: 14498_3 P= 0.36 d
ID: 15649_2 P= 0.37 d
ID: 03734_2 P= 0.37 d
ID: 09173_6 P= 0.37 d
ID: 11723_4 P= 0.37 d
ID: 11724_4 P= 0.37 d
ID: 10805_2 P= 0.37 d
ID: 05435_3 P= 0.37 d
ID: 18276_5 P= 0.37 d
ID: 16373_2 P= 0.38 d
ID: 06644_3 P= 0.38 d
ID: 18759_2 P= 0.38 d
ID: 27434_6 P= 0.38 d
ID: 08031_6 P= 0.38 d
ID: 08822_2 P= 0.38 d
ID: 00404_5 P= 0.39 d
ID: 01618_8 P= 0.39 d
ID: 21319_5 P= 0.39 d
ID: 20050_6 P= 0.39 d
ID: 01015_2 P= 0.39 d
R mag.
ϕ

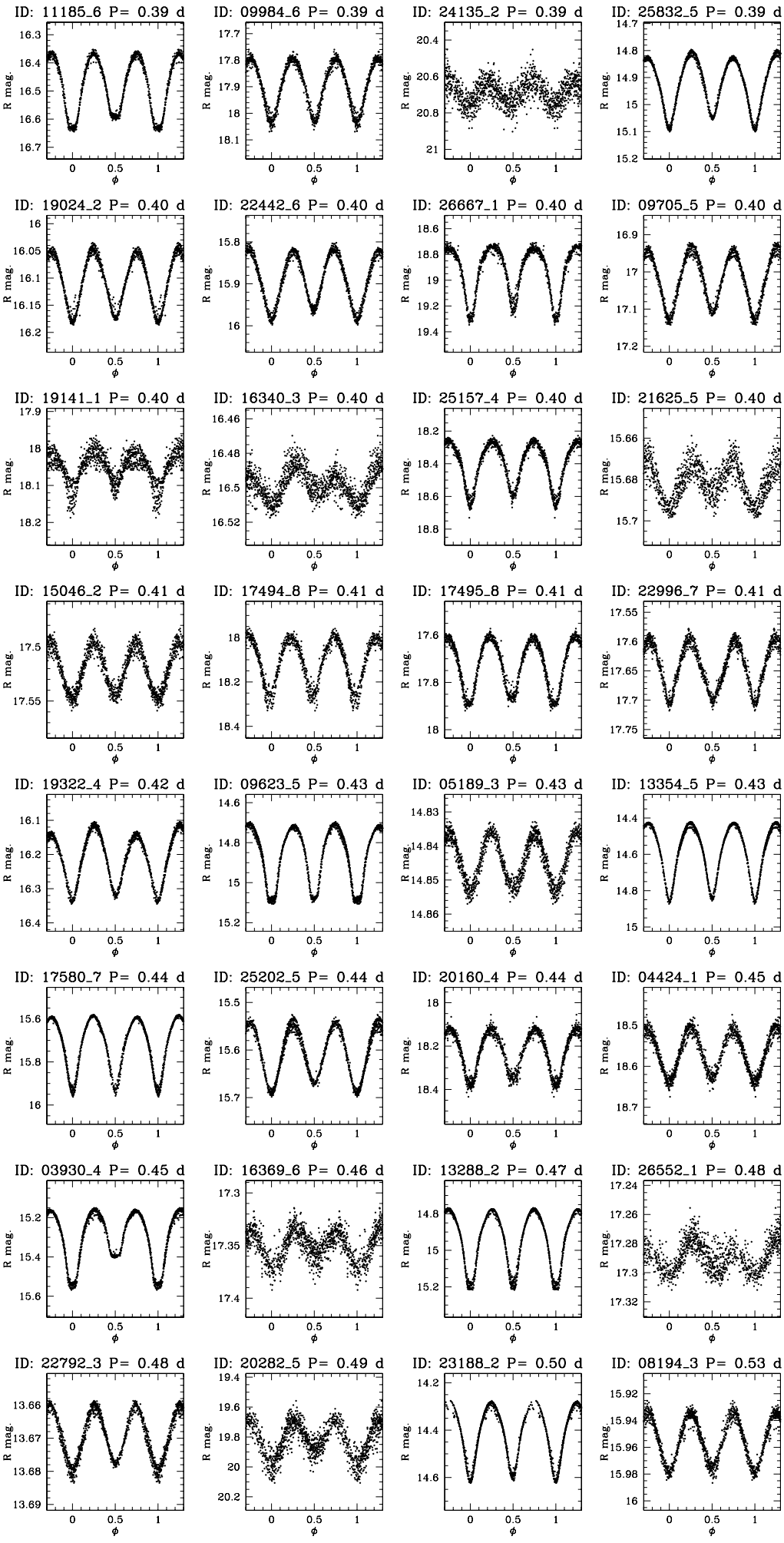
ID: 11185_6 P= 0.39 d
ID: 09984_6 P= 0.39 d
ID: 24135_2 P= 0.39 d
ID: 25832_5 P= 0.39 d
ID: 19024_2 P= 0.40 d
ID: 22442_6 P= 0.40 d
ID: 26667_1 P= 0.40 d
ID: 09705_5 P= 0.40 d
ID: 19141_1 P= 0.40 d
ID: 16340_3 P= 0.40 d
ID: 25157_4 P= 0.40 d
ID: 21625_5 P= 0.40 d
ID: 15046_2 P= 0.41 d
ID: 17494_8 P= 0.41 d
ID: 17495_8 P= 0.41 d
ID: 22996_7 P= 0.41 d
ID: 19322_4 P= 0.42 d
ID: 09623_5 P= 0.43 d
ID: 05189_3 P= 0.43 d
ID: 13354_5 P= 0.43 d
ID: 17580_7 P= 0.44 d
ID: 25202_5 P= 0.44 d
ID: 20160_4 P= 0.44 d
ID: 04424_1 P= 0.45 d
ID: 03930_4 P= 0.45 d
ID: 16369_6 P= 0.46 d
ID: 13288_2 P= 0.47 d
ID: 26552_1 P= 0.48 d
ID: 22792_3 P= 0.48 d
ID: 20282_5 P= 0.49 d
ID: 23188_2 P= 0.50 d
ID: 08194_3 P= 0.53 d
R mag.
ϕ

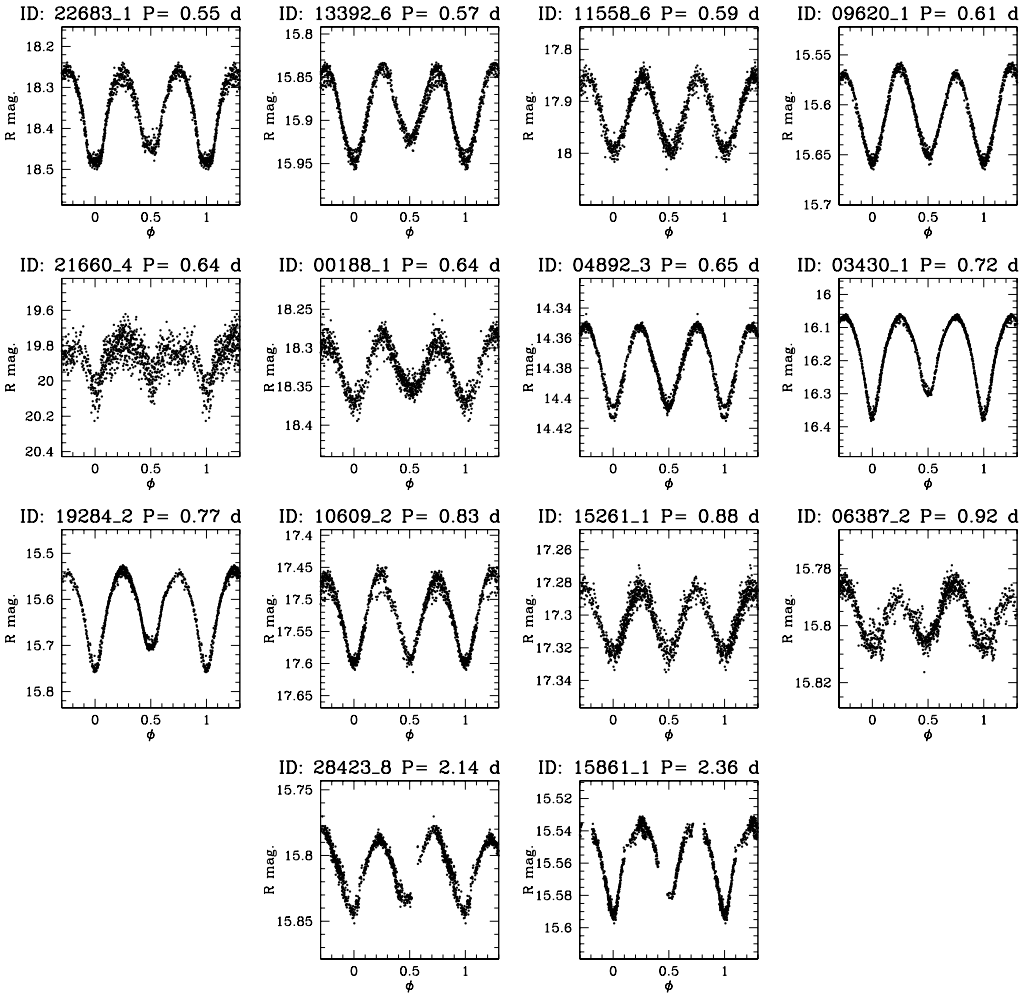

Figure B.9: EW-Type binaries.

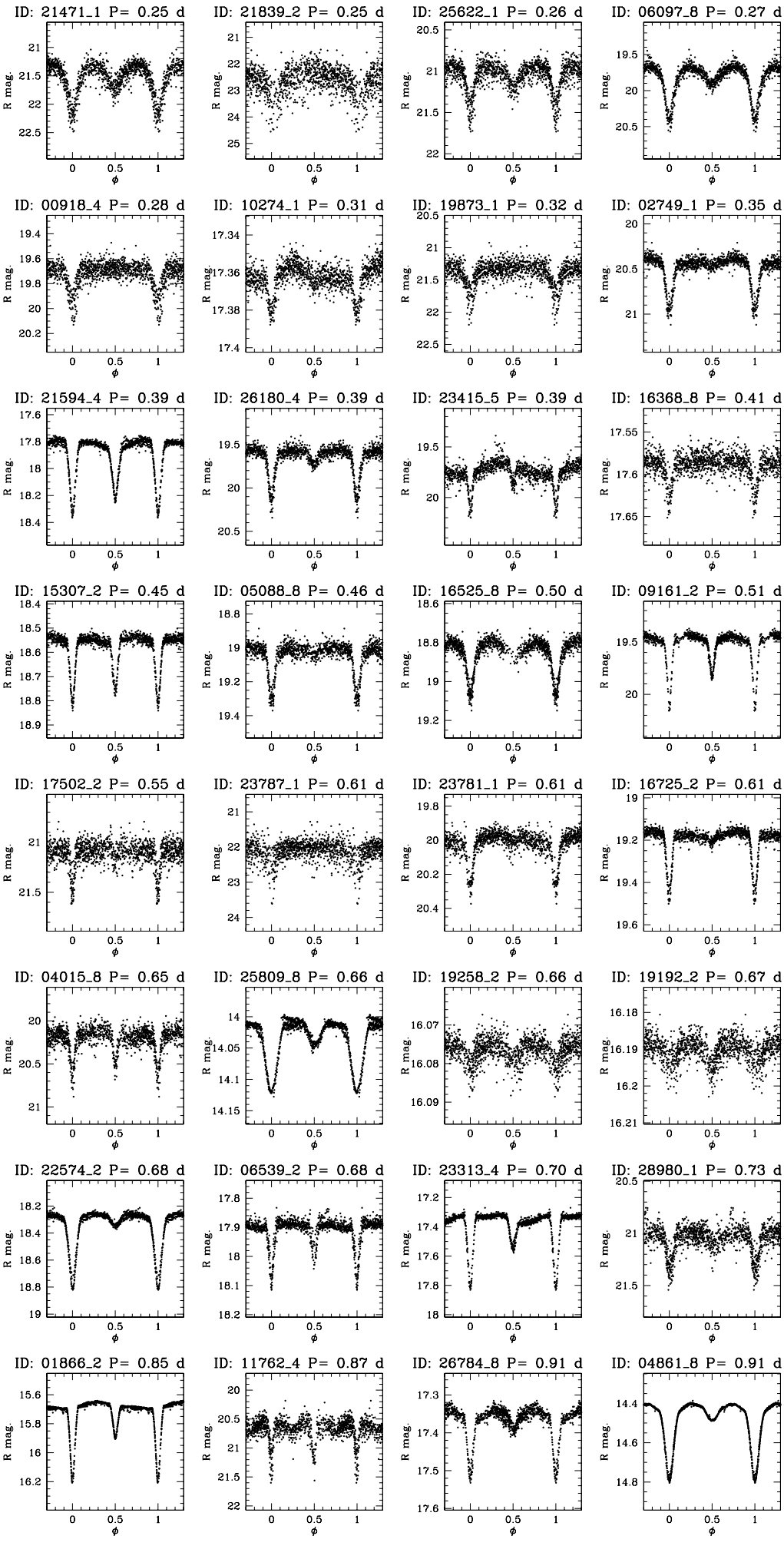
ID: 21471_1 P= 0.25 d
ID: 21839_2 P= 0.25 d
ID: 25622_1 P= 0.26 d
ID: 06097_8 P= 0.27 d
ID: 00918_4 P= 0.28 d
ID: 10274_1 P= 0.31 d
ID: 19873_1 P= 0.32 d
ID: 02749_1 P= 0.35 d
ID: 21594_4 P= 0.39 d
ID: 26180_4 P= 0.39 d
ID: 23415_5 P= 0.39 d
ID: 16368_8 P= 0.41 d
ID: 15307_2 P= 0.45 d
ID: 05088_8 P= 0.46 d
ID: 16525_8 P= 0.50 d
ID: 09161_2 P= 0.51 d
ID: 17502_2 P= 0.55 d
ID: 23787_1 P= 0.61 d
ID: 23781_1 P= 0.61 d
ID: 16725_2 P= 0.61 d
ID: 04015_8 P= 0.65 d
ID: 25809_8 P= 0.66 d
ID: 19258_2 P= 0.66 d
ID: 19192_2 P= 0.67 d
ID: 22574_2 P= 0.68 d
ID: 06539_2 P= 0.68 d
ID: 23313_4 P= 0.70 d
ID: 28980_1 P= 0.73 d
ID: 01866_2 P= 0.85 d
ID: 11762_4 P= 0.87 d
ID: 26784_8 P= 0.91 d
ID: 04861_8 P= 0.91 d
R mag.
φ

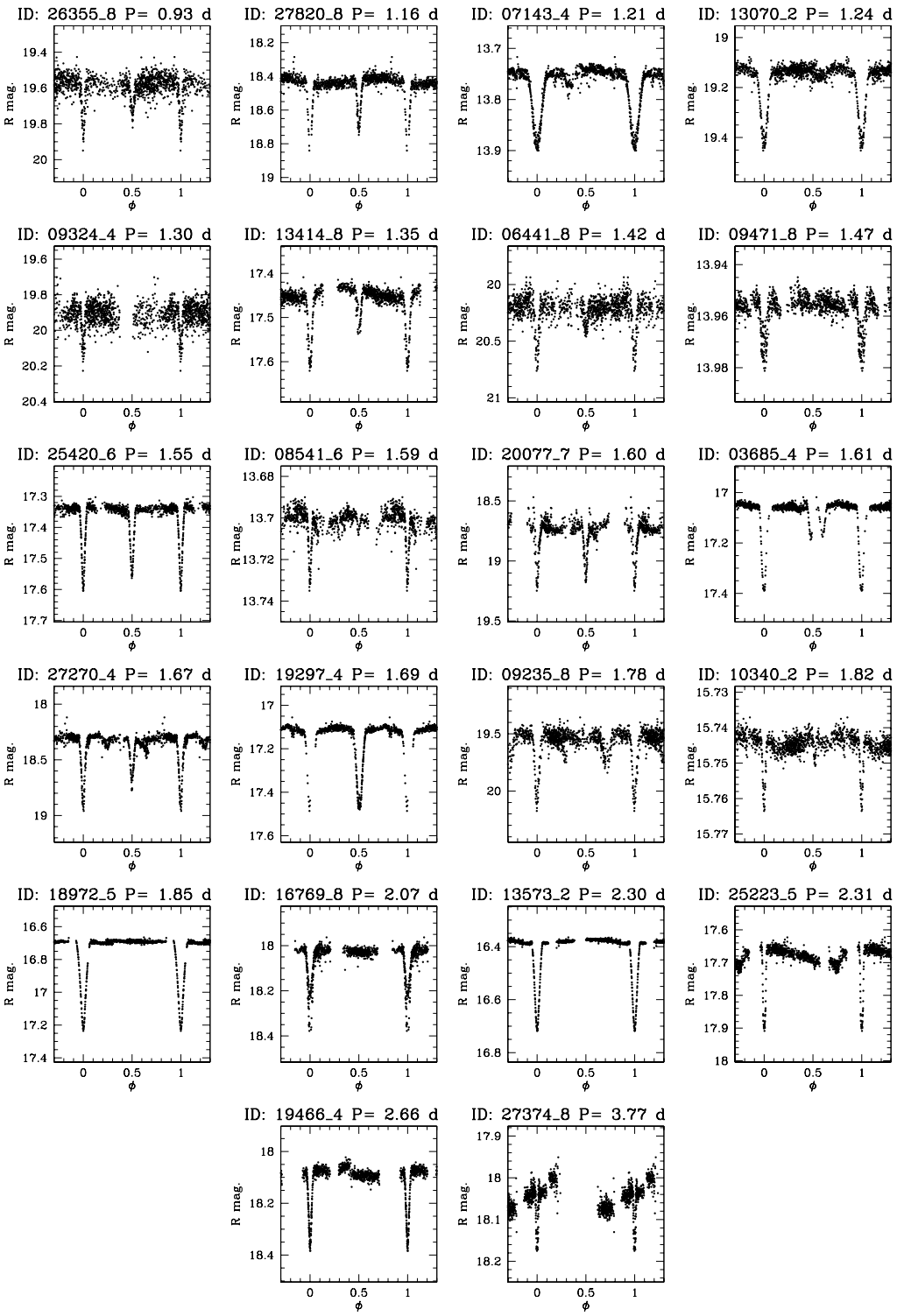

Figure B.11: EA-Type binaries.

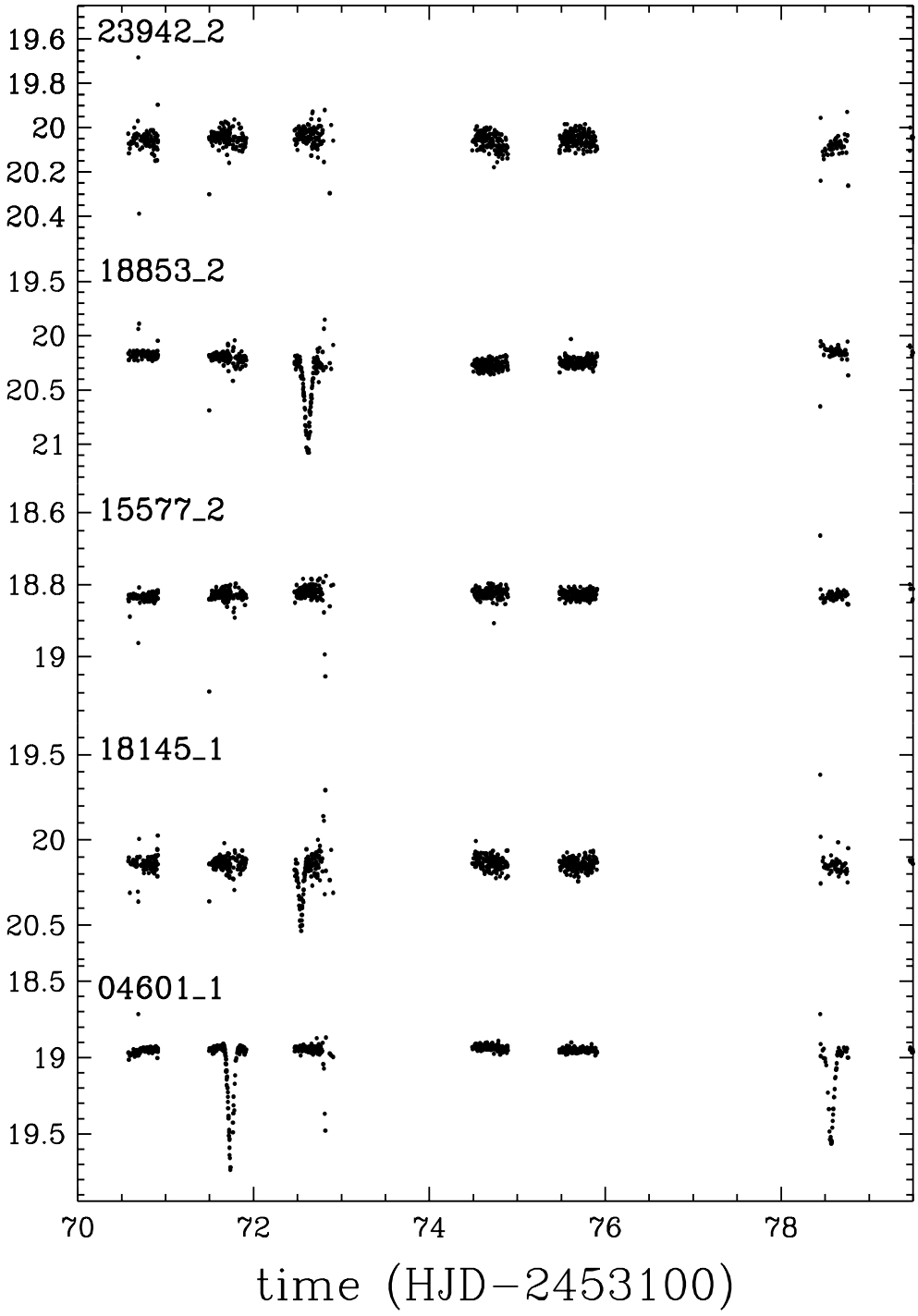

Figure B.12: EA-Type variables with undetermined periods.

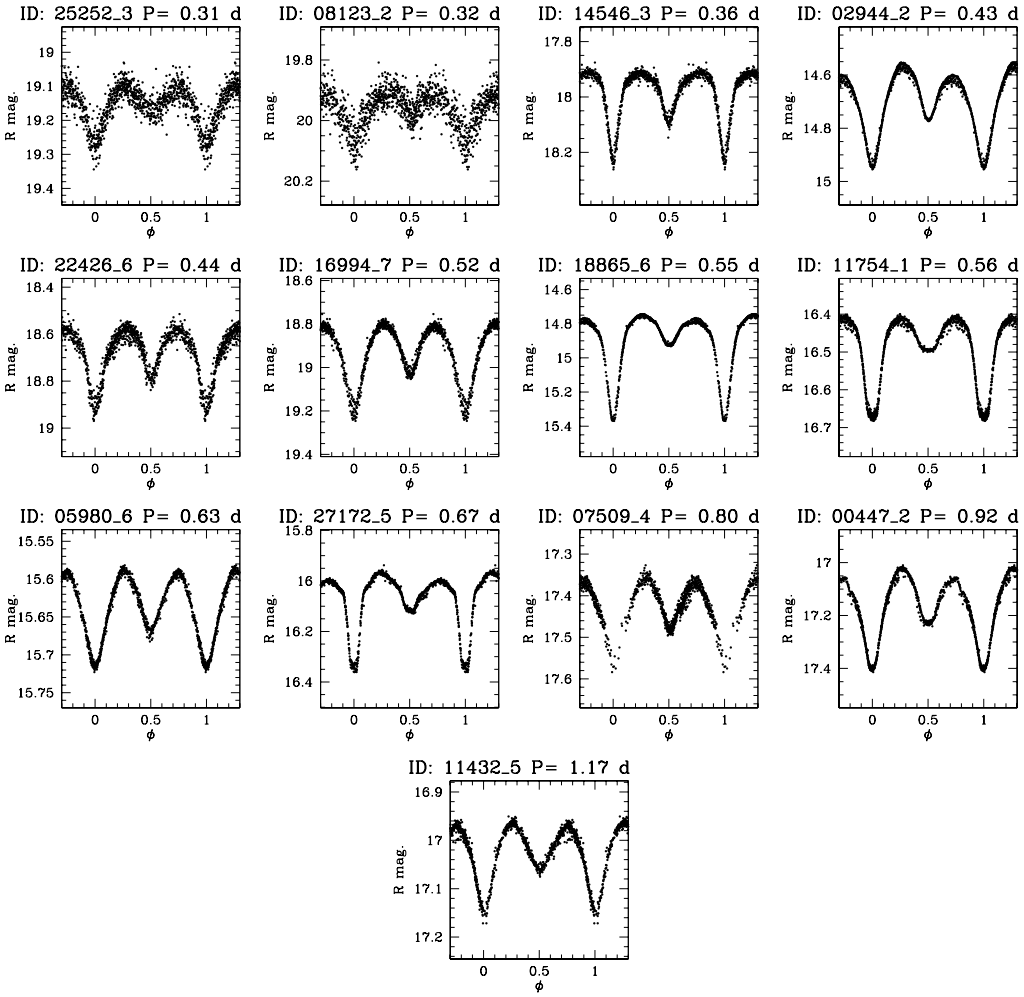

Figure B.13: EB-type systems.

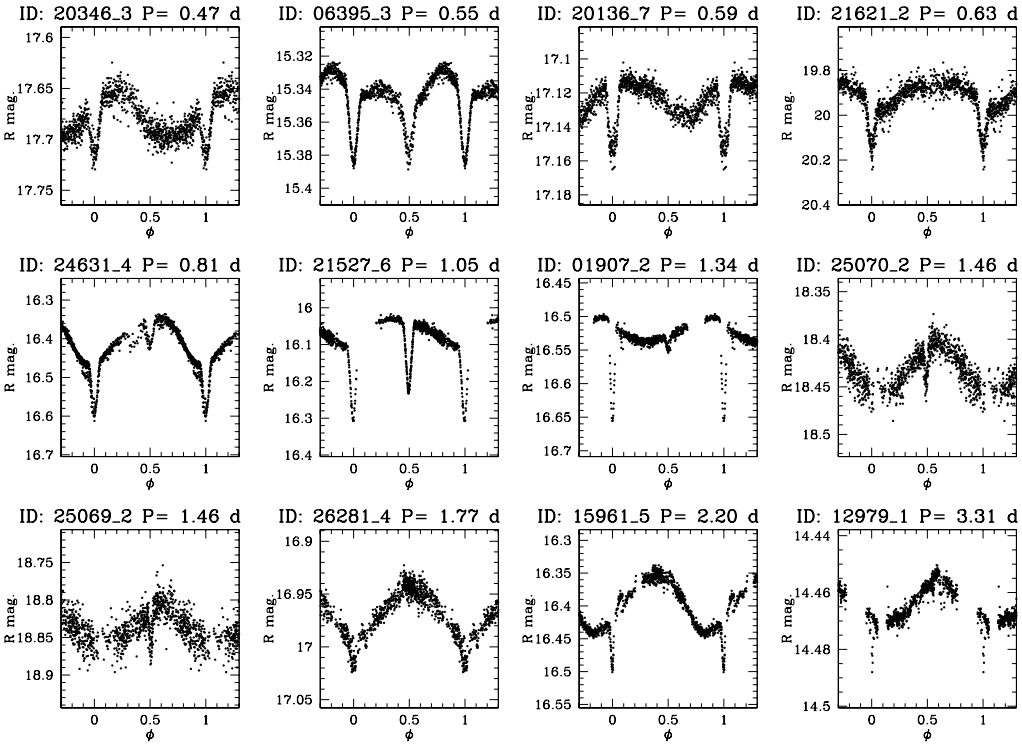

Figure B.14: RS-CVn variables.

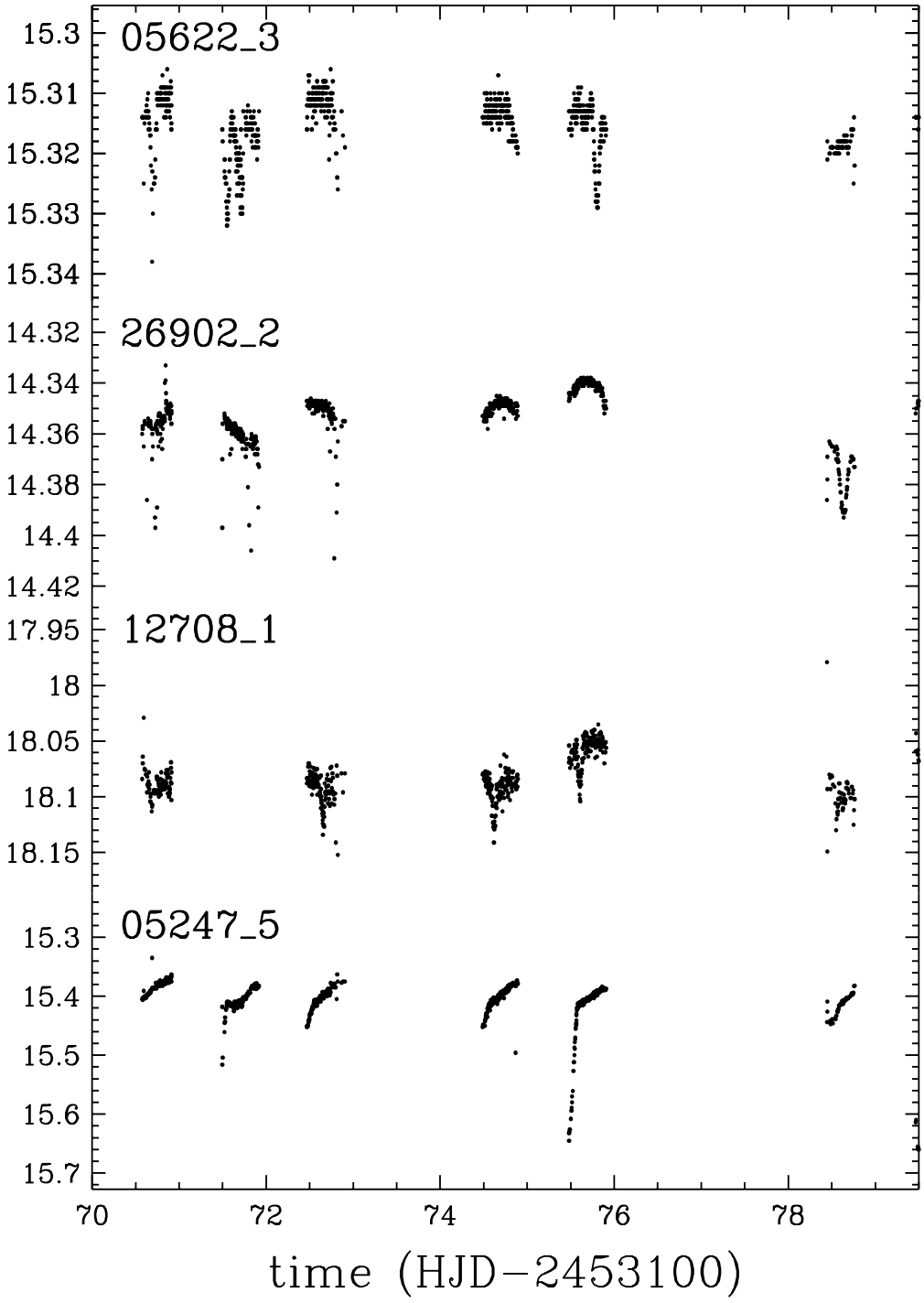

Figure B.15: RS-CVn variables with undetermined periods.

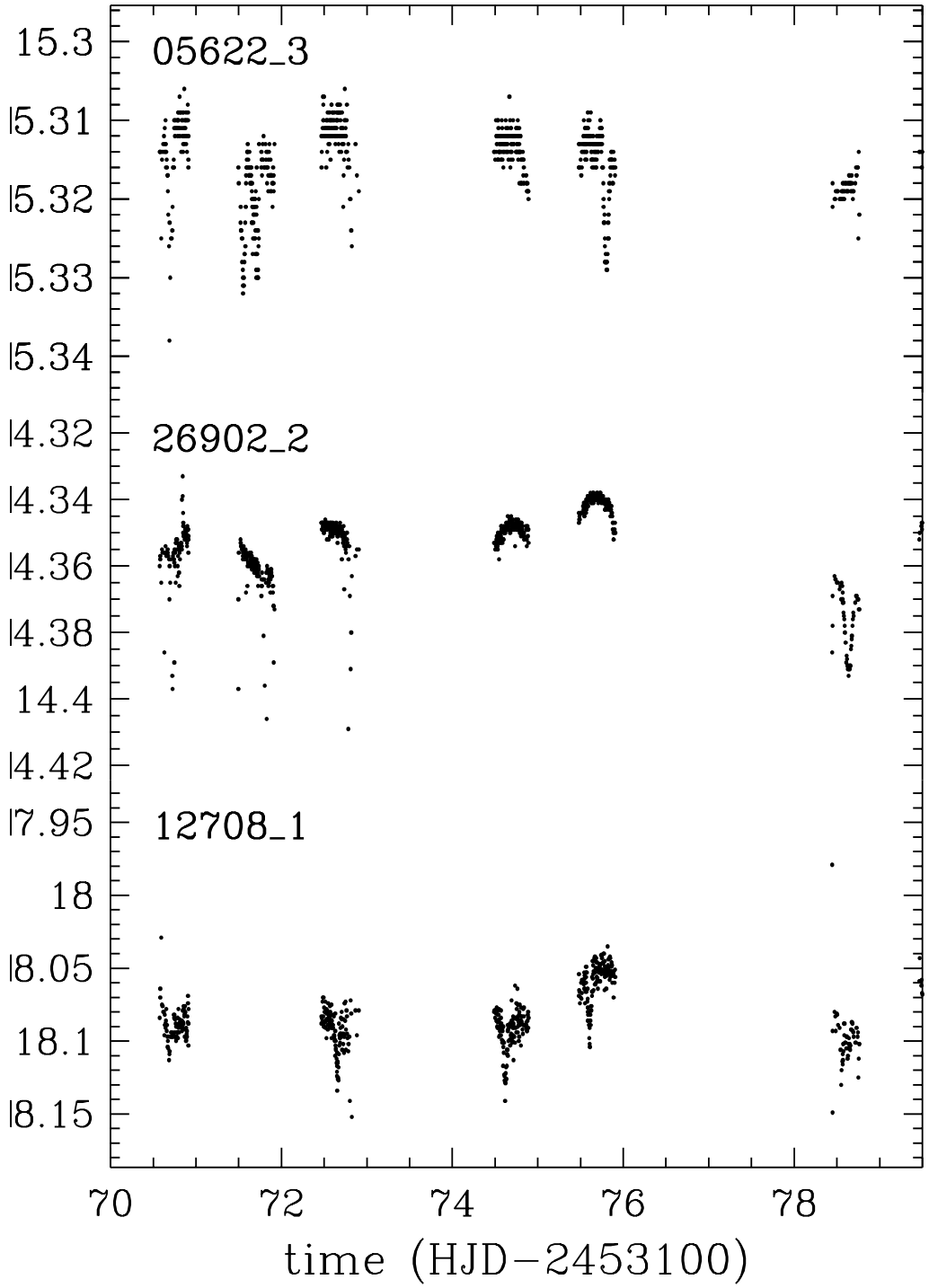

Figure B.16: RS-CVn variables with undetermined periods.

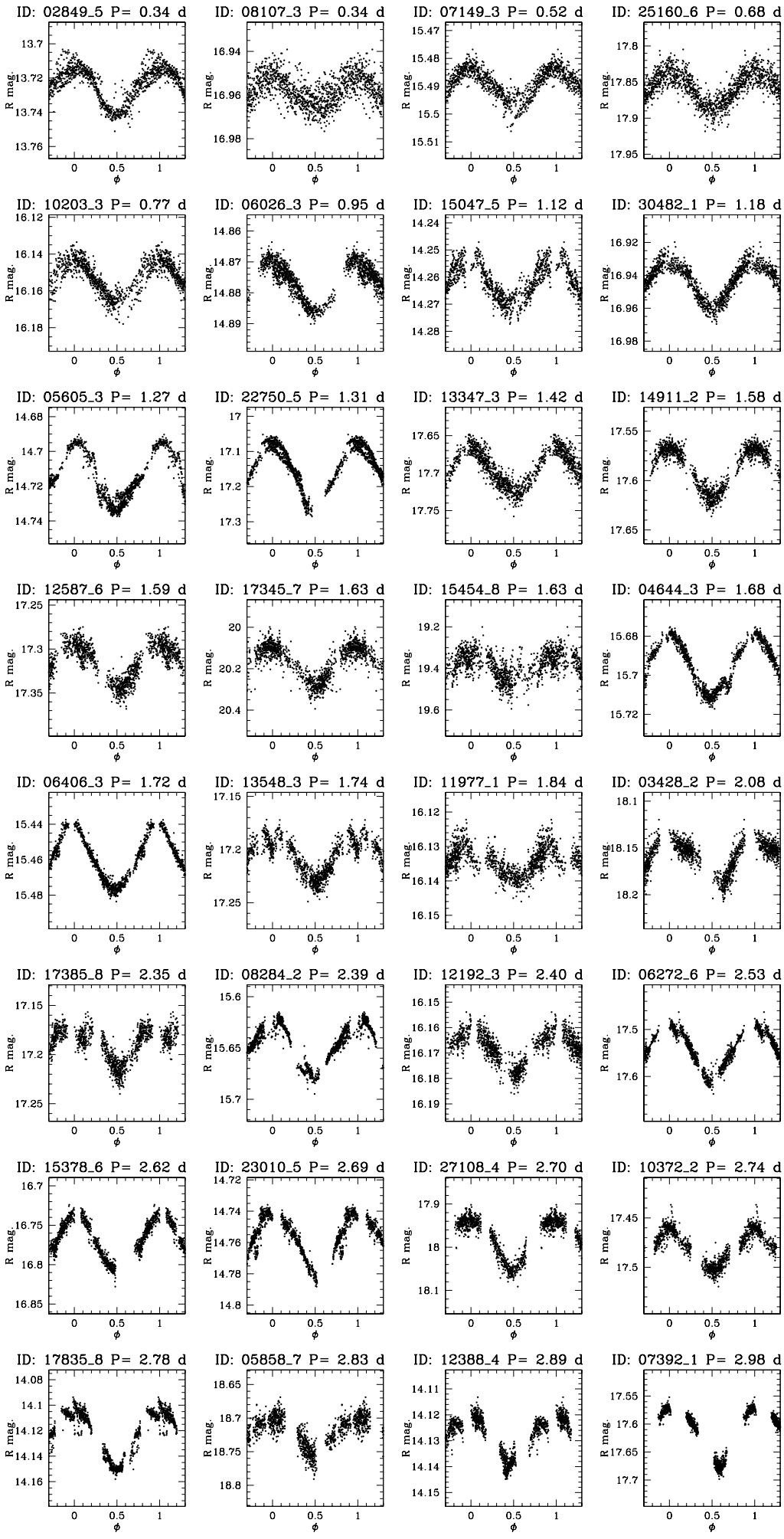
ID: 02849_5 P= 0.34 d
ID: 08107_3 P= 0.34 d
ID: 07149_3 P= 0.52 d
ID: 25160_6 P= 0.68 d
ID: 10203_3 P= 0.77 d
ID: 06026_3 P= 0.95 d
ID: 15047_5 P= 1.12 d
ID: 30482_1 P= 1.18 d
ID: 05605_3 P= 1.27 d
ID: 22750_5 P= 1.31 d
ID: 13347_3 P= 1.42 d
ID: 14911_2 P= 1.58 d
ID: 12587_6 P= 1.59 d
ID: 17345_7 P= 1.63 d
ID: 15454_8 P= 1.63 d
ID: 04644_3 P= 1.68 d
ID: 06406_3 P= 1.72 d
ID: 13548_3 P= 1.74 d
ID: 11977_1 P= 1.84 d
ID: 03428_2 P= 2.08 d
ID: 17385_8 P= 2.35 d
ID: 08284_2 P= 2.39 d
ID: 12192_3 P= 2.40 d
ID: 06272_6 P= 2.53 d
ID: 15378_6 P= 2.62 d
ID: 23010_5 P= 2.69 d
ID: 27108_4 P= 2.70 d
ID: 10372_2 P= 2.74 d
ID: 17835_8 P= 2.78 d
ID: 05858_7 P= 2.83 d
ID: 12388_4 P= 2.89 d
ID: 07392_1 P= 2.98 d
R mag.
ϕ

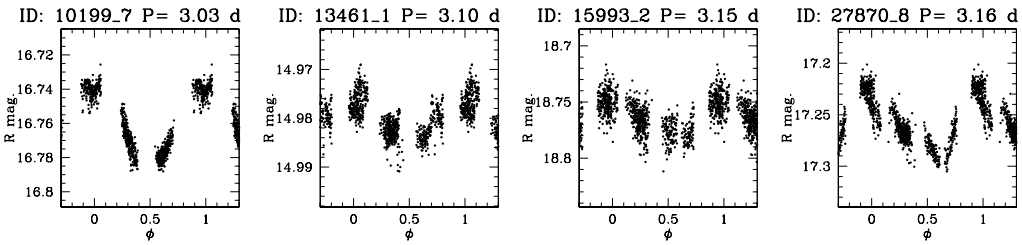

Figure B.18: Single-wave rotational variables

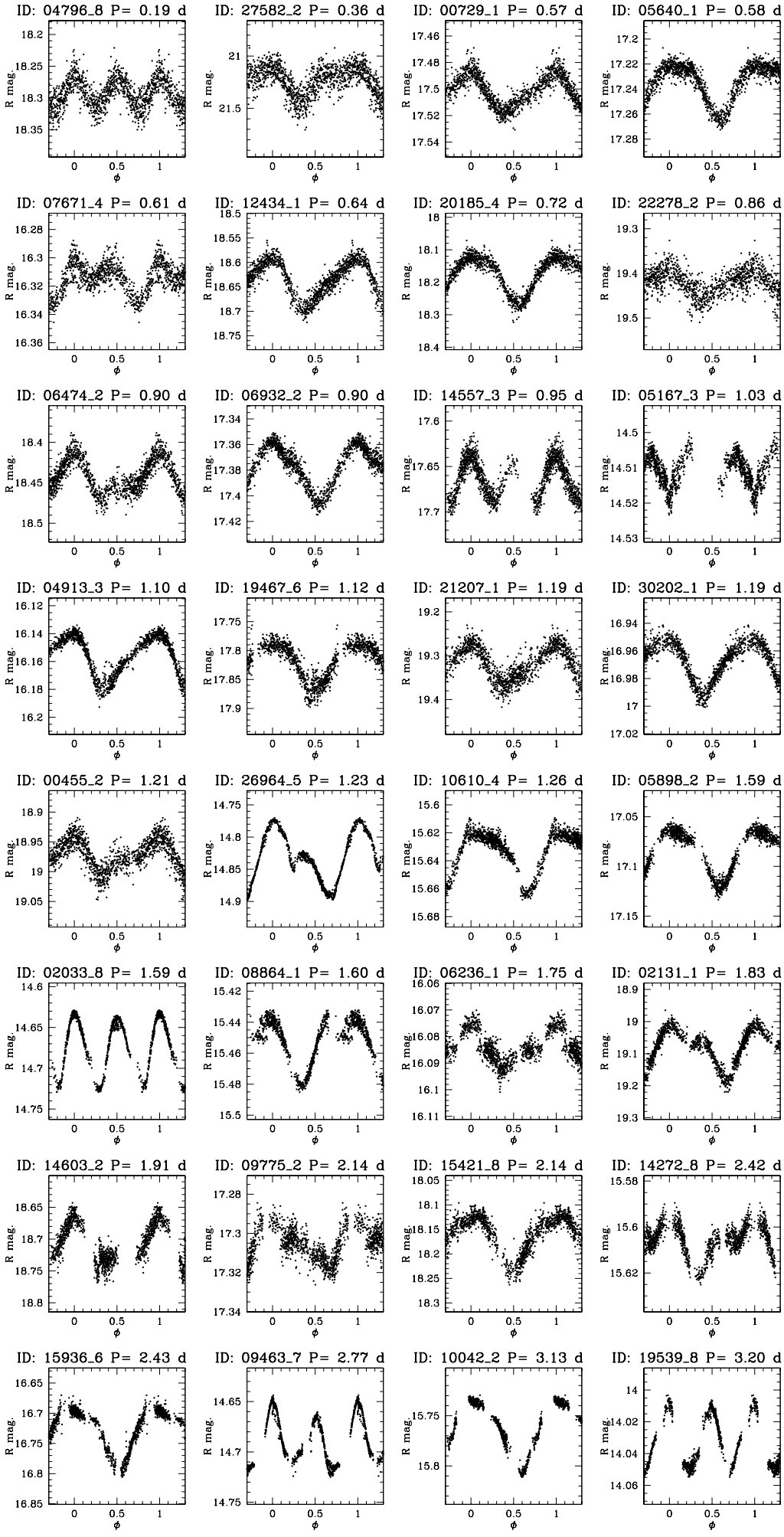
ID: 04796_8 P= 0.19 d
ID: 27582_2 P= 0.36 d
ID: 00729_1 P= 0.57 d
ID: 05640_1 P= 0.58 d
ID: 07671_4 P= 0.61 d
ID: 12434_1 P= 0.64 d
ID: 20185_4 P= 0.72 d
ID: 22278_2 P= 0.86 d
ID: 06474_2 P= 0.90 d
ID: 06932_2 P= 0.90 d
ID: 14557_3 P= 0.95 d
ID: 05167_3 P= 1.03 d
ID: 04913_3 P= 1.10 d
ID: 19467_6 P= 1.12 d
ID: 21207_1 P= 1.19 d
ID: 30202_1 P= 1.19 d
ID: 00455_2 P= 1.21 d
ID: 26964_5 P= 1.23 d
ID: 10610_4 P= 1.26 d
ID: 05898_2 P= 1.59 d
ID: 02033_8 P= 1.59 d
ID: 08864_1 P= 1.60 d
ID: 06236_1 P= 1.75 d
ID: 02131_1 P= 1.83 d
ID: 14603_2 P= 1.91 d
ID: 09775_2 P= 2.14 d
ID: 15421_8 P= 2.14 d
ID: 14272_8 P= 2.42 d
ID: 15936_6 P= 2.43 d
ID: 09463_7 P= 2.77 d
ID: 10042_2 P= 3.13 d
ID: 19539_8 P= 3.20 d
R mag.
ϕ

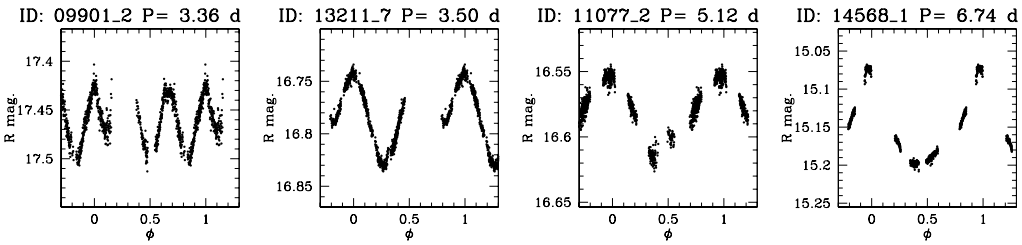

Figure B.20: Double-wave or distorted rotational variables.

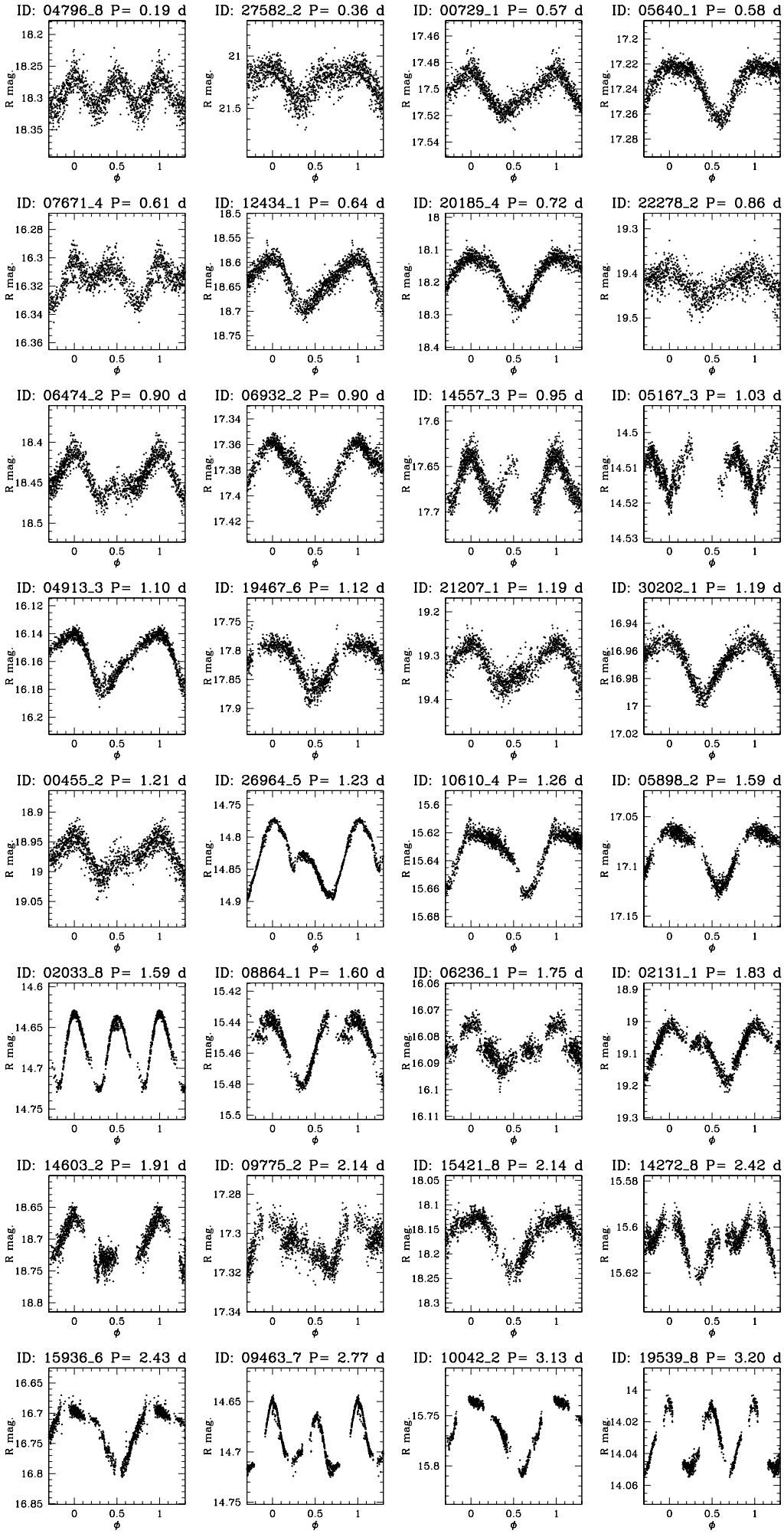
ID: 04796_8 P= 0.19 d
ID: 27582_2 P= 0.36 d
ID: 00729_1 P= 0.57 d
ID: 05640_1 P= 0.58 d
ID: 07671_4 P= 0.61 d
ID: 12434_1 P= 0.64 d
ID: 20185_4 P= 0.72 d
ID: 22278_2 P= 0.86 d
ID: 06474_2 P= 0.90 d
ID: 06932_2 P= 0.90 d
ID: 14557_3 P= 0.95 d
ID: 05167_3 P= 1.03 d
ID: 04913_3 P= 1.10 d
ID: 19467_6 P= 1.12 d
ID: 21207_1 P= 1.19 d
ID: 30202_1 P= 1.19 d
ID: 00455_2 P= 1.21 d
ID: 26964_5 P= 1.23 d
ID: 10610_4 P= 1.26 d
ID: 05898_2 P= 1.59 d
ID: 02033_8 P= 1.59 d
ID: 08864_1 P= 1.60 d
ID: 06236_1 P= 1.75 d
ID: 02131_1 P= 1.83 d
ID: 14603_2 P= 1.91 d
ID: 09775_2 P= 2.14 d
ID: 15421_8 P= 2.14 d
ID: 14272_8 P= 2.42 d
ID: 15936_6 P= 2.43 d
ID: 09463_7 P= 2.77 d
ID: 10042_2 P= 3.13 d
ID: 19539_8 P= 3.20 d
R mag.
ϕ

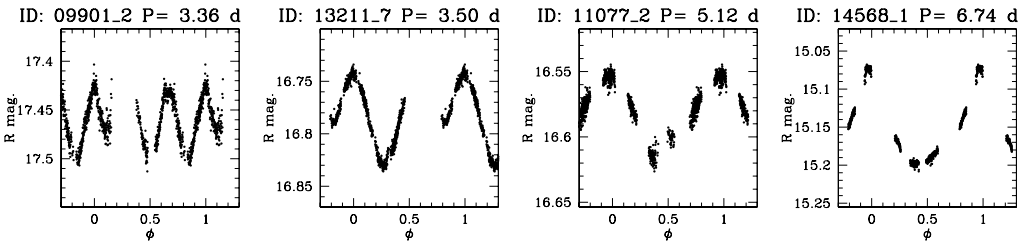

Figure B.22: Double-wave or distorted rotational variables.

Appendix C

Tables of results for transit simulations

In this Appendix we report the results of our simulations regarding the transits search described in Chapter 6.

For NGC 6791, simulations were made assuming three different dterminations for the metallicity (as explained in Sect. 6.3.1) and three different distributions for the radii of the simulated transiting planets (see Sect. 6.3.1)

The set of simulations now described were applyied on two sets of 3311 Main Sequence light curves: the ones obtained at the CFHT and that created by merging the data obtained at CFHT, Loiano and San Pedro Mártir (Tables C.1 and C.1 respectively).

For NGC 6253, simulations were made assuming two different dterminations for the metallicity (see Sect. 6.3.1) and the usual three different distributions for the planetary radii. Results are listed in Table C.2.

Moreover, other simulations were performed to evaluate the optimal observing time required to increase significatively the significance level of the results. For details about this topic see Sect. 6.5 Results are listed in Tables C.4, C.5, C.6, C.7, C.8 and C.9. A graphical representation of these results is plotted in Figures 6.15 and 6.16.

C.1 NGC 6791

[Fe/H]=0.17			
Planetary radii (R_J)	0.7±0.1	1.0±0.2	1.4±0.1
MS stars	3311	3311	3311
Number of stars with a planet	48.0	47.8	47.7
N_{geom}	5.4	5.6	5.7
Number of transiting planets (N1+)	2.4	2.5	2.6
N1	1.9	1.9	2.0
N2	0.5	0.5	0.5
N3	0.1	0.1	0.1
N4+	0.0	0.0	0.0
[Fe/H]=0.39			
Planetary radii (R_J)	0.7±0.1	1.0±0.2	1.4±0.1
MS stars	3311	3311	3311
Number of stars with a planet	131.5	131.5	131.5
N_{geom}	14.8	15.3	15.8
Number of transiting planets (N1+)	6.8	7.0	7.2
N1	5.2	5.4	5.6
N2	1.4	1.4	1.5
N3	0.2	0.2	0.2
N4+	0.0	0.0	0.0
[Fe/H]=0.47			
Planetary radii (R_J)	0.7±0.1	1.0±0.2	1.4±0.1
MS stars	3311	3311	3311
Number of stars with a planet	190.4	190.4	190.4
N_{geom}	21.4	22.1	22.8
Number of transiting planets (N1+)	9.7	10.1	10.4
N1	7.5	7.8	8.0
N2	2.0	2.1	2.1
N3	0.2	0.2	0.2
N4+	0.0	0.0	0.0

Table C.1: Results of our simulations for 3311 main sequence stars in NGC 6791.

[Fe/H]=0.17			
Planetary radii (R_J)	0.7±0.1	1.0±0.2	1.4±0.1
MS stars	3311	3311	3311
Number of stars with a planet	47.7	47.7	47.7
N_{geom}	5.3	5.5	5.7
Number of transiting planets (N1+)	4.6	4.8	4.9
N1	1.6	1.7	1.8
N2	1.7	1.8	1.8
N3	0.9	0.9	1.0
N4+	0.4	0.4	0.4
[Fe/H]=0.39			
Planetary radii (R_J)	0.7±0.1	1.0±0.2	1.4±0.1
MS stars	3311	3311	3311
Number of stars with a planet	131.6	131.6	131.5
N_{geom}	14.5	15.0	15.6
Number of transiting planets (N1+)	12.5	12.9	13.4
N1	4.4	4.6	4.8
N2	4.7	4.8	5.0
N3	2.4	2.5	2.6
N4+	1.0	1.0	1.1
[Fe/H]=0.47			
Planetary radii (R_J)	0.7±0.1	1.0±0.2	1.4±0.1
MS stars	3311	3311	3311
Number of stars with a planet	190.1	190.0	190.0
N_{geom}	21.0	21.6	22.4
Number of transiting planets (N1+)	18.0	18.6	19.3
N1	6.4	6.6	6.9
N2	6.7	7.0	7.2
N3	3.4	3.5	3.7
N4+	1.4	1.4	1.5

Table C.2: Results of our simulations for 3311 main sequence stars in NGC 6791 (considering all sites together).

C.2 NGC 6253

[Fe/H]=0.36			
Planetary radii (R_J)	0.7±0.1	1.0±0.2	1.4±0.1
MS stars	671.0	671.0	671.0
Number of stars with a planet	23.3	23.2	23.3
N_{geom}	2.4	2.4	2.6
Number of transiting planets (N1+)	1.5	1.6	1.6
N1	0.9	1.0	1.0
N2	0.5	0.5	0.5
N3	0.1	0.1	0.1
N4+	0.0	0.0	0.0
[Fe/H]=0.46			
Planetary radii (R_J)	0.7±0.1	1.0±0.2	1.4±0.1
MS stars	671.0	671.0	671.0
Number of stars with a planet	36.8	36.8	36.9
N_{geom}	3.7	3.9	4.1
Number of transiting planets (N1+)	2.4	2.5	2.6
N1	1.5	1.5	1.6
N2	0.8	0.8	0.8
N3	0.2	0.2	0.2
N4+	0.0	0.0	0.0

Table C.3: Results of our simulations for 671 selected main sequence stars in NGC 6253.

C.3 Other simulations

Nights	hours	N_{geom}	N_{tot}	N1	N2	N3	N4+	N_{tr}
5	1	1	0.00937	0.00918	0.00019	0.00000	0.00000	0.00956
5	2	1	0.09164	0.08840	0.00319	0.00005	0.00000	0.09492
5	3	1	0.15821	0.14888	0.00919	0.00010	0.00005	0.16779
5	4	1	0.21657	0.20238	0.01395	0.00019	0.00005	0.23109
5	5	1	0.27327	0.24894	0.02366	0.00057	0.00010	0.29846
5	6	1	0.32157	0.28777	0.03271	0.00100	0.00010	0.35666
5	7	1	0.37262	0.32666	0.04457	0.00129	0.00010	0.42015
5	8	1	0.42345	0.36385	0.05768	0.00186	0.00005	0.48504
5	9	1	0.46918	0.39409	0.07275	0.00229	0.00005	0.54669
5	10	1	0.51268	0.42213	0.08792	0.00259	0.00005	0.60596
5	11	1	0.55202	0.44052	0.10849	0.00296	0.00005	0.66663
5	12	1	0.59677	0.46300	0.13048	0.00320	0.00010	0.73403
5	13	1	0.63654	0.48616	0.14636	0.00398	0.00005	0.79104
5	14	1	0.67608	0.50361	0.16812	0.00425	0.00010	0.85304
5	15	1	0.71370	0.51623	0.19236	0.00496	0.00014	0.91647
5	16	1	0.75148	0.52934	0.21612	0.00588	0.00014	0.97983
5	17	1	0.78307	0.53583	0.24059	0.00650	0.00014	1.03714
5	18	1	0.81776	0.54095	0.26869	0.00778	0.00033	1.10306
5	19	1	0.85257	0.54428	0.29907	0.00884	0.00038	1.17051
5	20	1	0.88089	0.54021	0.33069	0.00941	0.00057	1.23221
5	21	1	0.90840	0.53229	0.36493	0.01055	0.00062	1.29645
5	22	1	0.93454	0.52117	0.40089	0.01163	0.00086	1.36141
5	23	1	0.95608	0.51045	0.43054	0.01423	0.00086	1.41770
5	24	1	0.98183	0.49012	0.47439	0.01645	0.00086	1.49175

Table C.4: Simulations regarding observative windows of 5 nights, with different number of hours per night. Note that all values, with the exception of N_{tr}, are normalized to N_{geom}.

Nights	hours	N_{geom}	N_{tot}	N1	N2	N3	N4+	N_{tr}
10	1	1	0.01749	0.01692	0.00052	0.00005	0.00000	0.01811
10	2	1	0.17529	0.16301	0.00913	0.00239	0.00076	0.19158
10	3	1	0.29716	0.26498	0.02503	0.00534	0.00181	0.33874
10	4	1	0.39191	0.33246	0.04728	0.00930	0.00286	0.46696
10	5	1	0.47447	0.38268	0.07248	0.01558	0.00374	0.58995
10	6	1	0.54926	0.41677	0.10186	0.02404	0.00658	0.72043
10	7	1	0.61059	0.42986	0.13999	0.03229	0.00845	0.84195
10	8	1	0.66694	0.42984	0.18386	0.04234	0.01090	0.96989
10	9	1	0.71412	0.42013	0.22246	0.05764	0.01390	1.09561
10	10	1	0.75509	0.39727	0.26574	0.07365	0.01844	1.22662
10	11	1	0.79148	0.37133	0.30435	0.09401	0.02179	1.35278
10	12	1	0.82129	0.34709	0.33490	0.11243	0.02688	1.46554
10	13	1	0.84666	0.31003	0.36775	0.13662	0.03225	1.58881
10	14	1	0.87054	0.27605	0.38723	0.16769	0.03957	1.71703
10	15	1	0.89473	0.24277	0.39970	0.20426	0.04799	1.85316
10	16	1	0.91233	0.21541	0.40369	0.23640	0.05683	1.96716
10	17	1	0.92962	0.18971	0.39636	0.27493	0.06861	2.09113
10	18	1	0.94648	0.16335	0.38840	0.31047	0.08426	2.21936
10	19	1	0.96013	0.14115	0.37499	0.34290	0.10109	2.33789
10	20	1	0.97400	0.11858	0.35408	0.37808	0.12326	2.47152
10	21	1	0.98428	0.09525	0.32989	0.40971	0.14944	2.60272
10	22	1	0.99130	0.07349	0.30138	0.44158	0.17485	2.72500
10	23	1	0.99680	0.05512	0.26855	0.46778	0.20535	2.84715
10	24	1	0.99967	0.03345	0.21655	0.50696	0.24271	2.99476

Table C.5: Simulations regarding observative windows of 10 nights, with different number of hours per night. Note that all values, with the exception of N_{tr}, are normalized to N_{geom}.

Nights	hours	N_{geom}	N_{tot}	N1	N2	N3	N4+	N_{tr}
15	1	1	0.02481	0.02353	0.00110	0.00010	0.00010	0.02643
15	2	1	0.25769	0.23209	0.01912	0.00453	0.00195	0.29297
15	3	1	0.41582	0.34707	0.05326	0.00972	0.00576	0.50977
15	4	1	0.53724	0.40986	0.09890	0.01760	0.01088	0.71137
15	5	1	0.62874	0.43251	0.15337	0.02592	0.01695	0.89604
15	6	1	0.69430	0.41726	0.21534	0.03768	0.02402	1.07192
15	7	1	0.75160	0.38409	0.27266	0.06180	0.03305	1.26779
15	8	1	0.79317	0.33566	0.32796	0.08785	0.04170	1.44809
15	9	1	0.82833	0.28090	0.36630	0.12502	0.05612	1.64571
15	10	1	0.85659	0.23273	0.38352	0.16083	0.07951	1.84236
15	11	1	0.87903	0.19266	0.38413	0.20105	0.10119	2.02026
15	12	1	0.89650	0.15516	0.36686	0.24368	0.13079	2.20509
15	13	1	0.91362	0.12769	0.33271	0.28006	0.17315	2.40385
15	14	1	0.92899	0.10306	0.30370	0.30536	0.21688	2.59158
15	15	1	0.93985	0.08170	0.27258	0.31688	0.26870	2.76999
15	16	1	0.95164	0.06666	0.24014	0.32309	0.32176	2.95183
15	17	1	0.96223	0.05626	0.19990	0.31987	0.38620	3.14933
15	18	1	0.97228	0.04484	0.16974	0.31218	0.44552	3.33890
15	19	1	0.97935	0.03600	0.14322	0.29141	0.50872	3.51800
15	20	1	0.98745	0.02781	0.11802	0.26543	0.57619	3.72140
15	21	1	0.99226	0.02050	0.10139	0.24134	0.62903	3.89034
15	22	1	0.99617	0.01345	0.07949	0.21168	0.69155	4.08772
15	23	1	0.99875	0.00743	0.06337	0.17960	0.74836	4.27791
15	24	1	0.99986	0.00148	0.04676	0.13554	0.81608	4.49713

Table C.6: Simulations regarding observative windows of 15 nights, with different number of hours per night. Note that all values, with the exception of N_{tr}, are normalized to N_{geom}.

Nights	hours	N_{geom}	N_{tot}	N1	N2	N3	N4+	N_{tr}
20	1	1	0.03277	0.03096	0.00158	0.00014	0.00010	0.03502
20	2	1	0.32955	0.28818	0.03240	0.00568	0.00329	0.38561
20	3	1	0.52006	0.40494	0.09050	0.01460	0.01002	0.68026
20	4	1	0.64586	0.43276	0.16866	0.02738	0.01706	0.93849
20	5	1	0.73207	0.40209	0.25365	0.04757	0.02875	1.19749
20	6	1	0.78681	0.33867	0.33136	0.07532	0.04146	1.43063
20	7	1	0.82677	0.26574	0.37606	0.12492	0.06005	1.68567
20	8	1	0.85922	0.20446	0.38318	0.18638	0.08519	1.94194
20	9	1	0.88271	0.15454	0.36346	0.24215	0.12256	2.18795
20	10	1	0.89954	0.11639	0.32227	0.28377	0.17711	2.44262
20	11	1	0.91633	0.08620	0.27801	0.31008	0.24203	2.69241
20	12	1	0.92810	0.06861	0.22675	0.31337	0.31937	2.94440
20	13	1	0.93918	0.05462	0.18147	0.30283	0.40027	3.19316
20	14	1	0.95000	0.04527	0.14492	0.27877	0.48104	3.44045
20	15	1	0.96088	0.03549	0.11750	0.24807	0.55982	3.70618
20	16	1	0.96907	0.02836	0.09684	0.21379	0.63008	3.95372
20	17	1	0.97656	0.02258	0.08124	0.17910	0.69363	4.20636
20	18	1	0.98028	0.01700	0.06748	0.15016	0.74563	4.43863
20	19	1	0.98564	0.01265	0.05459	0.12502	0.79338	4.69932
20	20	1	0.99207	0.00941	0.04513	0.10625	0.83129	4.95000
20	21	1	0.99508	0.00607	0.03393	0.09004	0.86504	5.19799
20	22	1	0.99757	0.00310	0.02609	0.07650	0.89188	5.44067
20	23	1	0.99929	0.00162	0.01738	0.06275	0.91754	5.70223
20	24	1	0.99995	0.00000	0.00826	0.04979	0.94190	6.00153

Table C.7: Simulations regarding observative windows of 20 nights, with different number of hours per night. Note that all values, with the exception of N_{tr}, are normalized to N_{geom}.

Nights	hours	N_{geom}	N_{tot}	N1	N2	N3	N4+	N_{tr}
25	1	1	0.04136	0.03869	0.00239	0.00014	0.00014	0.04465
25	2	1	0.39528	0.32995	0.05215	0.00786	0.00532	0.48459
25	3	1	0.60482	0.42597	0.14229	0.02205	0.01451	0.85179
25	4	1	0.72810	0.40152	0.25313	0.04676	0.02670	1.18889
25	5	1	0.79828	0.32038	0.34921	0.08697	0.04172	1.49408
25	6	1	0.84402	0.23287	0.39190	0.15112	0.06813	1.81436
25	7	1	0.86968	0.16250	0.37474	0.22508	0.10736	2.11342
25	8	1	0.89363	0.11687	0.32355	0.28597	0.16724	2.42315
25	9	1	0.90968	0.07724	0.26497	0.31692	0.25055	2.74097
25	10	1	0.92385	0.05619	0.20376	0.31457	0.34933	3.05896
25	11	1	0.93534	0.04166	0.15642	0.28970	0.44756	3.36901
25	12	1	0.94700	0.03420	0.11740	0.24683	0.54856	3.69416
25	13	1	0.95269	0.02683	0.09275	0.20074	0.63238	3.98840
25	14	1	0.96051	0.02056	0.07098	0.16446	0.70451	4.30141
25	15	1	0.96793	0.01692	0.05564	0.13375	0.76162	4.62075
25	16	1	0.97555	0.01351	0.04532	0.10955	0.80717	4.93238
25	17	1	0.98054	0.00916	0.03731	0.09150	0.84257	5.25184
25	18	1	0.98652	0.00791	0.02892	0.07409	0.87560	5.57166
25	19	1	0.98943	0.00536	0.02262	0.05998	0.90147	5.87033
25	20	1	0.99306	0.00326	0.01772	0.05252	0.91956	6.17969
25	21	1	0.99638	0.00205	0.01249	0.04191	0.93993	6.50708
25	22	1	0.99829	0.00100	0.00823	0.03245	0.95661	6.81722
25	23	1	0.99943	0.00043	0.00378	0.02604	0.96918	7.13170
25	24	1	1.00000	0.00000	0.00043	0.01787	0.98170	7.50745

Table C.8: Simulations regarding observative windows of 25 nights, with different number of hours per night. Note that all values, with the exception of N_{tr}, are normalized to N_{geom}.

Nights	hours	N_{geom}	N_{tot}	N1	N2	N3	N4+	N_{tr}
30	1	1	0.04791	0.04396	0.00362	0.00024	0.00010	0.05230
30	2	1	0.45246	0.35704	0.07461	0.01269	0.00811	0.58590
30	3	1	0.67358	0.41993	0.20264	0.03262	0.01839	1.01949
30	4	1	0.78145	0.33910	0.33193	0.07608	0.03434	1.41170
30	5	1	0.84093	0.23611	0.39094	0.14622	0.06766	1.80379
30	6	1	0.87194	0.15282	0.37016	0.23540	0.11356	2.15679
30	7	1	0.89747	0.09734	0.30503	0.29936	0.19573	2.54700
30	8	1	0.91324	0.06556	0.22756	0.31690	0.30322	2.91343
30	9	1	0.92749	0.04694	0.16458	0.29339	0.42257	3.29363
30	10	1	0.93980	0.03215	0.11569	0.25126	0.54069	3.68123
30	11	1	0.94659	0.02359	0.08749	0.19895	0.63656	4.02575
30	12	1	0.95453	0.01915	0.06457	0.15064	0.72017	4.40615
30	13	1	0.96182	0.01516	0.05042	0.11586	0.78038	4.78863
30	14	1	0.96822	0.01300	0.03656	0.08894	0.82973	5.15995
30	15	1	0.97551	0.01015	0.02868	0.07276	0.86392	5.55622
30	16	1	0.97890	0.00788	0.02272	0.05743	0.89087	5.91273
30	17	1	0.98381	0.00578	0.01734	0.04786	0.91283	6.28640
30	18	1	0.98746	0.00450	0.01282	0.03900	0.93115	6.66190
30	19	1	0.99117	0.00320	0.00898	0.03237	0.94662	7.03509
30	20	1	0.99417	0.00167	0.00674	0.02584	0.95992	7.43031
30	21	1	0.99685	0.00110	0.00400	0.01931	0.97245	7.80594
30	22	1	0.99818	0.00038	0.00225	0.01458	0.98098	8.17229
30	23	1	0.99952	0.00019	0.00096	0.00870	0.98967	8.54895
30	24	1	0.99995	0.00000	0.00000	0.00347	0.99648	9.00590

Table C.9: Simulations regarding observative windows of 30 nights, with different number of hours per night. Note that all values, with the exception of N_{tr}, are normalized to N_{geom}.

Bibliography

[1] Alard, C.; Lupton, Robert H. 1998, ApJ 503, 325

[2] Albrow, M. D.; Gilliland, R. L.; Brown, T. M. et al. 2001, ApJ, 559, 1060

[3] Anderson, J.; Bedin, L., R.; Piotto, G. et al. 2006 A&A 454,1029

[4] Anthony-Twarog, B.J.; Twarog, B.A.; Mayer, L.; preprint astro-ph/0612549

[5] Bedin, L. R.; Piotto, G.; Carraro, G.; King, I. R.; Anderson, J. 2006, A&A, 460, 27 (B06)

[6] Bedin, L. R.; Salaris, M.; Piotto, G.; King, I. R.; Anderson, J.; Cassisi S.; Momany Y. 2005, ApJ, 624, 45

[7] Beer, M. E.; King, A. R.; Pringle, J. E. 2004, MNRAS 355,1244

[8] Benz, W.; Hills, J. G. 1987 ApJ 323, 614

[9] Bonavita, M.; Desidera, S. 2007 A&A 468, 721

[10] Borucki, W.J. & Summers, A. L. 1984, Icarus, 58, 121

[11] Bragaglia, A.; Tessicini, G.; Tosi, M.; Marconi, G,; Munari, U. 1997, MNRAS 284, 477–488

[12] Bruntt, H.; Frandsen, S.; Gilliland, R. L.; Christensen-Dalsgaard, J.; Petersen, J. O.; Guhathakurta, P.; Edmonds, P. D.; Bono, G. 2001 A&A 371, 614

[13] Bruntt, H.; Grundahl, F.; Tingley, B. et al. 2003, A&A, 410, 323 (B03)

[14] Bruntt, H.; Stello, D.; SuÃ¡rez, J. C. et al. 2007 Mon. Not. R. Astron. Soc..378, 1371

[15] Carpino, M.; Milani, A.;& Nobili, A.M. 1987, A&A, 181, 182

[16] Carraro, G.; Villanova, S.; Demarque, P.; McSwain, M. V.; Piotto, G.; Bedin, L. R. 2006, ApJ, 643, 1151-1159

[17] Carretta, E.; Bragaglia, A.; Tosi, M.; & Marconi, G. 2000, in "Stellar Clusters and Associations: Convection, Rotation, and Dynamos", eds. R. Pallavicini, G. Micela, & S. Sciortino, ASPC vol. 198, p.273

[18] Carretta, E.; Bragaglia, A.; Gratton, R. G. 2007 A&A 473, 129C

[19] Chaboyer, B.; Green, E. M.; Liebert, J. 1999, AJ, 117, 1360

[20] Claret, A. 2000 A&A 363, 1081

[21] Clark, L. L.; Sandquist, E. L.; Bolte, M. 2004, AJ 128, 3019-3033

[22] Davies, M. B.; Sigurdsson, S. 2001, MNRAS 324, 612

[23] Davies, M. B.; Piotto, G.; de Angeli, F. 2004, MNRAS, 349, 129-134

[24] De Marchi, F.; De Angeli, F.; Piotto, G.; Carraro, G.; Davies, M. B. 2006, A&A, 459, 489-497

[25] De Marchi, F.; Poretti, E.; Montalto, M.; et al. 2007, A&A, 471, August IV 2007, 515-526 (D07)

[26] Edmonds, P. D.; Gilliland, R. L.; Heinke, C. O.; Grindlay, J. E 2003, ApJ, 596, 1197-1219

[27] Eggen, O J.; Iben, I. 1989 AJ 97, 431

[28] Eyer, L.; Mowlavi, N.; preprint astro-ph/0712.3797

[29] Ferraz-Mello S. 1981, AJ, 86, 4

[30] Fischer, D. A.; Valenti, J. 2005 ApJ 621, 1102

[31] Friel, E. D.; Janes, K. A. 1993, A&A, 267, 75

[32] Friel, E. D. 1995, ARA&A, 33, 381

[33] Gaudi, B. S. 2005 ApJ, 628, 73

[34] Gaudi, B. S. 2005 ApJ, 623, 472

[35] Gilliland, R. L.; Brown, T. M. 1992 AJ 103, 1945

[36] Gilliland, R. L.; Edmonds, P. D.; Petro, L.; Saha, A.; Shara, M. M. 1995 ApJ 447, 191

[37] Gilliland, R. L.; Brown, T. M.; Guhathakurta, P.; et al. 2000, ApJ, 545, L47

[38] Girardi, L.; Bertelli, G; Bressan, A. et al. 2002 A&A, 391, 195

[39] Gratton, R.; Bragaglia, A.; Carretta, E.; Tosi, M. 2006, ApJ, 642, 462-469

[40] Guillot, T.; Santos N.C.; Pont F. et al. 2006, A&A, 453, L21

[41] Hartman, J. D.; Stanek, K. Z.; Gaudi, B. S. et al. 2005, AJ, 130, 2241 (H05)

[42] Hénon, M. 1969 A&A 2, 151

[43] Kaluzny, J. 1990, Mon. Not. R. Astr. Soc. 243, 492

[44] Kaluzny, J.; Mazur, B.; Krzemiński, W. 1993 Mon. Not. R. Astron. Soc. 262, 49

[45] Kaluzny, J.; Thompson, I. B. 2003 AJ 125, 2534

[46] Kaluzny J. 2003, Acta Astronomica, 53, 51 (K03)

[47] Kaluzny, J.; Rucinski, S. M. 1993, MNRAS, 265, 34 (KR93)

[48] Kaluzny, J.; Rucinski, S. M. 1993, ASPC, 53, 164

[49] Kaluzny, J.; Rucinski, S. M. 1995, A&A Suppl., 114, 1

[50] Kaluzny J.; Stanek K. Z.; Garnavich P.M.; & Challis P. 1997, ApJ, 491, 153

[51] Kaluzny, J.; Udalski, A. 1992, Acta Astronomica, 42, 29

[52] Kaluzny, J.; Thompson, I. B.; Rucinski, S. M.; Pych, W.; Stachowski, G.; Krzemiński, W.; Burley, G. S. 2007 AJ 134, 541

[53] King, I. R.; Bedin, L. R.; Piotto, G.; Cassisi, S.; Anderson, J. 2005, AJ, 130, 626

[54] Kovács, G.; Zucker, S.; Mazeh, T. 2002, A&A, 391, 369

[55] Liebert, J.; Saffer, R. A.; Green, E. M. 1994, AJ, 107, 1408

[56] Lang, K. R. 1992 "Astrophysical Data: Planets and Stars." Springer-Verlag, Berlin

[57] Lomb, N. R. 1976, Astrophysics and space science, 39, 447

[58] Lombardi, J C.; Rasio, F. A.; Shapiro, S. L. 1996 ApJ 468, 797

[59] Mandel, K.; Agol, E. 2002 ApJ, 580, L171-L175

[60] Mateo, M.; Harris, H. C.; Nemec, J.; Olszewski, E. W. 1990 AJ 100, 469

[61] Mathieu, R. D.; van den Berg, M.; Torres, G.; Latham, D.; Verbunt, F.; & Stassun, K. 2003, AJ, 125, 246

[62] Mazur, B.; Krzemiński, W.; Kaluzny, J. 1995 Mon. Not. R. Astron. Soc. 273, 59

[63] Mazur, B.; Krzemiński, W.; Kaluzny, J. 1999 Acta Astronomica, 49, 551

[64] McCrea, W. H. 1964 Mon. Not. R. Astron. Soc. 128, 147

[65] McNamara, D. H. 1997, PASP, 109, 1221-1232

[66] McNamara, D. H.; Madsen, J. B.; Barnes, J.; Ericksen, B. F. PASP, 112, 202-216

[67] McNamara, D.H. 2000, in "Delta Scuti and Related Stars", M. Breger and M.H. Montgomery Eds., ASP Conf. Series, 210, 373

[68] Mochejska, B. J. & Kaluzny, J. 1999 Acta Astronomica., 49, 351

[69] Mochejska, B. J.; Stanek, K. Z.; Sasselov, D. D.; Szentgyorgyi, A. H. 2002, AJ, 123, 3460 (M02)

[70] Mochejska, B. J.; Stanek, K. Z.; Kaluzny, J. 2003, AJ, 125, 3175 (M03)

[71] Mochejska, B. J.; Stanek, K. Z.; Sasselov, D. D. et al. 2004 A&A, 128, 312

[72] Mochejska, B. J.; Stanek, K. Z.; Szentgyorgyi, A. H. et al. 2005, AJ, 129, 2856 (M05)

[73] Mochnacki, S., W. 1984 ApJ Suppl. 55, 551

[74] Mochnacki, S., W. 1985 ApJ Suppl. 59, 445

[75] Montalto, M.; Piotto, G.; Desidera, S.; et al. 2007, A&A, 470, 1137-1156

[76] Montgomery, K. A.; Janes, K.A.; Phelps, R.L. 1994 AJ. 108, 585 (MJ04)

[77] Pace, G. & Pasquini, I. 2004, A&A, 425, 1021

[78] Paulson, D.; Cochran, W.D.; Hatzes, A.P. 2004, AJ, 127, 3579

[79] Petersen, J. O.; & Christensen–Dalsgaard, J. 1996, A&A 312, 463

[80] Petersen, J. O.; & Christensen–Dalsgaard, J. 1999, A&A 352, 547

[81] Petersen, J. O.; Hog, E. 1998 MmSAI 69, 59

[82] Peterson, R. C.; Green, E. M. 1998, ApJ 502, 39

[83] Piatti, A. E.; Clatiá J. J.; Bica, E.; Geisler, D.; Minniti, D. 1998, AJ, 116, 801-812

[84] Piotto, G. & Zoccali, M., 1999, A&A, 345, 485

[85] Platais, I.; Kozhurina-Platais, V.; Mathieu, R. D.; Girard, T. M.; van Altena, W. F.2003 AJ, 126, 2922

[86] Platais, I.; Melo, C.; Mermilliod, J.-C.; et al. 2007 A&A 461, 509

[87] Poretti, E. 2001, A&A, 371, 986

[88] Preston, G. W.; Sneden, C. 2000, AJ 120, 1014-1055

[89] RodrÃguez, E.; Rolland, A.; López de Coca, P.; MartÃn, S. 1996 A&A 307, 539R

[90] Rosenblatt, F. 1971, Icarus, 14, 71

[91] Rucinski, S. M. 1995, PASP, 107, 648

[92] Rucinski, S. M. 2003, New Astronomy Reviews, Volume 48, Issue 9, p. 703-709.

[93] Rucinski, S. M.; Kaluzny, J.; Hilditch, R. W. 1996, MNRAS, 282, 705 (RK96)

[94] Sagar, R.; Munari, U.; & de Boer, K. S. 2001, MNRAS, 327, 23-45

[95] Santos, N. C., Israelian, G., & Mayor, M. 2001, A&A, 373, 1019

[96] Sato, B.; Fischer, D. A.; Henry, G. W. et al. 2005 ApJ 633, 465S

[97] Sestito, P.; Randich, S.; Bragaglia, A. 2007 A&A, 465, 185

[98] Sigurdsson, S.; Richer, H. B.; Hansen, B. M.; Stairs, I. H.; Thorsett, S. E. 2003, Science, 301, 193

[99] Simoda, M. 1991 IBVS, 3675, 1S

[100] Stellingwerf, R. F. 1978, ApJ, 224, 953-960

[101] Stetson, P. B. 1987 PASP 99, 191

[102] Stetson, P. B.; Bruntt, H.; Grundahl, F. 2003, PASP, 115, 413

[103] Sturve, O. 1952, The Observatory, 72, 199

[104] Taylor, B. J. 2001, A&A, 377, 473

[105] Tammann, G. A; Sandage, A.; Reindl, B. 2003, A&A, 404, 423-448

[106] Twarog, B. R.; Anthony–Twarog, B. J.; & De Lee, N. 2003, AJ, 125

[107] Vanicek, P. 1971, Astrophysics and Space Science, 12, 10

[108] Warner, B. 1995, Cataclysmic Variable Stars (Cambridge: Cambridge Univ. Press)

[109] Weldrake, D. T. F.; Sackett, P. D.; Bridges T. J.; Freeman, K. C. 2004, AJ, 128, 736

[110] Weldrake, D. T. F.; Sackett, P. D.; Bridges T. J.; Freeman, K. C. 2005, ApJ, 620, 1043

[111] Wittenmyrer, R. A.; Welsh, W. F.; Orosz, J. A.; et al. 2005, ApJ 632, 1157

[112] Worthey, G.; Jowett, K. J.; 2003 PASP 115, 96

[113] Xin, Y.; Zhang, X.; Deng, L. 2002, Chin. J. Astron. Astrophys. 2, 481

[114] Yan, L.; Mateo, M. 1994 AJ, 108, 1810

[115] Yan, L.; Reid, I. N. 1996 MNRAS, 279, 751

[116] Zhang, X. B.; Deng, L.; Zhou, X.; Xin, Y. 2004 Mon. Not. R. Astron. Soc. 355, 1369

[117] Zloczewski, K.; Kaluzny, J.; Krzemiński W.; Olech, A.; Thompson, I. B. 2007 Mon. Not. R. Astron. Soc., 380, 1191